

october 1960  
the  
institute  
of  
radio  
engineers

# Proceedings of the IRE

## in this issue

CHARGE CONTROL OF TRANSISTORS  
GAIN-BANDWIDTH OPTIMIZATION  
PHASED ARRAYS  
VACUUM EVAPORATED MEMORY  
NOISE IN TRANSISTORS  
EFFECTS OF SURFACE RECOMBINATION  
DC PUMPED QUADRUPOLE AMPLIFIER  
CONSTANT PHASE TECHNIQUE  
AUTOMATIC PHASE CONTROL  
**STANDARDS ON SEMICONDUCTOR TERMS**  
TRANSACTIONS ABSTRACTS  
ABSTRACTS AND REFERENCES

AMPLIFICATION IN AN ELECTRON BEAM PAGE 1750





# FILTERS FOR ALL APPLICATIONS FROM STOCK

HERMETICALLY SEALED TO MIL-T-27A & MIL-F-18327 SPECS.



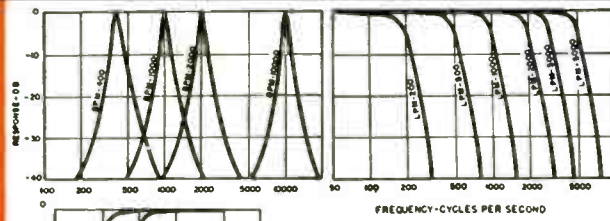
## MINIFILTERS

New Minifilters provide almost the same characteristics (with attenuation only slightly less) as the industry's standard interstage and line filters immediately below.

BPM band pass units are 10K input, output to grid; 2:1 gain. Attenuation is approximately 2 db  $\pm$  3% from center frequency, then 35 db per octave.

HPM high pass units; loss of less than 6 db at cut-off frequency; attenuation of 30 db at .67 cut-off frequency, 40 db at .5 cut-off frequency. Input and output 10K.

LPM low pass units; loss of less than 6 db at cut-off frequency; attenuation of 30 db at 1.5 cut-off frequency, 40 db at 1.65 cut-off frequency. Input and output 10K.



### STANDARD STOCK FREQUENCIES

(number in figure is cycles)

BPM-400	BPM-10000	LPM-1000
BPM-750	HPM-500	LPM-2000
BPM-1000	HPM-1000	LPM-3000
BPM-1500	LPM-200	LPM-5000
BPM-2000	LPM-500	

Write For NEW Catalog



BPM case (MIL AF)  
1/2" x 3/4" x 1 1/2"  
Weight .1 oz.



HPM and LPM case (MIL AB)  
1" x 1 1/2" x 1 1/2"  
Weight 2 1/2 oz.

## INTERSTAGE & LINE

These six basic types cover most popular filter applications and frequencies.

BMI band pass units are 10K input, output to grid; 2:1 gain. Attenuation is approximately 2 db at 3% from center frequency, then 40 db per octave.

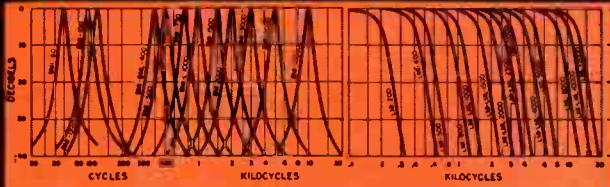
HMI high pass units are 10K in and out. Attenuation is less than 6 db at cut-off frequency and 35 db at .67 cut-off frequency.

LMI low pass units are 10K in and out. Attenuation is less than 6 db at cut-off frequency and 35 db at 1.5 cut-off frequency.

HML high pass filters are same as HMI but 500/600 ohms in and out.

LML low pass filters are same as LMI but 500/600 ohms in and out.

BML band pass units are same as BMI but 500/600 ohms input, output to grid, 9:1 gain.



### STANDARD STOCK FREQUENCIES

(number in figure is cycles)

BMI-60, 100, 120, 400, 500, 750, 1000, 1500, 2000, 3000, 4000, 5000, 10000
BTI-60, 100, 120
HMI-200, 400, 500, 800, 1000, 2000, 3000
LMI-200, 400, 500, 800, 1000, 1500, 2000, 2500, 3000, 4000, 5000, 10000
BML-400, 1000
HML-200, 300, 500, 1000
LML-1000, 1500, 2000, 2500, 4000, 8000, 10000, 12000



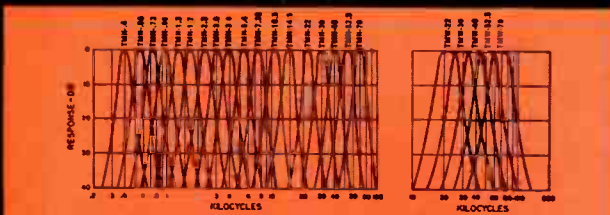
Base ..... 1 1/2" x 1 1/2"  
Height, BMI, LMI, BML ..... 1 1/2"  
Height, HMI, HML, LML ..... 2 1/2"  
Weight ..... 6 oz. and 9 oz.

## TELEMETERING BAND PASS

UTC standard telemetering filters provide extreme miniaturization with maximum stability, a complete set of 18 filters taking 19 cubic inches. They are 100K in and out and have an insertion loss of less than 6 db, 4 pin header for small Winchester socket.

TMN units are within 3 db at  $\pm$  7.5% of center frequency . . . down more than 18 db at  $\pm$  25% . . . more than 40 db beyond 1.75 and .58 center frequency.

TMW are within 3 db at  $\pm$  15% of center frequency . . . down more than 20 db at  $\pm$  50% . . . more than 40 db beyond 2.5 and .4 center frequency.



### STANDARD STOCK FREQUENCIES

(number in figure is KC)

TMN-.4	TMN-1.7	TMN-5.4	TMN-30	TMW-22
TMN-.56	TMN-2.3	TMN-7.35	TMN-40	TMW-30
TMN-.73	TMN-3.0	TMN-10.5	TMN-52.5	TMW-40
TMN-.96	TMN-3.9	TMN-14.5	TMN-70	TMW-52.5
TMN-1.3		TMN-22		TMW-70



TMN-2.3 thru TMN-70  
1/2" x 3/4" x 1 1/2"  
Weight .1-2 oz.

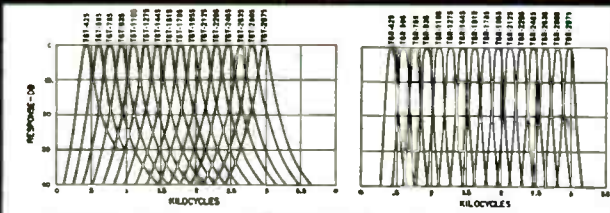
TMN-4 thru TMN-1.7  
1 1/2" x 1 1/2" x 2"  
Weight .3-5 oz.

## TELEGRAPH TONE CHANNEL

These band pass filters for multiplex transmitting and receiving provide maximum stability in miniature sizes. Both receiving and transmitting types are 600 ohms in and out, and employ 7 terminal header for sub-miniature 7 pin socket.

TGT transmitting filters are within 3 db at  $\pm$  42.5 cycles from center frequency . . . down more than 16 db at  $\pm$  170 cycles . . . down more than 7.5 db at adjacent channel cross-over.

TGR receiving filters are within 3 db at  $\pm$  42.5 cycles from center frequency . . . down more than 30 db at  $\pm$  170 cycles . . . down more than 15 db at adjacent channel cross-over.



### TRANSMITTING

TGT-425	TGT-1785
TGT-595	TGT-1955
TGT-765	TGT-2125
TGT-935	TGT-2295
TGT-1105	TGT-2465
TGT-1275	TGT-2635
TGT-1445	TGT-2805
TGT-1615	TGT-2975

### STANDARD STOCK FREQUENCIES

(number in figure is cycles)

### RECEIVING

TGR-425	TGR-1785
TGR-595	TGR-1955
TGR-765	TGR-2125
TGR-935	TGR-2295
TGR-1105	TGR-2465
TGR-1275	TGR-2635
TGR-1445	TGR-2805
TGR-1615	TGR-2975



TGT CASE  
1 1/2" x 1 1/2" x 2 1/2"  
Weight .8 oz.

TGR CASE  
1 1/2" x 1 1/2" x 4 1/2"  
Weight .15 oz.

And Special Units to Your Specifications

## UNITED TRANSFORMER CORP.

150 Varick Street, New York 13, N. Y.

PACIFIC MFG. DIVISION: 4008 W. JEFFERSON BLVD., LOS ANGELES 16, CALIF.  
EXPORT DIVISION: 13 EAST 40th STREET, NEW YORK 16, N. Y. CABLE: "ARLAB"

**October, 1960**

*published monthly by The Institute of Radio Engineers, Inc.*

**Proceedings of the IRE®**

*contents*

	<b>Poles and Zeros</b> .....	1693
	<b>Robert E. Moe, Director, 1960-1961</b> .....	1694
	<b>Scanning the Issue</b> .....	1695
<b>PAPERS</b>	A Study of the Charge Control Parameters of Transistors, <i>J. J. Sparkes</i> .....	1696
	Synthesis Techniques for Gain-Bandwidth Optimization in Passive Transducers, <i>H. J. Carlin</i> .....	1705
	Properties of Phased Arrays, <i>Wilhelm H. Von Aucock</i> .....	1715
	A Vacuum Evaporated Random Access Memory, <i>K. D. Broadbent</i> .....	1728
	Shot and Thermal Noise in Germanium and Silicon Transistors at High-Level Current Injections, <i>B. Schneider and M. J. O. Strutt</i> .....	1731
	Analytical Studies on Effects of Surface Recombination on the Current Amplification Factor of Alloy Junction and Surface Barrier Transistors, <i>T. Sugano and H. Yanai</i> .....	1739
	The DC Pumped Quadrupole Amplifier—A Wave Analysis, <i>A. E. Siegman</i> .....	1750
	Correction to "A Unified Analysis of Range Performance of CW, Pulse, and Pulse Doppler Radar," <i>J. J. Bussgang, P. Nesboda, and H. Safran</i> .....	1755
	High Selectivity with Constant Phase Over the Pass Band, <i>August W. Rihaczek</i> .....	1756
	Automatic Phase Control: Theory and Design, <i>T. J. Rey</i> .....	1760
	Correction to "A New Look at the Phase-Locked Oscillator," <i>Harold T. McAleer</i> .....	1771
	IRE Standards on Solid-State Devices: Definitions of Semiconductor Terms, 1960 .....	1772
<b>CORRESPONDENCE</b>	Esaki Diode Oscillators from 3 to 40 KMC, <i>R. Trambarulo and C. A. Burrus</i> .....	1776
	The Emitter Diffusion Capacitance of Drift Transistors, <i>J. Lindmayer and C. Wrigley</i> .....	1777
	Bomb-Excited "Whistlers," <i>B. A. Lippmann</i> .....	1778
	A Ferromagnetic Amplifier Using Dielectric Loading, <i>Harry Gruenberg</i> .....	1779
	Low Reverse Leakage Gallium-Arsenide Diodes, <i>J. Halpern and R. H. Rediker</i> .....	1780
	Scattering by a Spherical Satellite, <i>E. M. Kennaugh, S. P. Morgan, and H. Weil</i> .....	1781
	Scattering Properties of Large Spheres, <i>N. A. Logan</i> .....	1782
	WWV and WWVH Standard Frequency and Time Transmissions, <i>National Bureau of Standards</i> .....	1782
	Correction to "Direct Reading Noise Figure Measuring Device," <i>George Bruck</i> .....	1783
	Correction to "Absolutely Stable Hybrid Coupled Tunnel Diode Amplifier," <i>John J. Sie</i> .....	1783
	Some Results on Diode Parametric Amplifiers, <i>I. Goldstein and J. Zorzy</i> .....	1783
	Some Parametric Amplifier Circuit Configurations and Results, <i>I. Goldstein</i> .....	1783
	Gain Inconsistencies in Low-Frequency Reactance Parametric Up-Converters, <i>A. K. Kamal and A. J. Holub</i> .....	1784
	Parametric Amplification Properties in Transistors, <i>R. Zuleeg and V. W. Vodicka</i> .....	1785
	The Electron Content and Distribution in the Ionosphere, <i>T. G. Hane and W. D. Stuart</i> ..	1786
	Maximum Avalanche Multiplication in <i>p-n</i> Junctions, <i>Douglas J. Hamilton</i> .....	1787
	An Improvement in the Use of "Piecewise Approximations to Reliability and Statistical Design," <i>K. G. Ashar</i> .....	1788
	Modification of Pulse Amplifier Output Stages, Improving Their Response to Negative Edges, <i>I. Bar-David</i> .....	1788
	A Proposed Technique for F-Layer Scatter Propagation, <i>W. C. Vergara and J. L. Levatich</i> ..	1790
<b>REVIEWS</b>	Books:	
	"Fixed and Variable Capacitors," by G. W. A. Dummer and Harold M. Nordenberg, <i>Reviewed by Leon Podolsky</i> .....	1793
	"Infrared Radiation," by Henry L. Hackforth, <i>Reviewed by Sidney Passman</i> .....	1793
<b>COVER</b>	A novel electron-beam amplifier is described on page 1750 which makes use of the spiraling motion of electrons as they proceed along the beam. A time exposure of the beam would show that the various paths of individual electrons collectively form the interesting shape shown on the cover—a twisted ribbon which grows in width when the device is amplifying.	

published monthly by The Institute of Radio Engineers, Inc.

# Proceedings of the IRE®

continued

	"Advanced Engineering Mathematics," 2nd Ed., by G. R. Wylie, Jr., <i>Reviewed by Martin Katzin</i> .....	1793
	"Introduction to Modern Network Synthesis," by M. E. Van Valkenburg, <i>Reviewed by Thomas R. Williams</i> .....	1794
	"Introduction to Operations Research," by C. West Churchman, Russell L. Ackoff, and E. Leonard Arnoff, <i>Reviewed by C. L. Engelman</i> .....	1794
	"Electron Tube Life Factors," Craig Walsh and T. C. Tsao, Eds., <i>Reviewed by G. T. Bird</i> .....	1794
	"Photoconductivity of Solids," by Richard H. Bube, <i>Reviewed by M. S. Wasserman</i> .....	1794
	"A Primer of Programming for Digital Computers," by Marshall H. Wrubel, <i>Reviewed by Malcolm D. Smith</i> .....	1795
	SCANNING THE TRANSACTIONS .....	1795
<b>ABSTRACTS</b>	Abstracts of IRE TRANSACTIONS .....	1796
	Abstracts and References .....	1805
	Translations of Russian Technical Literature .....	1820
<b>IRE NEWS AND NOTES</b>	Current IRE Statistics .....	14A
	Calendar of Coming Events .....	14A
	Miscellaneous IRE Publications Available .....	18A
	Programs	
	1960 International Symposium on Engineering Writing and Speech .....	22A
	Twelfth Annual Mid-America Electronics Conference .....	22A
	1960 Radio Fall Meeting .....	24A
	Seventh Annual East Coast Conference on Aeronautical and Navigational Electronics ..	26A
	Thirteenth Annual Conference on Electrical Techniques in Medicine and Biology .....	28A
	1960 Electron Devices Meeting .....	32A
	1960 Nonlinear Magnetics and Magnetic Amplifier Conference .....	35A
	Northeast Electronics Research and Engineering Meeting (NEREM) .....	35A
	IRE Committees—1960 .....	42A
	IRE Representatives in Colleges .....	56A
	IRE Representatives on Other Bodies .....	60A
<b>DEPARTMENTS</b>	Contributors .....	1791
	IRE People .....	66A
	Industrial Engineering Notes .....	104A
	Meetings with Exhibits .....	8A
	Membership .....	121A
	News—New Products .....	62A
	Positions Open .....	128A
	Positions Wanted by Armed Forces Veterans .....	127A
	Professional Group Meetings .....	112A
	Section Meetings .....	121A
	Advertising Index .....	177A

## BOARD OF DIRECTORS, 1960

\*R. L. McFarlan, *President*  
 J. A. Ratcliffe, *Vice-President*  
 \*J. N. Dyer, *Vice-President*  
 \*W. R. G. Baker, *Treasurer*  
 \*Haraden Pratt, *Secretary*  
 \*F. Hamburger, Jr., *Editor*  
 \*D. G. Fink  
*Senior Past President*  
 \*Ernst Weber  
*Junior Past President*

## 1960

A. P. H. Barclay (R8)  
 \*L. V. Berkner  
 G. S. Brown  
 W. H. Doherty  
 A. N. Goldsmith

P. E. Haggerty  
 C. E. Harp (R6)  
 H. F. Olson (R2)  
 A. H. Waynick (R4)

## 1960-1961

C. W. Carnahan (R3)  
 B. J. Dasher (R3)  
 C. F. Horne  
 R. E. Moe (R5)  
 B. M. Oliver  
 J. B. Russell, Jr. (R1)

## 1960-1962

W. G. Shepherd  
 G. Sinclair

\*Executive Committee Members

## EXECUTIVE SECRETARY

George W. Bailey  
 John B. Buckley, *Chief Accountant*  
 Laurence G. Cumming, *Technical Secretary*  
 Emily Sirjane, *Office Manager*

## ADVERTISING DEPARTMENT

William C. Copp, *Advertising Manager*  
 Lillian Petranek, *Assistant Advertising Manager*

## EDITORIAL DEPARTMENT

Alfred N. Goldsmith, *Editor Emeritus*  
 F. Hamburger, Jr., *Editor*  
 E. K. Gannett, *Managing Editor*  
 Helene Frischauer, *Associate Editor*

## EDITORIAL BOARD

F. Hamburger, Jr., *Chairman*  
 A. H. Waynick, *Vice-Chairman*  
 E. K. Gannett  
 T. A. Hunter  
 J. D. Ryder  
 G. K. Teal  
 Kiyo Tomiyasu

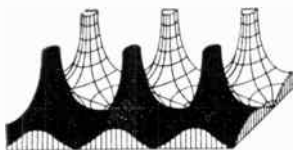


PROCEEDINGS OF THE IRE, published monthly by The Institute of Radio Engineers, Inc. at 1 East 79 Street, New York 21, N. Y. Manuscripts should be submitted in triplicate to the Editorial Department. Responsibility for contents of papers published rests upon the authors, and not the IRE or its members. All republication rights, including translations, are reserved by the IRE and granted only on request. Abstracting is permitted with mention of source.

Thirty days advance notice is required for change of address. Price per copy: members of the Institute of Radio Engineers, one additional copy \$1.25; non-members \$2.25. Yearly subscription price: to members \$9.00, one additional subscription \$13.50; to non-members in United States, Canada, and U. S. Possessions \$18.00; to non-members in foreign countries \$19.00. Second-class postage paid at Menasha, Wisconsin under the act of March 3, 1879. Acceptance for mailing at a special rate of postage is provided for in the act of February 28, 1925, embodied in Paragraph 4, Section 412, P. L. and R., authorized October 26, 1927. Printed in U.S.A. Copyright © 1960 by the Institute of Radio Engineers, Inc.



## Poles and Zeros



**The Communication of Ideas.** The basic and, perhaps, most important function of scientific and engineering journals

and periodicals is to promote the interchange of ideas on the part of a particular science or profession. It is essential that the several investigators or practitioners of an art or science become intimately aware of the progress of their colleagues. Duplication can be avoided and advance accelerated through the expeditious interchange of timely analytical and experimental successes or failures.

Before the establishment of professional societies and the days of rapid communications, the leaders in particular areas of scientific endeavor found it difficult to know what others were accomplishing. They either took recourse in private correspondence or were forced to travel to attain personal contact for the exchange of information. The earliest scientific publications, the precursors of today's journals, were truly journals of correspondence.

The formation of professional societies was, therefore, in a large measure engendered by the necessity for a better means of communicating ideas. The societies provided for the publication of the results of scientific investigations, and for the holding of meetings to facilitate the dissemination and the interchange of ideas. The foundation of the Royal Society (London), and the publication of its first *Transactions* in 1665 marked the inception of the scientific journal as such.

The Eighteenth Century saw the establishment of the first periodical limited to a particular branch of science; *Transactions of the American Philosophical Society* appeared first in 1771, *The Annales de Chimie et de Physique* appeared in 1789 and the *Journal der Physik* followed in 1790.

Scientific journals in the modern sense were born in the Nineteenth Century. Typical were the *Proceedings of the Royal Society of Sciences of Amsterdam*, *The American Journal of Science (Silliman's Journal)* which later became the *Proceedings of the American Philosophical Society*, and the *Proceedings of the American Academy of Arts and Sciences*. The specialized journal devoted to a single, often very narrow branch of science began its great development in this century. Journals devoted to the many branches of physics grew at the rate of eight new journals per year in the century beginning with 1810. The abstracting journal made its first appearance in the Nineteenth Century.

The late Nineteenth Century and the early Twentieth Century saw the beginnings of the development of the professional engineering societies in the United States. The American Society of Civil Engineers was founded in 1867, and the first volume of its *Transactions* appeared in 1872. *Transactions*

of the American Society of Mechanical Engineers appeared initially in 1880, those of the American Institute of Electrical Engineers in 1884, and of the American Society of Chemical Engineers in 1908. IRE was founded in 1912 and Volume I of the PROCEEDINGS was published in 1913. None of the initial volumes of these publications exceeded 400 pages, and the page size was approximately 6 by 9 inches rather than the present 8½ by 11 inches. Even as early as 1940, published pages had increased roughly four times without accounting for the increased page size.

As science and technology have progressed, the Twentieth Century has been marked by a remarkable increase in the number of journals published by each society. This increase was mandatory to attain adequate publication facilities for the expanding output of the growing society memberships. For example, the American Institute of Physics publishes 13 journals, ASME has 7 publications, AIEE publishes *Electrical Engineering* and three bi-monthly *Transactions*, and IRE publishes 28 *Transactions* in addition to the PROCEEDINGS. Using IRE as an indicator of the colossal growth in the number of printed pages, one may compare the 297 pages of 1913, the 586 pages of 1940, and the 1,480 pages of 1950 with the 17,968 pages of 1959!

From the early days of lack of publication and the meagerness of communication, we are now faced with a new problem in attempting to cope with a plethora of material. Complaints abound that there is so much now published that it is almost impossible to keep informed even in narrow areas of a particular interest. The overlapping of activities in societies makes it doubly or triply difficult to be assured that adequate coverage of a particular subject has been accomplished. One might conjecture, for example, that if an individual did nothing else but read in the area of his interest for an entire year, he might well find himself ten years behind at the end of his year of reading.

Selected reading has become a must. Techniques for selection are becoming more essential. Proper indexing, such as the newest IRE cumulative index, and comprehensive abstracting, which the PROCEEDINGS provides in the Abstracts and References Section each month, are important aids. Even these techniques are no longer completely satisfactory. The use of electronic scanning techniques, together with computers, presents a challenge to those interested in solving the problem under discussion. Someone will surely rise to the challenge and make a great contribution to the progress of science and engineering by solving the current and future problem of too little time for too much to read in too many scattered and uncorrelated publications.—F.H., Jr.



## R. E. Moe

*Director, 1960-1961*

Robert E. Moe (S'33-A'35-SM'46-F'55) was born in Appleton, Wis., on April 2, 1912. He was graduated from the University of Wisconsin, Madison, in 1933, with the B.S. degree in electrical engineering.

He joined the General Electric Company in May, 1934, as a student engineer, and was transferred to the Receiver Engineering Department in Bridgeport, Conn., in 1935, with assignments in components engineering, broadcast and television receiver design, and from 1941 to 1944 in government radar design. He was a member of Panel 9, Synchronizing Signal Standards, of the original National Television Systems Committee in 1939.

He was in charge of design activities on radar receivers and indicators for the Government division of the Electronics Department at Syracuse, N. Y., from 1944 to 1948. In 1947 he was awarded the U. S. Navy Certificate of Commendation for contributions to radar indicator design. He was transferred to Owensboro, Ky., in January, 1949, where he is now Manager of Engineering in the Receiving Tube Department. In 1958 he was appointed as an Industry Consultant to the Department of Defense Ad Hoc Study Group for Parts Specifications Management for Reliability, and served until the conclusion of its activities in May, 1960.

Mr. Moe has been chairman of the Evansville-Owensboro IRE Section and has held office in the Connecticut Valley and Syracuse Sections. He has served on the Papers Review Committee for a number of years.

He is a member of the Kentucky Society of Professional Engineers, the National Society of Professional Engineers, the American Society for Quality Control, Eta Kappa Nu and Tau Beta Pi, and is registered as a professional engineer in the states of New York and Kentucky.

## Scanning the Issue

**A Study of the Charge Control Parameters of Transistors** (Sparkes, p. 1696)—Many types of semiconductor and vacuum tube devices have in common the fact that their operation depends on the motion, control, and storage of charges. This charge approach to device analysis has aroused considerable interest lately because it provides a very useful common ground for characterizing and comparing the behavior of a wide variety of active devices. In this paper the author is interested specifically in investigating the concept of charge control as it applies to describing the action of transistors. He develops an important new method of specifying the characteristics of switching transistors that will be of interest to a large number of people using such transistors for electronic computation. It is not unlikely that an international standard method of measurement of switching-transistor performance will be based on this material.

**Synthesis Techniques for Gain-Bandwidth Optimization in Passive Transducers** (Carlin, p. 1705)—This paper is concerned with the problem of arriving at a design for an equalizer or matching network which will closely approach the ideal optimum in gain-bandwidth performance. The author evolves a technique which bypasses a complication which in the past has made this a very formidable problem to solve. The result is a paper which provides an effective and simple solution to a very difficult and significant network design problem. It is worth noting that this paper was originally considered for publication in the IRE TRANSACTIONS ON CIRCUIT THEORY. While it is relatively rare that TRANSACTIONS papers are referred to the PROCEEDINGS, the PGCT and IRE editors felt that this paper would be of fundamental and timely interest to a large segment of the PROCEEDINGS audience.

**Properties of Phased Arrays** (Von Aulock, p. 1715)—Although the majority of all operational radar systems use mechanically scanned antennas, there is greater interest today in electrical scanning because of the greater antenna rigidity, size and scanning speeds required by newly emerging radar systems. This interest goes well beyond methods of scanning. It also involves important differences in antenna beam characteristics which arise when electrical scanning is employed. The nature of these differences, and the resulting advantages and disadvantages, are made quite clear in this review of the scanning properties of electrically scanned arrays. The novelty of the author's approach and the manner in which he simplifies the visualization of the mode of operation of such antennas will be of interest to systems engineers as well as antenna designers.

**A Vacuum Evaporated Random Access Memory** (Broadbent, p. 1728)—The procession of important first papers on thin-film devices, which started in July, continues in this issue. Here again we are dealing with the evaporation of thin films of appropriate materials to form extremely compact structures of potentially great usefulness in microminiaturizing digital computers. However, in this paper the basic material employed is magnetic rather than superconductive. The structure described here consists of four layers of magnetic films interspersed with additional layers of insulators and of conductors for performing addressing and read-out functions. In fact, the total structure contains no less than 19 layers of magnetic, dielectric and conducting films. This multiple-layer deposition process is in itself a technological achievement of great interest.

**Shot and Thermal Noise in Germanium and Silicon Transistors at High-Level Current Injections** (Schneider and

Strutt, p. 1731)—During the past five years the PROCEEDINGS has published a number of papers and letters which have progressively developed a theoretical representation of noise in junction diodes and transistors, first for germanium and later for silicon. These studies were all made for the case of small current densities. The present paper complements this series by considering the case of high current densities. An interesting feature of the analysis is that at high current densities the equivalent circuit of a  $p-n$  junction includes an inductor as well as resistors and capacitors.

**Analytical Studies on Effects of Surface Recombination on the Current Amplification Factor of Alloy Junction and Surface Barrier Transistors** (Sugano and Yanai, p. 1739)—This paper provides analytical foundations for an area of transistor design which until now has been pretty much an empirical art. The authors develop a good approach to the computation of  $\beta$ , the survival factor of minority carriers, which gets around many difficulties that have stopped other investigators in the past. From this, the authors are able to develop much useful design data concerning optimum electrode geometries for transistors.

**The DC Pumped Quadrupole Amplifier—A Wave Analysis** (Siegman, p. 1750)—The quadrupole amplifier in the foregoing title takes its name from a low-noise parametric electron beam device described here just a year ago. Amplification was achieved by connecting an RF pump source to a four-pole structure to produce a transverse field which rotated synchronously with the spiralling motion of the electrons (*i.e.*, the cyclotron wave) as they proceeded along the beam path. In the present paper, the RF pumping field is replaced by a dc field applied via a twisted quadrupole structure. Thus the field, instead of rotating with time, rotates with distance along the beam axis. There is no idler frequency involved, nor does energy for amplification come from the pump. The result is a very promising form of microwave amplifier which, although it superficially resembles its earlier namesake, differs in a number of fundamental and interesting aspects.

**High Selectivity with Constant Phase over the Pass Band** (Rihaczek, p. 1756)—All types of linear networks that are highly selective introduce phase shifts which vary with frequency. In systems that use the phase of a signal as a carrier of information, this can cause troublesome distortions or errors. This paper describes a simple and novel technique for compensating for the phase shift in a filter so that the output phase will be independent of frequency. In essence, the signal is sent through two like filters, but in one case the signal frequency is inverted first by means of a mixer so that the phase change will be exactly opposite to that which the noninverted signal will experience in going through the second filter.

**Automatic Phase Control: Theory and Design** (Rey, p. 1760)—Automatic phase control serves to synchronize an oscillator with a sinusoidal reference signal of low power. The technique has a variety of uses, such as maintaining the phase close to that of the reference, tracking frequency changes, and purifying the oscillator spectrum. This study makes a very worthwhile contribution to a subject which is of considerable current interest in several fields, *e.g.*, binary data transmission, satellite tracking, radio interferometry, and TV.

**IRE Standards on Solid-State Devices: Definitions of Semiconductor Terms** (p. 1772)—This timely Standard defines over four score terms which are now among the most frequently used words in our technical language.

Scanning the Transactions appears on page 1795.

# A Study of the Charge Control Parameters of Transistors\*

J. J. SPARKES†

**Summary**—The present status of the concept of charge control of transistor action is considered, and what appear to be the most significant performance parameters for circuit design purposes are defined; also methods of measuring them surveyed. These parameters are the collector time constant  $\tau_C$ , the saturation time constant  $\tau_S$ , the “on demand current gain”  $\beta_S$ , the collector capacitance charge  $Q_V$  and the dc current gain  $\beta$ . The manner in which these parameters may be expected to vary with dc current level is analyzed, as far as possible, for homogeneous base transistors, and is considered qualitatively for graded base types.

A distinction is drawn between the technique of charge analysis of transistor action, and the concept of charge control of transistor performance. It is pointed out that only devices whose performance is determined by charges which are under the control of external circuitry can be regarded as charge *controlled* devices. This distinction strictly speaking excludes from the class of charge controlled devices those exhibiting the “wiggle” effect or possessing carrier storage in the collector region during operation in saturation. Although charge parameters can still be used for such devices, other parameters may be desirable as additions or alternatives.

IN the past few years, the description of the activity of active elements in terms of charge has been arousing a good deal of interest [1], [2] since it offers a method of unifying the analysis of all such electronic devices. Although a number of workers have independently studied the application of this principle to transistors [3], [4], the first explicit treatment of a transistor as a charge controlled device was published by Beaufoy and Sparkes [5], [6] in 1957. Since then, Sparkes [7] has defined those parameters which appear to be of most significance in circuit design and has outlined methods of measuring them. Beaufoy [8] has described a technique of circuit design using them. Further contributions to the subject have been made by Early [9], Grinich and Noyce [10], Kruithof [11] and Neeteson [12]. In most of these papers, it has been implicitly assumed that the parameters considered were constants of the devices although it was known, and the fact usually acknowledged, that they were in practice slowly varying functions of the dc conditions of operation. Furthermore, most of the work on transistors has been concerned with transistors possessing homogeneous base regions. The present paper is an attempt to consider the status of the concept of charge control of transistor action as applied to all types of present-day transistors, to define the significant parameters and show how their values may be expected to vary with operating conditions, and finally to point out the possible limita-

tions to the concept of charge control when applied to devices whose activity is not wholly under the control of charges accessible to external circuitry.

In previous articles, the time constants have been symbolized by the letter  $T$  ( $T_C$ ,  $T_S$ , etc.). But since this letter is normally reserved for temperatures, and since also the letter  $t$  is reserved for times, the symbol  $\tau$  is used throughout this paper to denote switching time constants. There is, of course, no change in meaning involved here, only a change of symbolism.

## TRANSISTOR SWITCHING PARAMETERS

Before a transistor is switched ON, the minority charge in the base region is approximately zero. Thermal generation leads to the presence of a small number of minority carriers and therefore also to a finite OFF collector current of the order of  $I_{CBO}$ . The actual value of the current is dependent upon  $I_{CBO}$ , but also upon the impedance and the reverse bias, if any, between the emitter and base terminals of the transistor [13].

The turn ON process consists in producing a forward bias across the emitter base junction. When the forward bias is applied to a  $p-n-p$  transistor, electrons flow into the base region via the base lead. These are majority carriers in the  $n$ -type base so that they transfer the applied potential immediately to the emitter junction and draw into the base a quantity of holes almost equal to the quantity of excess electrons which have been injected, since the condition of space charge neutrality must always be satisfied.

The quantity of holes is not exactly equal to the quantity of electrons because some of the electrons are used to charge up the emitter depletion layer capacitance, and the holes involved in this process remain in the emitter region. When the emitter junction is forward biased, the depletion layer gets narrower, so that some donors which were in the depletion layer move into the base region and require electrons to neutralize the charge they bring with them. Similarly, an equal number of acceptors emerge into the emitter region and require holes. This charge associated with charging the emitter depletion layer is called  $Q_{VE}$  and depends, of course, on the magnitude of the voltage swing on the emitter junction during turn-on. The total charge  $Q_B$  to turn on a specified collector current (at constant collector-base voltage) includes  $Q_{VE}$ , but also includes the magnitude of the minority charge which enters the base region. In homogeneous base transistors, the charge configuration shortly after switch-on is as shown in Fig. 1, and for

\* Received by the IRE, January 6, 1960; revised manuscript received, August 1, 1960.

† British Telecommunications Research Ltd., Taplow Court, Taplow. Nr. Maidenhead, Berks., England.

these transistors,  $Q_{VE}$  is usually a small fraction of  $Q_B$  at normal current levels. In graded base transistors the charge configuration is somewhat different (see, for example, Kruithof [11]), and since emitter capacitances tend to be relatively large in these devices,  $Q_{VE}$  may be a significant proportion of  $Q_B$ .

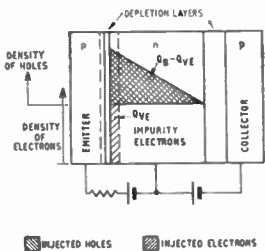


Fig. 1—Charge distribution in the base of a transistor after turn-on into short-circuit load. Dashed lines show the position of the emitter depletion layer before turn-on.

When the base charge has been set up and has reached equilibrium distribution (in a time of the order of  $\frac{1}{5}$  the steady-state transit time [13]), the collector current  $I_C$  is proportional to the base charge gradient at the boundary of the collector junction. In homogeneous base transistors (as illustrated in Fig. 1), the charge gradient is nearly linear throughout the base region and is proportional to the total base minority charge so that *the collector current is approximately proportional to this base charge*. In diffused base transistors, this latter proportionality still holds although the charge gradient is not linear. (Johnson and Rose [1] have shown that for this to be true, the carrier transit time should be substantially independent of current level.) The ratio of base charge to collector current is therefore a fundamental time constant of the transistor, and is called the Collector Time Constant  $\tau_C$ . Thus

$$\tau_C = Q_B / I_C \tag{1}$$

and if  $Q_{VE}$  can be neglected,  $\tau_C$  is equal to the mean carrier transit time across the base.

In general,  $Q_{VE}$  cannot be neglected so that the charge per unit collector current depends upon the current level in the ON state. It also depends to some extent upon the voltage at which the collector is held during turn-on as a result of collector depletion layer widening. The variation of  $Q_B$  with current level is considered later, but the effects of voltage can be taken into account for the purposes of definition by choosing a particular value of collector junction voltage. In practical applications, the most common ON state is one of saturation, so that at the edge of the saturation region when the collector base junction voltage is zero is a convenient ON state to regard as a standard test condition. Accordingly, the symbol  $\tau_{CO}$  is reserved for this state and is defined as

$$\tau_{CO} = Q_B / I_C \tag{2}$$

at zero collector junction voltage, and at specified collector current. This is the first switching parameter of importance.

The above discussion has been confined to short-circuit output conditions; in other words, it has been assumed that the turn-on of collector current has not resulted in a change of collector-base junction voltage. In practice, it usually happens (though not always) that a load resistance is present in the collector lead and that the turn-on process is accompanied by a drop of collector-base voltage. When this happens, further charge must be injected into the base region to charge up the collector-base capacitance in a manner exactly analogous to the charging of the emitter capacitance described earlier. In this case, however, the charge involved, to be called  $Q_V$ , is not usually negligible. It is shown later that

$$Q_V = M \cdot C_{ic} \cdot \Delta V_{CB} \tag{3}$$

where  $M$  is a numerical factor between 1 and 2,  $C_{ic}$  is the small signal depletion layer capacitance of the collector junction at the OFF collector voltage and  $\Delta V_{CB}$  is the change of collector junction voltage. (If extrinsic resistances are not negligible,  $V_{CB}$  is not equal to the collector junction voltage and corrections have to be made.)

The turn-on process into a finite load is illustrated for homogeneous base transistors in Fig. 2. Evidently, the charge  $Q_{ON}$  necessary to turn on a collector current  $I_C$ , if the OFF current is zero and if the transistor just bottoms, is given by<sup>1</sup>

$$Q_{ON} = Q_B + Q_V$$

or

$$Q_{ON} = I_C \tau_{CO} + Q_V. \tag{4}$$

$Q_V$  is the second design parameter of importance.

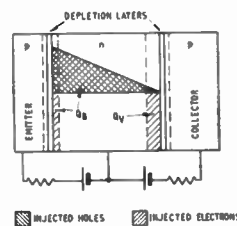


Fig. 2—Charge distribution in the base of a transistor after turn-on into finite load (active region only). Dashed lines show the position of the depletion layers before turn-on.

The third important parameter involved in active region operation is the common emitter dc current gain  $\beta$ . Thus, if  $\Delta I_C$  is the change in collector current as the base current is taken from zero to  $I_B$

<sup>1</sup> If the emitter is biased off turn-on,  $Q_{ON}$  is larger since charge is required to bring the emitter to the "just off" condition. This charge is related to the magnitude of the reverse bias and to  $C_{ie}$  by an equation similar to (3). This charge has been neglected in subsequent analysis in the paper, as it is usually small.

$$\beta = \Delta I_C / I_B \quad (5a) \quad \text{and}$$

at specified  $I_C$ .

It should be noted that  $Q_B / I_C$  is only slightly dependent upon temperature, because as  $Q_B$  increases with temperature as a result of thermal generation, so also does  $I_C$ .  $I_B$ , on the other hand, decreases as the temperature rises, and  $I_C / I_B$  increases markedly and can even change sign, so that for this reason  $\beta$ , as a near constant of the transistor is defined in terms of an increase in  $I_C$ . An alternative way of making allowance for thermal generation is to define  $\beta$  as

$$\beta = \frac{I_C - I_{CBO}}{I_B + I_{CBO}} \quad (5b)$$

at specified  $I_C$ .

To a good approximation, (5a) and (5b) are identical.

For circuit design purposes the value of  $\beta$  at zero collector junction voltage,  $\beta_0$ , is of primary importance, and in this condition  $I_{CBO}$  is zero so that

$$\beta_0 = h_{FE0} = I_C / I_B \quad (6)$$

at zero collector junction voltage and specified  $I_C$ . It should further be noted that in the measurement of  $\tau_c = Q_B / I_C$ , the charge injected to turn on a specified collector current is determined and this quantity is affected by temperature. Any charge in the base generated thermally is deducted from that which has to be injected to give rise to a predetermined  $I_C$ .

*Saturation Region*

When the transistor is driven into saturation, the collector current is circuit controlled so that an increase in base charge cannot lead to an increase in collector current. What happens is that a saturation charge accumulates in the base until its recombination rate exactly equals the rate at which extra current is supplied to the base. The saturation charge which accumulates in the base of a homogeneous base transistor is illustrated in Fig. 3.

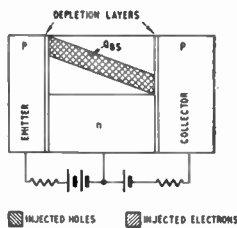


Fig. 3—Additional charge  $Q_{BS}$  which accumulates in the base after the transistor has been driven into saturation.

If the quantity of base charge in excess of that required to just bottom the transistor is  $Q_{BS}$  and if the base current required to maintain this saturation charge is  $I_{BS}$ , then

$$\text{total base charge} = I_C \tau_{CO} + Q_V + Q_{BS} \quad (7)$$

$$I_{B(\text{total})} = \frac{I_C}{\beta_0} + I_{BS} \quad (8)$$

and a saturation time constant  $\tau_S$  can be defined as

$$\tau_S = Q_{BS} / I_{BS} \quad (9)$$

at specified collector and base currents.

The turn-off process differs from turn-on because to turn on a transistor it is only necessary to take it from the OFF state to the edge of saturation, but to turn it off after it has been driven into saturation, it is necessary to remove  $Q_{BS}$  in addition to  $Q_{ON}$ . Thus (neglecting  $I_{CBO}$ )

$$Q_{OFF} = Q_{ON} + Q_{BS} \quad (10)$$

$$= Q_V + I_C \tau_{CO} + I_{BS} \tau_S \quad (11)$$

$$= Q_V + I_C \tau_{CO} + \tau_S \left( I_B - \frac{I_C}{\beta_0} \right) \quad (12)$$

The charge extraction necessary to turn the transistor off can evidently be calculated from the parameters defined above.

$\tau_S$  is the fourth and last independent parameter of importance. However, it is sometimes convenient to express this time constant as a multiple of  $\tau_c$ .

It often happens in transistorized equipment that a transistor is turned on with very small collector current, but that subsequently, a much larger current is suddenly required from it without additional input to the base. This, for example, can happen if gates are connected to the collector of the transistor which are opened by other parts of the circuitry and thus require additional current from the transistor.

If the base current supplied is  $I_C / \beta_0$  (where here  $I_C$  is the maximum current that will be required from the transistor), this will be sufficient to hold the transistor ON when in equilibrium, but will in general be insufficient to provide the required transient current. This can be understood as follows.

When a transistor is ON and just bottomed with  $I_C$  flowing, the active base charge is  $I_C \tau_{CO}$ .

If now the collector current is reduced to zero without altering the base current, then all the base charge becomes saturation base charge  $Q_{BS}$  and  $Q_{BS} = I_{BS} \tau_S$ .

The condition that the maximum collector current is immediately available again when required is simply that sufficient base charge should be present in the base region, and this is satisfied only if  $Q_{BS} \geq Q_B$ .

Thus

$$I_{BS} \tau_S \geq I_C \tau_{CO}$$

or

$$I_B \geq I_C \beta_S \quad (13)$$

where

$\beta_s$  is called "on demand" current gain and is defined as<sup>2</sup>  

$$\beta_s = \frac{\text{collector current instantly available on closing the circuit}}{\text{the steady base current}}$$

while the transistor remains bottomed, and as shown above is theoretically given by  $\beta_s = \tau_s / \tau_{CO}$ . (Experimental data are shown later indicating that this theoretical equation is not always well obeyed in practice.) If  $\beta_s$  is less than  $\beta_0$ , it is, of course, necessary to provide a larger base current to obtain a specified collector current than would be required for equilibrium conditions only.

$\beta_s$  is the fifth parameter of importance, but is not an entirely independent one.

In practice, all types of transistor possess extrinsic resistances in at least one of their electrodes. The base resistance is always present and sets an upper limit to the rate at which charge can be injected into or extracted from the base region, and thus slows down the rise and fall times of the output current. In general, however, except at high current levels, and particularly if allowance is made for it, this does not significantly modify the remarks made in this paper.

The series collector resistance exhibited by certain Mesa structures and grown junction types may cause "premature saturation" [10] since the collector junction voltage may fall to zero while collector base voltage is still significant. Again, however, if allowance is made for it, this consideration does not modify the discussions which follow.

For transient switching purposes, therefore, there-fore, five parameters may be regarded as of importance, namely  $\beta_0$ ,  $\tau_{CO}$ ,  $\tau_s$ ,  $\beta_s$  and  $Q_V$ . These parameters will now be considered in more detail.

DETAILED DISCUSSION OF THE PARAMETERS

Current Gain,  $\beta_0$

The subscript zero specifies that this parameter is restricted to the conditions of zero collector junction voltage. For any other junction voltage, the subscript is omitted. The variation of  $\beta$  at any specific reverse voltage on the collector with current level has been studied by a number of authors [15]-[17] and will not be considered further here, except to note that its value normally passes through a maximum at some intermediate value of collector current.

Collector Depletion Layer Charge  $Q_V$

The small signal collector depletion layer capacitance  $C_{tc}$  of a transistor varies, as is well known, with the magnitude of the applied bias voltage. The charge re-

<sup>2</sup> A very brief transient of collector current in excess of  $\beta_s I_B$  usually appears before the current  $\beta_s I_B$  is observed. It lasts for approximately the base transit time and results from the high carrier density adjacent to the collector just before turn-on. This transient is neglected in the definition of  $\beta_s$ .

quired to change the potential across the junction is not therefore a linear function of voltage. If  $V_{CB1}$  is the OFF collector base voltage and  $V_{CB2}$  is the ON voltage, then

$$Q_V = \int_{V_{CB1}}^{V_{CB2}} C_{tc} \cdot dV_{CB} \tag{14}$$

For abrupt junctions,  $C_{tc} = \text{const} (-\phi - V_{CB})^{-1/2}$ , where  $\phi$  is the contact potential between the collector and base regions and the sign convention is that reverse bias is negative, whence

$$Q_V = 2C_{tel} [-\phi - V_{CB1} - \sqrt{(\phi + V_{CB1})(\phi + V_{CB2})}] \tag{15}$$

where  $C_{tel}$  is the small signal collector depletion layer capacitance at the OFF voltage. It is convenient to write (15) as

$$Q_V = M \cdot C_{tel} \cdot \Delta V_{CB} \tag{3}$$

where

$$\Delta V_{CB} = |V_{CB1} - V_{CB2}|$$

and

$$M = \frac{2[-\phi - V_{CB1} - \sqrt{(\phi + V_{CB1})(\phi + V_{CB2})}]}{V_{CB1} - V_{CB2}} \tag{16}$$

If  $|V_{CB1} - V_{CB2}| \ll |V_{CB1}|$ , small signal conditions apply and, of course,  $M = 1$ . If, however,  $V_{CB2}$  is zero, as is common in switching circuits,  $M$  varies with  $V_{CB1}$  as shown in Fig. 4, assuming a value of  $-0.4$  volts for  $\phi$ . This figure also shows  $Q_V$  for various values of  $V_{CB1}$  when  $C_{tc}$  at  $V_{CB} = -6$  volts equals 10 pf and when  $V_{CB2} = 0$ . With graded junctions,  $C_{tc}$  varies inversely as the cube of the voltage so that  $M$  varies between the limits of 1 and 1.5.

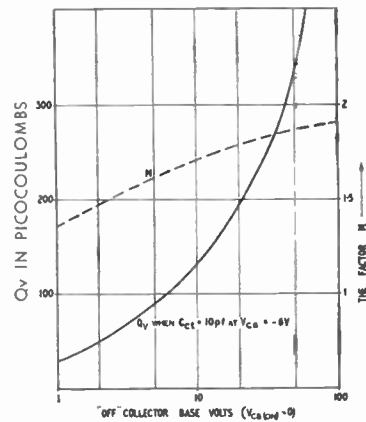


Fig. 4—The variation of  $Q_V$  and the factor  $M$  with the value of the OFF collector-base voltage, when the ON voltage is zero.

The calculation to determine  $Q_{VE}$ , the charge on the emitter junction, is, of course similar to the above.

Since both  $Q_{VE}$  and  $Q_V$  are charges on the depletion layer capacitance, they are both independent of the current switched, except in so far as this current is related to the change of junction voltage, as for example under forward bias conditions of the emitter.

Collector Time Constant  $\tau_c$

The collector time constant  $\tau_c$  as defined earlier is the base charge per unit collector current, when the collector junction voltage is held constant. ( $\tau_{c0}$  refers to the special case of zero junction voltage.) Part of this base charge is  $Q_{VE}$ , the charge on the emitter depletion layer capacitance, and since  $Q_{VE}$  is not directly proportional to  $I_c$ , it follows that  $\tau_c$  is not quite independent of  $I_c$ .<sup>3</sup> In transistors with homogeneous base, the effect of conductivity modulation of the base region at high injection levels leads to a further decrease of  $\tau_c$  with increasing collector current. For the purpose of analyzing this effect and the influence of  $Q_{VE}$  upon  $\tau_c$ , it is convenient to define an intrinsic time constant  $\tau_e$  equal to  $Q_B - Q_{VE} / I_c$ , which expresses the ratio of base charge to collector current involved in the diffusion process only. Meyer [18] has shown that this charge for a homogeneous base transistor with current gain equal to one is given by

$$Q_B - Q_{VE} = qANW \left[ \frac{y_0(1 + y_0)}{z} - 1 \right] \quad (17)$$

where

$$z = 2y_0 - \ln(1 + y_0) \quad (18)$$

and where  $q$  is the electronic charge,  $A$  is the emitter junction area,  $N$  the density of donors in the base region,  $W$  the base width and  $y_0 = p_1 / N$  where  $p_1$  is the density of holes at the emitter end of the base region. This charge is not significantly changed if the current gain is less than one.

Meyer also shows that

$$z = \frac{I_E W}{AqDN} \quad (19)$$

so that

$$\tau_e = \frac{Q_B - Q_{VE}}{I_E} = \frac{W^2}{D} \left[ \frac{y_0(1 + y_0)}{z^2} + \frac{1}{z} \right] \quad (20)$$

Curve *A* of Fig. 5 shows  $\tau_e$  normalized to  $W^2/2D$  plotted against  $z$  and it can be seen that theoretically

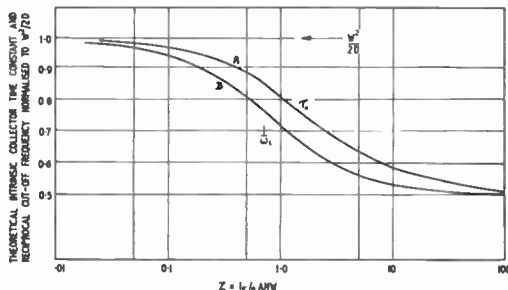


Fig. 5—Normalized intrinsic collector time constant,  $\tau_e$ , and  $1/\omega_c$  vs  $Z$  (theoretical).

<sup>3</sup> If  $Q_{VE}$  were regarded as a separate parameter, as suggested, for example, by Grinich and Noyce [10], this would result in a more constant value of  $\tau_c$ , but would render  $\tau_c$  extremely difficult to measure. For this reason,  $Q_B$  has been defined as including  $Q_{VE}$ .

$\tau_c$  decreases by a factor of 2 as the current increases from low to high values.

The parameter which is measured, and was defined earlier, is  $\tau_c$ , and evidently

$$\frac{\tau_c}{\tau_e} = \frac{Q_B}{Q_B - Q_{VE}} \quad (21)$$

The variation of this ratio with emitter current can be evaluated using the following relationships. Eq. (15) can be written for the emitter junction thus

$$Q_{VE} = 2C_{te1} [-\phi - V_{EB1} - \sqrt{(\phi + V_{EB1})(\phi + V_{EB2})}] \quad (22)$$

where  $C_{te1}$  is the emitter junction capacitance at the OFF emitter base voltage  $V_{EB1}$ , and  $V_{EB2}$  is the emitter base voltage in the ON state.

In the OFF state with  $I_E$  zero,  $V_{EB1} = 0$ . The ON value of emitter base voltage can be determined from the low-level expression

$$I_E = \text{const.} (\exp(qV_{EB2}/kT) - 1) \quad (23)$$

since in practice  $Q_{VE}$  is only a significant fraction of  $Q_B$  at low current levels. Thus, assuming also that  $\tau_e$  is constant at low levels, the ratio of  $\tau_c/\tau_e$  can be evaluated at any specific value of  $I_E$ . For example if  $\tau_e = 0.05 \mu\text{sec}$ ,  $C_{te} = 10 \text{ pF}$  at  $-3 \text{ V}$ ,  $\phi = -0.4 \text{ volts}$  and  $I_E = 1 \text{ mA}$  when  $V_{EB} = 0.15 \text{ volts}$ , the variation of  $\tau_c/\tau_e$  as derived from (21)–(23) is as shown in Fig. 6, curve *A*.

To a first approximation, curves *A* of Fig. 5 and 6 can be superimposed once the relationship between  $I_E$  and  $z$  has been established. For the case in which  $I_E = 2z \text{ ma}$  corresponding to a donor density of  $1.5 \times 10^{15}$  per cc in the base for the above value of  $C_{te}$ , curve *A* of Fig. 7 results.

Qualitative experimental confirmation of the above theory has been obtained and is illustrated for a typical alloy transistor in curve *A* of Fig. 8. Precise quantitative agreement requires an evaluation of  $z/I_E$  and this has not been attempted.

It may be concluded, therefore, that  $\tau_c$  should be specified at a particular value of ON and OFF current, and in particular it may be noted that the method of determining  $\tau_{c0}$  which involves measuring  $Q_{ON}$  at two values of ON current [7] will always lead to a value of  $\tau_{c0}$  which is too low.

The method here referred to is based upon [see (4)]

$$Q_{ON1} = I_{c1}\tau_{c01} + Q_{V1}$$

$$Q_{ON2} = I_{c2}\tau_{c02} + Q_{V2}$$

If the collector voltage swing during turn-on is the same in both cases, then  $Q_{V1} = Q_{V2}$ . If  $I_{c2} = 2I_{c1}$  and it is assumed that  $\tau_{c01} = \tau_{c02} = \tau_{c0}$ , then

$$\tau_{c0} = (Q_{ON2} - Q_{ON1}) / I_{c1} \quad (24)$$

However since  $\tau_{c02} < \tau_{c05c01}$ , the value of  $\tau_{c0}$  obtained from (24) is less than either  $\tau_{c01}$  or  $\tau_{c02}$ . For example, if  $\tau_{c01} = 0.054 \mu\text{sec}$  at 5 ma and  $\tau_{c02} = 0.051$  at 10 ma, as is the case for the transistor whose values are shown in Fig. 8, then the value of  $\tau_{c0}$  obtained is  $0.048 \mu\text{sec}$ .

It has been pointed out previously [7] that a measurement of  $f_T$  (or  $\omega_T = 2\pi f_T$ ) can be used to determine  $\tau_c$  since  $\tau_c \approx 1/\omega_T$  ( $f_T$  is the frequency at which  $|h_{fe}| = 1$ ). The following analysis, however, indicates that this method of determination will almost always be somewhat in error. Defining  $\omega_l$  as the angular frequency at which the modulus of the common emitter internal short-circuit current gain is equal to one, so that the effects of emitter depletion layer capacitance are not involved, the following expression applies

$$\frac{\omega_l}{\omega_T} = \frac{C_{b'e}}{C_{b'e} - C_{te}} \tag{25}$$

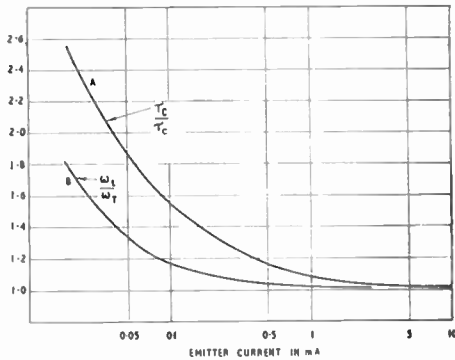


Fig. 6— $\tau_c/\tau_c$  and  $\omega_l/\omega_T$  vs  $I_E$  (theoretical) for  $\tau_c = 0.05 \mu\text{sec}$  and  $C_{te} = 10 \text{pF}$  at  $V_{EB} = -3$  volts.

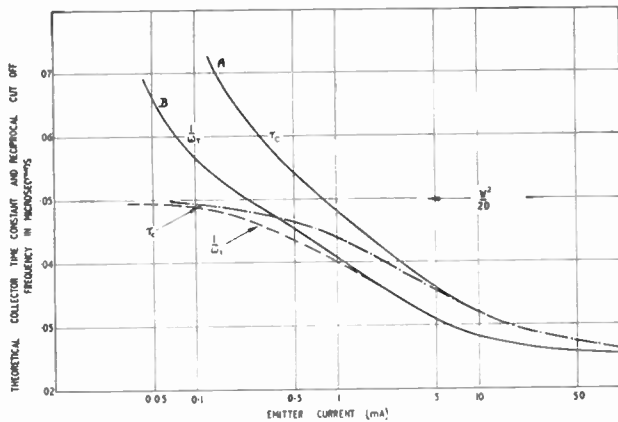


Fig. 7—Collector time constant  $\tau_c$ , and  $1/\omega_T$  vs  $I_E$  assuming  $Z = |I_E|/2$ .

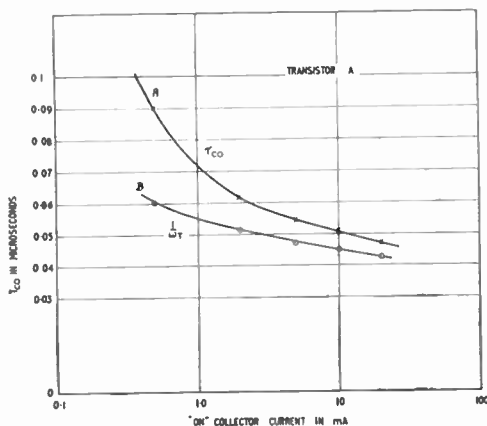


Fig. 8—Experimental variation of  $\tau_{c0}$  and  $1/\omega_T$  with collector current (normal transistor showing no wiggle effect).  $\omega_T$  measured with  $V_{CE} = -1$  volt.

where  $C_{b'e}$  is the emitter-base capacitance in the hybrid  $\pi$  equivalent circuit [19], at a particular value of emitter current, and  $C_{te}$  is the depletion layer capacitance at that current. At low currents

$$C_{b'e} - C_{te} = qI_E/kT\omega_l. \tag{26}$$

Misawa [16] has shown that

$$\omega_l = \frac{2D}{H^2} \left[ \frac{z}{2(1+y_0)(1-y_0/z)} \right] \tag{27}$$

where the parameters are as stated under (18).

From (23) and (25)–(27), the variation of  $1/\omega_l$  as a function of  $z$ , the variation of  $\omega_l/\omega_T$  as a function of  $I_E$  and the variation of  $\omega_T$  with assuming  $I_E = 2z$  can be plotted as shown in curves B of Figs. 5–7. Again qualitative experimental confirmation is shown in curve B of Fig. 8. It can be seen that the variation of  $\omega_T$  is less than that of  $\tau_c$ , and that the value of  $1/\omega_T$  is always less than  $\tau_c$  except at high current levels.<sup>4</sup> For example, for the transistor whose values are shown in Fig. 8 the value of  $\tau_{c0}$  is 0.054 at 5 ma, whereas  $1/\omega_T$  is 0.047. It should be pointed out, however, that  $\omega_T$  was measured at  $V_{CB} = -1$  volt since a small signal measurement at  $V_{CB} = 0$  is impracticable, a fact which leads in practice to a further reduction in  $1/\omega_T$  as compared with  $\tau_{c0}$ .

The above analyses apply strictly only to transistors whose dc current amplification factor is equal to one in common base. In practical transistors, a further phenomenon *sometimes* appears which overrides much of the foregoing calculations.

The phenomenon is characterized by a departure from the 6 db per octave fall of  $|h_{fe}|$  at high frequencies and by the appearance of a distorted wave during  $Q_{ON}$  or  $Q_{OFF}$  measurements.

The circuit of Fig. 9 is a basic circuit for the measurement of  $Q_{ON}$  or  $Q_{OFF}$ , and when  $R_B$  is set so that  $I_B = I_c\beta_0$ , and  $C_B$  is set so that  $V_a C_B = I_c\tau_{c0} + Q_V$ , a square-wave output is obtained with normal junction transistors. However, when a transistor is exhibiting this additional phenomenon, the output waveform is as shown in Fig. 10. A “wiggle” appears in the waveform so that a good square-wave is not observed. For simplicity, the effect is called the Wiggle Effect. The author has noted this effect previously [7] and has also offered an explanation of it [20]. It apparently arises from some technological defect in manufacture and will probably cease to appear as techniques advance. The importance of the effect in this context is that when waveforms similar to those shown in Fig. 10 are observed it is necessary to adjust  $C_B$  for a rapid fall of collector current and for *no subsequent rise* above the equilibrium off value [that is, the waveform of Fig. 10 (c) rather than that of Fig. 10 (b) should be observed when  $C_B$  is set].

<sup>4</sup> In practice it has been found that  $f_{\alpha} \approx 1.22 f_T$  passes through a maximum and decreases again at the highest current densities [18], and a theoretical explanation for this has been put forward by Matz [28]. Measurements by several workers (unpublished) indicate that  $1/\tau_c$  also goes through a maximum as  $I_E$  is increased.

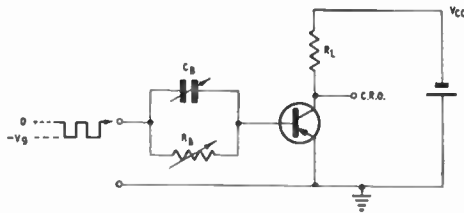


Fig. 9—A basic circuit for the measurement of transient switching parameters.

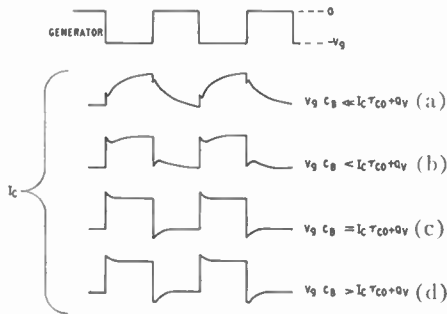


Fig. 10—Output waveforms obtained using the circuit of Fig. 9 (when  $R_B = \beta_0 R_L$  and  $C_B$  takes different values) for an abnormal transistor showing the "wiggle" effect.

The transistor must be turned off and held off, and this requires considerably more charge than is required simply to turn the transistor off. In other words, the measured value of  $\tau_c$  is being affected by charges not immediately under the control of the external circuitry, and these charges are not considered in the above theoretical analysis of  $\tau_c$ .

In transistors with graded base regions, the behavior is more complicated. In the first place,  $Q_{VE}$  is a much larger proportion of  $Q_B$ , so that  $\tau_c$  shows a significant decrease with current up to higher current densities [21]. Second, there is the possibility that the effect of the drift field may be swamped by the injection into the base region of minority carriers at higher current levels leading to an increase of  $\tau_c$ . Third, since carriers move by diffusion over the final portion of their transit across the base, conductivity modulation of this part of the base region will probably to some extent counteract the effects of swamping the drift field. Finally, in some diffused base structures the collector depletion layer moves away from the graded portion of the base at low values of collector-base voltage, causing a marked increase in base width and of transit time and leading to values of  $\tau_{CO}$  several times larger than  $\tau_c$  at  $V_{CB}$  of a few volts.

*The Saturation Time Constant*

On the basis of a one-dimensional analysis of a transistor in the saturation region, it can be shown [5] that

$$\tau_s = \frac{\omega_{T0} + \omega_{T10}}{\omega_{T0} \cdot \omega_{T10} (1 - \alpha_0 \alpha_{10})} \tag{28}$$

where the subscript  $I$  indicates inverse connection and the subscript zero indicates zero output junction voltage. Fairly satisfactory correlation between this expres-

sion and the measured quantities can be found at intermediate current levels for transistors of homogeneous base which do not exhibit the wiggle effect. A solution of the one-dimensional diffusion equations for such transistors, however, leads to the conclusion that  $\omega_{T0} = \omega_{T10}$  since both are approximately equal to  $2D/W^2$ , but in practice,  $\omega_{T0}$  is almost invariably several times greater than  $\omega_{T10}$  (except in symmetrical transistors), indicating that the one-dimensional theory is inadequate in the saturation region. Indeed, this can be readily understood since a significant proportion of saturation charge diffuses away from the region of the base which lies between emitter and collector, thus invalidating one-dimensional theory.

Qualitatively, it is to be expected that the variation of  $\tau_s$  with current level is fairly complicated. There are three principal factors affecting it. First, at low current levels it is to be expected that the change of collector depletion layer thickness as a transistor is taken from the just bottomed state into saturation should necessitate the injection of extra base charge leading to higher values of  $\tau_s$ . Second, the increase of current gain which occurs as the current level increases will tend to lead to values of  $\tau_s$  which rise with increasing current [see (28)], and third, the increase in  $\omega_I$  and  $\omega_{II}$  as a result of high injection levels will cause a decrease in  $\tau_s$ .

Typical experimental curves of the variation of  $\tau_s$  with  $I_{BS}$  at constant collector current for a transistor with homogeneous base are shown in Fig. 11. The tendency of  $\tau_s$  to fall initially, then rise and finally fall again is to be seen in these curves.

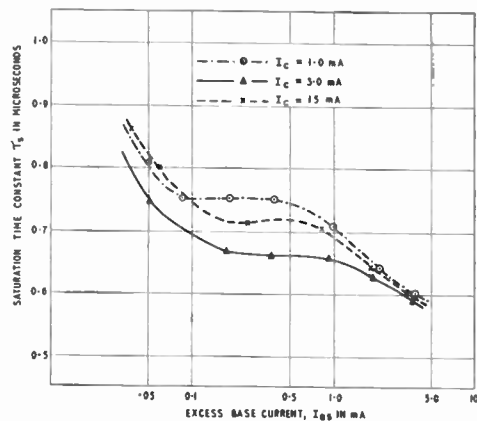


Fig. 11—The variation of the saturation time constant,  $\tau_s$ , with excess base current  $I_{BS}$  (collector current as parameter).

The wiggle effect, when it occurs (and here, too, it is not always present), tends to be more pronounced than in the active region, a fact which can again be qualitatively understood since more charges are being stored in the base remote from the junctions.

Diffused structures which possess comparatively large collector regions with high resistivity and lifetimes often exhibit minority carrier storage in this region when the transistor is driven into saturation. This has the

effect of producing very large measured values of  $\tau_s$ . The phenomenon arises because in saturation, the collector junction is forward biased and minority carriers are emitted into the collector region from the base. By making the resistivity of the collector region lower, the proportion of the collector forward current consisting of emission into the collector can be reduced; in alloyed structures, for example, the collector is so heavily doped that the collector forward current consists almost entirely of emission into the base. Alternatively the collector region can be filled with traps (e.g., by gold doping in silicon) so that the carrier lifetime in the collector region is small and the minority carrier storage there is so short-lived as to be unimportant. In one of these ways, the measured value of  $\tau_s$  can be kept less than  $\beta_0\tau_{co}$ , but in the absence of these techniques,  $\tau_s$  may well exceed  $1000\tau_{co}$ .

These high values of  $\tau_s$  are *measured* values in the sense that they represent the charge which has to be removed from the base *terminal* in order to turn off the collector current abruptly. In fact, of course, they do not represent the stored *base* charge  $Q_{BS}$  per unit excess base current  $I_{BS}$  since the charge in question is in the collector region. The fact that in many instances the collector current can be induced to fall off abruptly as a result of base drive probably results from the reverse biased collector junction clearing the collector region of minority carriers, but it sometimes happens that this does not occur, and no matter how hard the base is driven off the fall time of the transistor remains significant. Such transistors cannot any longer be regarded in their saturation region of operation as charge controlled devices. (See final section for further discussion.)

#### The "On Demand" Current Gain $\beta_s$

It was stated in an earlier section that  $\beta_s$  is the collector current immediately available on closing the collector circuit per unit steady base current. On the basis of a simple one-dimensional analysis which is applicable to all transistor types,  $\beta_s$  was also shown to be equal to  $\tau_s/\tau_{co}$ . These two expressions for  $\beta_s$  are not identical and it is of interest to determine whether or not direct measurements of  $\beta_s$ ,  $\tau_s$  and  $\tau_{co}$  confirm the relation  $\beta_s = \tau_s/\tau_{co}$ . In Table I are shown some typical results for alloy RF transistors. The correlation between  $\beta_s$  and  $\tau_s/\tau_{co}$  is good for transistors A, B and C, but is poor for the remaining types. The reason for the unsatisfactory correlation is not known. Those transistors which show good correlation do not exhibit the wiggle effect, but some of those that show poor correlation do not exhibit the effect either.

Transistors which exhibit the carrier storage in the collector region described in the previous section seldom, if ever, suffer from low values of  $\beta_s$ . As pointed out earlier, the difficulty with these transistors is not that collector current is unavailable when it is wanted, but rather that it cannot be turned off when it is *not* wanted. Preliminary experimental evidence seems to indicate,

moreover, that even diffused structures which do *not* exhibit carrier storage in the collector do not suffer from low values of  $\beta_s$  either, that is to say the current immediately available on closing the collector circuit is always at least as great as  $\beta_0 I_B$ , or in other words  $\beta_s > \beta_0$ . The reason for this has not yet been investigated.

TABLE I

Transistor Types	$\tau_s/\tau_{co}$	$\beta_s$	$\beta_0$
A	23.5	21.5	80
B	42.5	43	82
C	26.5	26.5	102
D	65	49	70
E	73	43	110
F	19.5	15.5	42
G	56	50.5	65

#### MEASUREMENT TECHNIQUES

A number of measurement techniques for determining the values of the switching parameters have been outlined by the author [7]. A comparative study of various methods of measurement of  $\tau_s$  has been carried out by Nanavati [22] in which reference is made to the techniques used by Simmons [23] and by RCA [24]. An additional method for the measurement of  $\tau_s$  has been proposed by Hilbourne [25]. The method proposed makes use of equipment normally used for measuring the charge stored in a diode. His technique involves connecting emitter and collector together to one terminal of the diode test circuit and the base lead to the other terminal. During the forward conduction period, charge is stored in the base region according to the magnitude of the base current, and on application of the reverse voltage, the charge is removed and measured directly on an integrating meter. Evidently,  $\tau_s$  in microseconds is simply the picocoulombs removed per microampere of forward current. This method must, of course, be used with care with diffused base transistors owing to the limited reverse emitter voltage they can withstand.

The degree of correlation obtained using the various techniques depends on the inherent accuracy of the equipment and to some extent upon the transistors used. Any techniques which involve an oscilloscopic display introduces some indeterminacy with transistors exhibiting the wiggle effect but those methods which do not display this abnormal waveform conceal it, so that they may be in error while being quite repeatable. In addition, however, not all the techniques measure the transistor under precisely the same conditions. For example, the methods of Simmons and Hilbourne for measuring  $\tau_s$  measure the transistor with zero collector current prior to turn-off, whereas Nanavati's methods and those of the author have finite collector currents, so that the base contains some active region charge  $Q_B$  in addition to the saturation charge  $Q_{BS}$ , although only  $Q_{BS}$  is being measured. (The RCA technique does not measure  $\tau_s$ ; it measures  $(Q_B + Q_{BS})/I_B$  and requires ad-

ditional information for the evaluation of  $\tau_S$ ). Again, Hilbourne's method imposes the condition of  $V_{CE}=0$  which means that the forward bias of the collector is abnormally large. This may lead to somewhat low values of  $\tau_S$  compared with other methods.

For transistor performance characterization, the kind of conditions encountered in practical circuit design have a bearing on the choice of measurement method. For example, the value of  $\tau_{CO}$  normally required is that related to the charge necessary to turn off a particular value of  $I_C$  and not to the charge needed to change the value of  $I_C$ , whereas the value of  $\tau_S$  usually needed is the ratio of  $Q_{BS}/I_{BS}$  when  $I_C$  has a value greater than zero. All these considerations make the choice of preferred test method somewhat difficult at this stage. However, it remains true that the charge control parameters vary only slowly with operating conditions and all of the methods of measurement, including those involving small signal techniques should not be much in error, and are likely to lead to more useful results than the normal rise time, fall time and storage time measurements, whose values are highly dependent on operating conditions and can only be adapted to other conditions with difficulty.

Concerning the measurement of  $\beta_S$ , the only available technique at present appears to be that described by the author [7].<sup>6</sup>

#### DISCUSSION AND CONCLUSION

Investigations of the behavior of charge in active devices is useful in two aspects of the study of the performance of semiconductor devices. First, there is the concept of charge control of activity considered in this paper, and second, there is the charge analysis of device characteristics as considered for example by Moll [26] or by Baker, *et al.* [27]. The difference between these two treatments is that *charge control* is only a valid concept if the charges which are significant in describing the activity of the device are accessible to some control terminal of the device, whereas *charge analysis* considers the behavior of charges within the device whether or not they are under the direct control of some terminal of the device.

This distinction is important since, strictly speaking, it excludes from the class of charge controlled devices *p-n-p-n* devices, transistors which exhibit minority carrier storage in the collector, and even those devices which exhibit the wiggle effect, since each of these devices in operation carry charges which are not immediately accessible to the control terminals. It follows, therefore, that to characterize these devices for transient performance, parameters additional to the charge control parameters may have to be required. In prac-

tice however, it may be that the charge control parameters are the most suitable even for those devices which are not strictly charge controlled. For example they can still be used for transistors which exhibit the wiggle effect, but in such cases  $Q_{OFF}$  becomes the charge necessary to turn off the device *and hold it off*, although in an ideal charge controlled device, removal of the control charge to turn off the output current necessarily entails the subsequent condition that the output current remains off until another control input is applied.

In conclusion, therefore, it may be said that the concept of charge control cannot necessarily be applied to all kinds of transistors, although for most it offers a convenient and useful method of performance characterization.

#### ACKNOWLEDGMENT

The author would like to thank C. S. den Brinker and R. Beaufoy for much helpful comment and the Director of Research of British Telecommunications Research for permission to publish this paper.

#### REFERENCES

- [1] E. O. Johnson and A. Rose, "Simple general analysis of amplifier devices with emitter, control and collector functions," *Proc. IRE*, vol. 47, pp. 407-418; March, 1959.
- [2] R. D. Middlebrook, "A modern approach to semiconductor and vacuum device theory," *Proc. IEE*, pt. B, vol. 106, suppl. 17, pp. 887-902; May, 1959. (Internatl. Convention on Transistors and Associated Semiconductor Devices, London, Eng.)
- [3] N. F. Moody, "Controlled saturation in transistors and its application in trigger circuits, part 1," *Electronic Engrg.*, vol. 30, pp. 121-127; March, 1958.
- [4] C. Le Can, "Fundamental Switching Properties of Junction Diodes and Transistors," Philips Technical Library, Eindhoven, The Netherlands; 1959.
- [5] R. Beaufoy and J. J. Sparkes, "The junction transistor as a charge controlled device," *ATE J.*, vol. 13, pp. 310-327; October, 1957.
- [6] J. J. Sparkes and R. Beaufoy, "The junction transistor as a charge controlled device," (Correspondence), *Proc. IRE*, vol. 45, pp. 1740-1742; December, 1957.
- [7] J. J. Sparkes, "The measurement of transistor transient switching parameters," *Proc. IEE*, pt. B, vol. 106, suppl. 15, pp. 562-567; May, 1959. (Internatl. Convention on Transistors and Associated Semiconductor Devices, London, Eng.)
- [8] R. Beaufoy, "Transistor switching circuit design in terms of charge parameters," *Proc. IEE*, pt. B, vol. 106, suppl. 17, pp. 1085-1091; May, 1959. (Internatl. Convention on Transistors and Associated Semiconductor Devices, London, Eng.)
- [9] J. M. Early, "Stored charge analysis of transistors," 1959 WESCON CONVENTION RECORD, pt. 2, p. 127. (Abstract.)
- [10] V. H. Grinich and R. N. Noyce, "Switching time calculations for diffused base transistors," 1958 WESCON CONVENTION RECORD, pt. 3, pp. 141-147.
- [11] A. Kruihof, "Transient response of junction transistors and its graphical representation," *Proc. IEE*, pt. B, vol. 106, suppl. 17, p. 1092; May, 1959. (Internatl. Convention on Transistors and Associated Semiconductor Devices, London, Eng.)
- [12] P. A. Neeteson, "Junction Transistors in Pulse Circuits," Philips Technical Library, Eindhoven, The Netherlands, pp. 94-122; 1959.
- [13] Private communication from J. R. W. Smith and J. L. Smith of British Telecommunications Research Ltd., Taplow. That the time is of the order of  $\frac{1}{2}\tau_c$  can be deduced from the rise time following a current impulse to the base evaluated, for example, by Kruihof [11] for drift transistors or by Steele [14] for diffusion transistors.
- [14] E. L. Steele and B. R. Gossick, "On the response time of junction transistors," *Proc. Symp. on the Role of Solid-State Phenomena in Electric Circuits*, Polytechnic Inst. of Brooklyn, Brooklyn, N. Y., pp. 163-173; 1957.
- [15] W. M. Webster, "On the variation of junction-transistor current-amplification factor with emitter current," *Proc. IRE*, vol. 42, pp. 914-920; June, 1954.

<sup>6</sup> An error appears in paragraph 5.3.2 of the author's previous work [7]. In measuring  $\beta_S$ , the value of  $R_B$  should be reduced until the off going transient at the collector does not take the transistor out of saturation. It is not necessary to decrease  $R_B$  until the transient disappears.

- [16] T. Misawa, "A note on the extended theory of junction transistors," *J. Phys. Soc. Japan*, vol. 11, pp. 728-739; July, 1956.
- [17] R. L. Pritchard, "Advances in the understanding of the  $p-n$  junction triode," *Proc. IRE*, vol. 46, pp. 1130-1141; June, 1958. This paper contains a survey of publications in the field.
- [18] N. I. Meyer, "On the variation of transistor small-signal parameters with emitter current and collector voltage," *J. Electronics and Control*, vol. 4, pp. 305-334; April, 1958.
- [19] L. J. Giacoletto, "Study of  $p-n-p$  alloy junction transistors from D.C. through medium frequencies," *RCA Rev.*, vol. 15, pp. 506-562; December, 1954.
- [20] J. J. Sparkes, "The effect of carrier storage in the emitter on transistor input admittance," *Proc. IEE*, pt. B, vol. 106, suppl. 17, pp. 1102-1107; May, 1959. (Internatl. Convention on Transistors and Associated Semiconductor Devices, London, Eng.)
- [21] F. J. Hyde, "An investigation of the current gain of a drift transistor at frequencies up to 105 Mc/s," *Proc. IEE*, pt. B, vol. 106, pp. 397-404; July, 1959.
- [22] R. P. Nanavati, "Prediction of storage time in junction transistors," *IRE TRANS. ON ELECTRON DEVICES*, vol. ED-7, pp. 9-15; January, 1960.
- [23] C. D. Simmons, "Hole storage delay time and its prediction," *Semiconductor Products*, pp. 14-18; May/June, 1958.
- [24] "Specification Sheet for 2N404 Junction Transistor," RCA Labs, Somerville, Mass.; 1958.
- [25] Private communication. R. A. Hilbourne is with the General Electric Co., Wembley, Eng.
- [26] J. L. Moll, "Avalanche transistors as fast pulse generators," *Proc. IEE*, pt. B, vol. 106, suppl. 17, pp. 1082-1084; May, 1959. (Internatl. Convention on Transistors and Associated Semiconductor Devices, London, Eng.)
- [27] A. N. Baker, J. M. Goldey, and I. M. Ross, "Recovery time of  $p-n-p$  diodes," 1959 WESCON CONVENTION RECORD, pt. 3, pp. 43-48.
- [28] A. W. Matz, "A modification of the theory of the variation of junction transistor current gain with operating point and frequency," *J. Electronics and Control*, vol. 7, pp. 133-152; August, 1959.

## Synthesis Techniques for Gain-Bandwidth Optimization in Passive Transducers\*

H. J. CARLIN†, FELLOW, IRE

The following paper appears in the PROCEEDINGS through the courtesy and upon the recommendation of the editors of the IRE Professional Group on Circuit Theory.—*The Editor*

**Summary**—This paper is concerned with an approximating technique for realizing the design of broad-band equalizers and matching networks which approach optimum gain bandwidth performance. Given an arbitrary load impedance, it is possible, by methods of Bode, Fano, LaRosa and Carlin, to derive the limiting constraints for optimum flat power or voltage transfer over a prescribed band. The synthesis of equalizer networks to approximate this optimum response is a difficult matter, particularly when the load has some degree of complexity. This is because methods proposed up till now prescribe an approximating transfer function which includes the load characteristics, and the problem of adjusting the parameters of such an approximating function is quite formidable. The technique proposed here bypasses this problem by producing from the idealized gain-bandwidth constraints a set of functions which specifies the equalizer alone. All load dependence is removed from the specifications as an initial step in the synthesis. The final transducer is then synthesized from the approximating functions which are obtained. Examples of one-port and two-port equalizer network designs utilizing this technique will be given.

\* Received by the IRE, May 2, 1960. The investigation reported herein was prepared for the Joint Services Technical Advisory Committee and made possible through the support of the AF Office of Scientific Res., the U. S. Army Signal Res. and Dev. Lab., and the ONR, under Contract AF-18(600)-1505, Expenditure Order No. 4-4750, Task No. 47501.

† Microwave Research Institute, Polytechnic Institute of Brooklyn, Brooklyn, N. Y.

### I. THE GAIN-BANDWIDTH SYNTHESIS PROBLEM

THE PROBLEM considered in this paper is that in which an arbitrary complex load (*i.e.*, one consisting of an assemblage of reactive and resistive elements rather than just a pure resistor) is fed from a prescribed source through an equalizer. The equalizer is to be designed so that the amplitude scale factor (or factors) of a prescribed shape of transfer characteristic (*i.e.*, voltage, current, power transfer) between source and load is maximized.

All such equalizer problems divide into two general parts. First, one must determine the parameters of an idealized transfer amplitude characteristic, and second, an equalizer must be synthesized so that the system approximates the idealized transfer characteristic shape.

The specification of the transfer characteristic of a system terminated in a complex load is rigidly constrained by the properties of the load. The amplitude characteristic of the entire system (including load) must be so prescribed that when a final network is synthesized, the given load may be separated out as the termination, and the remaining structure (the equalizer) is physically realizable.

Thus, if a transfer characteristic is required to be flat over a frequency band, the load constraints determine the maximum gain-bandwidth product which may be achieved. It should further be pointed out that except in very simple cases (e.g., a pure capacitance or inductance termination), the relation between achievable gain and bandwidth is not a simple linear one leading to a unique gain-bandwidth product constant. Rather, gain and bandwidth are generally related by a transcendental equation containing the constants of the load, and parameters describing the shape of the idealized transfer characteristic.

The usual approach to such problems [1]–[3] has been to determine first all the scale factors of the idealized transfer characteristic of the over-all system (including the load) by suitably taking into account the load constraints. This over-all idealized transfer characteristic is then approximated by a rational function which must have its parameters determined so as to simultaneously satisfy the following conditions.

- 1) The parameters of the rational function must be chosen so that all the constraints introduced by the load are satisfied.
- 2) The parameters of the rational approximating function must be chosen to maximize the scale factors of the transfer characteristic.
- 3) The shape of the rational function approximating the transfer characteristic must retain its prescribed form as the parameters are varied to satisfy 1) and 2).

Fano [2] has solved this problem in the case of power transfer from a finite source to a load through a reactive equalizer for a few simple loads, but points out that the solution is difficult to obtain if the load is moderately complex. It is the purpose of this paper to describe a relatively simple modification of the synthesis technique which utilizes straightforward computing methods and permits a solution for complicated loads.

In the technique described above, many of the difficulties ensue because of the problems entailed in handling the rational approximation to the over-all optimum system characteristic. However, in the method to be described here, the transfer characteristic is left as an idealized response and the load is extracted from this response, leaving a set of characteristics in *numerical form* which describes the equalizer *alone*. The rational approximation is now made for the equalizer network. This is a straightforward process, for no load constraints or optimization of parameters are involved (these have been taken care of previously in determining the idealized over-all system response).

The general approach proposed here for solving the equalizer problem is therefore broken down into the following steps.

- 1) Determine the parameters of an idealized over-all system transfer *amplitude* response characteristic

by optimizing a prescribed shape, taking into account the constraints imposed by the load. A simple idealized amplitude shape, for example one made up of straight lines, may be used to facilitate the evaluation of scale factors.

- 2) Use the phase-amplitude relations (see Bode<sup>1</sup> and Thomas [4]) to determine the phase associated with the optimum amplitude function.
- 3) Compute the characteristics of the equalizer from the numerically determined [in step 2)] complex transfer function; *i.e.*, phase and amplitude are known, by extracting the prescribed load characteristics.
- 4) Approximate the numerically determined data [in step 3)] for the equalizer by realizable rational functions. This approximation may, if desired, be carried out in a manner which permits realization of the equalizer in some special structural form, *e.g.*, as a ladder network without coupled coils.
- 5) Synthesize the equalizer as a network from the approximating rational function description.

The remainder of the paper will discuss some applications of this general technique to specific problems.

## II. THE DESIGN OF ONE-PORT EQUALIZERS

As an example of the application of the general method, a system will be considered which consists of an infinite current source feeding a load as in Fig. 1. It is

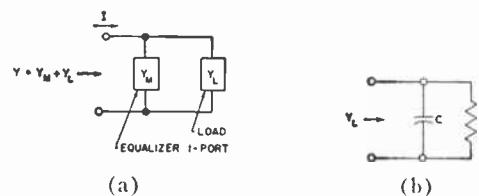


Fig. 1—(a) One-port equalizer. (b) Specific RC load.

desired to place a shunt two-terminal network (one-port) across the load so that maximum voltage transfer amplitude occurs at the load over a specified band of frequencies. The consideration of this type of system is motivated by certain types of wide-band transistor equalization problems. In this system, in addition to the usual load constraints, it is necessary to optimize the transfer characteristic so that the equalizer is realizable specifically as a physical one-port network. To the author's knowledge, the analysis of the particular configuration of Fig. 1 has not been published elsewhere.<sup>2</sup>

In order to apply the steps outlined at the end of Section I, it is first necessary to relate the transfer charac-

<sup>1</sup> Reference [1], pp. 301–302, 329.

<sup>2</sup> This problem has been treated in detail by W. Ku, "Design of Optimum Equalizers," M.E.E. thesis, Polytechnic Inst. of Brooklyn, Brooklyn, N. Y.; 1958. See also, W. Ku and H. J. Carlin, "Optimum Two-Terminal Interstage Design for High-Frequency Transistor Amplifier," Polytechnic Inst. of Brooklyn, MRI Rept. R-679-58; February 13, 1959.

teristic of the over-all system to the load, so that the constraints of the load may be properly introduced.

Since a constant current source is assumed, the gain of the system may be simply described as the total impedance amplitude  $|Z|$

$$\text{Gain} = \left| \frac{V}{I} \right| = |Z(j\omega)| = G(\omega^2). \quad (1)$$

Maximizing  $|Z(j\omega)|$  over a band of frequencies optimizes the voltage transfer to the load.

The load constraints and the fact that the equalizer must be a one-port are contained in the statement that, with  $Y_L(p)$  and  $Y_M(p)$ , respectively, the admittances of load and equalizer,

$$\frac{1}{Z(p)} = Y(p) = Y_L(p) + Y_M(p)$$

is a positive real function, e.g.,

- 1)  $Y(p)$  is a real, rational function of  $p$ ,
- 2)  $\text{Re } Y(j\omega) \geq 0$ ,
- 3)  $Y(p)$  is analytic in  $\text{Re } p > 0$ ,
- 4) poles of  $Y(p)$  along  $p = j\omega$  are simple with positive residues.

The admittance  $Y(p)$  is the function to be determined and must contain the prescribed load  $Y_L(p)$ . Hence, to satisfy proviso 2) above,

$$\text{Re } Y(j\omega) \geq \text{Re } Y_L(j\omega). \quad (2)$$

Thus

$$|Y(j\omega)| \cos \theta(\omega) \geq \text{Re } Y_L(j\omega) \quad (3a)$$

$$\frac{1}{G(\omega^2)} \cos \theta(\omega) \geq \text{Re } Y_L(j\omega). \quad (3b)$$

Eq. (3b) completely relates requirement 2) to the gain function of the system, for it must be noted that since  $Y(p)$  is a one-port, it is a minimum phase function [proviso (3)], hence  $\theta(\omega)$  is uniquely determined from  $|Y(j\omega)|$  by the Bode phase-amplitude relations.<sup>1</sup>

The residue requirement 4) provides additional load constraints for  $Y(p)$ , for, since  $Y(p)$  consists of  $Y_L$  and  $Y_M$  in parallel, it must contain all the real frequency ( $j\omega$ ) poles of the load admittance. These poles correspond to the zeros of the gain function  $G(\omega^2) = |Z(j\omega)|$ . For any pole at  $j\omega_k$  the residue must therefore satisfy

$$\text{Res } Y(p) \Big|_{p=j\omega_k} \geq \text{Res } Y_L(p) \Big|_{p=j\omega_k}. \quad (4)$$

This constraint equation may be related to the gain function by noting that the several Taylor series for  $Z(p)$  at the various  $\omega_k$  zeros of  $Z_L(p)$  must have first Taylor coefficients which are identical with those of  $Z_L(p)$ . Using integral relations for these Taylor coefficients [5]

$$\int_0^\infty f_k(\omega) R(\omega^2) d\omega = \int_0^\infty f_k(\omega) G(\omega^2) \cos \theta(\omega) d\omega \geq A_k \quad (5)$$

where  $f_k(\omega)$  are suitable weighting functions and the  $A_k$

are determined from the first Taylor coefficients of the load,  $Z_L(p)$ , obtained by expanding  $Z_L(p)$  at the zeros of gain  $\omega_k$ .

Eqs. (3) and (4), [or (5)], assure that the system will satisfy provisos 2) and 4) of the realizability requirements. It is readily apparent that if these are satisfied,  $Y(p)$  may then always be chosen so that all four restrictions are satisfied, and thus when the load is extracted in parallel from such a  $Y(p)$ , the remaining network is physically realizable as a physical passive one-port. As an example, an idealized optimum low-pass characteristic will be obtained for the specific  $RC$  load of Fig. 1(b). As a guide to determining a suitable shape for the gain characteristic in both pass and stop bands, consider first the limiting case in which  $R = \infty$  and the load is just a capacitor.<sup>3</sup> Then (5) becomes

$$\int_0^\infty R(\omega^2) d\omega = \int_0^\infty G(\omega^2) \cos \theta(\omega) d\omega = \frac{\pi}{2C} \quad (6)$$

and it is clear that for  $G$  to be as large as possible over a low-pass band of frequencies,  $\theta(\omega)$  should be  $\pm \pi/2$  outside the band so that the entire gain bandwidth area is concentrated in the pass band. This leads to an idealized optimum which is specified as:

$$G(\omega^2) = K \quad 0 \leq \omega \leq \omega_c \quad (7a)$$

$$\theta(\omega) = \frac{-\pi}{2} \quad \omega_c \leq \omega \leq \infty \quad (7b)$$

where  $\omega_c$  is the low-pass cutoff frequency, and  $K$  is a constant which must be maximized.

The details of this case will not be given here but are treated elsewhere.<sup>3</sup> Instead, we will be guided by (7a) and (7b) to choose a suitable gain characteristic. With the pure capacitor load, it was possible to hypothesize an idealized gain function whose phase was  $-\pi/2$  everywhere in the stop band. For the case of a load with a finite shunting  $R$  (a usual situation in transistor rather than tube equivalent circuits), we choose the phase in the stop band (the pass band is normalized to  $\omega_c = 1$ ) to deviate from the  $90^\circ$  characteristic as follows:

$$\theta(\omega) = \frac{m}{\omega} - \frac{\pi}{2} \quad 1 \leq \omega \leq \infty \quad (8a)$$

with flat gain in the pass band

$$G(\omega^2) = K \quad 0 \leq \omega \leq 1 \quad (8b)$$

and the parameter  $m$  must be chosen to permit the maximization of  $K$  consistent with (3) and (4).<sup>4</sup> The gain for  $1 \leq \omega \leq \infty$ , and the phase for  $0 \leq \omega \leq 1$  may be

<sup>3</sup> Reference [1], pp. 408-411.

<sup>4</sup> This choice of transfer characteristic is by no means unique. In the report referred to previously,<sup>2</sup> other choices were investigated and it was found that the one used here gave the highest scale factor of all those computed.

determined from the integral relations already referred to.<sup>1</sup>

$$\begin{aligned} & \frac{2\omega}{\pi} \int_0^1 \frac{\ln G(\lambda^2)}{(\lambda^2 - \omega^2)\sqrt{1 - \lambda^2}} \cdot d\lambda \\ & + \frac{2\omega}{\pi} \int_1^\infty \frac{\theta(\omega)}{(\lambda^2 - \omega^2)\sqrt{\lambda^2 - 1}} d\lambda \\ & = \begin{cases} \frac{\theta(\omega)}{\sqrt{1 - \omega^2}}, & 0 \leq \omega \leq 1 \\ -\frac{\ln G(\omega^2)}{\sqrt{\omega^2 - 1}}, & \infty \geq \omega \geq 1. \end{cases} \end{aligned} \quad (9)$$

The values of  $\theta(\omega)$  and  $\ln G(\omega^2)$  for the entire frequency band  $0 \leq \omega \leq \infty$  are then readily obtained:

$$\left. \begin{aligned} |Z(j\omega)| &= G(\omega^2) = K \\ \theta(\omega) &= -\frac{m}{\omega} [\sqrt{1 - \omega^2} - 1] - \sin^{-1}\omega \end{aligned} \right\} \omega \leq 1 \quad (10a)$$

$$|Z(j\omega)| = G(\omega^2) = K \left[ \frac{\epsilon^{m\sqrt{\omega^2 - 1}/\omega}}{\sqrt{\omega^2 - 1} + \omega} \right] \omega \geq 1 \quad (10b)$$

$$\theta(j\omega) = \frac{m}{\omega} - \frac{\pi}{2}.$$

These values are plotted in Figs. 2 and 3 for several values of  $m$ .

The residue restriction of (4) corresponding to the pole in  $Y_L(j\omega)$  at infinity is now determined from (10b)

$$\text{Res } Y(p) \Big|_{p \rightarrow \infty} = \lim_{\omega \rightarrow \infty} \frac{1}{\omega} |Y(j\omega)| = \frac{2}{K\epsilon^m}$$

and since the residue for the actual load  $Y_L(\omega)$  is  $C$ , we have by (4)

$$K \leq \frac{2\epsilon^{-m}}{C \cdot B} \quad (11)$$

where the bandwidth factor,  $B$ , instead of unity has been introduced.

The second restriction given by (3) is now applied by again utilizing (10a) and (10b). Thus

$$\begin{aligned} \text{Re } Y_L(j\omega) &= \frac{R\omega^2 C^2}{1 + \omega^2 C^2 R^2} \leq \text{Re } Y(j\omega) \\ &= \begin{cases} \frac{1}{K} \cos \left[ -\frac{m}{\omega} (\sqrt{1 - \omega^2} - 1) \right] - \sin^{-1}\omega, & 0 \leq \omega \leq 1 \\ \frac{1}{K} \left[ \frac{\sqrt{\omega^2 - 1} + \omega}{\epsilon^{m\sqrt{\omega^2 - 1}/\omega}} \right] \cos \left[ \frac{m}{\omega} - \frac{\pi}{2} \right], & \infty \geq \omega \geq 1. \end{cases} \end{aligned} \quad (12)$$

By a "cut and try" numerical procedure,  $m$  is determined to just satisfy requirements of (11), with the equal sign, and (12) and maximize  $K$ . A result is given below for typical transistor parameters:

$$\begin{aligned} C &= 6.5 \times 10^{-3} \mu\text{fd} \\ R &= 1000 \text{ ohms} \\ B &= 0.5 \times 10^6 \text{ rad/sec.} \end{aligned}$$

Then

$$\begin{aligned} m &= 0.42 \\ K &= 408 \\ K \cdot B &= \frac{1.314}{C} \quad (C \text{ numerically as above}). \end{aligned}$$

The value of  $K \cdot B$  may be compared to the result with no resistor present. This is

$$K \cdot B = \frac{2}{C} \quad (\text{for all } C; \text{ and } R = \infty).$$

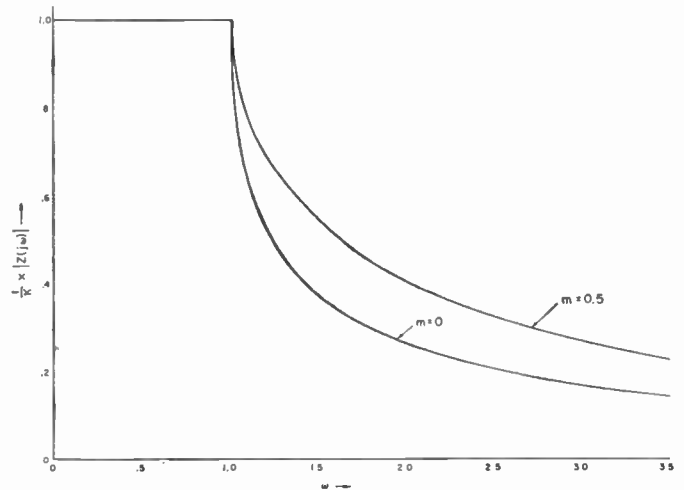


Fig. 2—Ideal one-port gain characteristics for phase parameter  $m=0, 0.5$ .

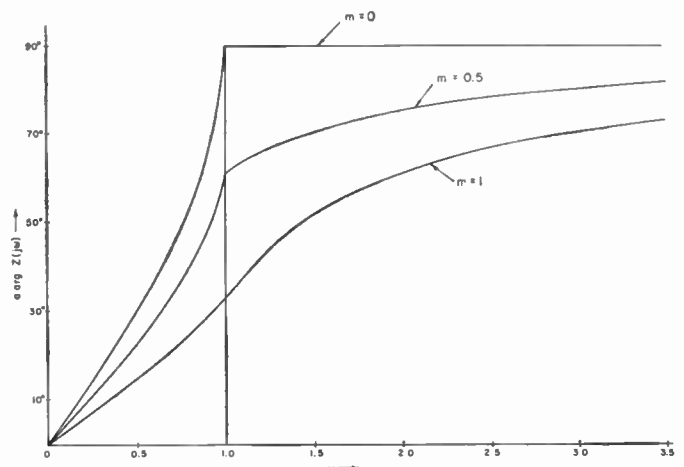


Fig. 3—Ideal one-port phase characteristics for phase parameter  $m=0, 0.5, 1.0$ .

The next step in the design technique is the extraction of the load from the idealized representation of  $Z(p)$ . The amplitude and phase of this function are given by (10a) and (10b), and the appropriate values of  $m$  and  $K$  may be inserted into these relations. The idealized description of  $Y_M(p)$  is then readily determined as

$$Y_M(p) = \frac{1}{Z(p)} - Y_L(p)$$

and one may then readily find  $|Y_M(j\omega)|$ . This is shown plotted on Fig. 4, and because of the manner in which this amplitude was determined, the fact that it corresponds to a physical, *i.e.*, positive real,  $Y_M(p)$  is assured.

The final step in the procedure is to find a  $PR$  rational approximation for  $Y_M(p)$  and then synthesize the network. In this case, since a realizable driving point impedance is a minimum phase network, one merely approximates the amplitude and the phase must follow. (The phase error as a function of amplitude approximation error is not easy to assess, but in the limit of zero amplitude error the phase will be automatically correct.) A potential analog computer gave the following  $PR$  rational function approximation  $Y_M'(p)$  for the idealized representation  $Y_M(p)$ .

$$Y_M(p) \cong Y_M'(p) = 0.328 \frac{p^3 + 4.5p^2 + 12.8p + 15.5}{p^3 + 2.69p^2 + 5.05p + 3.50}$$

The amplitude  $|Y_M'(j\omega)|$  is plotted on Fig. 4, where it may be compared with  $|Y_M(j\omega)|$ . The final network to represent  $Y_M'(p)$  is synthesized by a Brune process and is shown in Fig. 5. Fig. 6 shows a plot of the prescribed ideal gain characteristic of the over-all system, *i.e.*,  $|Z(j\omega)|$ , as well as the actual gain which results when the physical network shown in Fig. 5 is used. The agreement is good.

### III. TWO-PORT REACTIVE EQUALIZERS

The general problem to be considered in the remainder of this paper is the synthesis of a two-port reactive network to match a given load to a pure resistance generator impedance over a prescribed frequency band. The lossless matching network or equalizer is to produce approximately maximum scale factor for the stipulated power transfer characteristic shape (that is minimum reflection loss or mismatch) over the frequency band. Fig. 7 shows the system considered.

The first step in the procedure is the determination of the parameters for the prescribed amplitude of transfer characteristic. Referring to Fig. 7, with  $s_{jk}$  the scattering coefficients of the over-all network consisting of equalizer and load, the transfer function of interest is  $|s_{12}(j\omega)|^2$  which gives the ratio of power divided by available generator power when the load is represented in Darlington form [6] by a lossless two-port  $E$  termi-

nated in a one-ohm resistor. Since the system is lossless, the scattering matrix is unitary on  $p=j\omega$  and

$$s_{22}(p)s_{22}(-p) = 1 - s_{12}(p)s_{12}(-p) \tag{13a}$$

$$|s_{22}(j\omega)| = |s_{11}(j\omega)| \tag{13b}$$

and the load constraints on the transfer characteristic or the input reflection factor may be described in terms

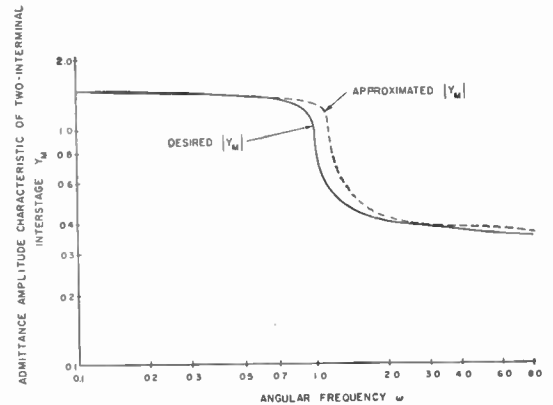


Fig. 4—Desired and approximated amplitude characteristic for one-port equalizer.

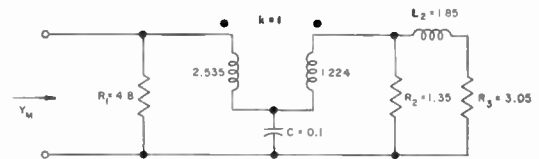


Fig. 5—One-port equalizer network.

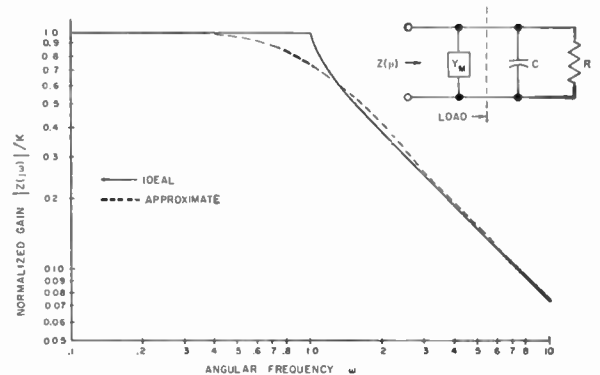


Fig. 6—Ideal and approximated gain characteristic of one-port equalizer system.

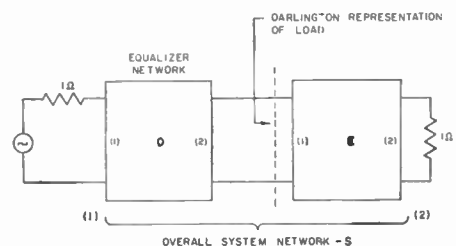


Fig. 7—Two-port equalizer system.

of  $s_{22}(p)$ , the load end reflection factor of the system consisting of  $D$  (matching network) and  $E$  (load reactance two-port) in cascade. These constraints are most conveniently expressed in terms of integral relations involving

$$\ln \left| \frac{1}{s_{22}(j\omega)} \right|,$$

and take the form [2]:

$$\int_0^\infty f_k(\omega) \ln \left| \frac{1}{s_{22}(j\omega)} \right| d\omega = A_k$$

$$k = 1, 2, \dots, n. \quad (14)$$

One such equation is written for each of the  $n$  zeros of transmission of the Darlington two-port associated with the load. These are the zeros of  $e_{12}(p)$  in the complex  $p$  plane. The constants  $A_k$  are essentially Taylor coefficients of  $e_{22}(p)$  when this function is expanded at the zeros of transmission of  $e_{12}(p)$ , but  $A_k$  is modified by appropriate constants found from right-hand zeros which are inserted into  $s_{22}(p)$  in order that all  $n$  equations of (14) be satisfied simultaneously. The  $f_k(\omega)$  are appropriate weighting functions which select the correct Taylor coefficients in the Cauchy integral expressions for such coefficients.

In order to simultaneously satisfy the system of (14), one has at one's disposal the possibility of modifying the prescribed shape

$$\ln \left| \frac{1}{s_{22}(j\omega)} \right|,$$

by introducing right-hand zeros into  $s_{22}(j\omega)$ , and if boundary zeros of transmission occur in  $e_{12}$  by changing the Taylor coefficients of  $s_{22}$  at such zeros by introducing these zeros into the matching network. With these adjustments available, the scale factor of  $s_{22}(j\omega)$  is minimized and at the same time all the equations in (14) at the various zeros of transmission are satisfied. This gives the appropriate load parameters. The performance of this process is not an easy matter, but if the function  $|s_{22}(j\omega)|$  is a simple curve so that the integrations can be performed readily, the solutions are simplified. If, however,  $s_{22}(j\omega)$  is in rational function form (*i.e.*, a rational approximation to the prescribed transfer curve is made at the outset) and contains constants which must be adjusted to optimize the scale of  $|s_{22}(j\omega)|$  at the same time as the equations in (14) are satisfied, a solution is generally quite difficult if the load consists of a number of elements. The essential feature of the technique described here is that  $s_{22}(j\omega)$  is left in idealized form, and an approximation is only made directly to the functions which describe the equalizer alone.

The first step in the design procedure is then to use a simple representation for  $|s_{22}(j\omega)|$  and for this idealized shape choose parameters which minimize this reflection amplitude in the pass band such that the equations in

(14) are satisfied. Referring to (13a), this maximizes the power transfer function  $|s_{12}(j\omega)|^2$  over the pass band.

The next step is to compute numerically the idealized complex function  $s_{22}(p)$ . The function  $s_{22}(p)$  may be written

$$s_{22}(p) = s_{22-0}(p)B(p) \quad (15)$$

where  $s_{22-0}(p)$  is a minimum phase function with

$$|s_{22-0}(j\omega)|^2 = |s_{22}(j\omega)|^2 \quad (16)$$

and  $B(p)$  is a Blaschke product, that is the product of all-pass factors of the form

$$\frac{\sigma_k - p}{\sigma_k + p}, \quad \frac{p_k - p}{p_k + p}, \quad \frac{p_k^* - p}{p_k^* + p}$$

$$\sigma_k \text{ real and } \sigma_k > 0$$

$$p_k \text{ complex and } \text{Re } p_k > 0$$

$$p_k^* \text{ the complex conjugate of } p_k.$$

The function  $B(p)$  is known, since the right-half-plane zeros  $\sigma_k$  and  $p_k$  can be chosen in the following manner. First observe that in terms of the  $D$  and  $E$  networks, the over-all function  $s_{22}(p)$  satisfies the following:

$$s_{22}(p) = e_{22}(p) + \frac{e_{12}^2(p)d_{22}(p)}{1 - d_{22}(p)e_{11}(p)}. \quad (17)$$

Then if the load functions  $e_{22}(p)$ ,  $e_{12}(p)$  have a coincident right-half-plane zero, this zero must appear in  $s_{22}(p)$  and is therefore inserted into the Blaschke product  $B(p)$ . The second way in which an all-pass factor is selected for  $B(p)$  is if, in the process of satisfying (14), it is necessary to choose right-half-plane zeros for  $s_{22}(p)$ . In this second case, such zeros only appear in the matching network, not in the load.

With  $B(p)$  determined, the phase of  $s_{22}(p)$  is readily computed, for the minimum phase,  $\arg s_{22-0}(p)$ , may be found by the Bode integral relations utilizing a graphical procedure (the Thomas tables [4] are particularly convenient), and this has added to it  $\arg B(p)$ . Thus

$$\arg s_{22}(p) = \arg s_{22-0}(p) + \arg B(p).$$

The complex function  $s_{22}(j\omega)$  is now known numerically and it is a simple procedure to completely calculate the scattering parameters of the equalizer. From (17), one may determine the function  $d_{22}(p)$  of the equalizer alone as

$$d_{22}(p) = \frac{s_{22}(p) - e_{22}(p)}{e_{12}^2(p) + e_{11}(p)[s_{22}(p) - e_{22}(p)]}. \quad (18)$$

Since all the complex functions of (18) are known either analytically or numerically on  $j\omega$ , the idealized amplitude and phase of  $d_{22}(j\omega)$  may be determined completely in numerical form. In a similar manner, one may find  $d_{12}(p)$  as a function of the scattering parameters of the

over-all network  $S$  and those of the load  $E$ . Thus

$$d_{12}(p) = \frac{s_{12}(p)e_{12}(p)}{e_{12}^2(p) + e_{11}(p)[s_{22}(p) - e_{22}(p)]} \quad (19)$$

Note that right-half-plane and  $j\omega$  zeros of  $e_{12}(p)$  are chosen for  $s_{12}$ , and because (17) is satisfied,  $s_{22} - e_{22}$  has these zeros with double multiplicity.<sup>5</sup> Hence these zero factors cancel from numerator and denominator and do not appear in  $d_{12}$ . The only points at which  $d_{12}(p)$  is zero for real  $\omega$  is where a zero is inserted in  $s_{12}$  but is not present in the load.

All the complex functions of (19) are known on  $j\omega$  except  $s_{12}(j\omega)$  and this too is readily calculated. The amplitude  $|s_{12}(j\omega)|$  may be numerically determined by (13) but the phase,  $\arg s_{12}(j\omega)$  needs some additional discussion. Recall that  $s_{22}(p)$  may require certain right-hand zeros, either to satisfy the integral relations (14) or because they are in the functions  $e_{12}(p)$ ,  $e_{22}(p)$  of the load. Since the system of  $D$  and  $E$  is unitary, the following relation must be satisfied

$$s_{11}(p) = -s_{22}(-p) \frac{s_{12}(p)}{s_{12}(-p)} \quad (20)$$

Using (15),

$$s_{22}(p) = \frac{M(p)}{Q_0(p)} \cdot \frac{B_1(-p)}{B_1(p)}$$

with  $B_1(-p)$  representing right-half-plane zeros [the zeros of  $B_1(p)$  are in the left-half plane] and with

$$s_{12}(p) = \frac{P(p)}{Q(p)}, \quad s_{22-0}(p) = \frac{M(p)}{Q_0(p)}, \quad B(p) = \frac{B_1(-p)}{B_1(p)}$$

[ $Q(p)$ ,  $Q_0(p)$  have no right-half-plane zeros], (20) becomes

$$s_{11}(p) = -\frac{M(-p)}{Q_0(-p)} \cdot \frac{B_1(p)}{B_1(-p)} \cdot \frac{P(p)}{Q(p)} \cdot \frac{Q(-p)}{P(-p)}$$

Now if

$$Q(p) = Q_0(p)$$

and

$$P(p) = P_0(p)B_1(-p),$$

where  $P_0(p)$  has no left-half-plane zeros, then  $s_{11}(p)$  is analytic in the right-half plane, hence realizable. Then

$$\begin{aligned} s_{11}(p) &= -\left[ \frac{M(-p)}{Q_0(-p)} \frac{B_1(p)}{B_1(-p)} \right] \\ &\quad \cdot \left[ \frac{P_0(p)B_1(-p)}{Q_0(p)} \frac{Q_0(-p)}{P_0(-p)B_1(p)} \right] \\ &= -\frac{M(-p)}{Q_0(p)} \cdot \frac{P_0(p)}{P_0(-p)} \end{aligned} \quad (21)$$

<sup>5</sup> For special case, see footnote 7.

$Q_0(p)$ ,  $P_0(-p)$  have no right-half-plane zeros (boundary zeros cancel in  $P_0(p)/P_0(-p)$  so that  $s_{11}(p)$  is analytic in  $\text{Re } p > 0$ ). Thus we conclude that if  $s_{22}(p)$  has a right-half-plane zero as part of an all-pass pair, that right-half-plane zero must appear in  $s_{12}(p)$  though not necessarily as an all-pass pair.

Returning to the numerical calculation of  $s_{12}(p)$  represent this function as

$$s_{12}(p) = s_{12-0}(p)B_1(-p) \quad (22)$$

where  $s_{12-0}(p)$  is a minimum phase function<sup>6</sup> whose amplitude is

$$|s_{12-0}(j\omega)| = \frac{|s_{12}(j\omega)|}{|B_1(j\omega)|} \quad (23)$$

and  $B_1(-p)$  are the right-half-plane zeros of the known all-pass factors of  $s_{22}(p)$ . The phase of  $s_{12-0}(p)$  is hence readily computed by the Thomas tables using the amplitude data of (23). Thus the phase of  $s_{12}(p)$  is given as

$$\arg s_{12}(p) = \arg s_{12-0}(p) + \arg B_1(-p). \quad (24)$$

With  $s_{12}(j\omega)$  known, the function  $d_{12}(j\omega)$  is completely determined numerically by (19), and  $d_{11}(p)$  then follows by (20).

If  $D$  is to be synthesized as a physical network  $d_{12}(p)$ ,  $d_{22}(p)$  must be approximated by rational functions which are analytic in the right-half plane, satisfy the unitary relations, and result in a  $d_{12}(p)$  function which has prescribed zeros which may lie on the boundary or in the right-half plane if the solution of the integral constraints calls for such zeros. Note, however, that fortunately the zeros of  $d_{22}(p)$  are not fixed in advance as are those of  $d_{12}(p)$  and may fall anywhere called for by the approximation.

In order to perform this multiple approximation in a practical manner, represent the rational function  $d_{22}'(p)d_{22}'(-p)$ , which approximates the numerically prescribed  $d_{22}(j\omega)d_{22}(-j\omega)$  function, as

$$d_{22}'(p)d_{22}'(-p) = \frac{F(p)F(-p)}{R(p)R(-p) + F(p)F(-p)} \quad (25)$$

where  $F(p)$  is a polynomial to be determined by the approximation process and  $R(p)$  is the product of all the prescribed right-half-plane and boundary zero factors which are known in advance to lie in  $d_{12}'(p)$ , the rational function which approximates  $d_{12}(p)$ . The denominator of (25) is an even polynomial which may be factored into its left- and right-half-plane root as

$$R(p)R(-p) + F(p)F(-p) = D(p)D(-p) \quad (26)$$

where  $D(p)$  has only left-half-plane root factors. Then  $d_{22}'(p)$  has the representation

$$d_{22}'(p) = \frac{F(p)}{D(p)} \quad (27)$$

<sup>6</sup> Referring to the discussion of (20) and (21),  $s_{12-0}(p)$  has no left-half-plane zeros.

Using (13a) for a lossless, hence unitary, equalizer,  $d_{12}'(p)d_{12}'(-p)$  is given as

$$d_{12}'(p)d_{12}'(-p) = \frac{R(p)R(-p)}{R(p)R(-p) + F(p)F(-p)} \quad (28)$$

and

$$d_{12}'(p) = \frac{R(p)}{D(p)} \quad (29)$$

with  $R(p)$  the required zeros of  $d_{12}'(p)$ , i.e., on the boundary and in the right-half-plane.

The problem may now be reduced to the approximation of a polynomial for

$$\frac{d_{22}'(p)}{d_{12}'(p)} = \frac{F(p)}{R(p)} \cong \frac{d_{22}(p)}{d_{12}(p)} \quad (30)$$

and since  $R(p)$  is known, with  $d_{22}(j\omega)$ ,  $d_{12}(j\omega)$  numerically determined

$$F(p) \cong R(p) \frac{d_{22}(p)}{d_{12}(p)}. \quad (31)$$

Substituting (18) and (19), (31) becomes

$$F(p) \cong R(p) \frac{s_{22}(p) - e_{22}(p)}{s_{12}(p)e_{12}(p)}. \quad (32)$$

It was previously shown in connection with (19), that zeros of  $e_{12}(p)$  must appear in  $s_{12}(p)$  and are found in double multiplicity in  $s_{22} - e_{22}$  so that all right-hand-plane and  $j\omega$  zeros of  $e_{12}$  cancel from the right-hand-side of (32).<sup>7</sup> Real frequency transmission zeros which for any reason are intended for the equalizer but do not appear in the load are common to  $s_{12}(p)$  and  $R(p)$  and hence again cancel.

Thus  $F(p)$  may be computed as a polynomial which approximates to the numerically specified function on the right side of (32) and  $d_{12}'(p)$  and  $d_{22}'(p)$  are completely specified by (27) and (29).

It must be emphasized at this point, however, that the phase,  $\arg F(j\omega)$ , is the difference in phase between  $d_{22}'(p)$  and  $d_{12}'(p)$ , whereas if the amplitude  $|F(j\omega)|$  is approximated satisfactorily, the amplitudes  $|d_{12}'(j\omega)|$  and  $|d_{22}'(j\omega)|$  are assured as close fits to the prescribed amplitude characteristics. In order that the *absolute* phase of  $d_{12}'(p)$  be a satisfactory approximation, it is not sufficient that its amplitude be correct in the pass band, but rather that its amplitude be correct over a much wider band, since amplitude deviations outside the band contribute phase errors in the band. This means that  $|F(j\omega)|$  must behave outside the pass band in the same manner as the prescribed functions. Thus if

<sup>7</sup> It is possible for  $(s_{22} - e_{22})$  to have a  $j\omega$  zero of order  $(2n - 1)$  if this zero occurs in  $e_{12}$  with order  $n$ . In this case this zero is of order  $(n - 1)$  in  $s_{12}$  and cancellation still occurs.

$d_{22}(j\omega)/d_{11}(j\omega)$  varies as  $\omega^n$  at large frequencies, so too must  $F(j\omega)$ , and therefore the degree of  $F(p)$  is dictated in advance by the shape of the idealized  $|s_{12}(j\omega)|$  and  $|s_{22}(j\omega)|$  functions at large frequencies. With this in mind, the polynomial  $F(p)$  may be approximated by any convenient technique.

Complex interpolation, for example, is particularly useful if a computer is handy, for the realizability of the  $D$  network functions is automatically assured in advance once  $F(p)$  is determined. This may be seen in the following manner. Note first that the factorization process makes the polynomial  $D(p)$  Hurwitz, so that  $d_{12}'(p)$ ,  $d_{22}'(p)$  are analytic in  $\text{Re } p > 0$ . In addition, the unitary relations are satisfied on  $p = j\omega$  for

$$|d_{12}'(j\omega)|^2 + |d_{22}'(j\omega)|^2 = 1.$$

Further  $d_{11}'(p)$  always satisfies the other unitary equation (20)

$$\begin{aligned} d_{11}'(p) &= -\frac{F(-p)}{D(-p)} \cdot \frac{R(p)}{D(p)} \cdot \frac{D(-p)}{R(-p)} \\ &= -\frac{F(-p)}{D(p)} \cdot \frac{R(p)}{R(-p)}. \end{aligned} \quad (33)$$

The function  $d_{11}'(p)$  is analytic in  $\text{Re } p > 0$  for  $R(-p)$  does not contain any right-half-plane factors, and any real frequency zeros in  $R(p)$  are cancelled by the same factors which must occur in  $R(-p)$ . The  $D$  network is hence physically realizable and may be synthesized by well-known procedures [6].

The method described is quite flexible, for the approximation procedure may be controlled to yield desired configurations for the equalizer network. Thus, suppose that the integral constraints are satisfied by appropriate choice of  $|s_{22}(j\omega)|$  without the need of right-half-plane zeros of transmission in  $D$ . Then the technique described can be manipulated to assure a constant  $K$  configuration ladder network representation of the equalizer. To do this, the function  $R(p)$  is chosen as unity and the result from (31) is

$$F(p) \cong \frac{s_{22}(p) - e_{22}(p)}{s_{12}(p)e_{12}(p)}, \quad [R(p) = 1] \quad (34)$$

with

$$d_{12}'(p) = \frac{1}{D(p)} \quad (35a)$$

$$d_{22}'(p) = \frac{F(p)}{D(p)}. \quad (35b)$$

The forms of (35a) and (35b) are necessary and sufficient for a ladder network representation of  $D$  containing at most one ideal transformer. If the further restriction is made that the constant term of  $F(p)$  is zero, then the ideal transformer is eliminated.

Restrictions of this kind may, of course, limit the closeness of approximation to the originally prescribed shape, but it may be desirable to trade optimum performance for simplicity of final network design.

Another example of the flexibility the procedure affords is in the design of cascaded transmission line matching networks for microwave loads. In this case, the functions are transformed by a change of frequency variable [7]

$$\lambda = \tanh \gamma p.$$

In the  $\lambda$  domain, the necessary and sufficient condition for the  $D$  network to be representable as  $n$  cascaded lines is that  $d_{12}'(\lambda)d_{12}'(-\lambda)$  have the form

$$d_{12}'(\lambda)d_{12}'(-\lambda) = \frac{(1 - \lambda^2)^n}{P_n(\lambda)P_n(-\lambda)}$$

where  $P_n(\lambda)$  is an  $n$ th degree polynomial without zeros in  $\text{Re } \lambda > 0$ . The  $n$ th order right-half-plane zero at  $\lambda = 1$  is first taken into account in computing the parameters of the idealized function  $|s_{22}(j\omega)|$ . Then one chooses

$$R(\lambda) = (1 - \lambda)^n$$

and approximates  $F(\lambda)$  as an  $n$ th degree polynomial.

$$F(\lambda) \cong (1 - \lambda)^n \frac{s_{22} - e_{22}}{s_{12}e_{12}}.$$

Note that this implies that the functions  $s_{22}$ ,  $s_{12}$  must be chosen so that the factor  $s_{22} - e_{22}/s_{12}e_{12}$  approaches a constant as  $\omega$  becomes infinite. If this can be done, the matching network is then guaranteed in advance to be synthesizable as a cascade of lossless transmission lines.

It must be emphasized that the general procedure described here is essentially a numerical method ideally suited to be carried out on a computer. A shortcoming of the technique is that although the result will converge to the prescribed response as the approximation to  $F(p)$  is improved, at this time there is no simple way of estimating the error in advance. The final approximating response  $|s_{12}'(j\omega)|^2$  should therefore be computed from

$$|s_{12}'(j\omega)|^2 = \left| \frac{e_{12}(j\omega)d_{12}'(j\omega)}{1 - e_{11}(j\omega)d_{22}'(j\omega)} \right|^2 \tag{36}$$

and checked against the prescribed idealized function  $|s_{12}(j\omega)|^2$ .

As an example of the procedure described above, consider the RRC load shown in Fig. 8. This is not an extremely pathologic network, but the structure is simple and has a right-half-plane zero in its  $e_{12}(p)$  and  $e_{22}(p)$  functions. Further, the synthesis will be carried out to eliminate ideal transformers. Thus, many facets of the synthesis technique described here can be illustrated.

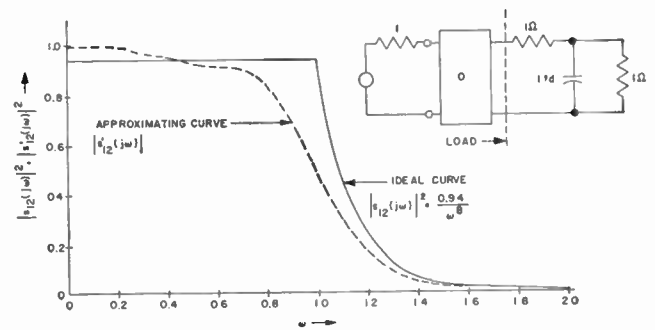


Fig. 8—Ideal and actual gain characteristics for RRC load equalizer.

The idealized transfer function amplitude chosen is shown in Fig. 8.

$$|s_{12}(j\omega)|^2 = \begin{cases} s_0^2, & 0 \leq \omega \leq 1 \\ \frac{s_0^2}{\omega^8}, & 1 \leq \omega \leq \infty \end{cases} \tag{36a}$$

Also

$$|s_{22}(j\omega)|^2 = \begin{cases} 1 - s_0^2, & 0 \leq \omega \leq 1 \\ 1 - \frac{s_0^2}{\omega^8}, & 1 \leq \omega \leq \infty \end{cases} \tag{36b}$$

The scattering parameters of the load two-port are

$$\begin{aligned} e_{11} &= \frac{p}{3p + 2}, & e_{22} &= \frac{p}{2 + 3p} \frac{(1/\sqrt{2} - p)}{(1/\sqrt{2} + p)}, \\ e_{12} &= 2\sqrt{2} \frac{1/\sqrt{2} - p}{2 + 3p}. \end{aligned} \tag{37}$$

There is a right-hand zero of transmission in the load at  $1/\sqrt{2}$  and the first Taylor coefficient of

$$\ln \frac{1}{e_{22}(p)} \frac{1/\sqrt{2} - p}{1/\sqrt{2} + p}$$

expanded about this zero is  $a_0 = \ln(3 + 2\sqrt{2})$ . There is only a single integral constraint, so no additional right-half-plane zeros are required in the equalizer network; the constraint is

$$\int_0^\infty \frac{\ln \left| \frac{1}{s_{22}(j\omega)} \right|}{\omega^2 + (1/\sqrt{2})^2} d\omega = \frac{\pi \ln(3 + 2\sqrt{2})}{\sqrt{2}}. \tag{38}$$

For the low-pass characteristic of (36b), the integral of (38) may be numerically evaluated for various choices of  $s_0^2$  and the equality is satisfied when  $s_0^2 = 0.94$ .

Since  $e_{12}$ ,  $e_{22}$  have a coincident right-half-plane zero, this zero is chosen as an all-pass factor in  $s_{22}(p)$  so as not to affect the amplitude shape  $|s_{22}(j\omega)|$  given in (36b).

Thus

$$s_{22}(p) = s_{22-0}(p) \frac{1/\sqrt{2} - p}{1/\sqrt{2} + p} \tag{39}$$

Further,  $s_{12}(p)$  must contain this zero (not necessarily as an all-pass) so that

$$s_{12}(p) = s_{12-0}(p)(1/\sqrt{2} - p) \tag{40}$$

If the equalizer is to be designed as a constant  $K$  configuration, the function  $F(p)$  is to approximate may then be written using (34), (37), (39), (40)

$$F(j\omega) \cong \frac{s_{22-0}(2 + j3\omega) - j\omega}{2\sqrt{2}s_{12-0}(0.5 + \omega^2)} \tag{41}$$

The phases  $\arg s_{22-0}$ ,  $\arg s_{12-0}$  are computed from the Thomas tables and with this information, plus the amplitude data of (36), as well as

$$|s_{12-0}(j\omega)|^2 = \frac{|s_{22}(j\omega)|^2}{0.5 + \omega^2} \tag{42}$$

the real and imaginary parts of the function on the right side of (41) are readily tabulated. These are shown plotted in Fig. 9. Because of the choice of  $|s_{12}(j\omega)|^2$  as a function which rolls off as  $1/\omega^8$ ,  $F(j\omega)$  must be approximated as a 4th degree polynomial to assure a reasonable fit to  $|s_{12}(j\omega)|^2$  at high frequencies. This constrains the number of equalizer elements to be 4 and does not provide the possibility of a really close approximation for  $F(j\omega)$ . An approximation was made by interpolation to obtain the function

$$F(p) = -0.835p - 0.945p^2 - 1.71p^3 - 0.369p^4 \tag{43}$$

and the real and imaginary parts of this are shown on Fig. 9. It should be noted that in performing the approximation of  $F(p)$ , its constant term was chosen to be zero so that no ideal transformer would be needed. This forces  $s_{12}'(0) = 1.0$  and contributes to the over-all error. From the polynomial  $F(p)$  of (43),  $d_{12}'(p)$  and  $d_{22}'(p)$  are readily computed<sup>8</sup> [see (35) with  $D(p)D(-p) = 1 + F(p)F(-p)$ ] and the ladder network is then synthesized as in Fig. 10. The actual response with this network as the equalizer is shown in Fig. 8. The approximation to the prescribed curve is reasonable considering the small number of elements and the fact that the approximation was made to exclude an ideal transformer.

<sup>8</sup>  $d_{22}'(p)$  is chosen as  $-F(p)/D(p)$  for best results.

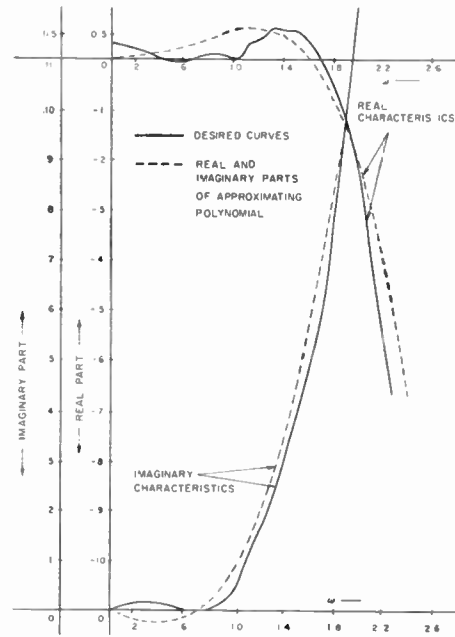


Fig. 9—Polynomial approximation for  $F(p) = 0.835p - 0.945p^2 - 1.710p^3 - 0.369p^4$ .

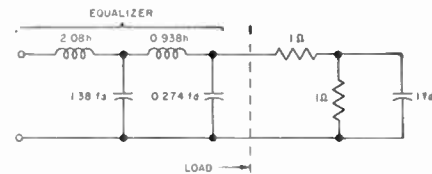


Fig. 10—Ladder equalizer for RRC load.

ACKNOWLEDGMENT

The author gratefully acknowledges the assistance of W. Ku and Mrs. M. Wang in preparing this paper.

REFERENCES

- [1] H. W. Bode, "Network Analysis and Feedback Amplifier Design," D. Van Nostrand Co., Inc., New York, N. Y., chs. 14 and 16; 1945.
- [2] R. M. Fano, "Theoretical limitations on the broadband matching of an arbitrary impedance," *J. Franklin Inst.*, vol. 249, pp. 57-98, January; pp. 139-154, February, 1950.
- [3] R. LaRosa and H. J. Carlin, "A general theory of wideband matching with dissipative 4-poles," *J. Math. and Phys.*, vol. 33, pp. 331-345; January, 1955.
- [4] D. E. Thomas, "Phase of a semi-infinite unit attenuation slope," *Bell Sys. Tech. J.*, vol. 26, pp. 870-899; October, 1947.
- [5] H. J. Carlin, "Gain bandwidth limitations on equalizers and matching networks," *Proc. IRE*, vol. 42, pp. 1676-1685; November, 1954.
- [6] H. J. Carlin and R. LaRosa, "On the synthesis of reactance 4-poles," *J. Appl. Phys.*, vol. 24, pp. 1336-1337; October, 1953.
- [7] P. I. Richards, "Resistor-transmission lines," *Proc. IRE*, vol. 37, pp. 217-219; February, 1948.

# Properties of Phased Arrays\*

WILHELM H. VON AULOCK†, ASSOCIATE MEMBER, IRE

*Summary*—This paper discusses in some detail the scanning properties of planar and linear phased arrays consisting of a large number of equispaced radiators, either omnidirectional or directive. Assuming that a suitable beam shape and sidelobe level in the broadside direction have been attained, it is shown how scanning of the array through introduction of a phase delay into the wave front distorts this pattern and introduces new sidelobes. The study uses contour maps of the antenna pattern in “ $\sin \theta$ -space,” which is a projection of the unit sphere on the plane of the array. In this space the antenna pattern remains invariant with scan angle and merely undergoes a translation proportional to the phase delay between adjacent radiators. Using a parallel projection of the unit sphere onto the plane of the array, the actual antenna patterns are then readily obtained in conventional spherical coordinates. This method also permits ready evaluation of the influence of the directivity of the radiating elements, including a slight shift of the beam maximum with respect to that of an array of isotropic radiators. Furthermore, a pictorial representation of the coverage of a tilted planar array of given scanning properties can be obtained in terms of an earth-fixed coordinate system. Finally, it is shown how the beam-pointing error in a phased array is related to systematic errors in the phase delay.

## I. INTRODUCTION

**M**ECHANICALLY scanned antennas were employed almost exclusively in the radar systems of World War II and are still being used in the majority of all operational radar systems. However, new requirements for radar systems, including rigidity and shock resistance of the antenna structure, volumetric rapid scanning of large antennas, and avoidance of any mechanical motion in the radar system, have led to an ever-increasing interest in electrically scanned antennas in which the antenna stays fixed in space and the radar beam is moved by introducing a phase delay into the radiated wave front. Such an antenna is called, briefly, a “phased array.” Its properties are well understood and readily amenable to numerical and graphic analysis.

Although the purpose of a two-dimensional phased array is the same as that of a parabolic reflector in a two-gimbal mount, namely, to scan a radar beam, the characteristics of these two antennas have some fundamental differences, thus making it impossible simply to substitute one for the other in an existing radar system. Phased arrays can provide scanning patterns and scanning rates which are impossible to attain with mechanically scanned antennas. Conversely, a parabolic reflector can be turned and tilted to radiate an identical

antenna pattern toward every point in a hemisphere, a task which is inherently impossible with a planar phased array. Furthermore, the scanning properties of a mechanically scanned antenna are readily described in a spherical coordinate system with its origin at the phase center of the antenna, whereas scanning of a phased array can be discussed more conveniently in a different coordinate system.

This paper presents a brief review of the scanning properties of phased arrays. The discussion is restricted to arrays of equispaced radiators located in a plane. Further, it is assumed that the variation of scan angle  $\theta_s$  of these arrays,<sup>1</sup> hereinafter referred to as “scan sector,” is large compared to the beamwidth. This assumption implies that the phased arrays consist of many radiating elements, possibly 50 to 100 radiators for a linear array and 2500 to 10,000 elements for two-dimensional arrays.

The introduction of a phase delay across the wave front radiating from an array has many consequences besides the obvious shift of the beam maximum.

- 1) The beamwidth increases as one scans away from broadside.
- 2) The beam shape changes slightly as one scans from broadside to moderate scan angles and is modified drastically for extreme scan angles close to  $90^\circ$  from broadside.
- 3) New sidelobes may appear at moderate to large scan angles.
- 4) The beam direction is slightly different from that computed by standard formulas.

All these effects are well understood. They have to be taken into account if one attempts to approximate the precise performance of a mechanically scanned antenna with a phased array. This discussion therefore deals with beam direction, beamwidth, and beam shape as functions of phase delay. Furthermore, the sensitivity of array performance to systematic excitation errors is reviewed.

As a result of this study, it is possible to state accuracy requirements for the phase delay of practical arrays. The capabilities and limitations of this type of scanning antenna will be apparent, and techniques for the design of such an array will emerge.

\* Received by the IRE, October 30, 1959; revised manuscript received, March 4, 1960.

† Bell Telephone Labs., Inc., Whippany, N. J.

<sup>1</sup> The scan angle  $\theta_s$  is defined as the angle between the array normal and the beam maximum.

The deterioration of array characteristics with random excitation errors has received considerable attention in the literature.<sup>2-5</sup> It is not to be discussed here because it is believed that systematic errors, rather than random errors, will limit the performance of multi-element phased arrays.

Whereas mechanically scanned antennas are adequately described by giving two antenna patterns in orthogonal planes, this method of presentation is entirely unsatisfactory for a phased array whose pattern changes appreciably as the beam is scanned away from the array normal. To appreciate fully the characteristics of both linear and two-dimensional phased arrays, their patterns must be studied in a hemisphere rather than in two planes, and a pattern representation which permits the study of pattern changes as a function of scan angle must be found. Thus, the hemisphere, rather than two orthogonal planes, becomes the preferred space to be considered, and the planar, rather than the linear, phased array emerges as the principal object of this discussion. In particular, the two-dimensional array of isotropic radiators is used to show the variation of beam position, beam shape, beamwidth, and secondary beams with phase delay. Directive radiating elements will be introduced later to demonstrate their contribution to beam distortion, sidelobe level, and beam-pointing errors.

## II. TWO-DIMENSIONAL PHASED ARRAYS OF ISOTROPIC RADIATORS

Consider a two-dimensional array of  $M \cdot N$  equispaced isotropic radiators in the  $xy$  plane (Fig. 1). The radiators are excited by individual currents  $I_{mn}$  and provisions are made to introduce independent progressive phase delays in the  $x$  and  $y$  directions, so that the delay between adjacent radiators is  $\psi_x$  and  $\psi_y$  (radians), respectively. We want to examine the motion of the radar beam as a function of the phase delays and to study the variations of beam shape with the scan angle. Hence, we are not concerned with the classic problem of array theory which attempts to correlate the antenna pattern with the complex excitation coefficients  $I_{mn}$ , but we simply assume that this problem has been solved and that means exist to produce an acceptable amplitude pattern in the  $z$  direction normal to the array when all array elements are excited in phase ( $\psi_x = \psi_y = 0$ ).

<sup>2</sup> L. A. Rondinely, "Effects of random errors on the performance of antenna arrays of many elements," 1959 IRE NATIONAL CONVENTION RECORD, pt. 1, pp. 174-189.

<sup>3</sup> L. A. Kurtz and R. S. Elliot, "Systematic errors caused by the scanning of antenna arrays: phase shifters in the branch lines," IRE TRANS. ON ANTENNAS AND PROPAGATION, vol. AP-4, pp. 619-627; October, 1956.

<sup>4</sup> D. K. Cheng, "Effect of arbitrary phase errors on the gain and beamwidth characteristics of radiation pattern," IRE TRANS. ON ANTENNAS AND PROPAGATION, vol. AP-3, pp. 145-147; July, 1955.

<sup>5</sup> R. S. Elliot, "Mechanical and electrical tolerances for two-dimensional scanning antenna arrays," IRE TRANS. ON ANTENNAS AND PROPAGATION, vol. AP-6, pp. 114-120; January, 1958.

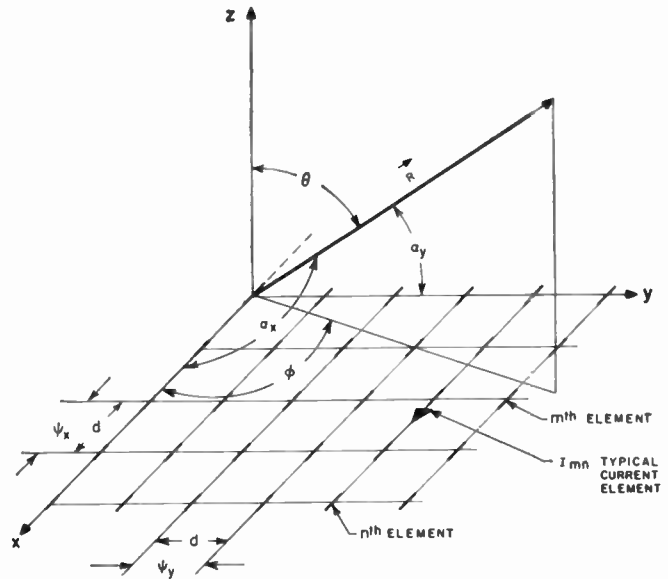


Fig. 1—Planar array of equispaced current elements.

### A. The Antenna Pattern

The amplitude pattern of an array of isotropic radiators is given by<sup>6</sup>

$$S_a = \sum_{m=0}^{M-1} \sum_{n=0}^{N-1} |I_{mn}| e^{jd_x(m\tau_x + n\tau_y)}, \quad (1)$$

where

$M, N$  = number of elements in  $x$  and  $y$  directions,

$|I_{mn}|$  = amplitude of excitation coefficient,

$d_x = 2\pi d/\lambda_0$  = spacing between radiating elements in radians,

$\lambda_0$  = wavelength in free space,

$\tau_x = \cos \alpha_x - \cos \alpha_{xs}$ ,

$\tau_y = \cos \alpha_y - \cos \alpha_{ys}$ ,

$\cos \alpha_x, \cos \alpha_y$  = direction cosines of radius vector specifying the point of observation,

$\cos \alpha_{xs}, \cos \alpha_{ys}$  = direction cosines of radius vector specifying beam maximum (scan direction).

The conventional pattern representation of this array uses a spherical coordinate system with azimuth and elevation angles  $\phi$  and  $\theta$  (Fig. 1). These angles are related to the direction cosines as follows:

$$\sin^2 \theta = \cos^2 \alpha_x + \cos^2 \alpha_y,$$

$$\tan \phi = \frac{\cos \alpha_y}{\cos \alpha_x}. \quad (2)$$

<sup>6</sup> S. Silver, "Microwave Antenna Theory and Design," M.I.T. Rad. Lab. Ser., McGraw-Hill Book Co., Inc., New York, N. Y., vol. 12, pp. 104-106; 1949.

After fixing the direction of the beam maximum by specifying  $\alpha_{zs}$  and  $\alpha_{ys}$  and computing  $\theta_s$  and  $\phi_s$  from (2), one selects a plane  $\phi = \text{const}$  and computes the pattern

$$S_a = f(\theta) \quad (\theta_s, \phi_s, \phi = \text{const}).$$

Similarly, one may compute the pattern

$$S_a = f(\phi) \quad (\theta_s, \phi_s, \theta = \text{const}).$$

Clearly, this pattern representation has two disadvantages.

- 1) The pattern depends on the position of the beam maximum  $\theta_s, \phi_s$ .
- 2) The pattern representation is valid only for one particular plane ( $\phi = \text{const}$ ) or conical surface ( $\theta = \text{const}$ ). Hence, a complete representation of the antenna pattern in the hemisphere requires many curves for many different planes.

Both these difficulties can be overcome by using the differences of direction cosines  $\tau_x$  and  $\tau_y$  as variables and plotting a contour map of the amplitude pattern,

$$f(\tau_x, \tau_y) - S_a = 0 \quad (S_a = \text{const}) \quad (3)$$

in direction cosine space.

Here we will assume that this particular contour is a circle for  $M = N$  and an ellipse for  $M \neq N$ . It is interesting to note that this assumption is justified in the case of uniform illumination ( $I_{mn} = I_0$ ). The amplitude pattern of an  $M \cdot N$  array with uniform illumination<sup>7</sup> is given by

$$S_a = \frac{\sin \frac{1}{2} M d_r \tau_x}{M \sin \frac{1}{2} d_r \tau_x} \cdot \frac{\sin \frac{1}{2} N d_r \tau_y}{N \sin \frac{1}{2} d_r \tau_y} \quad (4)$$

The contour map of the main beam can be approximated by

$$\begin{aligned} S_a &= \frac{\sin x}{x} \cdot \frac{\sin y}{y}, \\ x &= \frac{1}{2} M d_r \tau_x, \\ y &= \frac{1}{2} N d_r \tau_y. \end{aligned} \quad (5)$$

This map is shown in Fig. 2. It is apparent that the contour is an almost perfect circle at the half-power point but approaches a square as  $S_a$  approaches zero. Hence, one may talk of a beam broadening in the diagonal. This beam broadening amounts to less than 2 per cent at the half-power point and may be neglected (Fig. 3). Thus, the half-power beamwidth of a uniformly illuminated square array ( $M = N$ ) is given in  $\tau$  space by

$$2\Delta\tau = \frac{C_0}{A/\lambda_0}, \quad (6)$$

where  $C_0 = 0.888$  and  $A = Nd$  (aperture).

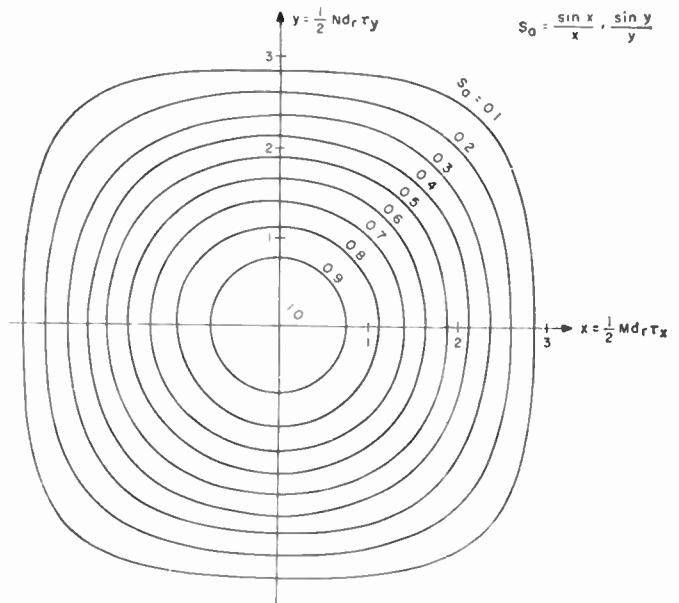


Fig. 2—Constant amplitude contours of the beam from a uniformly illuminated  $M \cdot N$  planar array.

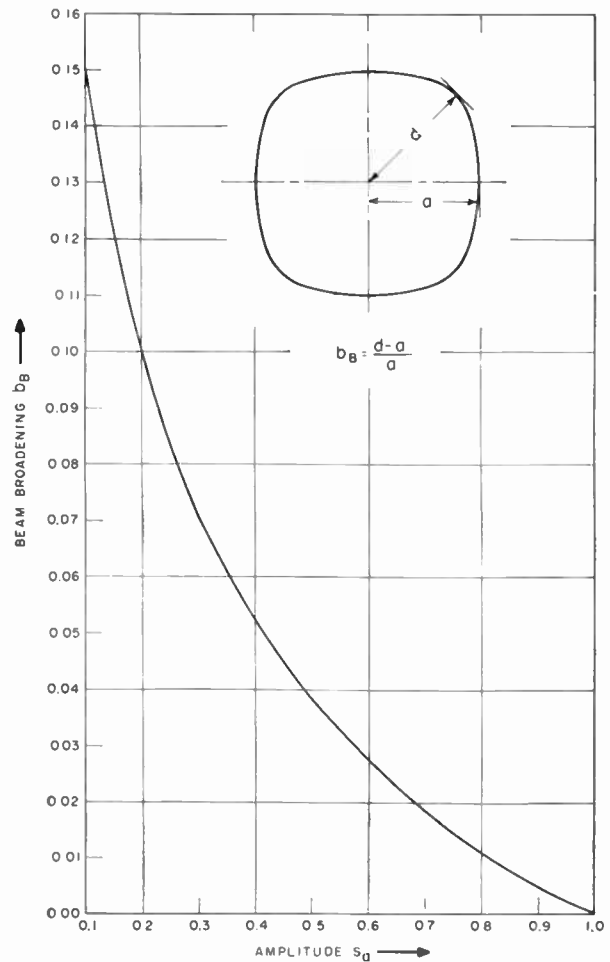


Fig. 3—Beam broadening of a uniformly illuminated planar array.

<sup>7</sup> J. D. Kraus, "Antennas," McGraw-Hill Book Co., Inc., New York, N. Y., ch. 4; 1950.

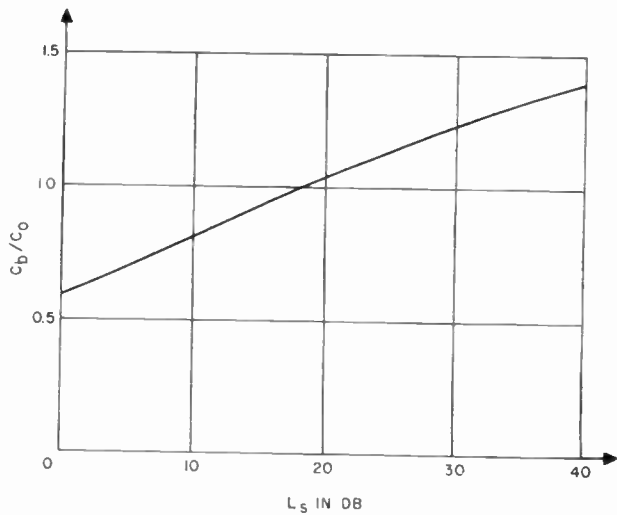


Fig. 4—Beamwidth of a Dolph-Tchebycheff array vs sidelobe level  $L_s$  relative to a uniformly illuminated array of equal aperture.

For a narrow beam array whose beam is oriented normal to the plane of the array,  $2\Delta\tau$  can be interpreted directly as half-power beamwidth in radians. The beamwidth is related to the sidelobe level of the array in such a manner that the beam broadens when the excitation coefficients  $I_{mn}$  are tapered to satisfy specific sidelobe requirements. For a Dolph-Tchebycheff excitation function\* (Fig. 4), the beamwidth can be expressed by

$$2\Delta\tau = \left(\frac{C_b}{C_0}\right) \left(\frac{C_0}{A/\lambda_0}\right), \quad (7)$$

where  $C_b/C_0$  expresses the beam broadening with respect to uniform excitation and as a function of design sidelobe level. Note that a design sidelobe level of 40 db introduces a beam broadening of 41 per cent for a given aperture.

*B. Scanning of the Beam*

The direction of the beam maximum is a function of the two phase delays  $\psi_x$  and  $\psi_y$  so that the direction cosines are proportional to the respective phase delays:

$$\cos \alpha_{zs} = \frac{\psi_x}{d_r} \quad \cos \alpha_{ys} = \frac{\psi_y}{d_r} \quad (8)$$

This fundamental property of phased arrays makes it desirable to discuss pattern shape and beam motion in a coordinate system which has  $\cos \alpha_x$  and  $\cos \alpha_y$  for the two axes.

For ease of manipulation, let us then define a complex  $T$  plane with coordinates  $\cos \alpha_x$  and  $\cos \alpha_y$ . This permits description of the point of observation by a

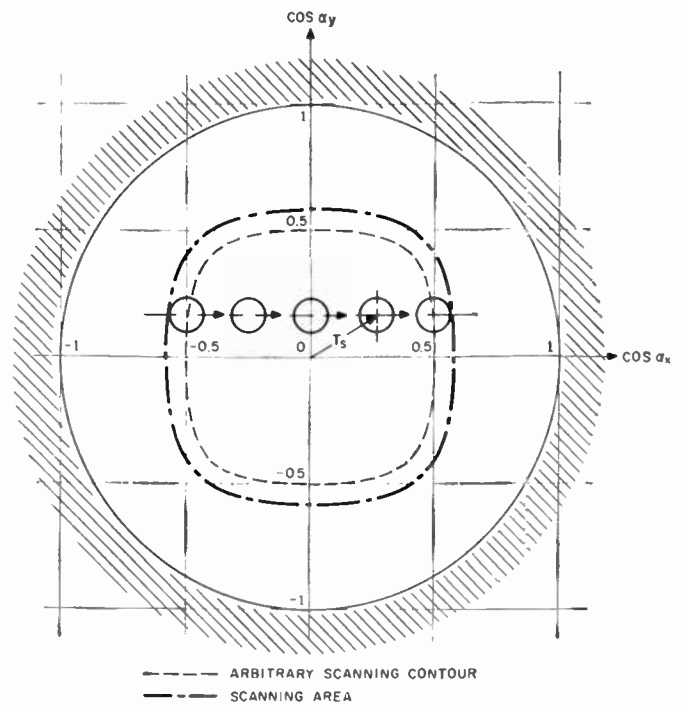


Fig. 5—Scanning in the complex  $T$  plane.

single complex number  $T$  and locates the beam maximum in the  $T$  plane by another complex number,  $T_s$ .

$$T = \cos \alpha_x + i \cos \alpha_y,$$

$$T_s = \cos \alpha_{xs} + i \cos \alpha_{ys} = \frac{\psi}{d_r}, \quad (9)$$

where  $\psi = \psi_x + i\psi_y$  (phase delay).

Similarly, we can define a complex  $\tau$  plane, which is suitable for contour maps of the amplitude pattern, by

$$\tau = T - T_s = \tau_x + i\tau_y. \quad (10)$$

The antenna pattern, which is a function of the complex variable  $\tau$ , is invariant in the  $T$  plane. Scanning the antenna by introducing the complex phase delay  $\psi = \psi_x + i\psi_y$  simply translates the pattern in space so that the pattern center moves to  $T_s = \psi/d_r$  (Fig. 5). If the phase delay is chosen so that  $|T_s| > 1$ , the half-power contour moves outside of the unit circle and becomes imaginary, *i.e.*, unobservable.

Two definitions are helpful in discussing array properties:

*The scanning contour*—a closed curve in the  $T$  plane, traced by the beam maximum when the beam is scanned through the largest required deviations from the array normal (Fig. 5);

*The scanning area*—the area whose boundary is the outer envelope of all the half-power contours of the main beam when the beam is scanned along the scanning contour.

\* L. B. Brown and G. A. Sharp. "Tchebyscheff Antenna Distribution, Beamwidth, and Gain Tables," Naval Ord. Lab., Corona, Calif., NAV-ORD Rept. No. 4629; 1958.

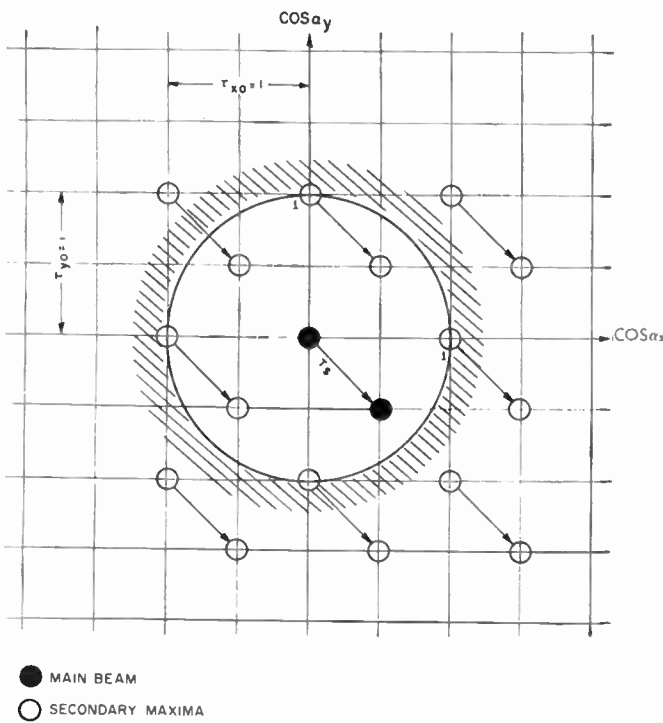


Fig. 6—Secondary maxima of a scanned array with one-wavelength element spacing.

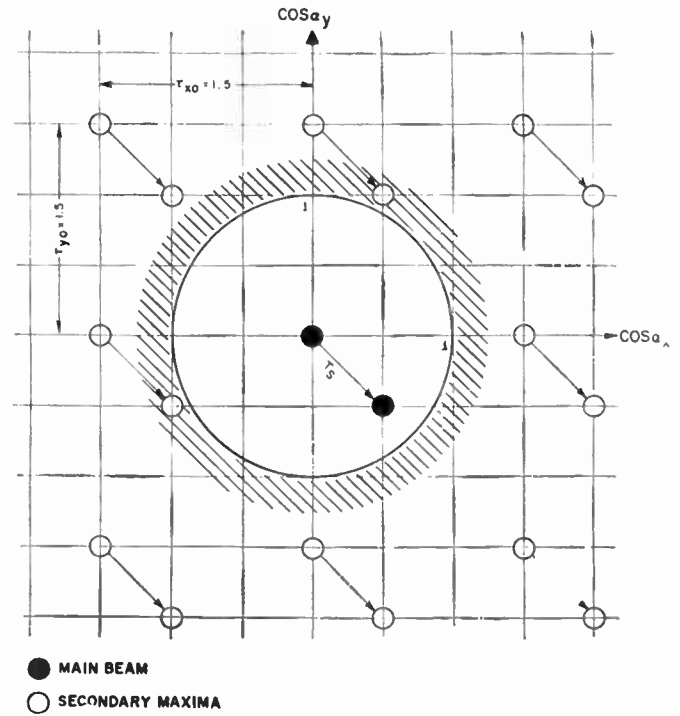


Fig. 7—Secondary maxima of a scanned array with two-thirds-wavelength element spacing.

C. Secondary Maxima

Let us now consider the effects of scanning on the beam pattern. The first is the occurrence of secondary maxima. An array of isotropic radiators has an infinite grid of these maxima spaced  $\tau_{x0} = \tau_{y0} = \lambda_0/d$ . The larger the element spacing, the closer the spacing of the maxima. Whenever the spacing is greater than  $\lambda_0/2$ , these maxima may become visible as they wander into the unit circle with each scanning of the array. If the elements in the array are spaced one free-space wavelength apart, the main beam and four endfire beams will be visible at zero scan angle (Fig. 6), and any scanning away from broadside will move a multiplicity of beams over the hemisphere. For example, if such an array is scanned by a phase delay  $\psi = (1+i)\pi$ , four beams will be seen on the circle  $\theta = 45^\circ$ . However, narrower spacing of the radiating elements (e.g.,  $d = 2\lambda_0/3$ ) will essentially suppress all secondary beams as long as  $|T_x| \leq \frac{1}{2}$  (Fig. 7).

Thus, the proper spacing of radiating elements is the first step in eliminating secondary beams in the array pattern. The second step is concerned with the proper choice of radiating elements (see Section IV).

D. Scanning of a Phased Array in a Spherical Coordinate System

All previous computations have been made in a coordinate system which was fixed with respect to the array, and it has been found that the antenna pattern remained invariant in direction cosine space ( $T$  plane).

To examine the scanning characteristics of a phased array in its associated spherical coordinate system (Fig. 1), we have to project the orthogonal coordinates  $\theta = \text{constant}$  and  $\phi = \text{constant}$  onto the  $T$  plane. This projection permits immediate interpretation of the antenna pattern for any desired scan angle in terms of the spherical  $\theta, \phi$  system.

Expressing the complex direction cosine  $T$  in polar coordinates

$$T = \cos \alpha_x + i \cos \alpha_y = \sin \theta (\cos \phi + i \sin \phi),$$

$$T = \sin \theta e^{i\phi}, \tag{11}$$

immediately yields the desired projection which can be described as the parallel projection of the unit sphere on the equatorial plane (Fig. 8). Each circle  $\sin \theta = \text{constant}$  corresponds to two values of  $\theta$ . Let us therefore define  $0 \leq \theta \leq \pi/2$  as the positive hemisphere and restrict our discussion to it.

E. Scanning Distortions in a Spherical Coordinate System

The resolution of a radar system is limited by the width of the radar beam. If this beamwidth depends on beam direction, then the resolution becomes a function of scan angle. To illustrate the magnitude of beam distortion in a phased array, consider a beam which is circular at the half-power points in  $T$  space. If this beam is scanned away from the array normal, it is then necessary to differentiate between two beamwidths in the  $\theta$  and  $\phi$  directions, respectively (Fig. 9). The reference

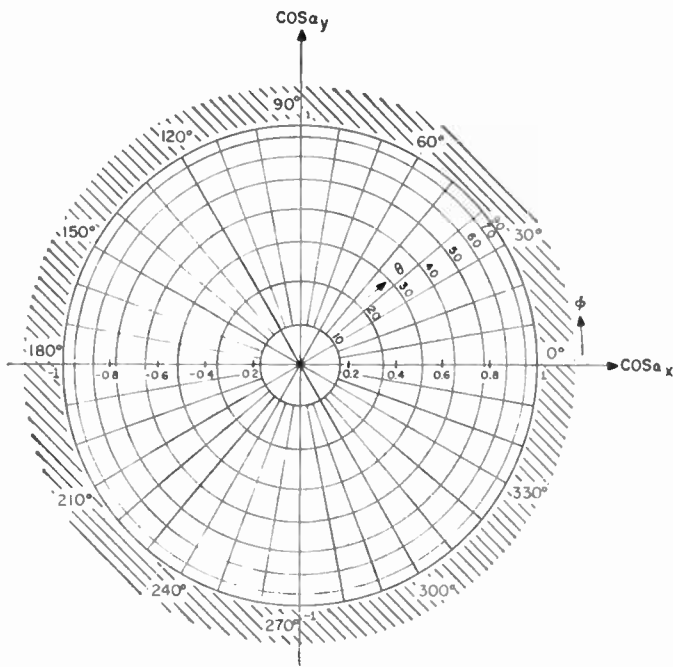


Fig. 8—Projection of unit sphere on  $T$  plane.

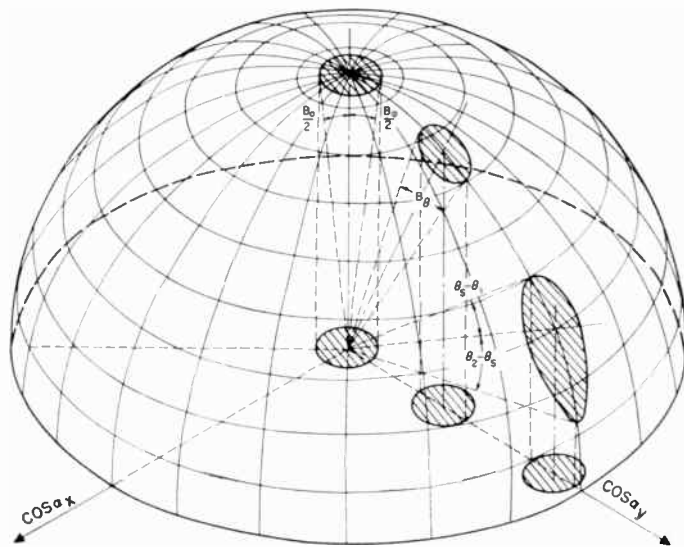


Fig. 9—Beamwidth and eccentricity of the scanned beam.

beamwidth is defined as [cf., (7)]:

$$B_0 = 2 \sin^{-1} (\Delta\tau) \text{ (radians)}, \quad (12)$$

where  $\Delta\tau = C_b \lambda_0 / 2A$ . The beamwidth in the  $\phi$  direction is constant and equal to  $B_0$ .

When the beam is directed away from the array normal, then the beamwidth  $B_\theta$  in the  $\theta$  direction is obtained from

$$2\Delta\tau = |T_2| - |T_1| = \sin \theta_2 - \sin \theta_1. \quad (13)$$

Thus

$$B_\theta = \theta_2 - \theta_1 = 2 \sin^{-1} \left( \frac{\Delta\tau}{\cos \frac{1}{2}(\theta_2 + \theta_1)} \right) \text{ (radians)}. \quad (14)$$

Eqs. (12) and (14) can be simplified for narrow-beam antennas in the usual manner, provided the scan angle  $\theta_s \simeq (\theta_1 + \theta_2) / 2$  is not larger than, say,  $45^\circ$ :<sup>9</sup>

$$B_0 = 2\Delta\tau \text{ (radians)},$$

$$B_\theta = \frac{2\Delta\tau}{\cos \frac{1}{2}(\theta_2 + \theta_1)} \simeq \frac{B_0}{\cos \theta_s} \text{ (radians)}. \quad (15)$$

As the beam is scanned away from the array normal, it broadens in the  $\theta$  direction. Hence, its contour at the half-power points changes gradually from a circle to an ellipse.

### F. Beam Eccentricity

The assumption in (15) that  $(\theta_2 + \theta_1) / 2 = \theta_s$  is inaccurate because the beam maximum is not centered between the two half-power points at  $\theta_2$  and  $\theta_1$ . Thus, a beam eccentricity (Fig. 9) can be defined as

$$2e = \frac{(\theta_2 - \theta_s) - (\theta_s - \theta_1)}{(\theta_2 - \theta_s) + (\theta_s - \theta_1)}. \quad (16)$$

Use of a trigonometric identity and (15) as applied to  $\theta_2 - \theta_s$  and  $\theta_s - \theta_1$ , the two "half" beams, in (16) yields

$$2e = \tan \frac{1}{4}(\theta_1 + \theta_2 + 2\theta_s) \tan \frac{1}{4}(\theta_2 - \theta_1). \quad (17)$$

As we are dealing with a second-order effect, (17) may be approximated by

$$e = \frac{B_\theta}{8} \tan \theta_s. \quad (18)$$

Note that the center of the beam moves relative to the contour by  $(B_\theta^2/8) \tan \theta_s$  radians. For a narrow beam, this eccentricity is very small and may be neglected; however, for a broad beam, it can be appreciable.

Additional beam eccentricity is observed when the isotropic radiators are replaced by actual radiating elements which exhibit a particular element pattern. This effect is discussed in Section IV-A.

### G. Endfire Beam

It has been shown that two phenomena limit the size of the practical scan sector,

- 1) the appearance of secondary maxima,
- 2) the broadening of the beam.

Both effects suggest maximum scan sectors of the order of  $\pm 30^\circ$  ( $|T_{\max}| = \frac{1}{2}$ ). If an array with  $2\lambda_0/3$  spacing is

<sup>9</sup> R. W. Bickmore, "A note on the effective aperture of electrically scanned arrays," IRE TRANS. ON ANTENNAS AND PROPAGATION, vol. AP-6, pp. 194-196; April, 1958.

scanned this far from its normal, maximum beam broadening in the  $\theta$  direction is about 13 per cent and secondary maxima begin to appear at  $\theta=90^\circ$ . It is this appearance of secondary maxima which requires a brief discussion of the beam shape close to  $\theta=90^\circ$ .

The secondary maximum of an array of isotropic radiators appearing at  $\theta=90^\circ$  is, in effect, an endfire beam directed parallel to the array. Its beamwidth in the  $\phi$  direction is equal to  $B_0$ , whereas its beamwidth  $B_{\theta_e}$  in the  $\theta$  direction<sup>10</sup> is obtained from (13) by noting that  $\theta_2=\pi/2$  and  $\theta_1=(\pi/2)-B_{\theta_e}$  and that  $\Delta\tau$ , rather than  $2\Delta\tau$ , applies (Fig. 10). We obtain the following approximation for a narrow-beam array:

$$B_{\theta_e} = \sqrt{2\Delta\tau} = \sqrt{B_0} \text{ (radians).} \quad (19)$$

Thus, an array with a reference beamwidth of  $1^\circ$  (0.017 radian) has an endfire beamwidth of  $B_{\theta_e}=7.5^\circ$ . Should the secondary maximum move just one-half beamwidth farther into the positive hemisphere, then its beamwidth increases by 41 per cent and is given by  $\sqrt{2}B_0$ . This substantial broadening of the endfire beam shows the importance of suppressing secondary maxima at  $\theta=90^\circ$  in a practical phased array through selection of appropriate radiating elements.

### III. SPECIAL CASES OF TWO-DIMENSIONAL PHASED ARRAYS

#### A. The Linear Array

The discussion of two-dimensional phased arrays (see Section II) includes linear arrays as a special case. Putting  $N=1$  in (1), we obtain the amplitude pattern of a linear array of isotropic radiators,

$$S_a = \sum_{m=0}^{M-1} |I_m| e^{jd_r m \tau_x} \quad (20)$$

The contour map of the pattern of a linear array in direction cosine space is just a grid of lines parallel to the  $y$  axis (Fig. 11). In particular, the beamwidth between half-power points is again given by

$$2\Delta\tau_x = \frac{C_b}{A/\lambda_0}, \quad (7)$$

where  $A=Md$  (aperture). Scanning of a linear array means moving a strip of width  $2\Delta\tau_x$  across the  $T$  plane so that

$$T_{zs} = \sin \theta_n \cos \phi = \frac{\psi_x}{d_r}. \quad (21)$$

<sup>10</sup> Consistent with our statement that we restrict our attention to the positive hemisphere, the endfire beamwidth is defined as  $B_{\theta_e}=(\pi/2)-\theta_1$ .

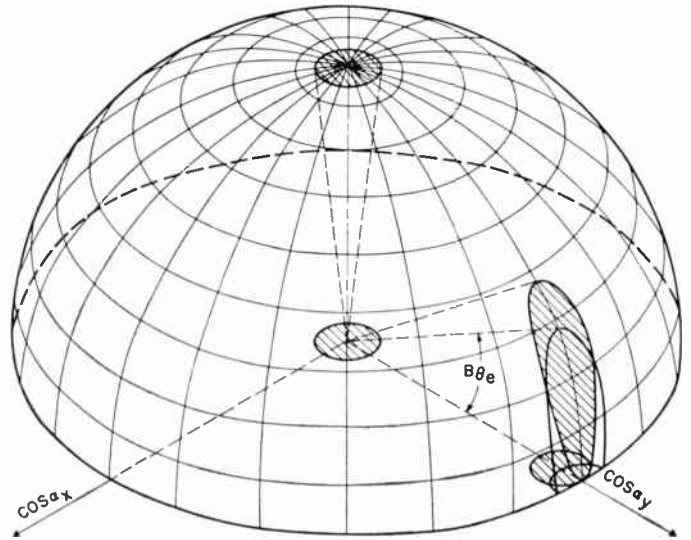


Fig. 10—Beam approaching endfire position.

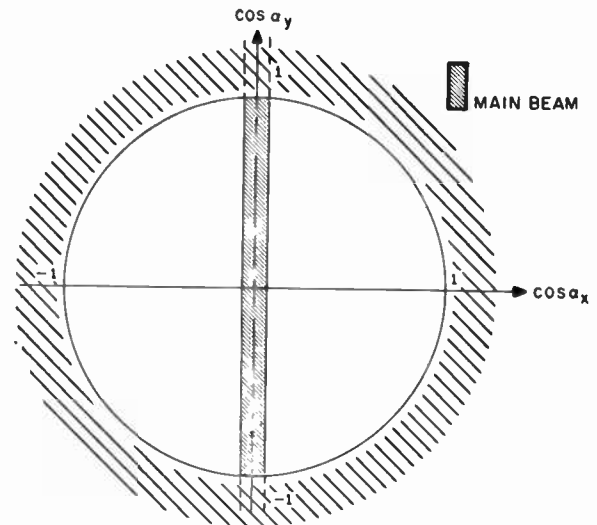
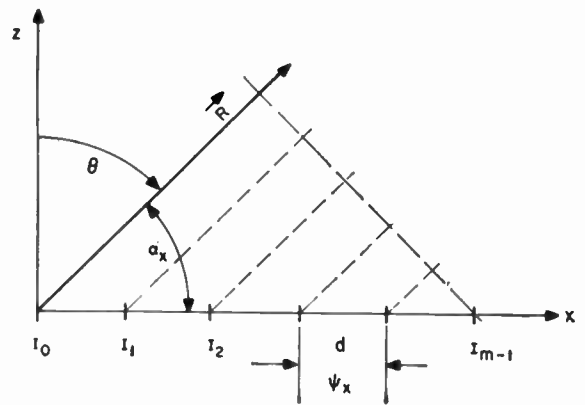


Fig. 11—Linear phased array.

If we again confine our attention to the positive hemisphere, then the actual beam of a linear array of isotropic radiators is a conical half shell. As the beam is scanned away from the array normal, the cone angle decreases and the cone contracts, much like an umbrella being folded, until at  $\theta = 90^\circ$  it becomes a single endfire beam. The discussion of the endfire beam in Section II-G is readily adapted to the linear array and secondary maxima have the same spacing as before,

$$\tau_{x0} = \frac{\lambda_0}{d},$$

but have the appearance of strips in the  $T$  plane (Fig. 12). Their suppression through proper element spacing and suitably chosen radiating elements is guided by the considerations outlined in Section II-C and Section IV.

*B. The Stacked Beam*

A two-dimensional array of  $M \cdot N$  radiators permits formation of a stacked beam (Fig. 13) by applying a multiplicity of fixed phase delays in the  $y$  direction. The stacked beam is then scanned by applying a variable phase delay in the  $x$  direction. There is a close similarity between the deformation of the stacked beam and of the beam of a linear array as a function of phase delay  $\psi_x$ . Here again, the aggregate of beams can be compared to a folding umbrella.

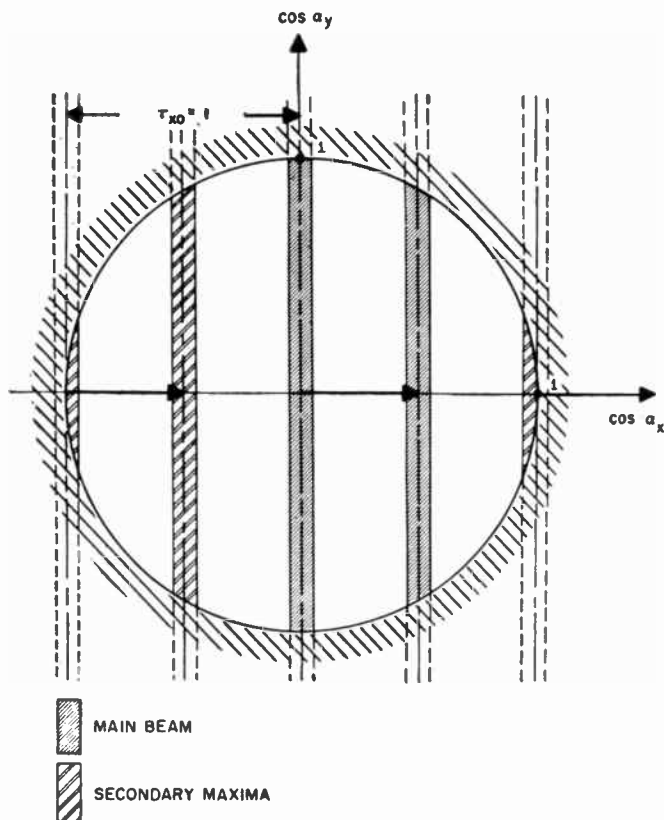


Fig. 12—Scanning of a linear array with one-wavelength element spacing.

*C. The Four-Beam Cluster*

In conventional radar systems, a four-beam cluster is employed to obtain monopulse information.<sup>11</sup> Such a four-beam cluster can readily be formed with a phased array by appropriate antenna feed structures with multiple outputs. In a phased array, the interpretation of the signal obtained from beams  $A, B, C, D$  (Fig. 14) must take into account the fact that the beam cluster cannot be rotated in the spherical coordinate system. Hence, the signals derived from  $(A - C)$  and  $(B - D)$  provide information relative to the  $\theta$  direction when the cluster is scanned along the  $x$  axis ( $\phi = 0$ ). The same beam combination supplies information pertaining to the  $\phi$  direction when the cluster is scanned along the  $y$  direction ( $\phi = 90^\circ$ ). Similar reasoning applies to the difference signals  $(A - B)$  and  $(C - D)$ .

<sup>11</sup> D. R. Rhodes, "Introduction to Monopulse," McGraw-Hill Book Co., Inc., New York, N. Y.; 1959.

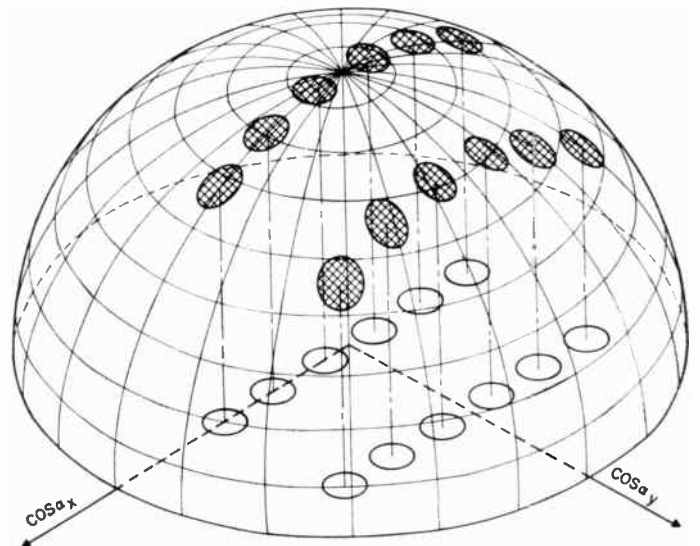


Fig. 13—Scanning of a stacked beam

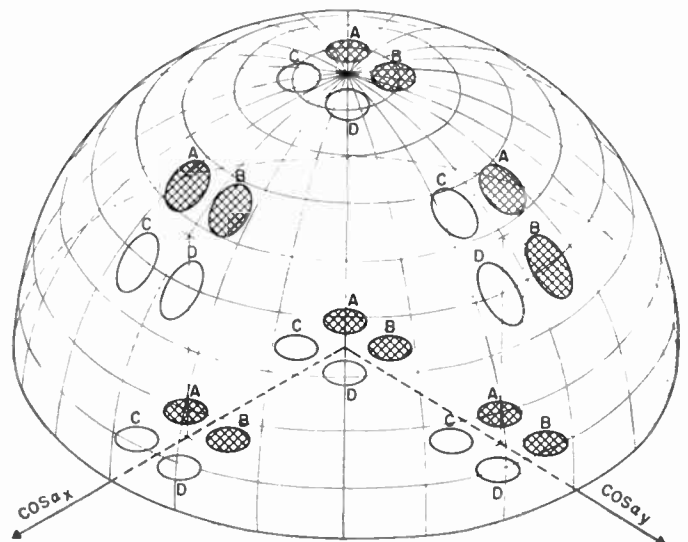


Fig. 14—Scanning of a 4-beam cluster.

IV. THE RADIATING ELEMENTS

In general, a phased array consists of identical directive radiators adjacent to a large reflecting ground plane. The pattern of such an array can be obtained by multiplying the pattern of the equivalent array of isotropic radiators  $S_a$  [see (1)] with the representative pattern of a single radiating element  $S_e$ , taking into account the effects of the ground plane and of mutual coupling between radiating elements. For the purpose of this discussion, let us assume that it is possible to find a single representative element pattern  $S_e$ . This implies that the array has many elements, thus providing a uniform environment for all elements except for a few at the very edge of the array. As the latter usually receive less illumination than the elements closer to the array center, their contribution to the over-all pattern is small.

Radiating elements assume many forms and shapes, such as dipoles, slots, open-end and tapered waveguides, polyrods, and helices. The free-space patterns of these radiators are reported in the literature and will not be discussed in detail. Rather, the requirements of an ideal radiating element will be stated, and the limitations of phased arrays will be discussed when the actual radiating elements fail to approximate this ideal.

First, the representative pattern  $S_e$  of the radiating element remains fixed in  $T$  space. It is, in effect, a window through which the scanned beam radiates into space. The ideal element factor  $S_e$  is therefore given by  $S_e = 1$  over the entire scanning area (Fig. 15) and  $S_e \leq L_s$  everywhere else ( $L_s$  is the highest acceptable sidelobe level).

Such an ideal pattern would permit scanning without introducing any additional distortion and would suppress all secondary maxima outside of the scanning area. In practical cases, the element pattern will drop from  $S_e = 1$  at  $\theta = 0$  to a prescribed value, such as  $S_e = 0.707$  (3 db), on the scanning contour. It is highly desirable to provide for a rapid decrease of  $S_e$  to 0 outside of the scanning area and for  $S_e = 0$  on the unit circle ( $\theta = 90^\circ$ ). As an example, the pattern of a half-wave dipole at a distance of  $\lambda_0/8$  from the ground plane is shown in Fig. 16.

Other radiating elements, such as horns or polyrods, can be designed to provide a better approximation to the ideal pattern. However, these radiators may not meet the fundamental requirement, namely, that their physical size permits close spacing of the radiating elements to suppress secondary maxima.

A detailed contour map of the representative pattern  $S_e$  of the array elements is required to determine the largest possible scanning contour (generally, the half-power contour) and the necessary element spacing. For example, the dipole pattern (Fig. 16) will permit scanning to  $40.5^\circ$  and  $48.5^\circ$  in  $x$  and  $y$  directions, respectively. This pattern has a sharp zero at  $\theta = 90^\circ$ . Hence, element spacing should be close to  $\lambda_0/2$  to insure that

secondary maxima stay outside the unit circle even at the largest practical scan angles.

If better radiating elements with steeper slopes of the pattern outside of the scanning area are available, the secondary maxima can be spaced closer to the main beam, thus permitting wider spacing of the radiating elements with attendant savings in hardware and circuitry. The theoretical maximum for element spacing is obtained from

$$\frac{\lambda_0}{d} = 2(\sin \theta_s + \Delta\tau). \tag{22}$$

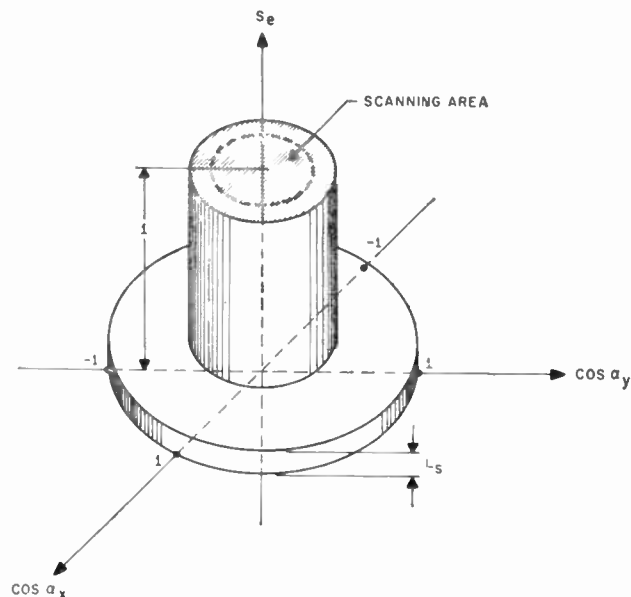


Fig. 15—Ideal element factor.

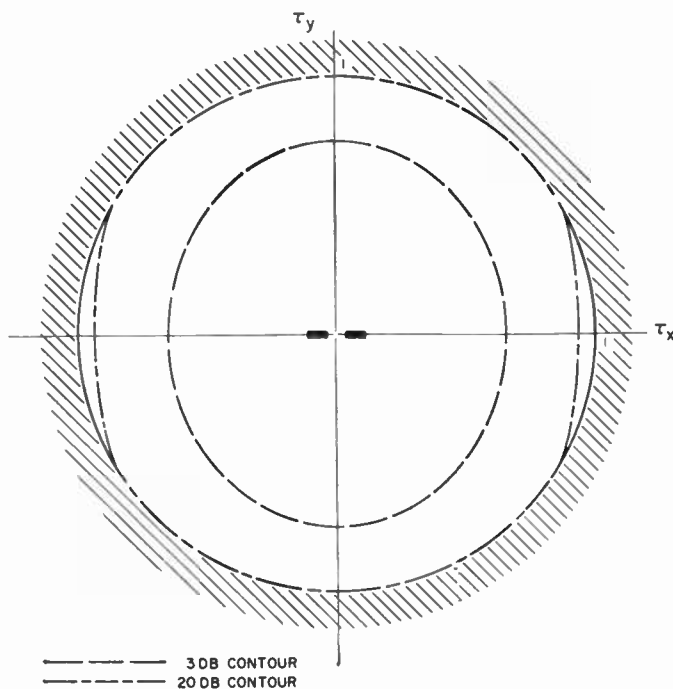


Fig. 16—Contour map of the pattern of a half-wave dipole located one-eighth wavelength above an infinite ground panel.

Hence, in special cases where only a small scan angle is desired, considerable savings can be realized by designing radiating elements which closely approximate the ideal pattern. If, for example, a  $\frac{1}{2}$ -degree beam were scanned  $\pm 15^\circ$ , the radiating elements could be spaced  $2\lambda_0$  apart, provided that the element factor  $S_e$  closely approximated Fig. 15.

For linear arrays, which are scanned in the  $x$  direction, the radiating elements determine the pattern shape in the  $y$  direction. Here, special requirements may have to be met, such as a squared cosecant pattern.

A. Correction for Beam Direction

The beam direction of an array of isotropic radiators was previously given [see (9)] as

$$\sin \theta_s e^{i\phi_s} = T_s = \frac{\psi}{d_r}$$

It can be shown that the scan angle  $T_s$  must be corrected by a small quantity  $\Delta T$  to account for the beam distortion (Fig. 17) which is introduced by the pattern  $S_e$  of the radiating elements. If  $S_e$  does not exhibit circular symmetry (e.g., if  $S_e$  is a dipole pattern of the type shown in Fig. 16), then  $\Delta T$  is a complex quantity; i.e., it contains corrections for the  $\theta$  and  $\phi$  directions. If  $S_e$  is independent of  $\phi$  or is circularly symmetric, the correction applies only to the  $\theta$  direction. Restricting this study to the latter case, let us assume scanning along the real axis, where  $T_s = \sin \theta_s$ . The radiated amplitude pattern is given by

$$S = S_a S_e \tag{23}$$

The correction for the beam maximum can be found by solving

$$\left. \frac{dS}{dT} \right|_{T=T_s-\Delta T} = 0 \tag{24}$$

for  $\Delta T$ .<sup>12</sup> To simplify computation, the logarithmic patterns  $F = \log S$ ,  $F_a = \log S_a$ , and  $F_e = \log S_e$  are introduced. Then the first derivative of (23) is

$$F'(T) = F_a'(T - T_s) + F_e'(T), \tag{25}$$

where  $T_s$  is assumed constant. Expanding the right-hand side of (25) into a power series about  $T_s$ , we can solve (24) for  $\Delta T$ ,

$$\Delta T = \frac{F_e'(T_s)}{F_a''(0) + F_e''(T_s)} \approx \frac{F_e'(T_s)}{F_a''(0)} \tag{26}$$

In general, the curvature of the element pattern  $F_e''(T_s)$  is much smaller than that of the array factor  $F_a''(0)$  and may be neglected.

<sup>12</sup> The minus sign is chosen because the expected shift of the beam maximum is toward the array normal, i.e., in the direction of decreasing  $T$ .

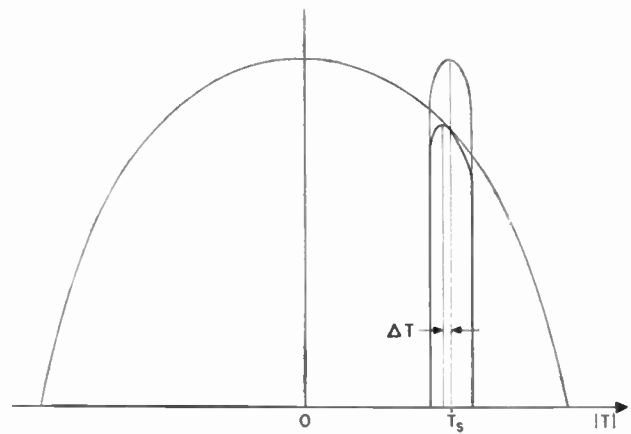


Fig. 17—Correction for beam direction of arrays consisting of directive radiators.

Thus, (26) permits ready evaluation of the correction factor  $\Delta T$  from measured or computed antenna patterns. As an example, consider an array where both the array factor and the element pattern can be approximated by  $S = (\sin x)/x$ . Using the logarithmic pattern

$$F = \log \sin x - \log x, \tag{27}$$

where  $x = Md_r T/2$ , we find

$$\frac{dF}{dT} = -\frac{1}{T} (1 - x \cot x). \tag{28}$$

$$\frac{d^2F}{dT^2} = -\frac{1}{T^2} \left[ \left( \frac{x}{\sin x} \right)^2 - 1 \right]. \tag{29}$$

Using (29) to obtain the curvature of the array factor at  $T=0$  and introducing the beamwidth  $2\Delta\tau_a$  from (6), we find that

$$F_a''(0) = -\frac{x^2}{3T^2} = -\frac{2.6}{(2\Delta\tau_a)^2} \tag{30}$$

The quantity  $F_a''(0)$  is inversely proportional to the square of the beamwidth. Using (28) to obtain the slope of the element factor at the half-power point and introducing the beamwidth  $2\Delta\tau_e$ , then

$$F_e'(T_s) = -\frac{1.5}{2\Delta\tau_e} \tag{31}$$

The slope  $F_e'$  is inversely proportional to the beamwidth. Thus the maximum correction term  $\Delta T_{\max}$ , which applies to the maximum scan angle, can be expressed in terms of array and element beamwidth,

$$\Delta T_{\max} = 0.57 \frac{(2\Delta\tau_a)^2}{2\Delta\tau_e} \tag{32}$$

For a narrow-beam array,  $\Delta T_{\max}$  is quite small and of the order of  $10^{-3}$  to  $10^{-4}$ . However,  $\Delta T_{\max}$  increases with the square of the beamwidth and cannot be ignored for phased arrays which have a relatively broad beam.

Thus, the radiating elements may introduce beam distortion, sidelobes, and a small shift in beam direc-

tion. It may be concluded that proper design of radiating elements for phased arrays is of crucial importance to insure optimum performance. Despite substantial information on free-space patterns of a large variety of radiators, there is not yet enough information on the representative patterns of such elements as part of multi-element phased arrays, and further investigations are needed.

V. ACCURACY OF PHASED ARRAYS

In this study, the accuracy of a phased array is defined as the accuracy with which the direction of the beam maximum can be determined and reproduced by measuring and adjusting the phase delay between radiating elements. Using the conventional method of expressing beam position and its accuracy, it can be stated that the radiated beam maximum is determined by the spherical coordinates  $\theta_s \pm \Delta\theta$  and  $\phi_s \pm \Delta\phi$ , with  $\Delta\theta$  and  $\Delta\phi$  designating the  $2\sigma$ -values of a normal distribution around  $\theta_s$  and  $\phi_s$ . If the antenna were mechanically scanned around two or more orthogonal shafts, it would be reasonable to give values for  $\Delta\theta$  and  $\Delta\phi$  which would apply to scanning throughout the entire hemisphere. It is readily seen, however, that no such numbers  $\Delta\theta$  and  $\Delta\phi$  can exist for phased arrays. If it can be assumed that all necessary phase delays between zero and  $\psi_{max}$  can be produced with equal accuracy, then the two direction cosines  $\cos \alpha_{xs}$  and  $\cos \alpha_{ys}$  will have constant tolerances but  $\Delta\theta$  and  $\Delta\phi$  will depend upon the scan angle  $\theta_s$ . From Section II-B, we obtain

$$d(\cos \alpha_{xs}) = \frac{1}{d_r} d\psi_x \quad d(\cos \alpha_{ys}) = \frac{1}{d_r} d\psi_y.$$

These statements can be combined into a single equation in the complex  $T$  plane,

$$dT = \frac{1}{d_r} d\psi \tag{33}$$

A small change in complex phase shift is given by

$$d\psi = |d\psi| e^{i\epsilon}. \tag{34}$$

The differential  $dT$  can be expressed as an arc  $d\gamma$  on unit sphere (Fig. 18) by rewriting it in spherical coordinates

$$dT = d(\sin \theta_s e^{i\phi_s}) = (\cos \theta_s d\theta + i \sin \theta_s d\phi) e^{i\phi_s}, \tag{35}$$

and computing  $d\theta$  and  $d\phi$

$$d\theta = \frac{\cos(\epsilon - \phi_s)}{d_r \cos \theta_s} |d\psi| \quad d\phi = \frac{\sin(\epsilon - \phi_s)}{d_r \sin \theta_s} |d\psi|. \tag{36}$$

Then the tolerance for a phased array can be stated in terms of the angle  $\Delta\gamma$ :

$$\begin{aligned} \Delta\gamma &\equiv \sqrt{(\Delta\theta)^2 + \sin^2 \theta_s (\Delta\phi)^2} \\ &= \frac{|d\psi|}{d_r} \sqrt{1 + \tan^2 \theta_s \cos^2(\epsilon - \phi_s)}. \end{aligned} \tag{37}$$

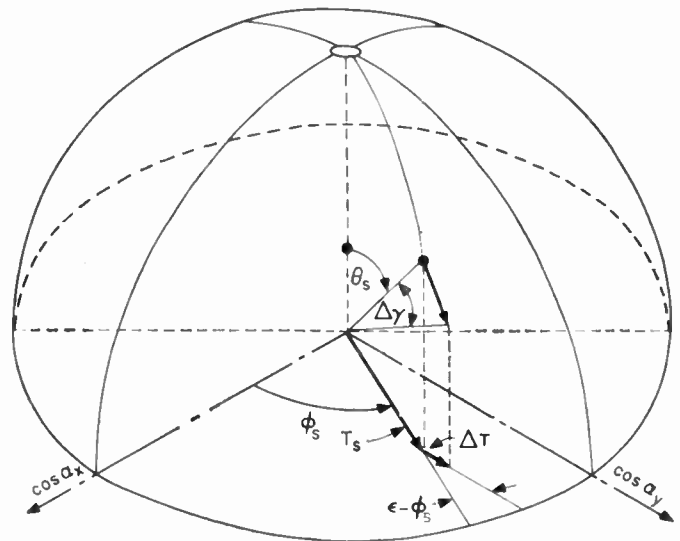


Fig. 18—Accuracy of phased arrays.

This result has the following significance:

- 1) Given a change in phase delay  $\Delta\psi$  in the  $\theta$  direction ( $\epsilon = \phi_s$ ), the beam motion is proportional to  $\Delta\psi$  in  $T$  space. Hence, for relatively small  $\theta_s$ , the tolerance  $\Delta\gamma$  is proportional to  $\Delta\psi$ . However,  $\Delta\gamma$  increases with  $\theta_s$  as  $1/\cos \theta_s$  in exactly the same way as the beam broadens (Section II-E).
- 2) Given a change in phase delay  $\Delta\psi$  in the  $\phi$  direction ( $\epsilon = \pi/2 + \phi_s$ ), the beam motion along the arc  $\Delta\gamma$  is proportional to  $\Delta\psi$  and hence independent of the scan angle  $\theta_s$ .
- 3) The tolerance  $\Delta\gamma$  is generally smaller than the tolerance  $|\Delta\psi|$  because the constant of proportionality  $1/d_r = \lambda_0/2\pi d$  is smaller than unity. For practical cases,  $\frac{1}{2} > 1/d_r > \frac{1}{10}$ ; typically,  $1/d_r = \frac{1}{4}$ . This implies that a systematic error in phase delay of, say,  $|\Delta\psi| = 1^\circ$  produces a beam-direction accuracy of the order of  $\frac{1}{4}$  degree, or less than 0.005 radian. This accuracy is not so good as that of modern, mechanically scanned antennas.

It is beyond the scope of this paper to discuss the design of accurate phased arrays, but we can point out here that the main problem appears to be the development of accurate methods to measure phase delay across the aperture of an array and of feedback and control circuitry which permits precise adjustment of phase shifters to the required values. Mechanical and electrical phase shifters are available for introducing the required phase delay.<sup>13-15</sup> Both appear to be capable of

<sup>13</sup> G. C. Southworth, "Principles and Applications of Waveguide Transmission," D. Van Nostrand Co., Inc., New York, N. Y., pp. 325-335; 1950.

<sup>14</sup> F. Reggia and E. G. Spencer, "A new technique in ferrite phase shifting for beam scanning of microwave antennas," Proc. IRE, vol. 45, pp. 1510-1517; November, 1957.

<sup>15</sup> F. E. Goodwin and H. R. Senf, "Volumetric scanning of a radar with ferrite phase shifters," Proc. IRE, vol. 47, pp. 453-454; April, 1959.

generating phase delays with an accuracy of  $|\Delta\psi| = 1^\circ$ . These phase shifters may be used in parallel and series feed structures as well as in combinations of both (Fig. 19). In a series feed, all phase shifts  $\psi_i$  are equal to  $\psi$ ; hence, programming is simple but errors in  $\psi$  show up directly as beam-direction errors. In a parallel feed,  $\psi_{i+1} - \psi_i = \psi$ ; this implies that all  $\psi_i$  are different, requiring elaborate programming, but systematic errors in  $\psi_i$  have a tendency to compensate each other, at least partially. Furthermore, phase shifters in a parallel feed can be designed with considerably lower peak-power rating than phase shifters in a series feed. Thus, each of these feeds has its own peculiar problem with respect to systematic errors, frequency dispersion, complexity, and power-handling capability.

VI. SCANNING OF PHASED ARRAYS IN A GROUND-BASED COORDINATE SYSTEM

So far, the scanning characteristics of a phased array have been described in a spherical coordinate system which is fixed with respect to the array (Fig. 1). If the array were horizontal and oriented so that its  $x$  axis pointed north and its  $y$  axis pointed west, then the same coordinate system could be used as a ground-based system and the beam position and pattern shape could be interpreted immediately in terms of the angles  $\theta$  and  $\phi$  of a ground-based coordinate system. In general, this will not be the case; the array normal will be inclined by an angle  $\theta_a$  from the vertical, and the plane of the array will not be horizontal. In fact, if the array were mounted on a ship or airplane, neither its  $x$  nor its  $y$  axis would normally be horizontal. Then the interpretation of beam direction in terms of a ground-based system would require a rotation of the array coordinate system through the Eulerian angles and a suitable coordinate transformation to find the beam direction and describe scanning distortions in a ground-based system.

This general case,<sup>16</sup> which is perfectly straightforward but somewhat involved and cumbersome, will not be treated here. But a simpler case, that of the ground-based tilted array, is given in some detail to show how its scanning performance can readily be studied by a parallel projection of a unit sphere belonging to the ground-based system on the  $T$  plane, which is fixed with respect to the array.

As an example, let the  $y$  axis of the array remain horizontal and point west. The array normal is then tilted forward through an angle  $\theta_a$  so that the normal points north (Fig. 20). The array coordinates are primed to distinguish them from the coordinates  $x, y, z$  of the ground-based system. Rotating the array in the  $xy$  plane to obtain a principal direction (that of the  $z'$  axis) different from north does not introduce any complications and therefore will not be considered.

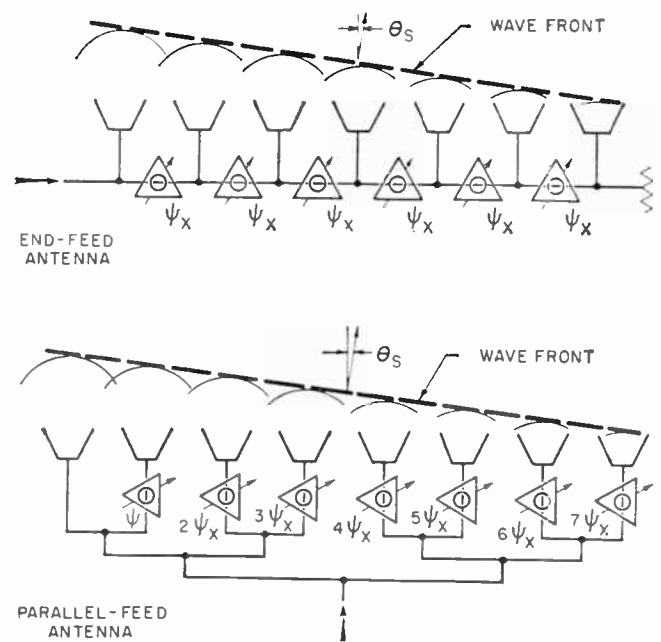


Fig. 19—Parallel-feed and series-feed antenna systems.

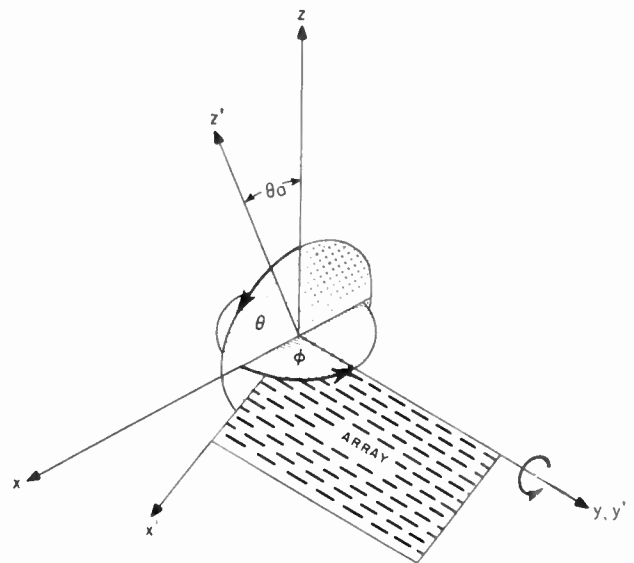


Fig. 20—Coordinate system of a tilted planar array.

Let  $\vec{x}$  and  $\vec{x}'$  be radius vectors in the ground-based and array coordinate systems, respectively:

$$\vec{x} = \begin{pmatrix} x \\ y \\ z \end{pmatrix} \quad \vec{x}' = \begin{pmatrix} x' \\ y' \\ z' \end{pmatrix}$$

Then  $\vec{x}$  and  $\vec{x}'$  are connected by the orthogonal transformations

$$\vec{x}' = \vec{A}\vec{x}, \tag{38}$$

$$\vec{x} = \vec{A}'\vec{x}'. \tag{39}$$

<sup>16</sup> H. Goldstein, "Classical Mechanics," Addison-Wesley Publishing Co., Inc., Reading, Mass., ch. 4; 1950.

where the rotation matrix  $\vec{A}$  is given by

$$\vec{A} = \begin{pmatrix} \cos \theta_a & 0 & -\sin \theta_a \\ 0 & 1 & 0 \\ \sin \theta_a & 0 & \cos \theta_a \end{pmatrix}, \quad (40)$$

and  $\vec{A}^T$  is the transpose of  $\vec{A}$ .

Two computations can be carried out, noting that on unit sphere

$$\begin{aligned} x &= \sin \theta \cos \phi &= \cos \alpha_x, \\ y &= \sin \theta \sin \phi &= \cos \alpha_y, \\ z &= \cos \theta &= \cos \alpha_z, \\ x^2 + y^2 + z^2 &= x'^2 + y'^2 + z'^2 = 1. \end{aligned} \quad (41)$$

First, for a desired beam direction  $\theta_s, \phi_s$  in the ground-based coordinate system, the required phase shift is derived immediately from (38), (41), and (8),

$$\begin{aligned} \frac{\psi_x}{d_r} &= \cos \theta_a \sin \theta_s \cos \phi_s - \sin \theta_a \cos \theta_s, \\ \frac{\psi_y}{d_r} &= \sin \theta_s \sin \phi_s. \end{aligned} \quad (42)$$

Second, a mapping of the ground-based  $\theta, \phi$  system on the  $T$  plane is obtained by expanding (39),

$$\begin{aligned} \sin \theta \cos \phi &= x' \cos \theta_a + z' \sin \theta_a, \\ \sin \theta \sin \phi &= y', \\ \cos \theta &= -x' \sin \theta_a + z' \cos \theta_a. \end{aligned} \quad (43)$$

Using (41) and rearranging terms, the equations for lines of constant longitude  $\phi$  and latitude  $\theta$  are, respectively,

$$\begin{aligned} (y' \cot \phi - x' \cos \theta_a)^2 &= (1 - x'^2 - y'^2) \sin^2 \theta_a, \quad (44) \\ (\cos \theta + x' \sin \theta_a)^2 &= (1 - x'^2 - y'^2) \cos^2 \theta_a. \quad (45) \end{aligned}$$

The latter can be rewritten to show that the lines of constant  $\theta$  are ellipses with centers on the  $x'$  axis (see Fig. 21),

$$\frac{(x' + \sin \theta_a \cos \theta)^2}{(\cos \theta_a \sin \theta)^2} + \frac{y'^2}{\sin^2 \theta} = 1. \quad (46)$$

The north pole ( $\theta=0$ ) is located at  $x' = -\sin \theta_a$ . We are interested only in that part of these ellipses which corresponds to the projection on the positive hemisphere. Hence, the intersection of these ellipses with the unit circle is located at  $x' = -\cos \theta / \sin \theta_a$ .

The lines  $\phi = \text{const}$  appear as ellipses whose main axes are rotated with respect to the  $x'$  and  $y'$  directions. By rearranging terms in (44) and applying additional algebra, the equation of an ellipse in polar form ( $x' = \rho \cos \epsilon; y' = \rho \sin \epsilon$ ) is obtained,

$$\frac{1}{\rho^2} = \frac{\cos^2(\epsilon - \epsilon_0)}{\sin^2 \theta_a \sin^2 \phi} + \sin^2(\epsilon - \epsilon_0), \quad (47)$$

in which  $\cot \epsilon_0 = -\tan \phi \cos \theta_a$ .

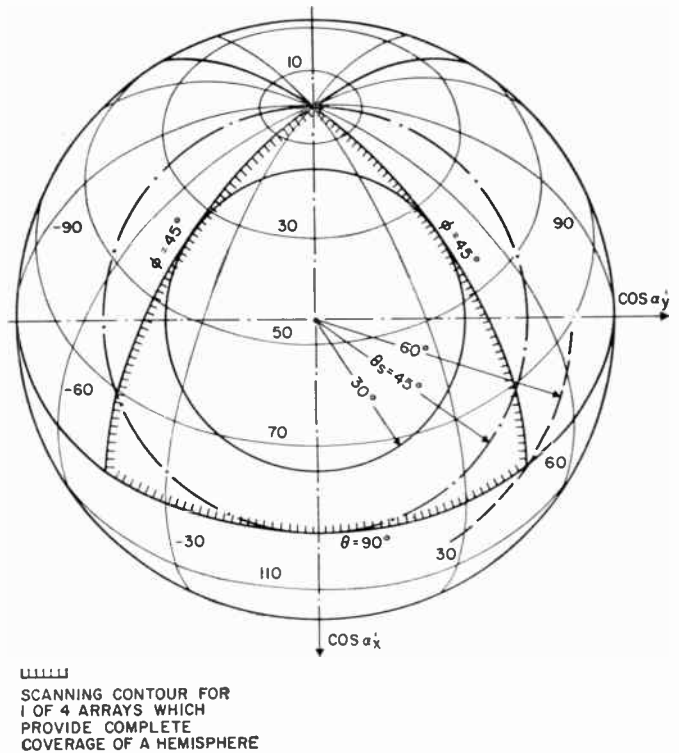


Fig. 21—Mapping of a ground-based spherical coordinate system onto the plane of an array whose normal is tilted 45° from the vertical.

The mapping given by (46) and (47) is very useful in determining the optimum tilt angle and scanning contour for a given scanning task. In general, a compromise will be needed between the scanning contour which gives the least beam distortion (see Sections II-E through II-G) and the scanning contour which provides the best coverage of the desired solid angle of the hemisphere. In the case of a phased array whose normal points straight up (Fig. 8), a circular scanning contour provides the best coverage. However, if complete coverage of a hemisphere is desired, then the scanning contours of several tilted arrays must be combined. If relatively large scanning distortions are permissible, then it is possible to cover the hemisphere with four phased arrays tilted 45° (Fig. 21). In this instance, a maximum scan angle of 45° would permit complete coverage to  $\theta = 70^\circ$ , down to 20° elevation, whereas a maximum scan angle of 60° would be required to cover all points down to zero elevation. A circular scanning contour would provide considerable overlap at the north pole. This could be avoided by suitable programming of the phased arrays to obtain triangular scanning contours.

ACKNOWLEDGMENT

The author is indebted to W. E. Danielson, J. N. Hines, and I. Jacobs for many stimulating discussions and to R. S. McCarter for his critical reading of the manuscript. Miss J. Peterson and W. Pelish were most helpful in the preparation of the figures.

# A Vacuum Evaporated Random Access Memory\*

K. D. BROADBENT†

**Summary**—The basic multiple-layer magnetic thin film structure described here has been shown to have special and desirable properties in coincident-signal switching applications such as those employed in binary random access memories. Its demonstrated advantages in this application include: 1) magnetic turnover times as low as 30m  $\mu$ sec; 2) wide latitude in selection currents, with greater than twelve-fold variations giving no appreciable change in the compensated signal-to-noise ratio of the cell's output; 3) extremely small volume of, typically, 0.025 inch  $\times$  0.010 inch  $\times$  0.0007 inch per complete cell; and 4) automated, microminiaturized production and assembly based on vapor phase handling techniques.

## INTRODUCTION

A NUMBER of applications of evaporated magnetic materials to computer memory systems have been realized;<sup>1-3</sup> however, the lack of reproducibility and uniformity in the characteristics of vacuum evaporated ferromagnetic films has in general imposed serious restrictions on attempts to use these materials as computer elements. This situation is further complicated by the difficulty experienced in sorting or selecting individual elements from within a complex deposited composite. The configuration to be described makes a minimum of stringent demands upon the evaporated magnetic material involved in a large system, but still provides a superior memory which takes advantage of vacuum processes and materials. These features are realized through the use of a complex, multiple plane, evaporated magnetic structure in conjunction with multiple evaporations of insulating and conducting materials. The approach places much of the critical emphasis in the matrix on configuration and geometry rather than on extremely uniform coercivity in the magnetic materials.

## MAGNETIC STRUCTURE AND BASIC CHARACTERISTICS

The structure employed to accomplish the selection and storage functions, within the deposited matrix, is comprised of four superimposed evaporated ferromagnetic films appropriately interlaced with evaporated selection and readout conducts. Fig. 1 is a schematic representation of the four magnetic planes as viewed in the plane of the substrate. In practice, the magnetic films which comprise these "planes" may actually be curved in some regions, but with extremely large radii

of curvature compared to their thickness. Fig. 1(a) is a view perpendicular to the quiescent direction of the magnetic vector  $M$  within the films, and Fig. 1(b) is a view in the direction of  $M$ . This schematic represents four single domain ferromagnetic films having different widths as shown in Fig. 1(a), and having equal magnetic cross sections as shown in Fig. 1(b). The scale ratio of the vertical to the horizontal dimensions has been increased several hundred times.

The four magnetic planes are disposed such that the magnetostatic energy for the over-all complex may be very high or relatively low depending upon the sense of the  $M$  vectors within the films. The lower magnetostatic energy levels, which correspond to statically stable configurations, can be obtained only with the condition that any two single domain films in Fig. 1(a) have their  $M$  vectors pointing right and the remaining two have their  $M$  vectors pointing left. Any other configuration, *i.e.*, with three or four of the  $M$  vectors pointing the same direction, results in excessively high magnetostatic energy levels which are unstable and quickly decay to the stable condition.

The difference in the widths of the various films depicted in Fig. 1(a) sets a control on the mode of decay or transition from the high to the low magnetostatic energy state. This decay will proceed by a path involving the least expenditure of energy. Because of the difference in the volume of magnetic material involved in each of the four films of Fig. 1, this minimum energy transition path is represented by the reversal of the narrowest or uppermost film which is available for reversal. To further insure this energy relationship, the lower film may be of magnetic material having a characteristically higher coercivity; however, in practice this has proved to be unnecessary.

This use of the magnetostatic energy relationships of complex magnetic structures is similar to that employed in the operation of "multiple path" ferrite devices.<sup>4-6</sup>

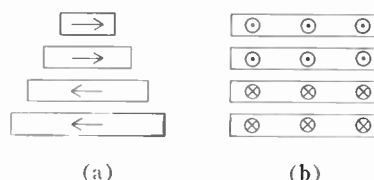


Fig. 1—Schematic representation of the four plane magnetic system. (a) End view, normal to  $M$  vector. (b) Side view, parallel to  $M$  vector.

\* Received by the IRE, November 9, 1959; revised manuscript received, May 9, 1960.

† American Systems, Inc., Inglewood, Calif. Formerly with Hughes Research Labs., Culver City, Calif.

<sup>1</sup> A. V. Pohm and S. M. Rubens, "A compact coincident-current memory," *Proc. Eastern Joint Computer Conf.*, New York, N. Y., pp. 120-123; December 10-12, 1956.

<sup>2</sup> J. I. Raffel, "Operating characteristics of a thin film memory," *J. Appl. Phys.*, vol. 30, pp. 605-615; April, 1959.

<sup>3</sup> D. O. Smith, "Thin magnetic films for digital computer memories," *Electronics*, pp. 44-45; June, 1959.

<sup>4</sup> J. A. Rajchman, "The transfluxor," *PROC. IRE*, vol. 44, pp. 321-332; March, 1956.

<sup>5</sup> L. P. Hunter and E. W. Bauer, "High speed coincident-flux magnetic storage principles," *J. Appl. Phys.*, vol. 27, pp. 1257-1261; November, 1956.

<sup>6</sup> U. F. Gianola and T. H. Crowley, "The laddic—a magnetic device for performing logic," *Bell Sys. Tech. J.*, vol. 38, pp. 45-71; January, 1959.

OPERATING MODE

A typical excursion of the four-plane magnetic complex will serve to illustrate the operating mode of this cell. Fig. 2 shows the sequence of stable states of the magnetic complex through such an excursion. The indicated magnetic coercing fields  $H$  are produced by passing current through vacuum deposited conducting sheets which enclose the top ("X winding") and next to the top ("Y winding") magnetic films. The state of the cell is indicated by the magnetic sense of the lowest film, and for the purpose of discussion will be represented as "zero" when pointing left and "one" when pointing right. The reversal of the  $M$  vector in the lower film is registered to the output circuitry by an evaporated inductive pickup loop deposited about the lower film.

Fig. 2(a) represents a stable configuration in which the  $M$  vectors of the two upper films point right and the two lower films point left. The cell is in the zero state in this figure. Fig. 2(b) shows the resulting state after driving the X select winding with a current sensed to reverse the magnetization in Film 1. Initially, such a reversal results in Film 1's complementing Film 2 to a low energy state, but leaving Films 3 and 4 in a non-

complementing configuration by reason of their parallel and similarly directed magnetizations. The resultant high energy state of these two lower films is unstable, requiring reversal of one of the films for stability to be obtained. Since the decay from the initial high energy state will proceed by a path involving a minimum energy expenditure, Film 3 will reverse, leaving Film 4 in its initial state, or from a readout standpoint, leaving the memory cell unaltered.

Fig. 2(c) shows the magnetic state resulting from driving the Y winding with a current required to reverse Film 2. Reversal of Film 2 initially places Films 1 and 2 in a high energy configuration, which by design is unstable. Decay to the equilibrium state proceeds by reversal of Film 1, since this represents the reversal involving the minimum switching of material and results in a complemented low magnetostatic energy configuration. Films 3 and 4 are not affected by this transition because of their existing mutual interaction and their longer lengths. Again, no alteration of the information content of the memory cell was accomplished. It can be seen that there now exist two essentially decoupled magnetic systems comprised of Films 1 and 2, and Films 3 and 4. Any single drive operations involving X and Y alone will affect only the system of Films 1 and 2. In order to change the state of the memory cell, that is, in order to reverse Film 4, X and Y must be driven simultaneously as shown in Fig. 2(d). This results in a high energy state of Films 1 and 2, which cannot be mutually complemented, but requires the reversal of Films 3 and 4 to provide the appropriate flux return and consequent stable low magnetostatic energy state. Thus, only with the excitation of X and Y simultaneously can the reversal of Film 4 or the lower layer be affected. This reversal represents a change of state of the memory cell from state zero to state 1.

The operational features described here provide all that is necessary to employ this memory cell in a two-dimensional random access memory. This mode of operation requires that the state of a storage site be changed only upon the simultaneous excitation of two address lines. In *single film* systems such a change is generally accomplished by a critical field threshold mechanism involving stringent material requirements as well as close control in peripheral instrumentation. No such stringent requirements are made on the material involved in this evaporated cell, but by reason of the special geometry-dependent energy characteristics, wide variation in both the coercive force of the magnetic films and the X and Y drive currents may be tolerated. Materials of a much greater latitude than the usual few per cent maximum deviation placed upon the coercivity in conventional systems may be used, and much less stringent demands are made upon peripheral equipment.

Calculations are being made of the magnetostatic energies involved in the various  $M$  configurations of this cell. The results of this work will be presented in a future paper.

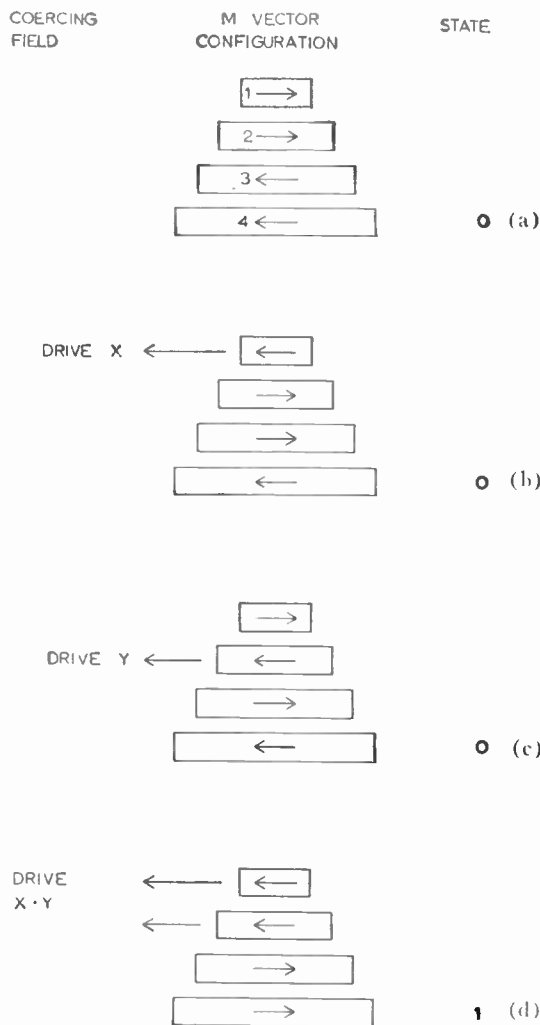


Fig. 2—A typical memory cell excursion.

CONSTRUCTION AND OPERATION

Fig. 3 is a distorted view of a section taken through a complete memory cell. For clarity, the height-to-width ratio has been increased several hundred times, and all radii of curvature have been severely reduced and distorted. The view corresponds to that of Fig. 1(a). As shown in Fig. 3, the complete cell requires 19 superimposed vacuum depositions involving insulating, conducting, and ferromagnetic materials.

Sequential vacuum evaporations such as these are performed without breaking vacuum between successive evaporations by the 21-stage mask and source changer shown in Fig. 4. This apparatus and its associated vac-

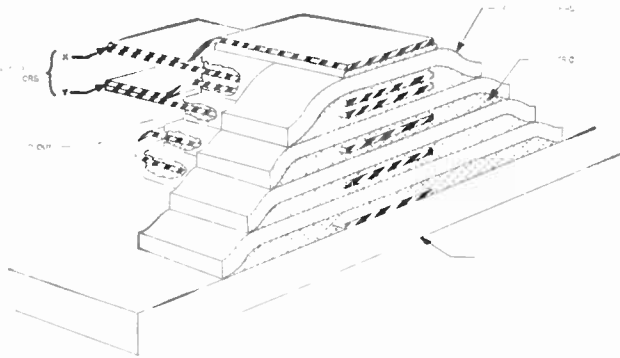


Fig. 3—Schematic section of an evaporated memory cell.

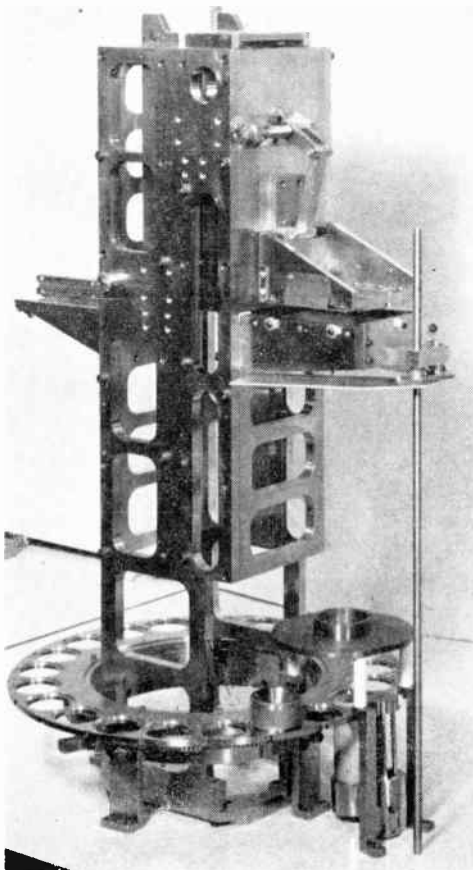


Fig. 4—21-stage mask and source changer.

uum system, including liquid nitrogen traps, allows sequential operations to be performed at pressures down to  $10^{-6}$  mm of Hg.

Fig. 5 shows oscillograms of voltages in the output circuit of an experimental evaporated memory cell of the type described. These signals were obtained using driving pulses on the *X* and *Y* windings which rose to 400 ma in  $0.1 \mu\text{sec}$ . The relatively slow rising drive signals employed here began their rise at point  $T_0$  on the time base. When the switching threshold for this cell of approximately 250 ma per select conductor was reached, the cell changed state in just under  $0.1 \mu\text{sec}$ . Using faster rising pulses and higher currents, cell reversal times as low as  $30 \text{ m}\mu\text{sec}$  have been observed. The 250-ma minimum selection current could be increased by a factor of twelve (the limit of our existing equipment) without causing any malfunction of the cell. For some applications, use of selection currents lower than 100 ma appear possible. The signals were obtained from a cell employing  $7000\text{-\AA}$  thick magnetic layers of 80 per cent Ni, 20 per cent Fe composition. The effective magnetic widths, as shown in Fig. 1(a), ranged from 0.011 inch to 0.025 inch, and the length, as shown in Fig. 1(b), was 0.200 inch. Conducting and insulating materials employed were aluminum and silicon oxide.

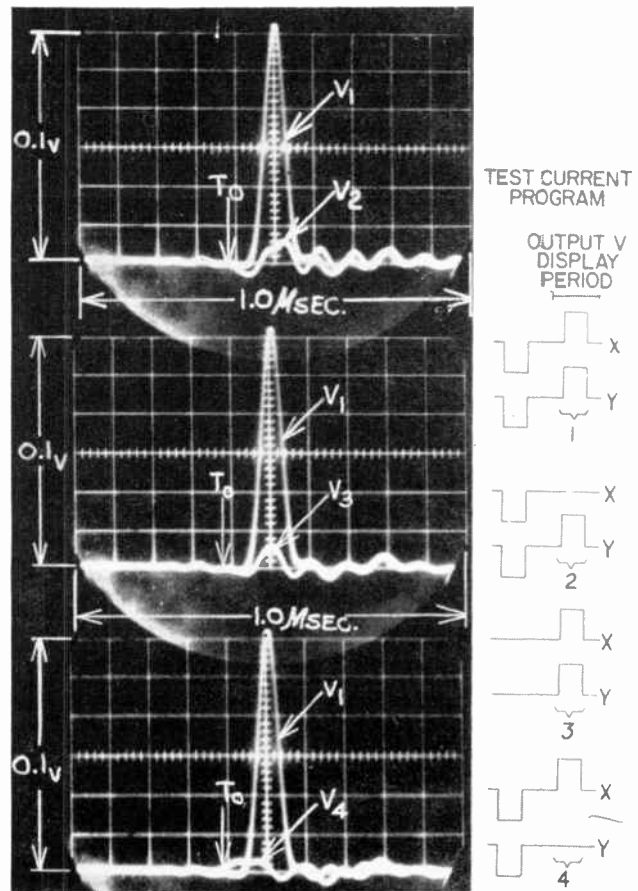


Fig. 5—Voltages in the memory cell output circuit and the associated test current program cycles.

Fig. 6 shows a random access memory matrix of one hundred sixty 0.100-inch long cells deposited on a 1 inch  $\times$  3 inch glass substrate. This matrix includes evaporated interconnected selection and readout conductors.

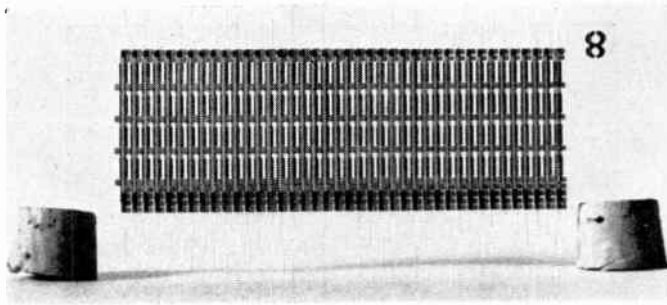


Fig. 6—A 160-bit random access memory matrix on a 3-inch by 1-inch substrate.

In applications involving large numbers of cells, a reduced cell length and reduced magnetic film thickness is used. One of the virtues of the cell is that, where desirable, thicker films and longer lengths may be employed to achieve substantial outputs, such as with the 0.200-inch cell in obtaining the voltages of Fig. 5. However, in large systems the problems of power dissipation per cell, back EMF per cell, output signal delay per

cell, and maximum storage density per surface area dictate the use of a smaller cell. Smaller size is feasible because of the vacuum techniques employed, and the use of a reacting system such as this, where flux may be switched at any location, becomes practical because of the minute amounts of magnetic material that can be employed using vacuum, vapor-phase processes.

An example of a practical reduced-size cell appears to be one having a length of 0.010 inch. Such a cell would be capable of providing several millivolts of output signal; and, considering conductor resistance and maximum back EMF on the drive line, approximately 1000 of these cells could be driven in series by a driver capable of supplying 30 volts at 0.2 a. The delay per bit in getting the read signal out of such an array, using straightforward series techniques, would be less than 0.05  $\mu$ sec per bit (based on analysis of the evaporated structure's transmission line characteristics). These numbers are based on existing cells and materials. A shortening of the cells in the transverse direction and an improvement in magnetic material characteristics would allow a further reduction in power requirements.

#### ACKNOWLEDGMENT

Special credit is due C. R. Pearce, M. Braunstein, and A. L. Berg, who contributed greatly to the development of this device.

## Shot and Thermal Noise in Germanium and Silicon Transistors at High-Level Current Injections\*

B. SCHNEIDER† AND M. J. O. STRUTT†, FELLOW, IRE

**Summary**—In previous papers, shot noise of germanium junction  $p$ - $n$  diodes and transistors was calculated and measured as dependent on frequency at small current densities, where good coincidence was obtained. At high current densities, when the density of minority carriers becomes comparable with the density of dotation, measured shot noise was higher than calculated values. In later papers, shot noise in silicon junction diodes and transistors was calculated and measured at small current densities, again obtaining good coincidence. In the present paper, the case of shot noise at high current densities is tackled for the first time, obtaining formulas in good agreement with experimental values. The crux of the new theory is the introduction of an equivalent circuit for  $p$ - $n$  junctions, containing an inductance besides resistances and capacitances.

\* Received by the IRE, January 4, 1960. This work was supported by the Swiss Federal Fund for the Advancement of Economy by Scientific Research.

† Dept. Adv. Elec. Engrg., Swiss Federal Institute of Technology, Zurich, Switzerland.

#### I. INTRODUCTION

A THEORY of shot and thermal noise of germanium  $p$ - $n$  diodes and of germanium junction transistors has been published and was found to be in satisfactory agreement with experimental values<sup>1-4</sup> at sufficiently small current densities. In the case of silicon diodes and transistors this theory had to

<sup>1</sup> W. Guggenbuehl and M. J. O. Strutt, "Theory and experiments on shot noise in semiconductor junction diodes and transistors," *PROC. IRE*, vol. 45, pp. 839-854; May, 1957.

<sup>2</sup> A. van der Ziel, "Shot noise in junction diodes and transistors," *PROC. IRE*, vol. 43, pp. 1639-1646; November, 1955.

<sup>3</sup> A. van der Ziel, "Shot noise in junction diodes and transistors," *PROC. IRE*, vol. 45, p. 1011; July, 1957.

<sup>4</sup> A. van der Ziel, "Noise in junction transistors," *PROC. IRE*, vol. 46, pp. 1019-1038; June, 1958.

be extended, in order to account for the influence of carrier generation and recombination in the depletion layer on the noise values.<sup>5,6</sup> When this generation-recombination noise was taken into account, satisfactory agreement with experimental values was also obtained in these cases,<sup>5,7,8</sup> when the current densities were sufficiently small.

At higher current densities, appreciable deviations of experimental from the said theoretical values occur. These deviations may be easily observed with transistors<sup>1</sup> and are due to high level injection. High level injection occurs when the density of injected minority carriers in a  $p$ - $n$  junction becomes equal to or larger than the density of dotation. This paper is devoted to the case of high level injection noise, which is narrowly connected with the fact that  $p$ - $n$  junctions then become inductive.

The mean square noise current of Germanium junction diodes is at small current densities represented by<sup>1,2</sup>

$$\bar{i}_n^2 = [4kT \operatorname{Re}(Y) - 2qI] \Delta f \quad (1)$$

This equation may be adapted to the case of silicon junction diodes, if the shot noise, represented by the second expression in brackets, is divided by the factor  $m$ , which accounts for the recombination-generation in the depletion layer.<sup>5,8</sup> It is relatively difficult to obtain satisfactory figures, showing the deviation of experimental values from (1) at high level injection, as the impedance of the junction decreases at increasing current density. Thus, the impedances of the  $p$ -region and of the  $n$ -region become relatively more important. At the same time, flicker noise, which is approximately proportional to the square of the forward current, makes itself increasingly apparent and renders the exact determination of shot and thermal noise sources increasingly difficult.

With junction transistors, conditions are more favorable. The noise figure  $F$  of germanium transistors for the grounded base and grounded emitter connections may be obtained from

$$4kTR_0F = 2qI_c \left| \frac{R_b + Z_0 + \frac{1}{y_{11}}}{\alpha_{fb}} \right|^2 - 2qI_E |R_b + Z_0|^2, \quad (2)$$

at small current densities.<sup>1</sup> With silicon transistors, generation-recombination in the space charge layer

may be accounted for by division of the second right-hand term of (2) by  $m_E$ .<sup>5,8</sup>

Fig. 1 shows typical deviations of measured noise figures at high current densities from those, calculated by (2), with germanium transistors of alloyed type. The deviations are small at low frequencies, if the decrease of  $y_{110}$  at high current densities as compared with the value  $qI_E/kT$  is taken into account. The experimental increase of  $F$  at higher frequencies begins earlier at high current densities than is obtained from (2). The deviations between (2) and experimental values are considerable at higher frequencies.

The ac current amplification factor  $\alpha_{fb}$  of transistors at high level injection shows a dependence on frequency which is different from the case of low level injection. Fig. 2 shows measured values of  $|\alpha_{fb}|$  at two current values with a germanium  $p$ - $n$ - $p$  transistor of alloyed type. The value  $I_E = 0.5$  ma is still in the low level region, but the value  $I_E = 4.0$  ma is certainly in the high level region. At high level injection  $|\alpha_{fb}|$  remains equal to its low frequency value  $\alpha_{fb0}$  up to much higher frequencies and then drops much more steeply. The differences between  $\alpha_{fb}$ -curves at low level and at high level injection are not always as pronounced as in Fig. 2. The general behavior of this Fig. 2 could, however, be observed with all transistors measured. The cut off frequency  $f_{ob}$  of the grounded base connection (see Fig. 2) remains practically equal at low and at high level injection.

## II. EQUIVALENT CIRCUIT OF JUNCTION DIODES AT HIGH LEVEL INJECTION

Experimental investigations have shown that the impedance of  $p$ - $n$  diodes at sufficiently high forward currents always turns inductive.<sup>9,10</sup> This behavior has not yet been satisfactorily investigated theoretically. The reason for this is that the system of differential equations, arising from the current and continuity equations for electrons and holes, has as yet only been solved under special assumptions. In some papers<sup>11-13</sup> the dc solution for special  $p$ - $n$  junctions is treated. The most important result of these papers is, in our case, that the ac differential resistance of the junction at high level injection becomes larger than the theoretical value at low level injection, which is  $kT/qI$ .

<sup>9</sup> T. Einsele, "Ueber die Tragheit des Flussleitwertes von Germanium-dioden," *Z. angew. Phys.*, vol. 4, pp. 183-185; May, 1952. (In German.)

<sup>10</sup> G. Kohn and W. Nonnenmacher, "Induktives Verhalten von  $p$ - $n$ -Uebergängen in Flussrichtung," *Arch. elektr. Übertragung*, vol. 8, pp. 561-564; December, 1954. (In German.)

<sup>11</sup> A. Herlet, "Das Verhalten von  $p$ - $n$ -Gleichrichtern bei hohen Durchlassbelastungen," *Z. Naturforsch.*, vol. 11a, pp. 498-510; June, 1956. (In German.)

<sup>12</sup> W. Guggenbuehl, M. J. O. Strutt, and W. Wunderlin, "Halbleiter-Kontaktgeräte," vol. 1, Birkhäuser, Bäle, Switzerland, to be published in 1960. (In German.)

<sup>13</sup> C. T. Sah, R. N. Noyce, and W. Shockley, "Carrier generation and recombination in  $p$ - $n$  junctions and  $p$ - $n$  junction characteristics," *Proc. IRE*, vol. 45, pp. 1228-1243; September, 1957.

<sup>5</sup> B. Schneider and M. J. O. Strutt, "Theory and experiments on shot noise in silicon  $p$ - $n$  junction diodes and transistors," *Proc. IRE*, vol. 47, pp. 564-554; April, 1959.

<sup>6</sup> A van der Ziel, "Shot noise in transistors," *Proc. IRE*, vol. 48, pp. 114-115; January, 1960.

<sup>7</sup> E. R. Chenette, "Frequency dependence of the noise and the current amplification factor of silicon transistors," *Proc. IRE*, vol. 48, pp. 111-112; January, 1960.

<sup>8</sup> B. Schneider, "Ueber einige spezielle Probleme beim Rauschen von Halbleiterdioden und Transistoren," M.S. thesis, Swiss Federal Institute of Technology, Zurich, Switzerland, nr. 2985; 1959. (In German.)

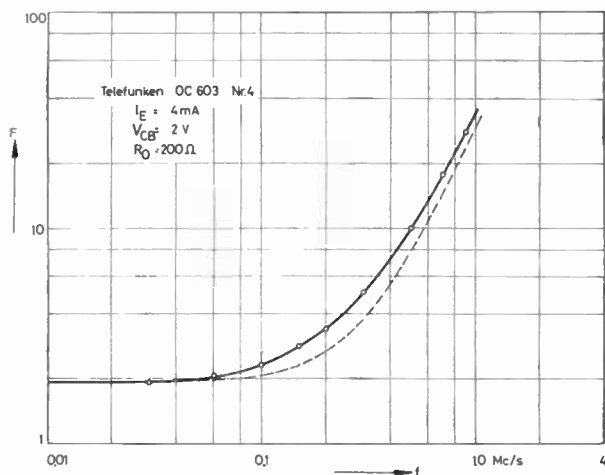


Fig. 1—Values of noise figure  $F$  as dependent on frequency for a germanium transistor in grounded base connection (Telefunken, type OC 603, with  $\alpha_{f,0} = 0.980$ ,  $R = 59$  ohms,  $1/y_{110} = 6.5$  ohms). Broken curve—calculated according to (2). Full curve—measured.

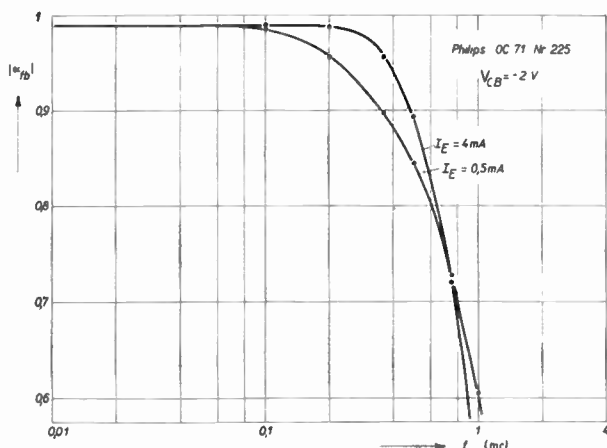


Fig. 2—Measured values of  $\alpha_f$  as dependent on frequency for a germanium  $p-n-p$  transistor.

The only ac solution of the said differential equations at high level injection is given by E. Spenke.<sup>14</sup> This solution, however, pertains to the case of a completely symmetrical diode, which is of little practical importance. Of special interest is the development of the border case at low frequencies from the formal complete solution using Bessel functions. Spenke successfully makes use of the equivalent circuit at high level injection, which was derived by G. Kohn and W. Nonnenmacher<sup>10</sup> from their measurements. The equivalent circuit of a  $p-n$  contact of considerable asymmetry, in which the resistance of the strongly doted semiconductor region is negligible with regard to that of the less doted semiconductor region on the other side of the space charge layer, is shown in Fig. 3. Measurements with strongly asymmetrical germanium junction diodes have confirmed this equivalent circuit.

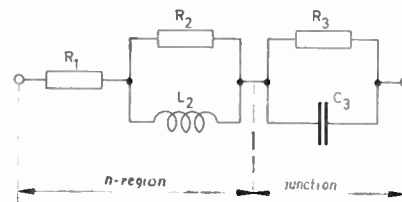


Fig. 3—Equivalent circuit of a strongly unsymmetrical  $p-n$  junction diode at high current densities. The dotation of the  $p$ -region is considerably higher than that of the  $n$ -region.  $C_3 \approx C_D$  is approximately equal to the diffusion capacity.

Fig. 4(a) and (b) show the real and the imaginary parts respectively of the impedance of a specially manufactured germanium diode (from Telefunken Company, Inc.) as dependent on frequency. The data and dimensions of this diode are shown in Fig. 5. The five elements of the equivalent circuit of Fig. 3 may be best determined from four points of the curve of Fig. 4(b) and from one additional point of the curve of Fig. 4(a). The elements of the equivalent circuit, calculated in this way, are shown in the following table for three different current values of the diode of Fig. 4(a) and (b).

According to Spenke<sup>14</sup> the time constant  $\tau_2 = L_2/R_2$  of a symmetrical diode should be independent of the forward current. Table I shows that this property holds also with an asymmetrical diode. If the equations of Spenke are used for the calculation of the elements of the equivalent circuit, the resulting values show bad coincidence with those of Table I. The measured values of  $\tau_2$  are independent of the current. The corresponding calculated value of  $\tau_2$  is  $2 \mu s$ , and this does not deviate very strongly from the measured values. As, however, the theory was derived for symmetrical diodes, these deviations are not unexpected.

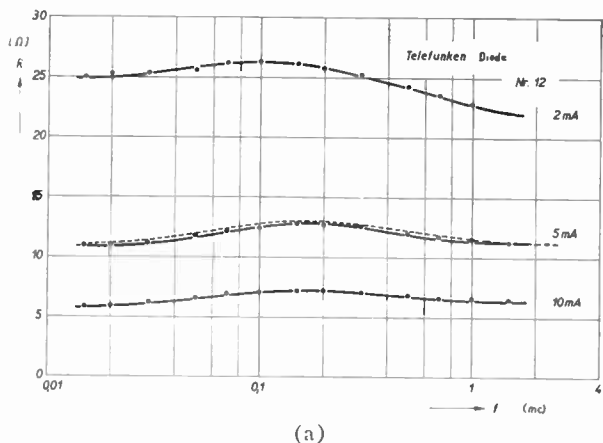
### III. NOISE OF DIODES AT HIGH LEVEL CURRENT INJECTION

The equivalent noise circuit of diodes at high level injection is shown in Fig. 6, in accordance with Section II. The noise voltage source  $u_n$  corresponds to the noise contribution of the semiconductor region of low dotation outside the space charge layer, the equivalent circuit elements of which are  $R_1$ ,  $R_2$  and  $L_2$ . W. Guggenbuehl<sup>15</sup> has shown that the noise of nondegenerated semiconductors, through which a current flows, is only negligibly different from Nyquist noise. Therefore, we may assume thermal noise for the above semiconductor region, the impedance  $Z_B$  of which becomes increasingly important as compared with the impedance of the junction at increasing forward current:

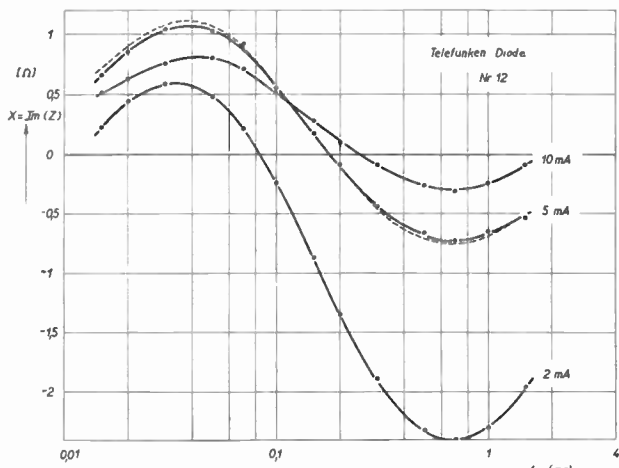
$$\overline{u_n^2} = 4kT \operatorname{Re}(Z_B)\Delta f. \quad (3)$$

<sup>14</sup> E. Spenke, "Das induktive Verhalten von  $p-n$  Gleichrichtern bei starken Durchlassbelastungen," *Z. angew. Phys.*, vol. 10, pp. 65-88; February, 1958. (In German.)

<sup>15</sup> W. Guggenbuehl, "Beiträge zur Kenntnis des Halbleiterrauschens mit besonderer Berücksichtigung von Kristalldioden und Transistoren," M.S. thesis, Swiss Federal Institute of Technology, Zürich, Switzerland, nr. 2515; 1955. (In German.)



(a)



(b)

Fig. 4—(a) Measured (full curves) and calculated (broken curves) values of the real part of the complex impedance of an unsymmetrical germanium diode as dependent on frequency. Length of *n*-region outside the junction is *b* = 250 microns (see Fig. 5). (b) The imaginary part of the impedance. The full curves correspond to measured values. The broken curves are calculated, using the equivalent circuit of Fig. 3 and the values of Table I.

The noise of the junction of impedance  $Z_J$  is accounted for in Fig. 6 by the noise current source  $i_n$ . The question as to whether and how the junction noise at high current densities deviates from (1) has been treated only tentatively up to the present. A. van der Ziel,<sup>4</sup> expects a considerable space charge outside the junction, caused by the injected carriers. This space charge would result in a certain correlation between the carriers at their entrance into the junction. The supposition was put forward by Guggenbuehl and Strutt<sup>1</sup> that the number of carriers drawn into the junction might be influenced by voltage variations, which were caused by variations of the carrier concentration outside the junction. In both cases the shot noise term (second right hand term) of (1) would decrease, thus causing an increased total mean square noise current of the diode.

In all previous papers on high level injection the assumption has been that complete neutrality of charge, or at least a very small space charge as compared with the density of dotation, occurs in the regions outside the junction. Following this notion, we shall base this paper on the assumption that the said decrease of shot

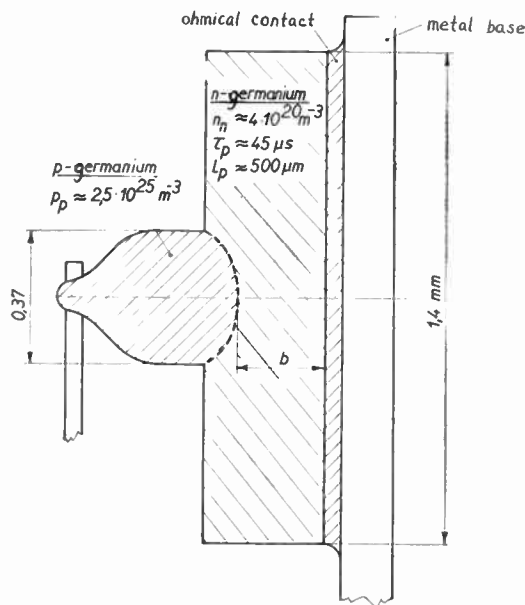


Fig. 5—Dimensions and data of germanium junction diode, specially manufactured by the Telefunken Company, Uhm, Germany (Dr. W. Engbert).

TABLE I

Element of Equivalent Circuit	Diode Current			
	2	5	10	ma
$R_1$	19.7	8.7	4.8	$\Omega$
$R_2$	1.7	2.6	1.8	$\Omega$
$L_2$	5.8	9.2	6.3	$\mu H$
$R_3$	5.1	1.9	0.85	$\Omega$
$C_3$	0.058	0.17	0.37	$\mu F$
$\tau_2$	3.37	3.55	3.45	$\mu s$

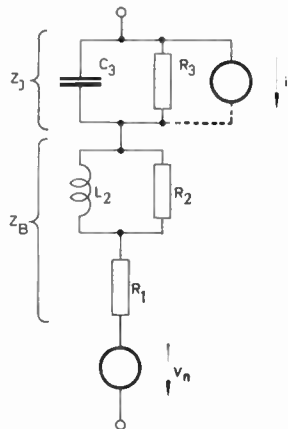


Fig. 6—Equivalent noise circuit of strongly unsymmetrical *p-n* junction diodes at high current densities.

noise is negligible with respect to the over-all noise. Hence, the noise source has a mean square noise current

$$\overline{i_n^2} = 4kT \operatorname{Re}(Y_J)\Delta f - 2qI\Delta f. \quad (4)$$

The experimental determination of the junction noise at high current densities, *i.e.*, of the noise current  $i_n$  of (4), is rather difficult, due to flicker noise, which makes itself felt even with selected junction diodes.

The measurements of diode noise of Fig. 7 were carried out using a set-up which was described in a previous paper.<sup>5</sup> The resulting measured absolute values of the impedance of the junctions of the two germanium diodes drop to about 0.5 ohm at frequencies above 0.5 mc. The noise of the junction is hence negligible with respect to total noise. Thus, these measurements confirm the assumption that the regions outside the junction contribute pure Nyquist noise. Due to flicker noise, it is not possible to draw valid conclusions as to the noise of the junctions.

IV. EQUIVALENT CIRCUIT OF JUNCTION TRANSISTORS AT HIGH LEVEL INJECTION

No papers have hitherto been published on high level injection behavior of transistors with a view to deduce their corresponding noise. The relative minority carrier density as compared with the density of dotation approaches unity and higher values primarily in the base region, if the emitter current is increased. Hence, this base region primarily determines the high level injection properties of transistors. If the Shockley theory is assumed to be valid for the emitter and collector junction, the boundary conditions for the theory of the base region are given. However, the theory of high level injection conditions is very difficult and has hitherto only been approached under very simplified conditions.<sup>12,16,17</sup> Especially, no papers are available treating the ac case.

As a starting point for the practical treatment of the high level injection properties of transistors we shall use the frequency dependence of the ac current amplification factor  $\alpha_{fb}$ . The frequency dependence of  $\alpha_{fb}$  at high current densities according to Section I (Fig. 2) may be understood from the equivalent  $y$ -circuit of the intrinsic transistor in grounded base connection (Fig. 8). The difference from the corresponding equivalent circuit at low level injection manifests itself in the representation of  $y_{11}$  by four frequency independent elements. Of these,  $R_3$  corresponds to the resistance and  $C_3$  to the diffusion capacitance of the emitter junction at low level injection. The ohmic resistance  $R_2$  and the inductance  $L_2$  may be similarly accounted for as the impedance of the region outside the junction of a diode at high forward current (see Fig. 3). The seat of  $R_2$  and  $L_2$  is in the base region. The capacitance  $C_3$  is not in parallel to the emitter resistance  $R_3$ . It is shunted to the intrinsic base connection. The reason for this is as follows.

We consider a slight increase of emitter current with a  $p-n-p$  transistor of alloyed type at high current densities. Some of the holes, which have passed the emitter junction, must be stored in the base region as a result of this current increase. The charge neutrality is re-

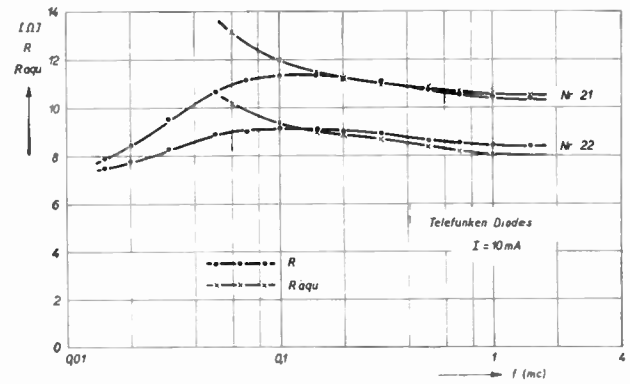


Fig. 7—Measured curves for the equivalent noise resistance (crosses) and for the real part of the impedance (circles) of germanium diodes as dependent on frequency. Data of the diodes as in Fig. 5. Length  $b$  of  $n$ -region is 500 microns.

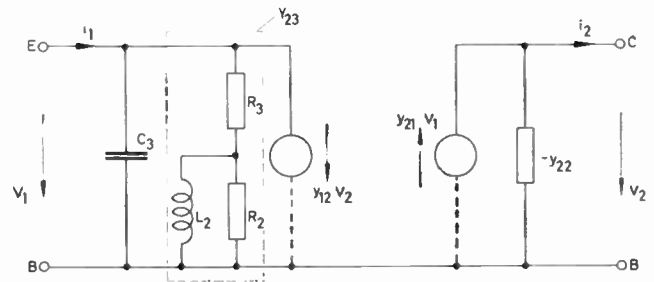


Fig. 8—Equivalent circuit of intrinsic junction transistors in grounded base connection at high current densities.

stored by a corresponding electron current, which flows from the base contact into this region. These carrier motions result in the capacitance  $C_3$ . The part of the emitter current, which reaches the collector junction, flows transversely to the above electron current. As the base region is represented by  $R_2$  and  $L_2$ , the series connection with  $R_3$  may be understood.

The most important result of the equivalent circuit of Fig. 8 resides in the fact that only a part of the capacitive storage current has to be delivered by the emitter input current. This is due to the said inductance  $L_2$ . The current flowing through  $R_3$  is transferred to the output. This output current, at ac short circuit, is

$$i_2 = \alpha_{fb0} Y_{23} v_1. \tag{5}$$

The ac current amplification factor  $\alpha_{fb0}$  at LF accounts for the emitter efficiency and for the recombination in the base region. By (5) and  $i_1 = y_{11} v_1$ , the current amplification factors become

$$\alpha_{fb} \approx \frac{i_2}{i_1} = \alpha_{fb0} \frac{Y_{23}}{y_{11}}. \tag{6}$$

Introducing the time constants,

$$\tau_2 = \frac{L_2}{R_2} \quad \text{and} \quad \tau_3 = R_3 C_3, \tag{7}$$

<sup>16</sup> E. S. Rittner, "Extension of the theory of the junction transistor," *Phys. Rev.* vol. 94, pp. 1161-1171; June, 1954.

<sup>17</sup> K. E. Mortenson, "High-level transistor operation and transport capacitance," *IRE TRANS. ON ELECTRON DEVICES*, vol. ED-6, pp. 174-189; April, 1959.

the amount of  $\alpha_{fb}$  may be written as

$$|\alpha_{fb}| = \alpha_{fb0} \left[ \left( 1 - \frac{R_2}{R_3} \frac{\omega^2 \tau_2 \tau_3}{1 + \omega^2 \tau_2^2} \right)^2 + \omega^2 \tau_3^2 \left( 1 + \frac{R_2}{R_3} \frac{\omega^2 \tau_2^2}{1 + \omega^2 \tau_2^2} \right)^2 \right]^{-1/2} \quad (8)$$

From the measured curve of  $|\alpha_{fb}|$  as dependent on frequency the values of  $R_2/R_3$ ,  $\tau_2$  and  $\tau_3$  may be determined. This determination requires the solution of a system of equations of higher order, which leads to complicated formulas. It is therefore preferable to seek an approximation to this solution by means of an equivalent circuit, serving as an analog computer, which is shown in Fig. 9.

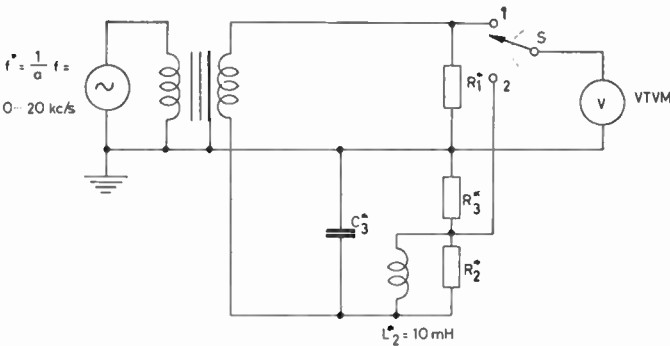


Fig. 9—Analog computer circuit for the determination of  $y_{11}$  of junction transistors at high current densities.  $R_1^*$ ,  $R_2^*$  and  $R_3^*$  are precision resistance decades of small inductance.  $C_3^*$  is a precision capacitance decade. The transformer is screened and of General Radio type 578 A. The resistances  $R_1^*$  and  $R_3^*$  are always made equal. Furthermore,  $R_2^* = L_2^*/a\tau_2$ ,  $R_3^* = R_2^*R_3/R_2$ , and  $\tau_3 = C_3^*R_3^*/a$ .

In order to facilitate the application of this computer circuit, the frequency is divided by  $a$ , and a fixed inductance  $L_2^*$  is used instead of  $L_2$ . These simplifications are made possible by the fact that only the ratio  $R_2/R_3$  and the time constants  $\tau_2$  and  $\tau_3$  have to be determined and not the values of  $R_2$ ,  $L_2$ ,  $R_3$  and  $C_3$  separately.

The effective values of the ac through  $R_2^*$  and  $R_3^*$  (Fig. 9) are indicated by  $I_1^*$  and  $I_3^*$  respectively. The effective values of  $i_1$  and  $i_2$  of Fig. 8 are indicated by  $I_1$  and  $I_2$  respectively. Then we may deduce from (6) and from the relationship  $|y_{11}| = I_1/V_1$ ,

$$\frac{|\alpha_{fb}|}{\alpha_{fb0}} = \frac{|Y_{23}|}{|y_{11}|} = \frac{|Y_{23}| V_1}{I_1} = \frac{I_3^*}{I_1^*} \quad (9)$$

As the resistances  $R_1^*$  and  $R_3^*$  are of equal value, the ratio of the voltages at the switch positions 2 and 1 is equal to the ratio

$$|\alpha_{fb}| / \alpha_{fb0}$$

By a suitable choice of  $R_2/R_3$  and of  $\tau_2$ , the values  $R_2^*$  and  $R_3^* = R_1^*$  of the computer circuit are given. The capacitance  $C_3^*$  is adjusted so as to make the current amplification factor, obtained from the computer, coincident with the measured value of  $|\alpha_{fb}|/\alpha_{fb0}$  of the

transistor in question in the vicinity of the cut off frequency. If this is accomplished, the frequency curve of  $|\alpha_{fb}|$  obtained from the computer circuit in general shows deviations from the measured curve of the transistor. This means that the values of  $R_2/R_3$  and of  $\tau_2$  have to be corrected, in order to obtain a better approximation. By applying this procedure three to ten times, if necessary, a set of values  $R_2/R_3$ ,  $\tau_2$  and  $\tau_3$  may be obtained, which gives close coincidence between the measured  $|\alpha_{fb}|$ -curve of the transistor and the corresponding curve of the computer circuit. As an example, Fig. 10 shows the measured curve of  $|\alpha_{fb}|$  for a germanium  $p-n-p$  transistor of alloyed type together with the corresponding curve, obtained from the computer circuit.

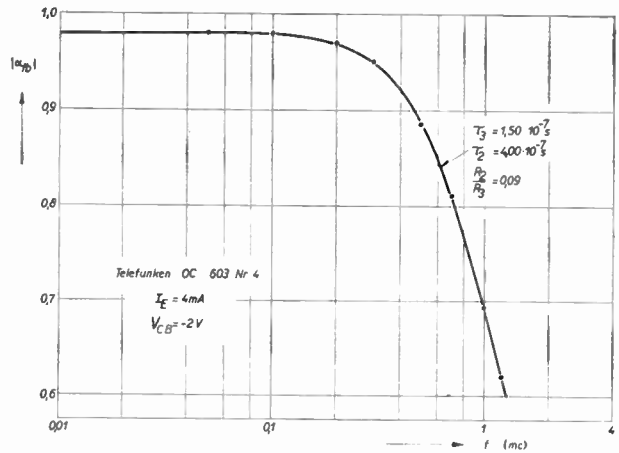


Fig. 10—Measured points of  $|\alpha_{fb}|$  as dependent on frequency for a germanium transistor of Telefunken type OC 603. The full curve was obtained by the equivalent circuit of Fig. 8, using the values shown here. The values of  $\tau_2$ ,  $\tau_3$ , and  $R_2/R_3$  were obtained by the use of the analog computer circuit of Fig. 9.

The absolute values of the equivalent transistor circuit (Fig. 8) elements  $R_2$ ,  $L_2$ ,  $R_3$  and  $C_3$  cannot be obtained from the measured  $|\alpha_{fb}|$ -curve. By the application of a further experiment, yielding, e.g. the input impedance  $h_{11}$  of the transistor at shorted output, the above values may be determined. In the grounded base connection,  $h_{11}$  is approximately given by

$$h_{11} \approx h_{11}' + R_b(1 - h_{21}'). \quad (10)$$

The measured curve of  $h_{11}$  as dependent on frequency yields, therefore, approximately the value of  $R_b$ , if the frequency  $f$  is large compared with the cut off frequency  $f_{ab}$ , i.e.,  $h_{21}' \approx 0$ . If  $R_b$  is known, we may also determine the low frequency value of  $h_{11}'$ , assuming  $h_{21}' \approx \alpha_{fb}$ . According to the equivalent circuit of Fig. 8 the value of  $h_{11}'$  at low frequencies coincides with  $R_2$ .

#### V. NOISE OF JUNCTION TRANSISTORS AT HIGH LEVEL CURRENT INJECTION

Under equal assumptions as for junction diodes at high current densities, i.e., Nyquist noise in the regions outside the junctions and complete shot noise of the junctions, we obtain the equivalent noise circuit of Fig. 11 for junction transistors at a grounded base connec-

tion. The two noise current sources  $i_{n2}$  and  $i_{n3}$  correspond to the emitter diode and are given by

$$\overline{i_{n2}^2} = 4kT \operatorname{Re}(Y_2)\Delta f, \tag{11}$$

$$\overline{i_{n3}^2} = 4kT \frac{1}{R_3} \Delta f - 2qI_E \Delta f, \tag{12}$$

if the admittance  $Y_2$  indicates the parallel connection of  $R_2$  and  $L_2$ . These two noise current sources are supposed to be uncorrelated. A single noise current source  $i_{ne}$  connected in parallel to  $y_{11}$  may be substituted for both of them,

$$i_{ne} = y_{11} \frac{i_{n3}R_3 + i_{n2}Z_2}{1 + j\omega C_3 Z_2}. \tag{13}$$

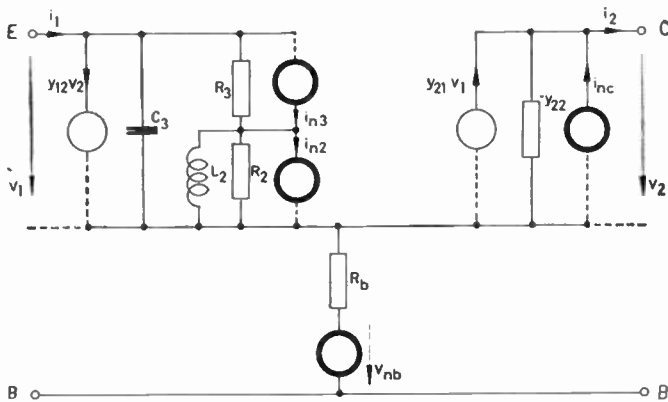


Fig. 11—Equivalent noise circuit of junction transistors in grounded base connection at high current densities.

This equation, taking into account (6) and the relation  $y_{11} = Y_{23} + j\omega C_3$ , yields

$$i_{ne} = \frac{\alpha_{fb}}{\alpha_{fb0}} y_{11}(i_{n3}R_3 + i_{n2}Z_2). \tag{14}$$

The base lead resistance contributes Nyquist noise, as previously, and the noise of the collector diode is represented by a noise current source according to (1). [See Guggenbuehl and Strutt<sup>1</sup> and van der Ziel.] We obtain

$$\overline{v_{nb}^2} = 4kTR_b\Delta f; \tag{15}$$

$$\overline{i_{nc}^2} = 2qI_C\Delta f - 4kT \operatorname{Re}(y_{22})\Delta f. \tag{16}$$

The derivation of an equation for the correlation between  $i_{nc}$  and  $i_{ne}$  may be carried out similarly as in Guggenbuehl and Strutt.<sup>1</sup> We obtain

$$\overline{i_{nc}^* i_{ne}} = 2kT(y_{21} - y_{12}^*)\Delta f. \tag{17}$$

For the calculation of the noise figure  $F$  we connect a source impedance  $Z_0$  to the input terminals of Fig. 11 and in series to this impedance the noise voltage source,

$$\overline{v_{n0}^2} = 4kT \operatorname{Re}(Z_0)\Delta f.$$

As  $F$  is independent of the impedance connected to the output terminals, we may apply a short-circuit to these.

Furthermore, we assume

$$|y_{11}| \gg |y_{12}|, \quad |v_{21}| \gg |y_{22}|, \quad |y_{22}R_b| \ll 1. \tag{18}$$

The noise figure for the grounded base and the grounded emitter connections is then given by

$$4kTR_0F = 2qI_C \left| \frac{1}{y_{11} + R_b + Z_0} \right|^2 - 2qI_E |R_b + Z_0|^2 R_3^2 |Y_{23}|^2, \tag{19}$$

where

$$R_3^2 |Y_{23}|^2 = \frac{1 + \omega^2\tau_2^2}{1 + \omega^2\tau_2^2 \left(1 + \frac{R_2}{R_3}\right)^2}. \tag{20}$$

The formal difference between (19) and (2) at low current densities consists in the multiplication of the second right-hand term by  $R_3^2 |Y_{23}|^2$ . The frequency curve of this multiplier at  $R_2/R_3 = 0.5$  is shown in Fig. 12 as an example.

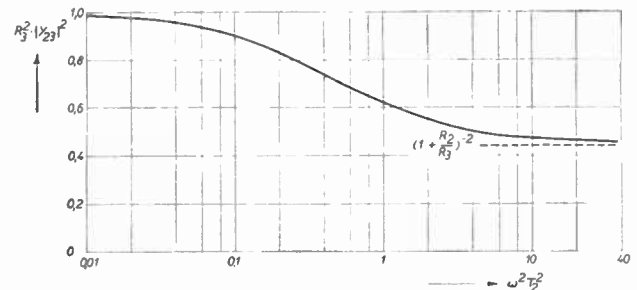


Fig. 12—Multiplier  $R_3^2 |Y_{23}|^2$  of eq. (19) as dependent on  $\omega^2\tau_2^2$ . The asymptotic value corresponding to  $\omega\tau_2 \rightarrow \infty$  is shown by a broken line.

As long as we stay within the frequency-independent region of the  $y_{11}$ -curve; i.e., if  $R_3^2 |Y_{23}|^2 = 1$ , (19) is identical with (2). The low-frequency value of  $F$ , barring flicker noise, is indicated by  $F_0$ . The value of  $F_0$  at high current densities differs from the corresponding value at low current densities by the fact that  $y_{11}$  is smaller than  $qI_E/kT$  in the former case, whereas  $y_{11}$  is equal to this value in the latter case. The multiplier  $R_3^2 |Y_{23}|^2$  causes an increase of  $F$  at increasing frequency, even if  $\alpha_{fb}$  is still independent of frequency. The influence of  $R_3^2 |Y_{23}|^2$  is weakened at frequencies above the cut off frequency, as the second right-hand term of (19) does not affect  $F$  strongly in this range.

In order to check the validity of the equivalent noise circuit of Fig. 11 and of (19), measurements were carried out using germanium and silicon transistors of alloyed type and of small flicker noise. The setup has been described earlier.<sup>18</sup> At low current densities,  $I_E$ ,

<sup>18</sup> W. Guggenbuehl, B. Schneider, and M. J. O. Strutt, "Messungen ueber das Hochfrequenzrauschen von Transistoren," *Nachrichtentech Fachberichte*, vol. 5, pp. 34-36; 1956. (In German.)

$I_C$ ,  $R_b$ ,  $1/y_{11}$ , and  $\alpha_{fb}$  are required for the calculation of the noise figure  $F$ . At high current densities,  $\tau_2$  and  $R_2/R_3$  are also required. The latter quantities have been determined as described in the preceding section.

As examples of these measurements, Fig. 13 shows the measured and the calculated curve of  $F$  as dependent on frequency for a germanium transistor. The  $F$ -values, obtained by the new formula, (19), which is valid at high current densities, are in satisfactory agreement with the experimental values. Especially, the experimental increase of  $F$  at higher frequencies, which is different at high current densities from the increase at low current densities, is checked very well by the new theory. The emitter current density of the transistor of Fig. 13 is  $1.1 \text{ A/cm}^2$  at  $I_E = 2 \text{ ma}$ .

From measurements and calculations of  $F$  which have been quoted, and from other analogous ones, the following trend may be stated. The calculated values of  $F$  in the frequency range, where  $F$  is independent of frequency, are often somewhat larger than the experimental values, if the calculations are based on the experimental value of  $1/y_{110} = R_3$ . Due to the base lead resistance it is rather difficult to determine  $1/y_{110}$  with a better accuracy than within about  $\pm 10$  per cent, as the base lead resistance is usually large compared with  $1/y_{110}$ . The said discrepancy is slight only at values of the input source resistance  $R_0$  above 200 ohms. It cannot be explained by an eventual space-charge noise suppression at the emitter diode. This would cause a decrease of the second right-hand term of (19);  $F$  would therefore be increased. Thus, an eventual discrepancy between experiment and calculation would also be increased.

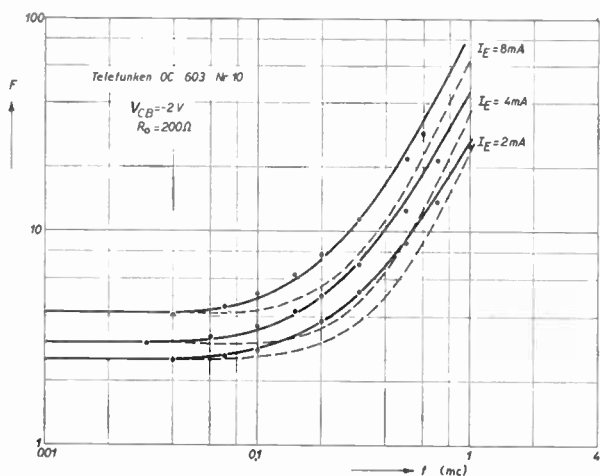


Fig. 13—Noise figure  $F$  as dependent on frequency for a germanium  $p-n-p$  transistor. The emitter current  $I_E$  is used as a parameter for the separate curves. Full curves are calculated by (19). Broken curves are calculated by (2). Points are measured values. The values underlying the calculations are shown in the table.

$I_E$ ma	$I_C$ ma	$\alpha_{fb0}$	$R_b$ ohm	$R_2/R_3$	$\tau_2$ $\mu\text{s}$	$\tau_3$ $\mu\text{s}$	$1/y_{110}$ ohm
2	1.978	0.983	165	0.10	0.30	0.130	12.5
4	3.943	0.980	150	0.18	0.22	0.125	6.0
8	7.848	0.976	134	0.25	0.15	0.139	2.7

The noise behavior of transistors hence confirms the assumption of Section III, according to which the shot noise term of (1) with diodes is not appreciably influenced at higher current densities.

Some noise curves of silicon transistors at high current densities are shown in Fig. 14. A value  $I_E = 0.2 \text{ ma}$  of the type OC 470 still lies within the low current density range. The experimental values are not very different from the values, calculated by taking into account recombination and generation of carriers in the emitter space charge layer.<sup>5</sup> At high current densities, recombination and generation may be neglected ( $m_E = 1.01$ ). In principle, this silicon transistor shows a similar behavior to the behavior of germanium transistors. The coincidence between theory and experiments at high current densities seems to be worse. The reason for this may be found in the difficulties of the determination of several quantities entering (19), due to the high base lead resistance. Thereby the accuracy of the calculated curves is appreciably lower in Fig. 14 than with corresponding germanium transistors.

LIST OF SYMBOLS

- $a$  = factor for reduction of frequency in analog computer.
- $b$  = length of the  $p$ - or  $n$ -region in diodes.
- $C_3$  = total capacitance in the equivalent circuit of diodes and transistors at high level injection.
- $f_{ab}$  = cut off frequency of the ac amplification factor of transistors in grounded base connection ( $f$  for  $\alpha_{fb} = \alpha_{fb0}/\sqrt{2}$ ).
- $F_0$  = LF noise figure without flicker noise.

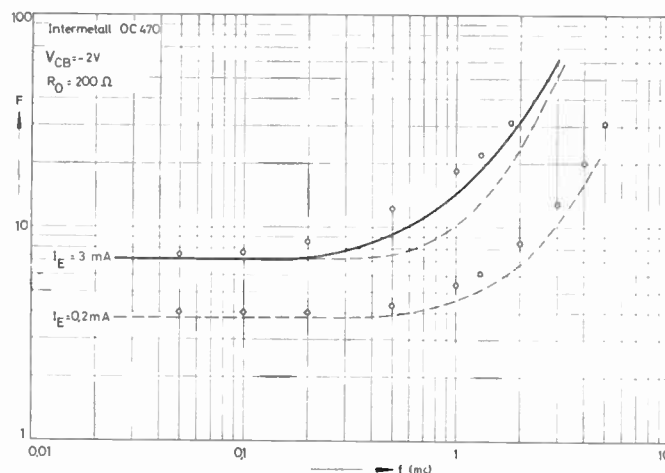


Fig. 14—Noise figure  $F$  as dependent on frequency for a silicon  $p-n-p$  transistor of alloyed type. Curves are indicated as in Fig. 13.

- $I_E = 0.2 \text{ ma}$ :  
 $R_b = 320 \text{ ohms}$ ,  
 $\alpha_{fb0} = 0.962$ ,  
 $m_E = 1.07$ ;
- $I_E = 3 \text{ ma}$ :  
 $R_b = 220 \text{ ohms}$   
 $\alpha_{fb0} = 0.957$ ,  
 $m_E = 1.01$ ,  
 $\tau_2 = 0.1 \mu\text{s}$ ,  
 $\tau_3 = 0.0435 \mu\text{s}$ ,  
 $R_2/R_3 = 0.15$ .

$h_{11}, \dots, h_{22}$  =  $h$ -parameters of the nonintrinsic transistor in grounded base connection.  
 $h_{11}', \dots, h_{22}'$  =  $h$ -parameters of the intrinsic transistor in grounded base connection.  
 $i_{nc}$  = noise current of the collector diode.  
 $i_{ne}$  = noise current of the emitter diode.  
 $i_{n2}, i_{n3}$  = noise currents of the emitter diode at high level injection.  
 $I$  = total current in a  $p$ - $n$  junction.  
 $I_C$  = collector current.  
 $I_E$  = emitter current.  
 $L_2$  = inductance in the equivalent circuit of diodes and transistors at high level injection.  
 $m_E$  = multiplication factor of the emitter junction in silicon transistors, accounting for generation-recombination of carriers in space charge layer.  
 $R = \text{Re}(Z)$  = total resistance of a  $p$ - $n$  junction.  
 $R_b$  = base lead resistance.  
 $R_{nq}$  = equivalent noise resistance.  
 $R_0 = \text{Re}(Z_0)$  = source resistance.  
 $R_1, R_2, R_3$  = resistances of the equivalent circuit of diodes and transistors at high level injection.  
 $v_n$  = noise voltage.  
 $y_{11}, \dots, y_{22}$  =  $y$ -parameters of the intrinsic transistor in grounded base connection.

$y_{110}$  = LF input admittance of the intrinsic transistor at shorted output.  
 $Y = 1/Z$  = total admittance of a  $p$ - $n$  junction.  
 $Y_J = 1/Z_J$  = diffusion admittance.  
 $Y_2 = 1/Z_2$  = admittance of the parallel connection of  $R_2$  and  $L_2$ .  
 $Y_{23} = 1/Z_{23}$  = admittance of the series connection of  $Z_2$  and  $R_3$ .  
 $Z_B$  = impedance of the  $p$ - and  $n$ -region.  
 $Z_0$  = source impedance.  
 $\alpha_{fb}$  = ac current amplification factor in grounded base connection.  
 $\alpha_{fb0}$  = LF ac current amplification factor.  
 $\tau_2 = L_2/R_2$  = time constant of the parallel connection of  $R_2$  and  $L_2$ .  
 $\tau_3 = R_3C_3$  = time constant of the parallel connection of  $R_3$  and  $C_3$ .

#### ACKNOWLEDGMENT

The authors take pleasure in expressing their thanks for the support of the Swiss Federal Fund for the Advancement of Economy by Scientific Research.

The diode measurements of Sections II and III were made possible by the use of junction diodes, especially manufactured for us by the Telefunken Company at Ulm, Germany. The authors express their thanks to Dr. W. Engbert and to the said company for this kindness.

## Analytical Studies on Effects of Surface Recombination on the Current Amplification Factor of Alloy Junction and Surface Barrier Transistors\*

T. SUGANO† AND H. YANAI†, MEMBER, IRE

**Summary**—The survival factor of minority carriers is one of the important factors which determine the current amplification factor of a junction transistor, and is generally known to be much more affected by the surface recombination of the minority carriers than by the volume recombination in the base region. It is therefore quite necessary in the design of transistors to get an expression of the survival factor  $\beta$  in terms of the surface recombination velocity, the dimensions of the emitter and the collector electrodes, and the thickness of the base region.

Because of the complexity of their geometries, however, analytical expressions of  $\beta$  have not yet been obtained for alloy junction and other similar types of transistors.

In this paper, analytical formulas for various idealized geometries are derived by means of approximating methods. From these results,

many useful design data such as the optimum radius ratio of the emitter electrode and the collector are obtained and the effect of curvature of the electrode surfaces is made clear. It is also pointed out that the survival factor can be expressed by four dimensionless quantities, thus establishing the principle of similitude among transistors having different surface recombination velocities and different geometrical dimensions of electrodes.

The values of  $\beta$  calculated from these formulas are in good agreement with the experimental values previously obtained by Stripp and Moore from an analogy of three-dimensional electrolytic conductance.

#### I. INTRODUCTION

IN designing the junction transistor, the consideration on the alpha cutoff frequency and the emitter current dependency of current amplification factor are different, whether the transistor is a high frequency

\* Received by the IRE, August 25, 1959; revised manuscript received, May 17, 1960.

† Faculty of Engrg., University of Tokyo, Japan.

device or a high power device, but in all cases it is desirable that the survival factor of minority carriers  $\beta$  be nearly equal to unity.

And  $\beta$  is generally known to be much more affected by the surface recombination of the minority carriers rather than by the volume recombination in the base region.<sup>1,2</sup> Therefore,  $\beta$  is closely related to the surface recombination velocity and the geometry of the electrodes, and it has become known empirically that it is desirable that the radii of the emitter electrode and the collector be much larger than the thickness of the base region and that the area of collector be made twice as large as that of the emitter for the case of alloy junction transistors.

On the other hand, theoretically, Rittner<sup>1</sup> made the analysis for grown junction transistors and estimated the effect of surface recombinations on the current amplification factor, but for alloy junction transistors only experiments by an electric analog method<sup>2,3</sup> were carried out because of the complexity of their geometries.

However, the results of the experiments are not universal; *i.e.*, the experiments must be repeated whenever the geometries of electrodes are altered, and the magnitudes of influences of each factor cannot be estimated easily. Therefore, we have made an analysis for alloy junction transistors by approximating methods and have obtained analytical formulas.

In our equations,  $\beta$  is expressed in terms of the geometrical dimensions of the electrodes and the surface recombination velocity; and the optimum emitter radius, when the base thickness and the collector radius are given, is determined. Also it is pointed out that the principle of similitude among transistors having different surface recombination velocities and geometrical dimensions of electrodes is established, and that this is convenient in order to understand systematically the current amplification factor experimentally obtained from various transistors.

Experimental verification of the analytical formulas has not been attempted because of the difficulty of measuring the surface recombination velocities of completely assembled alloy junction transistors, but the values of  $\beta$  calculated from the formulas are in good accordance with the experimental values previously obtained by Stripp and Moore<sup>3</sup> from an analogy of three-dimensional electrolytic conductance.

## II. PRESUPPOSITION OF ANALYSIS AND APPROXIMATING METHOD<sup>4</sup>

Recently some experiments to make uniform planar

<sup>1</sup> E. S. Rittner, "Extension of the theory of the junction transistors," *Phys. Rev.*, vol. 94, pp. 1161-1171; June, 1954.

<sup>2</sup> A. R. Moore and J. I. Pankove, "The effect of junction shape and surface recombination on transistor current gain," *PROC. IRE*, vol. 42, pp. 907-913; June, 1954.

<sup>3</sup> K. F. Stripp and A. R. Moore, "The effect of junction shape and surface recombination on transistor current gain—part 2," *PROC. IRE*, vol. 43, pp. 856-866; July, 1955.

<sup>4</sup> Hereafter, we will consider only *p-n-p* transistors for simplicity. For *n-p-n* transistors, only the symbol must be changed.

alloy junctions have been attempted, but generally it is characteristic of alloy junction transistors that the junction surfaces are curved and that the radii of the emitter and of the collector are different. Consequently, it is desirable for  $\beta$  to be calculated for arbitrary electrode constructions such as the one illustrated in Fig. 1(a); unfortunately, it is too complicated to analyze.

Therefore, in this paper two ideal cases are treated and a real construction is approximated by them. The first case is of the planar collectors such as illustrated in Fig. 1(b) and 1(c), and the second is of the emitter and collector with apparently equal radii such as in Fig. 1(d). The former resembles a transistor with a planar collector or with a slightly curved collector; the latter resembles a transistor with a heavily curved collector of diameter nearly equal to that of emitter.

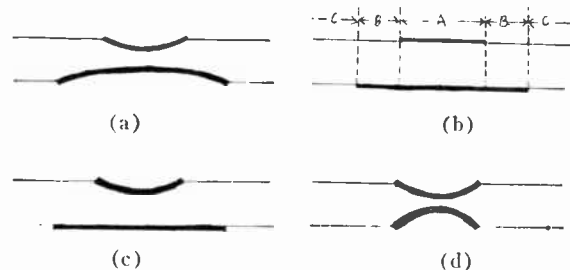


Fig. 1—Idealized electrode constructions of alloy junction and surface barrier transistors.

The process of calculation is as follows: the curved surfaces of electrodes are approximated by the coordinate surface of a prolate spheroidal coordinate; the base region of a transistor is divided into three regions; and in each region the hole distribution is solved under the proper boundary conditions.

The region under the emitter junction is named the *A* region. The region in which the emitter side is the free base surface and the collector side is the collector junction, is called the *B* region. The residual region, in which both sides are free base surfaces, is the *C* region.

In *A* region the hole distribution is assumed to be of one dimension. The assumption is comparatively reasonable, because the radii of junctions are much larger than the base width, and the survival factor of minority carriers is approximately equal to unity. At the boundaries between *A* and *B* regions, and *B* and *C* regions the hole density distribution is connected continuously.

For simplicity, the transistor in the low injection level is treated. Therefore, the equation determining the hole distribution in these regions is the diffusion equation in the steady state.

$$\nabla^2 p - \frac{p - p_0}{L_p^2} = 0 \quad (1)$$

where  $p$  is the hole density in the base region,  $p_0$  is the equilibrium hole density in the base region and  $L_p$  is the diffusion length of holes.

The boundary condition is as follows:

- 1) The hole density at the emitter junction is a constant value, *i.e.*, a self-bias cutoff effect is neglected.
- 2) The hole density at the collector junction is a thermal equilibrium value.<sup>5</sup>
- 3) The surface recombination current density is proportional to the hole density on the free base surface.
- 4) The hole density far from the emitter and collector is the equilibrium value.<sup>6</sup>

After the hole density distribution in each region is solved, the desired emitter current  $I_e$  and surface recombination current  $I_s$  are obtained from the surface integrals of the solution, *i.e.*,

$$I_e = qD_p \int |\nabla p| d\sigma \text{—over emitter junction surface, (2)}$$

$$I_s = qS \int (p - p_0) d\sigma \text{—over free base surface, (3)}$$

where  $q$  is the charge of a hole,  $D_p$  is the diffusion constant of a hole,  $S$  is the surface recombination velocity and  $d\sigma$  is the area element.

Then  $\beta$  is given by

$$1 - \beta = I_s/I_e,$$

for the volume recombination current is much smaller than the surface recombination current.

### III. THE DERIVATION OF ANALYTICAL FORMULAS OF $\beta$

According to the above-mentioned approximating method,  $\beta$  of the transistor with geometries of electrodes illustrated in Fig. 1, is calculated as follows, under the condition

$$\frac{a}{W'} > 1, \quad \frac{SW'}{D_p} \ll 1, \quad (4)$$

where  $a$  is the emitter cross-sectional radius and  $W$  is the wafer thickness.

$$A_m = \frac{2(p_1 - p_0) \left( \frac{1}{L_p} \sin \theta_m \cosh \frac{W'}{L_p} - \frac{\theta_m}{W'} \cosh \theta_m \sinh \frac{W'}{L_p} \right)}{\left( \frac{\theta_m^2}{W'^2} + \frac{1}{L_p^2} \right) \frac{W'}{\theta_m} \left( \theta_m - \frac{1}{2} \sin 2\theta_m \right) \sinh \frac{W'}{L_p} K_0 \left( \sqrt{\frac{\theta_m^2}{W'^2} + \frac{1}{L_p^2}} a \right)}, \quad (8)$$

<sup>5</sup> Speaking exactly, the hole density on the base side of the collector junction is much smaller than the equilibrium value, because the collector junction is reversely biased. But the emitter current is proportional to the gradient of hole density in the base region, and the hole density at the emitter junction is much greater than that at the collector. Therefore the error resulting from the above mentioned assumption is small and negligible, and the analysis is much simplified.

<sup>6</sup> Speaking exactly, this condition is not to be used at the calculation of the hole distribution in the *B* region. However, its use is equivalent to neglecting the end effect, and it greatly simplifies the calculation, so the condition is used at the calculation in the *B* region.

#### A. The Case of the Planar Electrode Construction, Illustrated in Fig. 1(b)

Taking the cylindrical coordinate as shown in Fig. 2,

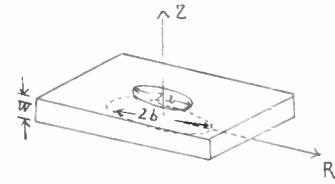


Fig. 2—Setting of the coordinate in the case of the planar electrode construction.

the origin of which is at the center of the collector, and the approximating method mentioned in Section II, we find that the hole density distributions in the *A*, *B* and *C* regions are given by (5), (6), and (7), respectively.

$$p - p_0 = (p_1 - p_0) \frac{\sinh \frac{Z}{L_p}}{\sinh \frac{W}{L_p}}, \quad (5)$$

where  $p_1$  is the hole density at the emitter junction, and  $Z$  is the axial coordinate.

$$p - p_0 = \sum_{m=1}^{\infty} A_m \sin \left( \theta_m \frac{Z}{W'} \right) K_0 \left( \sqrt{\frac{\theta_m^2}{W'^2} + \frac{1}{L_p^2}} R \right), \quad (6)$$

where  $R$  is the radial coordinate.  $\theta_m$  is the  $n$ th root of (7)

$$\theta_m \cos \theta_m + \frac{SW'}{D_p} \sin \theta_m = 0. \quad (7)$$

Also

where  $K_0$  is the second kind modified Bessel function of the zero order.

$$p - p_0 = \sum_{n=0}^{\infty} B_n \left\{ \sin \left( \phi_n \frac{Z}{W'} \right) + \frac{D_p}{SW'} \phi_n \cos \left( \phi_n \frac{Z}{W'} \right) \right\} K_0 \left( \sqrt{\frac{\phi_n^2}{W'^2} + \frac{1}{L_p^2}} R \right), \quad (9)$$

where  $\phi_n$  is the  $n$ th root of

$$2\phi_n \cos \phi_n - \left( \frac{D_p}{SW} \phi_n - \frac{SW}{D_p} \right) \sin \phi_n = 0. \quad (10)$$

Now  $B_n$ , when it is rigorously determined under the boundary condition in Section II that the hole density distribution at the boundary between  $B$  and  $C$  regions is connected continuously, is expressed by the double series of  $m$  and  $n$ , and it is very complicated.

We therefore determine  $B_n$  by using the approximated hole density distribution in the region where  $R$  is equal to  $b$ , which is the collector cross-sectional radius.

Because  $A_m$  is determined under the boundary conditions that the hole density distribution at the boundary between  $A$  and  $B$  regions is connected continuously, in one case, in which  $a$  is nearly equal to  $b$ , the hole density distribution is reasonably approximated by the following, because it is nearly equal to (5):

$$p - p_0 = (p_1 - p_0) \frac{Z}{W} \frac{K_0 \left( \sqrt{\frac{\theta_1^2}{W^2} + \frac{1}{L_p^2}} b \right)}{K_0 \left( \sqrt{\frac{\theta_1^2}{W^2} + \frac{1}{L_p^2}} a \right)}; \quad (11)$$

and in another case, in which  $a$  is much smaller than  $b$ , by the following, because the first term of (6) predominates over the succeeding terms:

$$p - p_0 = 2(p_1 - p_0) \frac{\sin \left( \theta_1 \frac{Z}{W} \right)}{\theta_1^2} \frac{K_0 \left( \sqrt{\frac{\theta_1^2}{W^2} + \frac{1}{L_p^2}} b \right)}{K_0 \left( \sqrt{\frac{\theta_1^2}{W^2} + \frac{1}{L_p^2}} a \right)}. \quad (12)$$

Then,  $B_n^{(1)}$  which is  $B_n$  determined by using (11), is given by

$$B_n^{(1)} = \frac{2(p_1 - p_0) \left\{ \frac{1}{\phi_n} \left( \frac{\sin \phi_n}{\phi_n} - \cos \phi_n \right) + \frac{D_p}{SW} \left( \sin \phi_n - \frac{1 - \cos \phi_n}{\phi_n} \right) K_0 \left( \sqrt{\frac{\theta_1^2}{W^2} + \frac{1}{L_p^2}} b \right) \right\}}{\left[ \left\{ 1 + \left( \frac{D_p}{SW} \right)^2 \right\} - \frac{D_p}{2SW} (\cos 2\phi_n - 1) \right] K_0 \left( \sqrt{\frac{\theta_1^2}{W^2} + \frac{1}{L_p^2}} a \right) K_0 \left( \sqrt{\frac{\theta_1^2}{W^2} + \frac{1}{L_p^2}} b \right)} \quad (13)$$

and  $B_n^{(2)}$ , which is  $B_n$  determined by using (12), by

$$B_n^{(2)} = \frac{2(p_1 - p_0) \left[ \frac{\sin(\theta_1 - \phi_n)}{\theta_1 - \phi_n} - \frac{\sin(\theta_1 + \phi_n)}{\theta_1 + \phi_n} + \frac{D_p}{SW} \phi_n \left\{ \frac{1 - \cos(\theta_1 + \phi_n)}{\theta_1 + \phi_n} + \frac{1 - \cos(\theta_1 - \phi_n)}{\theta_1 - \phi_n} \right\} \right] K_0 \left( \sqrt{\frac{\theta_1^2}{W^2} + \frac{1}{L_p^2}} b \right)}{\theta_1^2 \left[ \left\{ 1 + \left( \frac{D_p}{SW} \right)^2 \right\} - \frac{\sin \phi_n}{2\phi_n} \left\{ 1 - \left( \frac{D_p}{SW} \phi_n \right)^2 \right\} - \frac{D_p}{2SW} (\cos 2\phi_n - 1) \right] K_0 \left( \sqrt{\frac{\theta_1^2}{W^2} + \frac{1}{L_p^2}} a \right) K_0 \left( \sqrt{\frac{\theta_1^2}{W^2} + \frac{1}{L_p^2}} b \right)}. \quad (14)$$

Now the hole density distribution is determined and currents are derived from them, that is to say, the emitter current  $I_e$  is derived by means of (2):

$$I_e = \frac{\pi a^2 q D_p}{L_p} (p_1 - p_0) \coth \frac{W}{L_p}, \quad (15)$$

and the surface recombination current  $I_s$  by means of (3):

$$I_s = I_{seB} + I_{sec} + I_{sc}, \quad (16)$$

where

$$I_{seB} = 2\pi q S \sum_{m=1}^{\infty} A_m \frac{\sin \theta_m}{\sqrt{\frac{\theta_m^2}{W^2} + \frac{1}{L_p^2}}} \cdot \left\{ a K_1 \left( \sqrt{\frac{\theta_m^2}{W^2} + \frac{1}{L_p^2}} a \right) - b K_1 \left( \sqrt{\frac{\theta_m^2}{W^2} + \frac{1}{L_p^2}} b \right) \right\}, \quad (17)$$

$$I_{sec} = 2\pi q S \sum_{n=0}^{\infty} B_n \left( \sin \phi_n + \frac{D_p}{SW} \phi_n \cos \phi_n \right) \cdot \frac{b}{\sqrt{\frac{\phi_n^2}{W^2} + \frac{1}{L_p^2}}} K_1 \left( \sqrt{\frac{\phi_n^2}{W^2} + \frac{1}{L_p^2}} b \right), \quad (18)$$

$$I_{sc} = 2\pi q S \sum_{n=0}^{\infty} B_n \frac{D_p}{SW} \phi_n \cdot \frac{b}{\sqrt{\frac{\phi_n^2}{W^2} + \frac{1}{L_p^2}}} K_1 \left( \sqrt{\frac{\phi_n^2}{W^2} + \frac{1}{L_p^2}} b \right). \quad (19)$$

Here  $K_1$  is the second kind modified Bessel function of the first order.

The second suffix of  $I_s$  means that the current is due to the surface of either the emitter side or the collector side, and the third suffix means that the current is due to the surface of either the  $B$  region or the  $C$  region.

Furthermore, using the approximated relations

$$\left. \begin{aligned} \theta_m &\equiv \left(m - \frac{1}{2}\right)\pi, \quad m = 1, 2, 3, \dots \\ \phi_0 &\equiv \sqrt{2} \frac{SW}{D_p}, \quad \phi_n = n\pi, \quad n = 1, 2, 3, \dots \end{aligned} \right\}, \quad (20)$$

we can find the analytical formula of

$$1 - \beta = \frac{z}{x} \left[ 1.1 + \left(\frac{y}{x}\right)^{1/2} e^{-\pi(y-x)/2} \cdot \left\{ -1.0 + \frac{2.0}{\sqrt{2z}} \frac{K_1(y\sqrt{2z})}{K_0(y\sqrt{2z})} \right\} \right], \quad (21)$$

where  $x = a/W$ ,  $y = b/W$ ,  $z = SW/D_p$ .

But the one by means of  $B_n^{(2)}$  differs slightly, that is to say, the constant which is  $-1.0$  in (21) is  $-0.96$ , but the difference is meaningless in the case in which  $a$  is much smaller than  $b$ ; in the case in which  $a$  is nearly equal to  $b$ ,  $B_n^{(1)}$  gives us better approximated results. Therefore it is reasonable to adopt (21).

*B. The Case of the Curved Electrode Construction, Illustrated in Fig. 1(c)*

Expressing the electrode surfaces by the coordinate surfaces of the prolate spheroid, as shown in Fig. 3, we find the relations between the dimensions of electrodes and coordinates  $(\xi, \eta)$  to be

$$c = W_0 \sqrt{\frac{a^2}{W^2 - W_0^2} + 1}, \quad \eta_0 = \frac{W_0}{c}, \quad \xi_0 = \frac{W}{W_0}, \quad (22)$$

where  $c$  is the  $Z$  coordinate of confocal point.

Now (1), which determines the hole density distribution in the  $A$  region, must be written in the prolate spheroidal coordinate, but the general solution is not yet known. However, it is reasonable to assume that  $L_p$  is infinitely long because the volume recombination in the base region is neglected, and in the  $A$  region the hole flow is assumed to be of one dimension.

Therefore, the solution is expressed by the Legendre functions of the zero order, as

$$p - p_0 = (p_1 - p_0) \frac{Q_0(\eta)}{Q_0(\eta_0)}, \quad (23)$$

where  $Q_0$  is the Legendre function of the zero order of the second kind.

The hole density distribution in the  $B$  region is given by (6) in the same manner as in the case of the planar electrode construction, but in this case  $A_m$  is given by

$$A_m = \frac{p_1 - p_0}{Q_0(\eta_0)} \frac{\frac{W}{\theta_m} \sqrt{c^2 + a^2} \left\{ 1 + \frac{W^2}{c^2 + a^2} \left( 1 - \frac{2}{\theta_m^2} \right) \right\} \sin \theta_m + \left( 2 \frac{W^3}{\theta_m \sqrt{c^2 + a^2}} - Q_0(\eta_0) \right) \cos \theta_m}{\frac{1}{2} \left( \theta_m - \frac{1}{2} \sin 2\theta_m \right) K_0 \left( \sqrt{\frac{\theta_m^2}{W^2} + \frac{1}{L_p^2}} a \right)}. \quad (24)$$

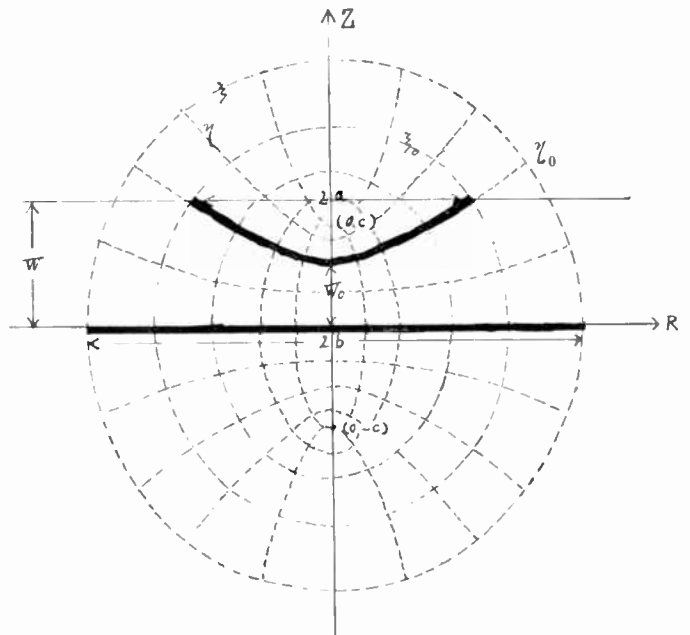


Fig. 3—Setting of the coordinate in the case of the curved electrode construction.

Similarly, the hole density distribution in  $C$  region is given by (9) and (10), but two approximated values of  $B_n$  are considered according to the approximation of hole density distribution in the region, in which  $R$  is equal to  $b$ .

In one case, in which  $a$  is nearly equal to  $b$ , the hole density distribution is reasonably approximated by the following, from the same reason as in section A:

$$p - p_0 = (p_1 - p_0) \frac{Q_0(\eta)}{Q_0(\eta_0)} \frac{K_0 \left( \sqrt{\frac{\theta_1^2}{W^2} + \frac{1}{L_p^2}} b \right)}{K_0 \left( \sqrt{\frac{\theta_1^2}{W^2} + \frac{1}{L_p^2}} a \right)}, \quad (25)$$

and in another case, in which  $a$  is much smaller than  $b$ , it is

$$p - p_0 = \frac{p_1 - p_0}{Q_0(\eta_0)} \frac{\sin \left( \theta_1 \frac{Z}{W} \right)}{\theta_1^2} \frac{W}{\sqrt{c^2 + a^2}} \cdot \left\{ 1 + \frac{W^2}{c^2 + a^2} \left( 1 - \frac{2}{\theta_1^2} \right) \right\} \frac{K_0 \left( \sqrt{\frac{\theta_1^2}{W^2} + \frac{1}{L_p^2}} b \right)}{K_0 \left( \sqrt{\frac{\theta_1^2}{W^2} + \frac{1}{L_p^2}} a \right)}. \quad (26)$$

Then  $B_n^{(1)}$ , which is  $B_n$  determined by using (25), is given by

$$\begin{aligned}
 B_n^{(1)} = \frac{(\rho_1 - \rho_0)}{Q_0(\eta_0)} \cdot \frac{\frac{W^2 \sin \phi_n}{\phi_n^2 \sqrt{c^2 + a^2}} \left\{ 1 + \frac{W^2}{c^2 + a^2} \left( 1 - \frac{2}{\phi_n^2} \right) \right\} + \frac{W \cos \phi_n}{\phi_n} \left\{ \frac{2W^3}{\phi_n^2 (\sqrt{c^2 + a^2})^3} \right.}{\frac{W}{2} \left[ \left\{ 1 + \left( \frac{\phi_n D_p}{SW} \right)^2 \right\} - \frac{\sin 2\phi_n}{2\phi_n} \left\{ 1 - \left( \frac{\phi_n D_p}{SH} \right)^2 \right\} \right.} \\
 \left. - Q_0(\eta_0) \right\} + \frac{D_p}{S} \left[ Q_0(\eta_0) \sin \phi_n - \frac{W}{\phi_n \sqrt{c^2 + a^2}} \left\{ 1 - \cos \phi_n + \frac{1}{c^2 + a^2} \right. \right. \\
 \left. \left. - \frac{D_p}{2SW} (\cos 2\phi_n - 1) \right] K_0 \left( \sqrt{\frac{\theta_1^2}{W^2} + \frac{1}{L_p^2} a} \right) K_0 \left( \sqrt{\frac{\phi_n^2}{W^2} + \frac{1}{L_p^2} b} \right) \right. \\
 \left. \left( -W^2 \cos \phi_n + 2W^2 \frac{\sin \phi_n}{\phi_n} - 2W^2 \frac{1 - \cos \phi_n}{\phi_n^2} \right) \right] \quad (27)
 \end{aligned}$$

and  $B_n^{(2)}$ , which is  $B_n$  determined by using (26), is given by

$$\begin{aligned}
 B_n^{(2)} = \frac{(\rho_1 - \rho_0)}{Q_0(\eta_0)} \cdot \frac{\frac{W}{\theta_1^2 \sqrt{c^2 + a^2}} \left\{ 1 + \frac{W^2}{c^2 + a^2} \left( 1 - \frac{2}{\theta_1^2} \right) \right\} \left[ \left\{ \frac{\sin(\theta_1 - \phi_n)}{\theta_1 - \phi_n} - \frac{\sin(\theta_1 + \phi_n)}{\theta_1 + \phi_n} \right\} \right.}{\frac{W}{2} \left[ \left\{ 1 + \left( \frac{\phi_n D_p}{SW} \right)^2 \right\} - \frac{\sin 2\phi_n}{2\phi_n} \left\{ 1 - \left( \frac{\phi_n D_p}{SH} \right)^2 \right\} \right.} \\
 \left. + \frac{\phi_n D_p}{SW} \left\{ \frac{1 - \cos(\theta_1 + \phi_n)}{\theta_1 + \phi_n} + \frac{1 - \cos(\theta_1 - \phi_n)}{\theta_1 - \phi_n} \right\} K_0 \left( \sqrt{\frac{\theta_1^2}{W^2} + \frac{1}{L_p^2} b} \right) \right. \\
 \left. - \frac{D_p}{2SW} (\cos 2\phi_n - 1) \right] K_0 \left( \sqrt{\frac{\theta_1^2}{W^2} + \frac{1}{L_p^2} a} \right) K_0 \left( \sqrt{\frac{\phi_n^2}{W^2} + \frac{1}{L_p^2} b} \right)} \quad (28)
 \end{aligned}$$

Therefore, the emitter current becomes

$$I_e = \frac{2\pi q D_p c (\rho_1 - \rho_0)}{Q_0(\eta_0)} \left( \frac{W}{W_0} - 1 \right), \quad (29)$$

the surface recombination current is obtained from (17), (18) and (19), into which (27) and (28) are taken, and  $\beta$  is calculated from them.

The question whether  $B_n^{(1)}$  or  $B_n^{(2)}$  is to be used is solved from the same consideration as in the foregoing Section A, and by considering that the analytical formula of  $\beta$  must coincide with (21) when  $W_0$  is equal to  $W$ , because then the emitter is planar. Thus in this case,  $\beta$  is given by

$$\begin{aligned}
 1 - \beta = \frac{z}{x} \left[ 1.1 + \left( \frac{y}{x} \right)^{1/2} e^{-\pi(y-x)/2} \right. \\
 \left. \left\{ -1.0 + \frac{2.0}{\sqrt{2z}} \cdot \frac{K_1(y\sqrt{2z})}{K_0(y\sqrt{2z})} \right\} \frac{1+w}{2}, \quad (30)
 \end{aligned}$$

where  $w = W_0/W$  and  $W_0$  is the thinnest width of base region.

C. The Case of the Curved Electrodes Construction, Illustrated in Fig. 1(d)

Expressing the electrode surfaces by the coordinate surfaces of the prolate spheroid, as shown in Fig. 4, we find the relations between the dimensions of electrodes and coordinates  $(\xi, \eta)$  as follows:

$$\left. \begin{aligned}
 c &= W_{01} \sqrt{1 + \frac{a^2}{W_1^2 - W_{01}^2}} \\
 &= W_{02} \sqrt{1 + \frac{a^2}{W_2^2 - W_{02}^2}} \\
 \eta_1 &= \frac{W_{01}}{c}, \quad \eta_2 = \frac{W_{02}}{c}, \quad \xi_1 = \frac{W_1}{W_{01}}, \quad \xi_2 = \frac{W_2}{W_{02}}
 \end{aligned} \right\}, \quad (31)$$

where  $W_{01}$ ,  $W_0$ ,  $W_1$  and  $W_2$  are shown in Fig. 4.

Now, the hole density distribution in the A region is obtained in the same manner as in Section B, as follows:

$$\rho - \rho_0 = (\rho_1 - \rho_0) \frac{Q_0(\eta_2) + Q_0(\eta)}{Q_0(\eta_1) + Q_0(\eta_2)}, \quad (32)$$

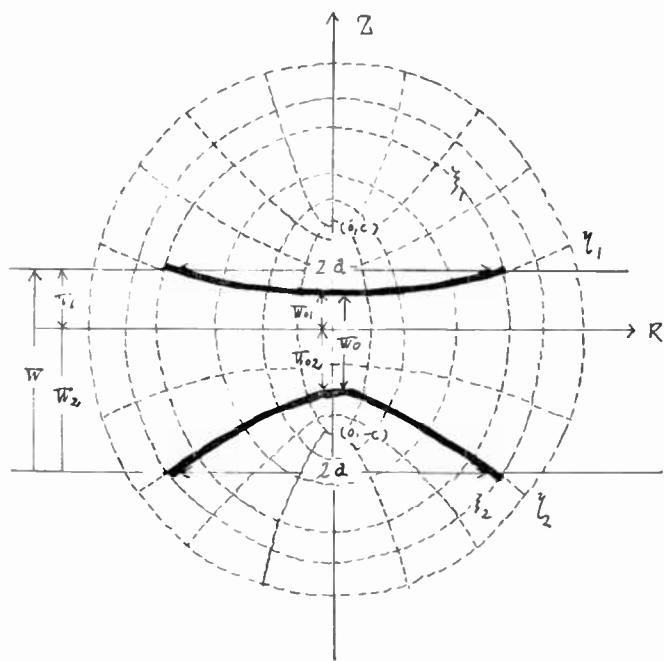


Fig. 4—Setting of the coordinate in the case of the curved electrodes construction.

and the hole density distribution in the C region is obtained from (9) and (10), in which Z must be replaced by Z + W<sub>2</sub>.

Because of the vacancy of B region, B<sub>n</sub> is simply determined as follows:

$$B_n = \frac{(\rho_1 - \rho_0)}{Q_0(\eta_1) + Q_0(\eta_2)} \cdot \frac{Q_0(\eta_2) \frac{W}{\phi_n} \left\{ (1 - \cos \phi_n) + \frac{\phi_n D_p}{SW} \sin \phi_n \right\} - \frac{W}{\phi_n} \{ Q_0(\eta_1) \cos \phi_n + Q_0(\eta_2) \}}{\frac{W}{2} \left[ \left\{ 1 + \left( \frac{\phi_n D_p}{SW} \right)^2 \right\} - \frac{\sin 2\phi_n}{2\phi_n} \left\{ 1 - \left( \frac{\phi_n D_p}{SW} \right)^2 \right\} \right]} + \frac{D_p}{S} \sin \phi_n Q_0(\eta_1) - \frac{1}{\sqrt{c^2 + a^2}} \left[ -\frac{W}{\phi_n} \left\{ \left( \frac{W}{\phi_n} \sin \phi_n - \frac{D_p}{2SW} (\cos 2\phi_n - 1) \right) K_0 \left( \sqrt{\frac{\phi_n^2}{W^2} + \frac{1}{L_p^2} a} \right) + \frac{\phi_n D_p}{SW} (\cos \phi_n - 1) \right\} + \left\{ 1 + \frac{1}{\phi_n^2} \frac{W^2}{c^2 + a^2} \right\} \left\{ -\frac{2WW_2}{\phi_n} + \sin \phi_n \left( 2 \frac{W^2 W^2}{\phi_n} - W_1^2 \right) - \frac{2WW_1 \cos \phi_n}{\phi_n} + \frac{\phi_n D_p}{SW} \left( W_2^2 - 2 \frac{W^2}{\phi_n^2} + \frac{2W_1^2 \sin \phi_n}{\phi_n} + \left( \frac{W^2}{\phi_n^2} - 1 \right) \cos \phi_n \right) \right] \right] \quad (33)$$

Then the emitter current becomes

$$I_e = \frac{2\pi q D_p c (\rho_1 - \rho_0)}{Q_0(\eta_1) + Q_0(\eta_2)} \left( \frac{W_1}{W_{01}} - 1 \right), \quad (34)$$

and the surface recombination current is obtained from (18) and (19), into which (33) is taken.

Therefore, β is given by

$$1 - \beta = \sqrt{\frac{z}{2}} \cdot \frac{1}{x} \cdot \frac{K_1(x\sqrt{2z})}{K_0(x\sqrt{2z})} \cdot w \cdot (1 + v), \quad (35)$$

where

$$v = \frac{W_1}{W_{01}}.$$

But the determination of v from the observed value of electrode dimensions is very laborious. So calculating v in the cases that the emitter is planar, and the emitter and the collector are symmetrical, and in the cases that the dimensions of electrodes are slightly altered from the above mentioned two cases, we find in all cases

$$v = \frac{1}{w}. \quad (36)$$

Thus we obtain

$$1 - \beta = \frac{z}{x} \cdot \frac{2}{\sqrt{2z}} \cdot \frac{K_1(x\sqrt{2z})}{K_0(x\sqrt{2z})} \cdot \frac{1 + w}{2}. \quad (37)$$

According to the assumption of one-dimensional hole flow in the A region, all flow lines must arrive at the collector; therefore another condition is added, namely the validity range of (21)

$$a \leq b, \quad (38)$$

of (30)

$$a \sqrt{1 + \frac{W^2 - W_{\sigma}^2}{a^2}} \leq b, \quad (39)$$

and of (37) is that the curvature of collector is not smaller than that of the emitter.

IV. DISCUSSION AND NUMERICAL EXAMPLES

Eqs. (21), (30) and (37) give us  $\beta$  of alloy junction and surface barrier transistors in terms of geometrical dimensions of electrode constructions and surface recombination velocity. They also give us many useful design data. Therefore, discussions follow on the results from equations and numerical examples which are necessary to design transistors.

A. Principle of Similitude

As it is seen from the analytical formulas of  $\beta$ ,  $\beta$  is expressed by the four dimensionless quantities  $w$ ,  $x$ ,  $y$  and  $Z$ . Therefore the data on  $\beta$  from transistors with different geometrical dimensions of electrodes and different surface recombination velocities are understood systematically.

B. Influence of Electrodes Curvature

The influence of electrodes curvature on  $\beta$  is included in the correction factor  $(1+w)/2$ . When the wafer thickness  $W$  is held at a constant,  $\beta$  approaches to unity as the thinnest width  $\bar{W}_0$  is smaller. This results from the fact that holes flow mostly along the center axis of electrode where the gradient of hole density is the greatest, even though part of the hole's flow lines approach to the free base surface.

C. Numerical Values of  $\beta$

Because, as mentioned above, (30) is the same function of  $x$ ,  $y$ , and  $z$  as (21), except for the correction factor of the electrode curvature, the relations between  $\beta$  and  $y$ , calculated from (21), are shown in Figs. 5-7 when parameters are  $x$  and  $z$ .

In Section V-A, we will point out that the analytical formulas of  $\beta$ , obtained under the assumption that the radius of collector electrode is infinitely large, are able to be applied in most cases and are in good accordance with the experimental values obtained by Stripp and Moore.<sup>3</sup>

Now we will look for the limit of collector electrode radius, *i.e.*,  $y$ , in which the assumption is allowed.

From (21) and (30), it is easily understood that the assumption is allowed if

$$1.1 \gg \left(\frac{y}{x}\right)^{1/2} e^{-\pi(y-x)/2} \left\{ -1.0 + \frac{2.0}{\sqrt{2z}} \cdot \frac{K_1(y\sqrt{2z})}{K_0(y\sqrt{2z})} \right\} \quad (40)$$

Therefore, the contributions of various factors being considered, (40) is reduced to

$$1 \gg \frac{10}{\sqrt{2z}} e^{-\pi(y-x)/2} \quad (41)$$

Therefore  $y$  may be considered as infinity if

$$y - x \geq 5,$$

extending over

$$1 \geq Z \geq 10^{-5},$$

and this conclusion is verified in Figs. 5-7.

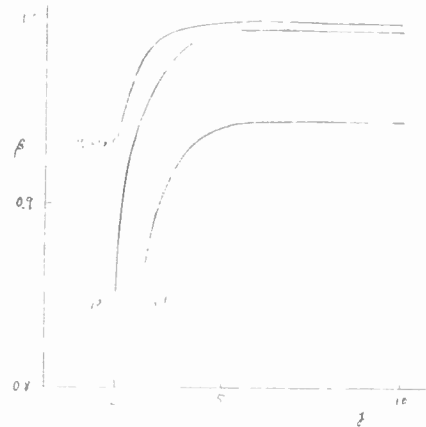


Fig. 5—Variation of  $\beta$  as a function of  $y$ .  $x=2$ .

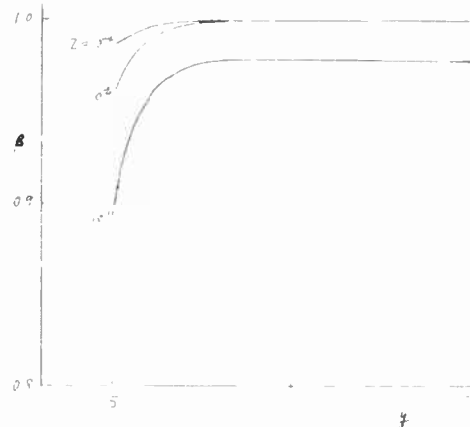


Fig. 6—Variation of  $\beta$  as a function of  $y$ .  $x=5$ .

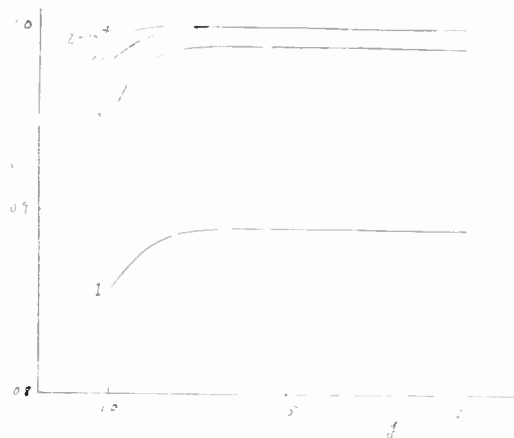


Fig. 7—Variation of  $\beta$  as a function of  $y$ .  $x=10$ .

Then it is very useful to illustrate  $1/1-\beta$  ( $\equiv \alpha_{cb}$ —common emitter current amplification factor) as a function of  $x$ , calculated from (21), when  $y$  may be considered as infinity, and a parameter  $z$ , shown in Fig. 8 by real lines, of which the gradient is  $\tan(1/1.1z)$ .  $\beta$  given by (37) is nearly equal to  $\beta$  given by (30) when cross-sectional electrodes radii are equal; the difference is as small as 5 per cent even when  $z$  equals to unity, and it becomes trivial as  $z$  is smaller. Then  $1/1-\beta$ , as a function of  $x$  when a parameter is  $z$ , is illustrated in Fig. 8 by dotted lines.

Comparing the real lines with the dotted ones, it is easily seen that  $1/1-\beta$  decreases when the emitter and collector have equal radii, especially for small  $z$ .

*D. Cross-Sectional Radius Ratio of Emitter and Collector Electrode*

As easily seen,  $\beta$  is a monotonic function of  $y$  when  $x$  and  $z$  are given, but  $\beta$  has a value  $x_{opt}$  in which  $\beta$  takes the maximum, when  $y$  and  $z$  are given.

The fact has been shown in the experiments by Moore and Pankove,<sup>2</sup> but it has not been clear what factors participate and how. From this calculation, it can be understood quantitatively; that is, the surface recombination in the  $C$  region, especially on the collector side, is remarkable when  $x$  is extremely large, and the one in

the  $B$  region near the emitter electrode is marked when  $x$  is extremely small.

In Fig. 9,  $x_{opt}$  is shown when  $y$  is given and  $z$  is a parameter, from which it is seen that  $\beta$  takes the maximum when the cross-sectional radius ratio is comparatively close to unity.

The real lines in Fig. 10 show the variation of  $\beta$  as a function of  $x$  when  $y$  is a parameter and  $z$  is  $10^{-2}$ , and indicate that  $x$  smaller than  $x_{opt}$  is in the safety side, which is also adequate from the standpoint of the eccentricity between the emitter electrode and the collector.

The dotted lines in Fig. 10 show the variation of  $\beta$  as the parameter  $z$  is changed to  $10^{-1}$  and  $10^{-3}$ , which indicates that  $\beta$  approaches to unity and changes only a little in terms of  $x/y$  as  $Z$  is a small quantity.

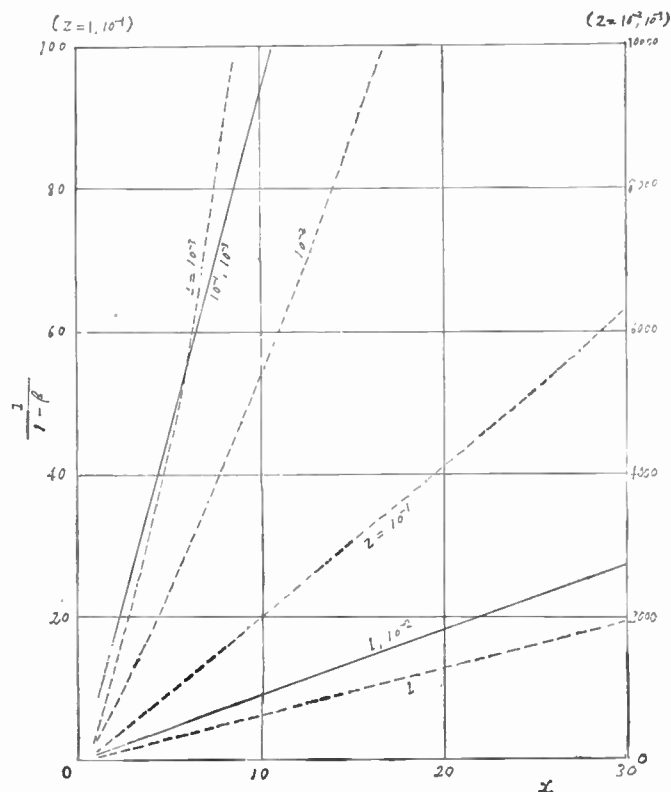


Fig. 8—Numerical values of  $\beta$ . Real line—cases of  $y \rightarrow \infty$ ; scales on both sides. Dotted line—cases of  $x = y$ ; scales on left side only.

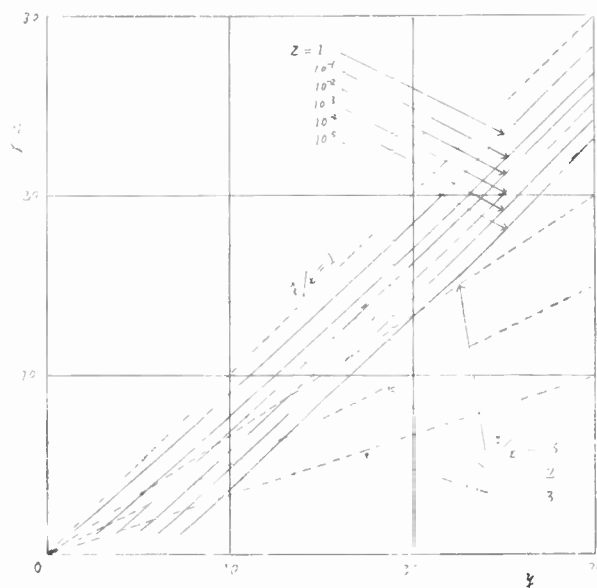


Fig. 9—Cross-sectional radius of emitter maximizing  $\beta$  when  $y$  and  $Z$  are given.

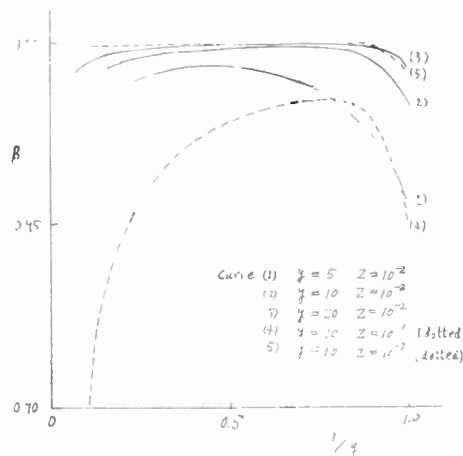


Fig. 10— $\beta$  as a function of  $x/y$ .

### E. Recommended Constructions When One Electrode or Two are Curved Unavoidably

As is easily seen from (30) and (37),  $\beta$  is always smaller as the electrodes are more curved when the minimum spacing in base region is held at a constant, which is physically recognized as the increase of surface recombination current due to the oblique intersection between the free base surface and the flow lines of holes.

Therefore, having the constructions in which the flow lines of holes are at right angles to the free base surface at the periphery of electrodes, one expects that effects of surface recombination on  $\beta$  in the construction with surfaces of the curved electrodes are nearly equal to one with the planar electrodes' surfaces. Fig. 11 shows a recommended electrode construction when one electrode is curved unavoidably, which seems to be made by using the fabrication technique of surface barrier transistors<sup>7</sup> or drilled junction transistors.<sup>8</sup>

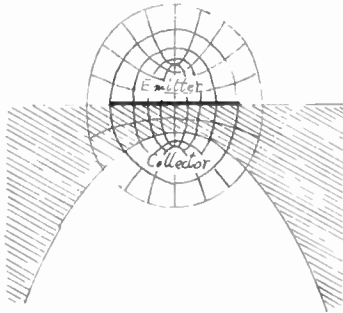


Fig. 11—A recommended construction when one electrode is curved unavoidably.

## V. COMPARISON WITH EXPERIMENTAL RESULTS

Because the analytical formulas of  $\beta$ , (21), (30), and (37), are obtained by the approximating method, they must be verified by experiments.

Unfortunately, however, it is very difficult to measure the volume lifetime of minority carriers and surface recombination velocity separately from completely assembled alloy junction transistors. We will therefore compare the calculated results of (21) and (30) with the experimental results obtained by Moore and Pankove,<sup>2</sup> and Stripp and Moore.<sup>3</sup>

### A. Numerical Values of $\beta$

Stripp and Moore have obtained the empirical formula of  $\beta$  in terms of surface recombination velocity, as follows:

$$\begin{aligned} \beta_{cb} &= \frac{\beta}{1 - \beta} \left( \cong \frac{1}{1 - \beta} \right) \\ &= \frac{K_M}{S} (1 + C_M \sqrt{S}) \cong \frac{K_M}{S}, \end{aligned} \quad (42)$$

<sup>7</sup> W. E. Bradley, *et al.*, "The surface-barrier transistor," *Proc. IRE*, vol. 41, pp. 1702-1720; December, 1953.

<sup>8</sup> C. W. Miller and J. I. Pankove, "A *p-n-p* triode alloy junction transistor for radio-frequency amplification," *Proc. IRE*, vol. 42, pp. 386-391; February, 1954.

where

$K_M, C_M$  = experimentally determined constants,  
 $\beta_{cb}$  = common emitter current amplification factor,

from an analogy of three-dimensional electrolytic conductance when

$$a = 7.5 \text{ mils}, \quad b = 22 \text{ mils}, \quad W = 5 \text{ mils}. \quad (43)$$

Therefore, it is most appropriate to compare  $K_M$  with our corresponding quantity  $K_c$ ,

$$K_c = \frac{aD_p}{1.1W^2} \cdot \frac{1}{\left(1 + \frac{W_0}{W}\right)/2}, \quad (44)$$

which is given from (30) by taking  $y$  infinitely great.

The first column of Table I shows the results of comparison of  $K_c$  with  $K_M$ , especially of the planar collector, which are in very good accordance irrespective of the emitter electrode curvature.

The second and succeeding columns of Table I show the comparison of  $K_M$  with  $K_c$ , calculated from the above mentioned approximation, and indicate that the approximation is valid if the depth of collector electrode is not beyond a third of wafer thickness.

TABLE I  
COMPARISON OF  $K_c$  WITH  $K_M$

$W_{\text{eff}}$ (mils)	$W_0$ (mils)	$K_c$	$K_M$	$K_M/K_c$
5	5	4,490	4,700	0.96
	4	5,150	5,200	0.99
	3	5,580	5,900	0.95
	2	6,230	6,700	0.93
	1	7,370	7,900	0.93
4	4	7,820	7,400	1.06
	3	8,640	8,400	1.03
	2	9,410	9,800	0.96
	1	10,730	12,000	0.89
3	3	11,230	13,000	0.86
	2	11,160	16,000	0.76
	1	14,900	20,000	0.75
2	2	19,170	30,000	0.64
	1	22,500	39,000	0.58
1	1	49,470	120,000	0.41

### B. Applied Limit When a Collector Is Curved

As mentioned above, exactly speaking, (21) and (30) are applied only to the case of planar collector, but a practically used transistor has the curved collector, even though the curvature is usually small, and in most cases the collector is considered as planar.

In such cases, it is reasonable to use, instead of the real wafer thickness, the effective wafer thickness  $W_{\text{eff}}$ , defined as the spacing between the free base surface at the emitter side and the top of the collector as illustrated in Fig. 12, and this corresponds to considering the virtual collector at the top of collector.

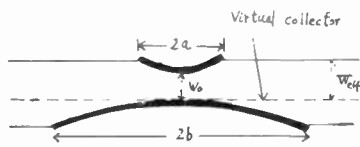


Fig. 12—Virtual collector.

C. Cross-Sectional Radius Ratio of Emitter and Collector Electrode

Moore and Pankove<sup>2</sup> have experimentally obtained the variation of  $\beta$  as a function of cross-sectional radius ratio of emitter and collector electrode in alloy junction transistors, which is shown by the real line (1) in Fig. 13.

Though they could not know the surface recombination velocities, they assumed it as 5000 cm/second and obtained the real line (2) in Fig. 13, by which they verified their two-dimensional analog experiment with a resistive sheet.

Therefore we also assume the surface combination velocity as the same value and the base width as 2.2 mils, which was written as a mean base width in their paper.

Then we obtain the dotted line (3) in Fig. 13, which is in comparatively reasonable accordance with their experimental results, but the reasonableness is insufficient, probably owing to the curvatures of emitter and collector electrodes.

Because the electrode construction of their alloy junction transistors is not known, we assume the construction of the collector as the same as that of the T A 153 alloy junction transistor shown in Fig. 14, which was in their paper.

From the considerations mentioned in Section V-B,  $W_{eff}$  is taken as 2.5 mils, and the surface recombination velocity is assumed to be 4000 cm/second; then the dotted line (4) in Fig. 13 is obtained, and it is in good accordance. The value of  $y/x$ , which maximizes  $\beta$ , is 1.4 experimentally and 1.3 theoretically. The difference, which is just smaller than 10 per cent, is due to the fact that in this case  $z$  is nearly equal to 0.5, though the analytical

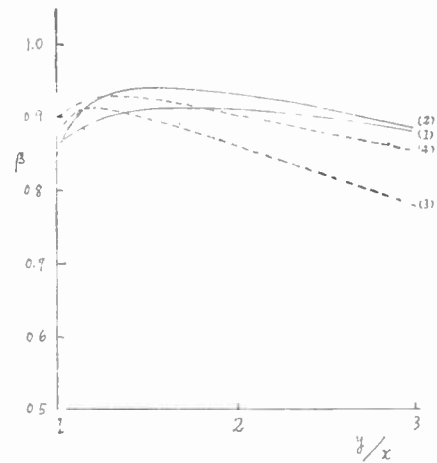


Fig. 13—Variation of  $\beta$  as a function of  $y/x$ . Comparison with experimental and calculated values.

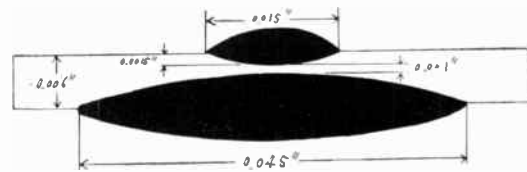


Fig. 14—TA 153 p-n-p junction transistor.

formulas of  $\beta$  in this paper are good standing only when  $z$  is much smaller than unity, and the electrode constructions are not known.

And also the statistical variation of experimental results was reported as great. Therefore, we cannot seek further for the cause of the discrepancy.

ACKNOWLEDGMENT

We are indebted to the members of the Departments of Electronic and Electrical Engineering of the University of Tokyo, in particular to Prof. T. Sakamoto, Prof. S. Okamura, and Assistant Prof. Y. Adachi; and to Dr. H. Osafune of Nippon Electric Co. for many valuable suggestions and help.

# The DC Pumped Quadrupole Amplifier— A Wave Analysis\*

A. E. SIEGMAN†, MEMBER, IRE

**Summary**—Gordon, Buchsbaum, and Feinstein have proposed a new quasi-parametric electron-beam amplifier which uses the same transverse cyclotron waves as the Adler-Wade quadrupole parametric amplifier, but which is pumped with dc voltage applied via a twisted or staggered quadrupole structure. This paper analyzes the dc pumped twisted-quadrupole case in terms of the four transverse beam waves and their coupling. Amplification is found to result from the coupling of the slow and fast cyclotron waves. The pump voltage does not actually pump, i.e., does not supply energy. An alternative dc pumping scheme is also examined and found to give coupling of the waves but no amplification.

## INTRODUCTION

A LOW-CURRENT filamentary electron beam traveling parallel to a longitudinal dc magnetic field will propagate small RF transverse disturbances in the form of two small-signal RF waves, called the fast and slow cyclotron waves. (There are also two other related transverse waves, sometimes called the synchronous waves.) The quadrupole amplifier recently developed by Adler, Hrbek, and Wade uses the fast cyclotron wave as a medium for parametric amplification.<sup>1</sup> In the Adler-Wade tube, fast cyclotron waves at signal and idle frequencies are amplified by pumping the beam with transverse RF electric fields at the pump frequency. The RF pump fields are applied to the beam via a quadrupolar structure, hence the name quadrupole amplifier. The slow cyclotron waves are not involved in this device.

More recently, at a private conference in June, 1959, Gordon, Buchsbaum, and Feinstein of the Bell Telephone Laboratories pointed out that amplification of the cyclotron waves on a beam could also be obtained by applying transverse dc electric fields to the beam with a set of staggered quadrupoles or a twisted quadrupole structure. An analysis of such a dc quadrupole device, considering the growing trajectories of individual electrons, was developed by Gordon.<sup>2</sup> The present author, having just carried out an analysis of cyclotron and synchronous waves,<sup>3</sup> was led to analyze the dc quadrupole device from a wave viewpoint. This latter

analysis forms the principal content of the present paper. The chief result of the analysis is to show clearly that the dc quadrupole device amplifies by coupling together the fast and slow cyclotron waves so that both of them grow exponentially with distance along the beam. The growing positive energy in the fast cyclotron wave is just balanced by the growing negative energy in the slow cyclotron wave. The device is analogous in many ways to the velocity-jump amplifier for space-charge waves, which amplifies by coupling together the fast and slow space-charge waves.

The dc quadrupole amplifier is sometimes referred to as a dc pumped parametric amplifier. The phrase is somewhat misleading, as the dc quadrupole amplifier differs from usual parametric amplifiers in important ways. There is no idle frequency involved, and the energy for amplification does not come from the pump. The dc pump fields deliver no energy to the electrons. The device has also been called the Larmoratron, although the Larmor frequency does not seem to be involved.

## DESCRIPTION OF THE DC QUADRUPOLE AMPLIFIER

A general sketch of a quadrupole amplifier is shown in Fig. 1. Such a sketch might apply to either an RF or dc pumped amplifier, although the details of the coupling structures and the pump structure will differ for the two types. We will describe only the dc case, and will be concerned primarily with the amplification process in the quadrupole section. Very little will be said about the couplers for exciting and extracting the beam waves.

Gordon, *et al.*, originally described a staggered quadrupole structure in which alternate quadrupoles along the length of the pumping section were rotated by 90° about the central axis. Such a structure can be viewed as a superposition of two twisting quadrupoles rotating equally but oppositely. The amplification process results only from the twisting component which rotates in the same direction as an electron spirals about the dc magnetic field, and so we will consider here such a twisted quadrupole, rather than a set of staggered quadrupoles. The twisted-quadrupole pumping section might look something like the sketch of Fig. 2, with voltages applied to the various wires as shown.

Since analysis shows that the fast and slow cyclotron waves grow equally in the dc quadrupole amplifier, we consider the appearance of an electron beam propagating fast and slow cyclotron waves of equal amplitude. In this case, the trajectory of an individual electron is a

\* Received by the IRE, January 25, 1960; revised manuscript received, April 11, 1960.

† Dept. of Electrical Engrg., Stanford University, Stanford, Calif.

<sup>1</sup> R. Adler, G. Hrbek, and G. Wade, "The quadrupole amplifier, a low-noise parametric device," *Proc. IRE*, vol. 47, pp. 1713-1723; October, 1959.

<sup>2</sup> E. I. Gordon, "A transverse-field traveling-wave tube," *Proc. IRE*, vol. 48, p. 1158; June, 1960.

<sup>3</sup> A. E. Siegman, "The transverse waves on a filamentary electron beam in a transverse-field slow-wave circuit," *J. Appl. Phys.*, vol. 31, pp. 17-26; January, 1960.

helical path with the center on the axis of the tube. The frequency with which the electron orbits around the center is, of course, the cyclotron frequency. If the fast and slow waves are equally excited, it can be shown that the instantaneous position of the beam at any given transverse plane moves back and forth along a straight line during the RF cycle. (The RF frequency is not necessarily equal to the cyclotron frequency.) If one could take a time exposure of the beam over one cycle or longer, the electron trajectories would form a twisted ribbon of constant width, such as is sketched (rather badly) in Fig. 3. The heavy line is the trajectory of an electron coming through at the peak of the RF cycle. An electron coming through at the midpoint of the cycle passes straight along the axis of the tube. Note that the twist rate of the ribbon depends only on the cyclotron frequency. The RF or signal frequency simply determines how fast the beam spot at any transverse plane swings back and forth from one side of the ribbon to the other.

To obtain amplification, the twisted ribbon of Fig. 3 must be fitted neatly into the twisted quadrupole of Fig. 2, with the same twist rate. The amplification which then occurs is such that the width of the ribbon increases exponentially with distance, the twist rate remaining the same. In terms of individual electron

trajectories, the radius of each helical trajectory grows exponentially with distance.

One way of viewing the amplification process is to consider a set of sketches such as Fig. 4, showing cross sections of the quadrupole and the beam locus at various distances along the beam. At any instant, the beam is a spot somewhere on each locus, the spot moving back and forth along the locus at the RF frequency. The arrows indicate transverse velocities of the electrons. One might at first be tempted to explain the amplification by noting that each electron is clearly in a transverse electric field, accelerating it in its direction of transverse motion. Therefore, each electron is receiving energy from the transverse dc field. By twisting the quadrupole, we keep the twisting electron always in a favorable transverse electric field. This explanation is spoiled, however, by noting that an electron actually always stays on the same equipotential line of the quadrupole, and hence cannot be receiving energy from the quadrupole fields. Thus, consider a coordinate system which moves axially at the same rate as a given electron, and also rotates at the same rate as the quadrupole. Fig. 5 shows what the trajectory of the given electron would look like in this coordinate system. The outward motion represents the amplification. Clearly, no energy is received from the dc fields. The fact is, of course, that the twisted quadrupole also has axial field components, and these axial components extract energy from each individual electron at the same rate that the transverse fields put energy in. Explanations of the amplification mechanism must be sought, instead, in the wave picture.

THE WAVE ANALYSIS

An idealized filamentary electron beam (vanishingly small spot size, low space charge) in a longitudinal dc magnetic field propagates the four waves summarized in Table I, when the beam is unperturbed by external influences.<sup>3</sup> We will be concerned with how these waves couple together and grow when the beam is subjected to the dc fields of the twisted quadrupole.

The transverse RF modulation on such a beam can be written as a summation of the four waves. Thus, the  $x$  and  $y$  displacements of the beam, as functions of axial distance and time, are given by

$$\begin{aligned}
 x(z, t) &= (k\omega_c)^{-1} e^{j(\omega t - \beta_0 z)} [A_s e^{-j\beta_c z} - A_f e^{j\beta_c z} - A_{e1} + A_{e2}] \\
 y(z, t) &= j(k\omega_c)^{-1} e^{j(\omega t - \beta_0 z)} [A_s e^{-j\beta_c z} + A_f e^{j\beta_c z} - A_{e1} - A_{e2}] \quad (1)
 \end{aligned}$$

where  $k \equiv (\omega I_0 / 2\eta\omega_c)^{1/2}$ ,  $I_0$  being the dc beam current, and  $\eta$  the charge-to-mass ratio for an electron. As is the usual practice in these problems, the transverse displacement of the *beam* has been written. To find the transverse displacement of an *individual electron*, one must note that the  $z$  position of an individual electron is given by  $z = u_0(t - t_0)$ , where  $t_0$  is the time when the

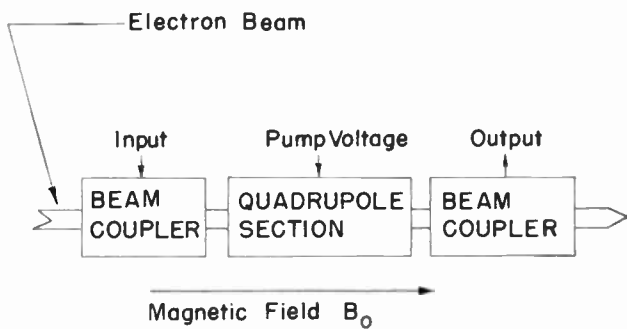


Fig. 1—Sketch of a generalized quadrupole amplifier.

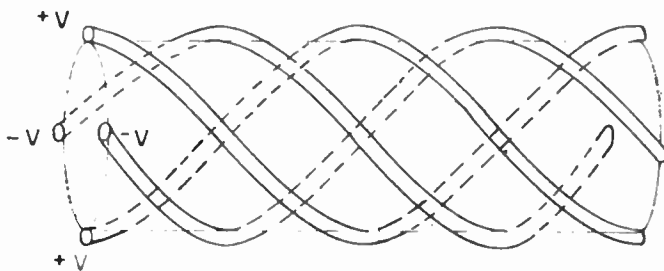


Fig. 2—A twisted quadrupole for a dc quadrupole amplifier.



Fig. 3—Individual electron trajectories for a beam carrying equal amounts of slow and fast cyclotron waves. The collection of trajectories forms a twisting ribbon.

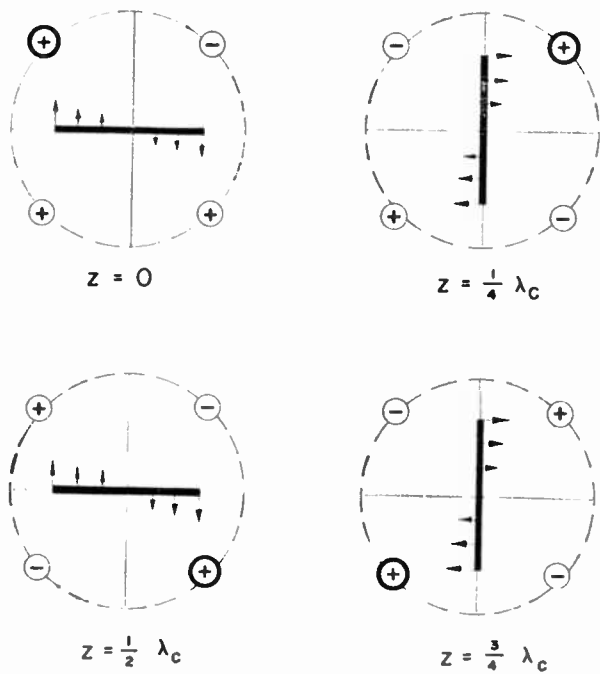


Fig. 4—Cross sections of the dc quadrupole amplifier at various distances along the twisted quadrupole.

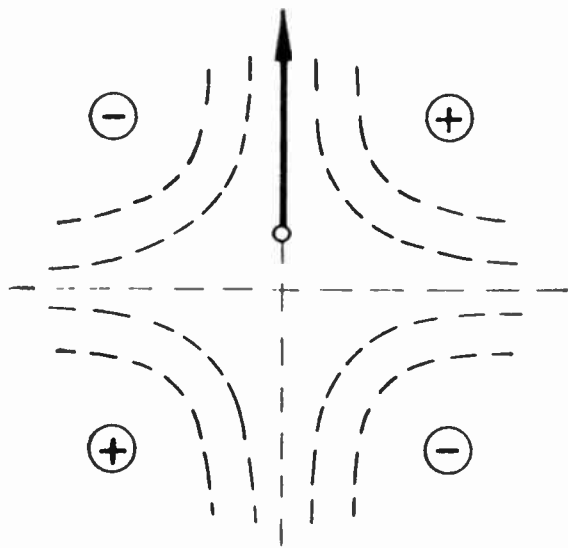


Fig. 5—The path of a single electron being amplified in the twisted quadrupole, as seen in a coordinate system which moves axially with an electron and also rotates at the same rate as the twisted quadrupole.

TABLE I  
TRANSVERSE BEAM WAVES

Wave	Amplitude	Free Propagation Constant	RF Energy Carried	Sense of Circular Polarization
Fast cyclotron	$A_f$	$\beta_r - \beta_c$	+	-
Slow cyclotron	$A_s$	$\beta_r + \beta_c$	-	+
Synchronous	$A_{e1}$	$\beta_r$	+	+
Synchronous	$A_{e2}$	$\beta_s$	-	-

$\beta_r = \omega/u_0$ ,  $\beta_s = \omega_c/u_0$ ,  $\omega_c$  = cyclotron frequency,  $u_0$  = dc electron velocity

electron passes  $z=0$ . The total time derivative of displacement for an individual electron, such as  $dx/dt$  for an individual electron, is obtained by writing

$$\frac{dx}{dt} = \frac{\partial x(z, t)}{\partial t} + \frac{\partial x(z, t)}{\partial z} \frac{dz}{dt} \approx j\omega x(z, t) + u_0 \frac{\partial x(z, t)}{\partial z} \tag{2}$$

Since the analysis is intended to be linearized and small signal, the electron  $z$  velocity is taken to be constant and equal to  $u_0$ ; i.e., RF displacements in the  $z$  direction are not considered.

The entire following analysis, in fact, is entirely in terms of transverse displacements, ignoring longitudinal effects. This assumption can be shown to be valid for this type of problem in a first-order or small-signal analysis such as the present. Longitudinal effects are definitely present—for example, most of the energy in a transverse wave really resides in the dc slowing down or speeding up of the beam that inevitably occurs when a transverse wave is excited—but correct answers are still obtained by solving only the transverse equations of motion and properly interpreting the results.<sup>3</sup>

The transverse equations of motion for an electron are

$$\begin{aligned} \frac{d^2x}{dt^2} + \omega_c \frac{dy}{dt} - \eta \frac{\partial V}{\partial x} &= 0 \\ \frac{d^2y}{dt^2} - \omega_c \frac{dx}{dt} - \eta \frac{\partial V}{\partial y} &= 0. \end{aligned} \tag{3}$$

We are interested in the case where the electric potential  $V$  is furnished by a twisted quadrupole. The potential of such a quadrupole can be written as

$$V = -\frac{1}{2}K[(x^2 - y^2) \sin 2\beta_q z - 2xy \cos 2\beta_q z], \tag{4}$$

where  $\lambda_q$  is the full axial pitch of the quadrupole and  $\beta_q \equiv 2\pi/\lambda_q$ . The exact Bessel functions for a quadrupolar potential have been approximated by the formula given. For the moment we will keep the analysis more general by not equating  $\lambda_q$  to the cyclotron wavelength  $\lambda_c = 2\pi u_0/\omega_c$ . If (1), (2), and (4) are substituted into the equations of motion (3), and if one assumes that the wave amplitudes  $A_s$ ,  $A_f$ ,  $A_{e1}$  and  $A_{e2}$  vary with distance, then the equations of motion become

$$\begin{aligned} \frac{dA_s}{dz} e^{-j\beta_c z} + \frac{dA_{e1}}{dz} &= \kappa e^{-2j\beta_q z} [A_f e^{j\beta_c z} - A_4] \\ \frac{dA_f}{dz} e^{j\beta_c z} + \frac{dA_{e2}}{dz} &= \kappa e^{2j\beta_q z} [A_s e^{-j\beta_c z} - A_3]. \end{aligned} \tag{5}$$

These are the desired equations which describe the coupling together of the four waves by the quadrupole perturbation. The coupling coefficient or gain coefficient  $\kappa$  is given by

$$\kappa = \frac{\eta K}{\omega_c u_0}, \tag{6}$$

so that it is proportional to the pump voltage. We should note that this coupling coefficient is assumed to be small,  $\kappa \ll \beta_c$ , in obtaining the equations in (5).

In the dc quadrupole amplifier described above, the beam and the quadrupole twist at the same rate, *i.e.*  $\beta_q = \beta_c$ . Putting this into (5) and then separating out terms with different  $z$  dependence, one obtains

$$\begin{aligned} \frac{dA_s}{dz} &= \kappa A_f, & \frac{dA_f}{dz} &= \kappa A_s, \\ \frac{dA_{e1}}{dz} &= \frac{dA_{e2}}{dz} = 0. \end{aligned} \quad (7)$$

Clearly, the fast and slow cyclotron waves are coupled to each other, while the two synchronous waves are to first order unaffected. If one solves these equations in terms of initial conditions at  $z=0$ , one obtains growing and decaying terms for the fast and slow cyclotron waves

$$\begin{aligned} A_s(z) &= \frac{1}{2}[A_s(0) + A_f(0)]e^{+\kappa z} + \frac{1}{2}[A_s(0) - A_f(0)]e^{-\kappa z} \\ A_f(z) &= \frac{1}{2}[A_s(0) + A_f(0)]e^{+\kappa z} - \frac{1}{2}[A_s(0) - A_f(0)]e^{-\kappa z}. \end{aligned} \quad (8)$$

Note that the total RF power in the beam, given by

$$P = -|A_s|^2 + |A_f|^2 + |A_{e1}|^2 - |A_{e2}|^2, \quad (9)$$

remains constant even though the fast and slow waves grow. The amplified power is ultimately obtained by extracting the power in the amplified fast cyclotron wave with a fast-wave coupler, leaving the negative-energy slow cyclotron wave on the beam.

#### PRACTICAL DESIGN CONSIDERATIONS

To give a general idea of the practical possibilities of the dc quadrupole amplifier, we will discuss some of the design parameters. From (6), if the gain is large enough so that the growing wave predominates at the output coupler, and if the output coupler takes off all the energy in the fast wave, then the gain in decibels of the amplifier is given by

$$\begin{aligned} G(\text{db}) &= 10 \log_{10} \left[ \frac{|A_f(0) + A_s(0)|^2}{4P_{\text{in}}} \right] \\ &\quad + 10 \log_{10} [e^{2\kappa L}] \\ &= A + 8.68\kappa L, \end{aligned} \quad (10)$$

where  $L$  is the length of the quadrupole section. The initial loss term  $A$  depends on what is used for the input coupler, *i.e.*, on how the input power  $P_{\text{in}}$  is distributed among the various waves. A coupler which excites equal amounts of fast and slow cyclotron waves with equal phase will make the initial loss zero,  $A=0$  db. Note, however, that if the fast and slow waves are equally excited but  $180^\circ$  out of phase at the input to the pump section, no growing wave at all will be excited; the initial

loss will be infinite. This situation corresponds physically to the beam loci being at right angles to those shown in Fig. 4, so that the electron trajectories are all attenuated. Since the relative phase of  $A_f$  and  $A_s$  will change in any drift section between the input coupler and the quadrupole section, careful design is obviously required to get  $A=0$  and not  $A=-\infty$ . A safer procedure would be to use a fast-wave input coupler, exciting  $A_f$  only, in which case one obtains

$$A = -6 \text{ db} \quad (\text{fast-wave input coupler}). \quad (11)$$

A slow-wave coupler would work equally well.

The pitch of the twisted quadrupole must be physically reasonable. An expression for the cyclotron wavelength, and hence also the full pitch (one complete turn or four staggered sections) of the quadrupole, is

$$\lambda_c(\text{inches}) = 8.35 \frac{V_0^{1/2}(\text{volts})}{B(\text{gauss})}, \quad (12)$$

where  $V_0$  is the dc voltage corresponding to the axial velocity of the electrons, and  $B$  is the longitudinal dc magnetic field. Fig. 6 shows the voltages and magnetic fields required for typical cyclotron wavelengths. To obtain a simple formula for the gain in the twisted quadrupole section, we can note that if the elements of the quadrupole are located at radius  $R$  and carry dc pump voltages  $\pm V_p$ , then from (4) one can write  $V_p = \frac{1}{2}KR^2$ . Obtaining  $K$  from this in terms of  $V_p$  and  $R^2$ , one can after a little manipulation write the gain expression in the form

$$G(\text{db}) = A + 1.38 \left( \frac{\lambda_c}{R} \right)^2 \left( \frac{V_p}{V_0} \right) N, \quad (13)$$

where  $N$  is the number of cyclotron wavelengths in the length  $L$  of the quadrupole section.

Using these expressions, a reasonable set of parameters might be

$$\begin{aligned} V_0 &= 1000 \text{ volts}, \\ B_0 &= 1000 \text{ gauss}, \\ \lambda_c &= \frac{1}{4} \text{ inch}, \\ \lambda_c/R &= 2, \quad R = \frac{1}{8} \text{ inch}, \\ V_p/V_0 &= 0.8, \\ N &= 8, \\ A &= -6, \\ G &= 30 \text{ db}. \end{aligned}$$

Thus, these conditions would give an over-all gain of 30 db in a 2-inch long quadrupole section, including the initial loss. The low gain per unit length assumption  $\kappa \ll \beta_c$  made earlier can, incidentally, be rewritten as  $G(\text{db}) \ll 27N$ , which is fairly well satisfied in this example.

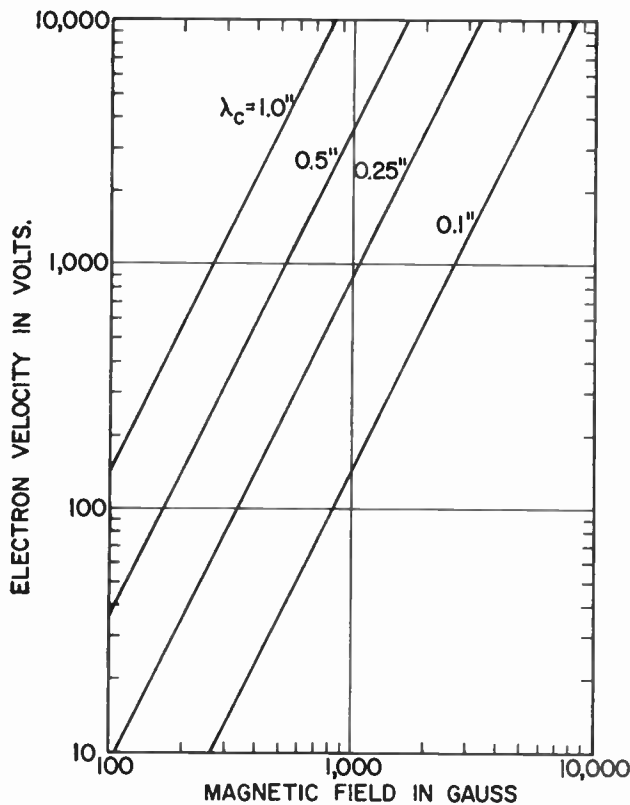


Fig. 6—Beam velocities and longitudinal dc magnetic fields required for various cyclotron wavelengths.

Note the fact, perhaps surprising at first glance, that the design parameters thus far involve neither frequency nor current. The gain mechanism is totally independent of frequency, at least to first order, and has infinite bandwidth. Moreover, the gain simply represents the exponential growth of individual electron trajectories and is thus independent of current. However, frequency and current considerations will certainly enter into the design of input and output couplers, and into power output considerations.

So far as power output is concerned, one can show that for a beam with equal amounts of fast and slow waves, the half width  $r_0$  of the beam ribbon (*i.e.*, the radius of the largest electron orbit) is related to the power in the fast wave by

$$P = \frac{1}{8} \omega B I_0 r_0^2, \quad (14)$$

where all quantities are in mks units. Picking some easily obtainable numbers, with no attempt to obtain high power, one might have a design such as

- Beam voltage = 1000 volts, as above,
- Beam current = 200 microamperes,
- Beam diameter = 0.01 inch,
- Current density = 0.1 amp/cm<sup>2</sup>,
- Beam power = 200 milliwatts,
- Frequency = 3000 mc,
- Magnetic field = 1000 gauss.

With such a beam, even if the fast-wave power reached the clearly impossible level of being equal to the dc power, the maximum beam radius would still be only 0.075 inch. Thus, the beam would be in no danger of striking the quadrupole structure. In the particular case given here, the condition  $\omega = \omega_c$  holds, so that a simple Cuccia fast-wave coupler<sup>4</sup> could be used. The beam current quoted is probably too low to permit coupling with any very substantial bandwidth, however.

#### ANOTHER DC QUADRUPOLE DEVICE

In the early stages of this work, the author was led to consider the situation where the twisted quadrupole twists at only one-half the twist rate of the electrons in the beam. As will be shown, this condition does not lead to growing waves on the beam.

The reasoning behind this alternative scheme may be appreciated by considering Fig. 7. Suppose that at the input the electrons enter on the tube axis, but with RF modulated transverse velocities upwards and downwards. This is the type of modulation that results, for example, from a very short pair of deflection plates. It corresponds to equal excitation of all four transverse beam waves. As Fig. 7 shows, the electrons will then follow helical orbits displaced from the tube axis. Only the outermost or largest orbits are shown; the heavy lines indicate the beam locus during the RF cycle, as previously. Examination of Fig. 7 will show that, during most of its cycle, an electron sees at least some dc pump field component parallel to its transverse motion. Therefore, amplification might be expected, at least by analogy with the case in Fig. 4. Note that the quadrupole is twisting at only one-half the beam rate.

This case corresponds to putting the condition  $\beta_q = \frac{1}{2}\beta_c$  into the general equations of motion in (5). If one does this and separates out terms with similar  $z$  dependence, one obtains the set of equations

$$\begin{aligned} \frac{dA_s}{dz} &= -\kappa A_{e2}, & \frac{dA_{e2}}{dz} &= \kappa A_s, \\ \frac{dA_f}{dz} &= -\kappa A_{e1}, & \frac{dA_{e1}}{dz} &= \kappa A_f. \end{aligned} \quad (15)$$

The solutions to these equations, including initial conditions, are

$$\begin{aligned} A_s(z) &= A_s(0) \cos \kappa z - A_{e2}(0) \sin \kappa z, \\ A_f(z) &= A_f(0) \cos \kappa z - A_{e1}(0) \sin \kappa z, \\ A_{e1}(z) &= A_{e1}(0) \cos \kappa z + A_f(0) \sin \kappa z, \\ A_{e2}(z) &= A_{e2}(0) \cos \kappa z + A_s(0) \sin \kappa z. \end{aligned} \quad (16)$$

In other words, the two negative-energy waves  $A_s$  and  $A_{e2}$  couple to each other in such a way that they beat

<sup>4</sup> C. L. Cuccia, "The electron coupler," *RCA Rev.*, vol. 10, pp. 270-303; June, 1949.

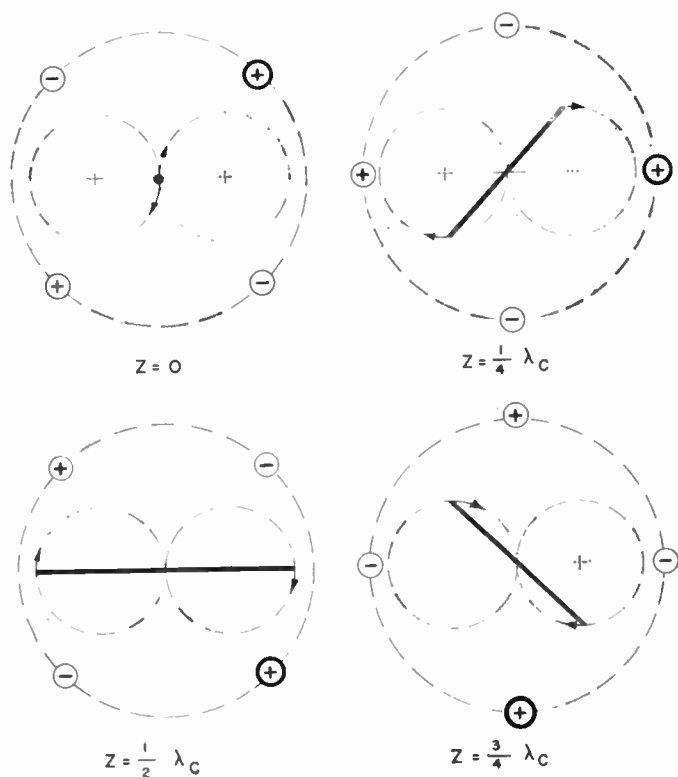


Fig. 7—Cross sections of a quadrupole device in which the quadrupole twists at only one-half the cyclotron rate. Amplification does not result.

together and interchange energy, and similarly for the two positive-energy waves. There is no exponential growth or amplification. The only apparent use for this effect might be as a mode coupler in some sophisticated noise-interchanging scheme.

DISCUSSION

The dc quadrupole amplification principle, either in the staggered quadrupole form as originally proposed by Gordon, Buchsbaum, and Feinstein or in the twisted quadrupole form, appears to have great promise as a microwave electron-beam amplifier, although, of course, only further development will prove its usefulness. The unlimited bandwidth of the amplification mechanism is attractive, although the problem of broad-band input and output coupling has not yet been solved. The absence of any slow-wave circuit in the amplification region makes the device attractive for higher-frequency application. Finally, the device may even have usefulness as a low-noise amplifier. The dc quadrupole amplifier is not a true fast-wave parametric amplifier like the Adler-Wade quadrupole amplifier. It has the same problem of slow-wave noise as do all other nonparametric electron-beam amplifiers. Nonetheless, there are methods for removing or lessening cyclotron-wave noise, in effect cooling the beam, which are different from and not available to the space-charge-wave beam tubes.<sup>5</sup> It may prove possible to use these methods to make a low-noise dc quadrupole amplifier.

ACKNOWLEDGMENT

The author gratefully acknowledges many discussions with, among others, Drs. G. Wade, D. A. Watkins, W. Kluver, and E. I. Gordon, and with Mr. Shing Mao of the Stanford Electronics Laboratory.

<sup>5</sup> G. Wade, Stanford Electronics Labs., Stanford, Calif.; R. Adler, Zenith Radio Corp., Chicago, Ill., and W. Kluver, Bell Telephone Labs., Inc., Murray Hill, N. J. (Private communications.)

CORRECTION

In "A Unified Analysis of Range Performance of CW, Pulse, and Pulse Doppler Radar," by J. J. Busgang, P. Nesbeda, and H. Safran, which appeared on pages 1753–1762 of the October, 1959, issue of PROCEEDINGS, Lee E. Davies, of the Stanford Research Institute, has called the following to the attention of the *Editor*.

In (33), page 1759, the plus sign should be a minus sign.

Since this equation is said to be good when  $\lambda_1^2/\lambda_2$  is large, the equation is more convenient for calculation if written:

$$S = \left[ \left( \frac{V_T}{\lambda_1} \right)^{1/3} - 1 \right] \left[ \frac{3\lambda_1}{\sqrt{\lambda_2}} \right] + \frac{\sqrt{\lambda_2}}{3\lambda_1}$$

although, of course, this does not show the derivation as clearly.

# High Selectivity with Constant Phase Over the Pass Band\*

AUGUST W. RIHACZEK†

**Summary**—The frequency dependence of the phase in selective circuits causes problems in systems that utilize the signal phase as a carrier of information. For example, in a Doppler system the phase change originating within the receiver represents an error in the measurement. A relatively simple method for compensation of phase shifts in filters, resulting in a constant output signal phase, has been developed. In principle, the signal frequency is inverted by means of a mixer, and the signal is passed through a filter to create a phase shift in one direction. The signal frequency is then reinverted in another mixer, and the resulting signal is again passed through a filter which now effects a phase change in the opposite direction. By properly choosing the filter constants and combining the two signals, the two phase shifts will compensate each other, giving an output signal whose phase is independent of the frequency. The method of phase compensation is not restricted to a particular frequency range or a particular type of circuitry. What is needed in addition to conventional circuitry without phase compensation is a local oscillator and simple mixers. In some applications, a local oscillator is provided already (for example, parametric amplifiers or frequency converters), making the adaptation of the compensation principle very simple and economical. The method was developed for the slow frequency variations in Doppler systems, but should also be applicable to the rapid variations of frequency or phase modulation, where a phase change with frequency may be undesirable in some applications. The principle may be equally useful in circuitry where variations of the phase cause problems of operation rather than merely signal distortions or errors in the measurement.

## INTRODUCTION

IN designing highly selective circuits, difficulty is encountered in achieving a narrow-band characteristic without, simultaneously, introducing a strong frequency dependence of the phase. This sensitivity of the phase to frequency changes, greater in filters of higher selectivity, will be of no interest in a system utilizing solely the amplitude of the signal as a carrier of information. If, however, the phase of the signal conveys a part or all of the information, any variation in phase may greatly restrict the system capabilities. For example, in Doppler instrumentation for missile and satellite trajectory measurements, a phase shift originating within the equipment, rather than as a result of movement of the object being tracked, will introduce an error in the measurement.

Because of the increasing importance of Doppler systems, extensive work has gone into the development of selective, constant-phase transponders and receivers. Until now the only successful approach to this problem has been the phase-lock system or tracking filter, which uses a feedback loop to tie the phase of the output signal

to that of the input signal. In addition to providing the desired constancy of phase over its narrow pass band, a tracking filter can follow a signal of changing frequency within a wide frequency band. This is more than is needed for many practical applications where a constant phase is of paramount importance rather than the extremely narrow bandwidth which can be realized with a tracking filter. There is need for a simple selective circuit of fixed center frequency with a bandwidth just wide enough to accommodate the expected frequency shift of the signal and a phase shift which is independent of the frequency. This simple and more reliable device could be substituted for the complex tracking filter in applications where stability of the phase and equipment simplicity are more important than the ultimate in selectivity.

Work in the field of Doppler instrumentation has led to the development of a simple method for compensation of frequency-dependent variations of the phase in a selective circuit. Since this principle is not restricted to particular equipment, it should find more applications than merely for the trajectory measuring systems for which it was developed.

## PHASE COMPENSATION FOR SELECTIVE AMPLIFIERS

Linear filtering techniques do not permit the design of a highly selective filter without simultaneously obtaining, within the pass band, a strong dependence of the phase on the signal frequency. This is true for all types of passive and active linear networks. For a minimum phase shift networks theory shows that phase and attenuation characteristics are uniquely related to each other.<sup>1</sup> Unfortunately, the slope of the phase characteristic increases with decreasing bandwidth so that the variation of the phase cannot be suppressed without destroying the selective properties of the filter. Furthermore, because of the unique relation between phase and attenuation, it is impossible to design two selective filters with phase variations in the opposite direction and compensate the over-all phase variation by using the filters in series. These results are still valid when all-pass filters are included, for the phase characteristic of an all-pass filter is of the same type as that of a band-pass filter within its pass band. Finally, these conclusions must hold even when active elements are incorporated, since active elements can only add positive or negative attenuation.

\* Received by the IRE, January 29, 1960; revised manuscript received, June 7, 1960.

† Space Technology Labs., Inc., El Segundo, Calif.

<sup>1</sup> H. W. Bode, "Network Analysis and Feedback Amplifier Design," D. Van Nostrand Company, New York, N. Y.; 1945.

The problem of phase shift can be illustrated by the circuits most commonly used in selective amplifiers, namely, tuned parallel circuits and coupled bandfilters. In a single tuned circuit, the slope of the phase characteristic increases with the quality factor  $Q$  of the circuit; however, lowering  $Q$  to reduce the variation of the phase would also widen the pass band. Coupled bandfilters, on the other hand, provide an additional means of reducing the variations of the phase by increasing the degree of coupling, but stronger coupling also means a wider pass band. A reasonably constant phase can be attained only at the expense of greatly increased bandwidth.

As the tracking filter has shown, the solution to the narrow-band, constant-phase filter must be looked for in nonlinear circuit techniques. One particularly simple approach to the problem is derived by the following reasoning: The selective filters under consideration all show the same type of phase characteristic within their pass band, for example an increasing phase for increasing frequency. Therefore, a positive change in frequency will be accompanied by a positive change in phase, and a negative change in frequency will cause a negative phase shift. As discussed above, this relation cannot be altered without destroying the selective properties of the filter, but, instead of attempting to change the characteristics of the filter, we can reverse the sign of a phase shift by reversing the frequency trend of the signal by subtracting the signal frequency from a higher reference frequency, as is done by a frequency inverting demodulator. What was an increasing frequency before inversion becomes a decreasing frequency after inversion, and vice versa. A phase shift caused in the noninverted signal will have the opposite sign from a phase shift caused in the inverted signal. Thus, we can compensate the phase shift of one filter by inverting the signal frequency, passing the inverted signal through a second filter of the same type, and suitably combining the filtered inverted with the filtered noninverted signal.

The described method of phase compensation will be successful if the frequency inversion can be accomplished without simultaneously changing the sign of the signal phase, since this change in the sign would nullify the attempted reversal of the sign of the phase shift and would restore the original frequency trend of the phase. For example, by subtracting the signal frequency in a nonlinear element from a higher reference frequency, the output frequency will be inverted with respect to the signal frequency; however, any phase shift caused by a filter at this inverted frequency will again be changed in its sign when, in order to restore the original frequency, the higher reference frequency is again subtracted from the inverted frequency. To avoid the second reversal of the sign of the phase shift, and thus the cancellation of the desired effect, the original signal frequency must be restored in a mixing process which subtracts the now lower reference frequency from the

changed signal frequency. This may seem to be a contradiction to the above, but it will be shown that this requirement merely increases the number of nonlinear elements by one. The circuitry necessary to realize the principle of compensation remains simple.

#### EXAMPLES OF PRACTICAL CIRCUITS

Because of the generality of the compensation method, many ways of arranging practical circuitry can be found; the particular configuration will depend on the requirements of an application. For this reason, we will restrict ourselves to illustrative examples which show how to proceed in the design of equipment. We may write down the equations describing the operations needed to invert the signal frequency and, after filtering, restore the original frequency. Then we may interpret these equations in terms of circuitry, if we keep in mind that 1) each addition or subtraction corresponds to the use of a nonlinear element for mixing, and 2) an equal sign in any equation means the selection of one particular frequency after the mixer and hence requires a filter.

If we use brackets to indicate terms that represent a single frequency signal and write  $[f_s]$  for the signal frequency and  $[f_L]$  for the reference frequency (local oscillator), we can construct a possible set of operations as follows: At first, the signal frequency must be inverted by generating the lower sideband  $[f_L - f_s]$ , and the lower sideband must be filtered out among all possible products of the mixing process. The filter also introduces the unavoidable dependence of the phase of the lower sideband on its exact frequency, considering frequency variations within the pass band of the filter. Next, we have to use a noninverted signal whose phase shift with frequency would have the opposite direction so that the combination of both signals results in a compensation of the changes in the phase, that is, a total phase shift which is independent of the signal frequency.

To achieve the reversal of the frequency trend after one type of phase shift has already been introduced, we transform the (inverted) lower sideband  $[f_L - f_s]$  into the upper sideband  $[f_L + f_s]$  by simply adding twice the signal frequency. The filter required to select the (noninverted) upper sideband from the various mixing products will now introduce a variation of the phase which has the opposite sign as compared to the first filter. The remaining task is the conversion of the upper sideband into the original signal frequency, and this is accomplished in a third mixer by subtracting the reference frequency from the upper sideband  $[f_L + f_s]$ . Again, this mixer must be followed by a filter that selects the desired output signal, and this filter introduces a phase shift of the same sign as the preceding filter. Hence, for cancellation of the over-all phase variation, the phase shift introduced in the first filter must have the same magnitude as the sum of the phase shifts caused by the other two filters.

The described procedure can be summarized in the following three steps:

- a)  $[f_L] - [f_s] = [f_L - f_s]$ ,
- b)  $[f_L - f_s] + [2f_s] = [f_L + f_s]$ , and
- c)  $[f_L + f_s] - [f_L] = [f_s]$ . (1)

Since a mixer reverses the phase shift of a signal if and only if the signal frequency is subtracted from a higher reference frequency or vice versa, the "negative" phase shift introduced in the filtering process of a) is not reversed in the two subsequent mixing operations of b) and c).

Eqs. (1) can be readily realized by practical circuitry: The input signal is mixed with a local oscillator signal, and the lower sideband is filtered out from the many products of the mixing process. In a second nonlinear element we then mix the lower sideband with the input signal and select, by means of another filter, the second order mixing product  $[f_L - f_s] + 2f_s$  to obtain the upper sideband  $[f_L + f_s]$ . Finally, this upper sideband is combined with the local oscillator signal in a third mixer, and the original frequency is selected by a filter. The corresponding block diagram is shown in Fig. 1, neglecting Filter I' for the moment.

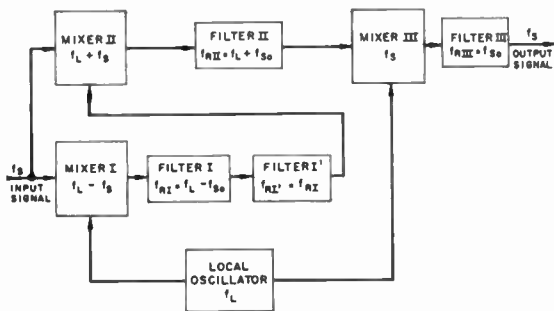


Fig. 1—Basic arrangement for compensation of phase variations. Filters are tuned to the signal frequency, upper sideband, and lower sideband.

In accordance with the above explanation, a change in the input frequency  $f_s$ , which effects a phase shift in each of the selective filters in Fig. 1, will not change the phase of the output signal if the magnitude of the phase shift in Filter I equals the sum of the phase shifts of Filters II and III. However, even the phase characteristic of the simplest type of filter is too complicated to achieve equality of one phase function to the sum of two such functions over the entire bandwidth of the circuit. For this simple reason, the filter following Mixer I has been split into two decoupled parts, Filters I and I', permitting perfect cancellation of the phase variations over the entire pass band. With four filters, one obvious solution (out of many possible ones) for the choice of the filter constants is to make, individually, the phase shifts of Filters I and II equal in magnitude, and likewise those of Filters I' and III.

The derivation of the filter constants to achieve perfect cancellation of the over-all variation of the phase is straightforward. For purposes of illustration, the simple case will be considered where each filter in Fig. 1 consists of a single tuned parallel circuit. It can be easily shown that the total phase shift is simply the sum of the phase shifts of all filters. Variations in the phase of the local oscillator signal will cancel out, since a phase angle added in Mixer I is again subtracted in Mixer III. For a single tuned parallel circuit of given quality factor  $Q$  and resonance frequency  $f_R$ , the phase shift  $\phi$  is determined by

$$\tan \phi = -Q \left( \frac{f}{f_R} - \frac{f_R}{f} \right). \quad (2)$$

The resonant frequencies to which the circuits are tuned are indicated in Fig. 1. Using these values and introducing the relative deviation from the resonance frequency,  $\zeta = 2\Delta f/f_{s0}$ , where  $\Delta f = f_s - f_{s0}$ , and  $f_{s0}$  denotes the center frequency of the signal, the total phase shift  $\tan \phi = \tan(\phi_I + \phi_{I'} + \phi_{II} + \phi_{III})$  may be computed as

$$\tan \phi = \frac{K_1 \zeta - K_2 \zeta^3}{1 + K_3 \zeta^2 + K_4 \zeta^4}. \quad (3)$$

In the derivation of (3), the approximation  $1/(1+\zeta) \approx 1 - \zeta$  was used, but this approximation is valid over the entire pass band of narrow-band amplifiers. The algebra that leads to (3) also yields the constant  $K_n$ , of which  $K_1$  and  $K_2$  are of interest:

$$K_1 = Q_I \frac{1}{a-1} + Q_{I'} \frac{1}{a-1} - Q_{II} \frac{1}{a+1} - Q_{III},$$

$$K_2 = -Q_I Q_{I'} Q_{II} \frac{1}{(a-1)^2} \frac{1}{(a+1)} - Q_I Q_{I'} Q_{III} \frac{1}{(a-1)^2}$$

$$+ Q_I Q_{II} Q_{III} \frac{1}{(a^2-1)} + Q_{I'} Q_{II} Q_{III} \frac{1}{(a^2-1)}, \quad (4)$$

with  $a = f_L/f_{s0}$  designating the ratio of local oscillator frequency to center frequency of the signal. For zero over-all phase shift both  $K_1$  and  $K_2$  must be made zero. Because of the alternating signs for the terms in (4), the condition  $K_1 \equiv K_2 \equiv 0$  can easily be met through suitably choosing the circuit  $Q$ 's and the local oscillator frequency.

The value of  $a$  must be chosen such that the undesired products of the mixing processes are sufficiently separated in frequency from the desired signal to permit its selection by simple filtering; thus, the choice for  $a$  is somewhat restricted. That still leaves four circuit  $Q$ 's to choose with only the contingencies of (4) imposed. This fact usually allows one to accommodate additional requirements of over-all bandwidth of the circuit ar-

rangement, preferred circuit constants, or available components. The special case where the constants  $K_1$  and  $K_2$  are made zero by choosing the phase shifts of Filters I and II and Filters I' and III, respectively, equal in magnitude, leads to the design requirements

$$\begin{aligned} Q_I/Q_{II} &= (a - 1)/(a + 1), \\ Q_{I'}/Q_{III} &= a - 1. \end{aligned} \quad (5)$$

If filter types other than the single tuned circuit are considered, the computation of the circuit requirements for compensation of the phase shift is quite analogous. For coupled bandfilters, consisting of two coupled parallel tuned circuits of the same  $Q_n$ , the relations corresponding to (5) become

$$\begin{aligned} Q_I/Q_{II} &= (a - 1)/(a + 1) = k_{II}/k_I, \\ Q_{I'}/Q_{III} &= a - 1 = k_{III}/k_{I'}. \end{aligned} \quad (6)$$

The  $k$ 's denote the coefficients of coupling for each bandfilter. The actual adjustment of these filters in practical circuitry is not difficult, as the over-all phase shift of the output signal can be checked with a swept frequency input signal as the adjustment is made.

VARIATIONS OF THE CIRCUIT ARRANGEMENT

With the circuit configuration shown in Fig. 1, the filtering with the "negative" phase shift is done at the lower sideband frequency  $[f_L - f_s]$ , while the compensating phase shift of opposite direction is created through filtering at the higher sideband frequency  $[f_L + f_s]$  and at the signal frequency  $f_s$ . For some applications, it may be inconvenient to operate at these three appreciably different frequency levels. The phase compensation principle is general enough to permit variations of the chosen circuit of Fig. 1. For example, if filtering at approximately the same frequency level is desired, the steps of (1) may be rearranged as follows:

- a)  $[f_L] - [f_s] = [f_L - f_s],$
- b)  $[2f_s] - [f_L] = [2f_s - f_L],$
- c)  $[f_L - f_s] + [2f_s - f_L] = [f_s].$  (7)

As compared to (1), only b) and c) have been changed for a different sequence of operations. All filters will be at more nearly the same frequency level, if the reference frequency  $f_L$  is chosen about one and a half times the signal frequency  $f_s$  (yet not at such a value that the selection of the desired mixing product becomes difficult). The corresponding circuit diagram, realizing (7), is depicted in Fig. 2. Filter I' is again included merely to allow perfect cancellation of the phase shift over the entire pass band. Furthermore, since mixing the signal frequency with the local oscillator frequency will result in the end products of both a) and b) of (7), one of the mixers can be eliminated to permit simplification of the circuit as shown in Fig. 3.

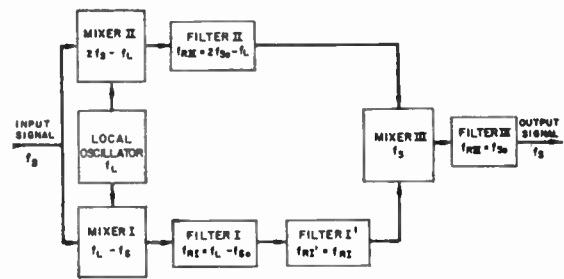


Fig. 2—Alternate circuit for phase compensation, with filters at more nearly the same frequency level.

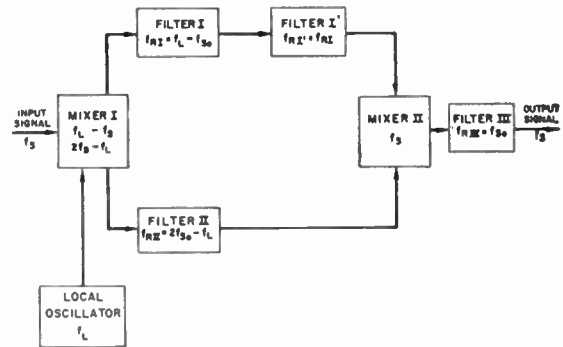


Fig. 3—Simplified circuit for phase compensation with only two mixers.

DISCUSSION

The method of compensating the phase shift of selective filters by filtering both at the inverted and noninverted signal frequency can be realized by simple equipment. Conventional nonlinear elements, such as tubes, transistors, or crystal diodes, can serve as mixers. The filters which must succeed the mixers in order to select the proper mixing product can simultaneously perform the task of interference and noise rejection and thus are needed in a selective amplifier regardless of whether or not phase compensation is attempted. If higher amplification is desired than obtained from the compensation circuit, the arrangement may be preceded by an amplifier with its pass band sufficiently wide to avoid the introduction of an appreciable phase shift. Obviously, it is also quite immaterial where, in the circuit, amplification is introduced, if such is desired.

As compared to conventional amplifiers of high selectivity, the local oscillator required by the phase compensation circuit is an addition. However, if down-conversion is desired, the local oscillator must be provided even for conventional circuitry. An interesting application of the method of phase compensation offers itself for parametric amplifiers. These amplifiers, at least the cavity types, must employ filters to select the desired product of the parametric mixing process and hence should have the problem of phase shift with frequency. On the other hand, parametric amplifiers already use the local oscillator needed to implement the phase compensation principle, namely the "pump." It appears that the described compensation method should be

particularly simple and economical to adapt to parametric amplifiers.

The principle of compensation was developed for systems that involve signals of slow and narrow-band changes of the signal frequency; however, the method should apply equally well to systems with rapidly changing frequency of the signal, or frequency and phase modulation systems. It could serve in critical applications to eliminate the effects caused by the frequency dependence of the phase in filters.

There may be other types of applications for the compensation principle described here. It can be said,

generally, that the method should be useful either to avoid the introduction of errors through phase shifts in the equipment, or to improve the operation of equipment in which phase shifts of selective circuits impose limitations on equipment performance.

#### ACKNOWLEDGMENT

The work reported here was done at White Sands Missile Range, Las Cruces, N. M. The author wishes to thank W. E. Wohlenberg for interesting discussions and suggestions, and W. H. Lentz for help in carrying out the tests of practical circuitry.

## Automatic Phase Control: Theory and Design\*

T. J. REY†, SENIOR MEMBER, IRE

**Summary**—Automatic Phase Control (APC) systems with sinusoidal reference are analyzed, and design criteria are presented. The limit of the pull-in range is derived; the result is believed to be novel, and is found to be in agreement with experiment.

#### GLOSSARY

- $a$  = lead parameter of RC filter (Fig. 6)  
 $B$  = noise bandwidth (17)  
 $G$  = forward transfer function of filterless APC system at lock (6)  
 $J_0$  = Bessel function of order 0  
 $\pm K$  = limits of the control range (frequencies are in radians per second)  
 $N(\omega) = N_\omega \exp(-i\psi_\omega)$  = filter transfer function ( $N(0) = 1$ )  
 $t$  = real time  
 $v$  = control voltage  
 $\hat{V}$  = amplitude of the first-order beat  
 $Y$  = closed-loop transfer function of locked APC system  
 $W$  = open-loop transfer function of locked APC system  
 $\mu$  = modulation index  
 $\nu$  = frequency of FM in locked system  
 $\tau$  = time constant of RC filter (Fig. 6)  
 $\varphi$  = a small change in  $\phi$

- $\phi$  = oscillation phase relative to reference (1)  
 $\omega$  = frequency, error frequency in closed loop  
 $\omega_s$  = reference frequency  
 $\Omega$  = tuning error in open loop  
 $\hat{\Omega}$  = maximum pull-in frequency

#### I. INTRODUCTION

##### A. General

**A**UTOMATIC Phase Control (APC) serves to synchronize an oscillator with a sinusoidal reference signal of low power. It differs from AFC systems wherein a frequency discriminator supplies the control signal so that a frequency error remains. APC has developed from a method of motor tuning in which the oscillation and the reference are combined to generate a field that rotates at the error frequency.<sup>1-3</sup>

The electronic system contains a phase detector (e.g., a balanced mixer), a frequency modulator (e.g., a reactance tube) and a low-pass filter between these parts (Fig. 1). The filtered beat between the oscillation and the reference signal controls the modulator, and tends to compensate the open-loop error frequency  $\Omega$ . The desired control signal is dc proportional to  $\sin \phi_\infty = \Omega/K$ ; the limit of the control range is  $\pm K$ , where

<sup>1</sup> D. G. Tucker, "Carrier frequency synchronization," *P.O. Elec. Engrs. J.*, vol. 33, p. 75-81; July, 1940.

D. G. Tucker, "The synchronization of oscillators," *Electronic Engrg.*, vol. 16, pp. 26-30; June, 1943.

<sup>2</sup> W. J. Gruen, "Theory of AFC synchronization," *Proc. IRE*, vol. 41, pp. 1043-1048; August, 1953.

<sup>3</sup> E. Labin, "Théorie de la synchronisation par contrôle de phase," *Philips Res. Repts.*, vol. 4, pp. 291-315; August, 1949.

\* Received by the IRE, November 27, 1959; revised manuscript received April 15, 1960. Presented in summary at the NEREM Meeting in Boston, Mass., November 19, 1958. The work reported in this paper was performed by Lincoln Laboratory, a center for research operated by Massachusetts Institute of Technology, with the joint support of the U. S. Army, Navy, and Air Force.

† M.I.T. Lincoln Lab., Lexington, Mass.

$K$  = maximum beat voltage  $\hat{V} \times$  modulator sensitivity,  
 $\hat{V}$  = smaller of the inputs to the detector  $\times$  conversion gain  $\times$  dc gain between detector and modulator.

The angle  $\phi_\infty$  accounts for the static phase difference between the reference and the locked oscillation (Fig. 2). When  $\Omega > K$ , the system is in its asynchronous state and  $\Omega$  must be reduced to the value  $\hat{\Omega}$  for lock to occur. When the "pull-in ratio"  $(\hat{\Omega}/K) < 1$ , a hysteresis effect (sometimes called "pulling effect") exists since, if  $\Omega$  drifts slowly, the state does not change when  $\Omega$  enters the interval between  $\hat{\Omega}$  and  $K$  from either side (Fig. 3).

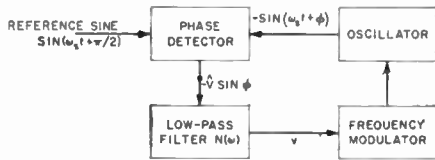


Fig. 1—Block diagram of APC system.

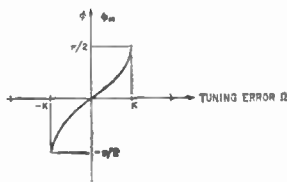


Fig. 2—Phase vs tuning error characteristic.

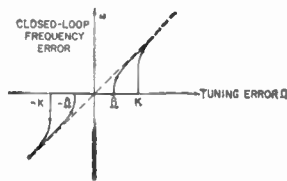


Fig. 3—Hysteresis effect.

The objects of synchronization are varied and sometimes conflicting, e.g.,

- 1) Power in excess of the reference
- 2) Spectral purity in excess of the reference (frequency synthesis)
- 3) Phase close to the reference (TV, Radio interferometry)
- 4) Tracking of frequency changes (e.g., satellites)<sup>4,5</sup>
- 5) Spectral purification of the oscillation (microwaves)<sup>6-8</sup>

<sup>4</sup> R. Leek, "Phase-lock AFC loop, tracking signals of changing frequency," *Electronic and Radio Engr.*, vol. 34, pp. 141-146, 177-183; April/May, 1957.

See also R. Jaffe and E. Rechten, Jet Propulsion Lab., California Institute of Technology, Progress Rept. No. 20-243; December, 1954.  
<sup>5</sup> L. V. Berkner, "Annals of the International Geophysical Year," Pergamon Press, New York, N. Y., vol. 6, pp. 410-416; 1958.

<sup>6</sup> M. Peter and M. W. Straudberg, "Phase stabilization of microwave oscillators," *Proc. IRE*, vol. 43, pp. 869-873; July, 1955.

<sup>7</sup> G. Winkler, "Progress in Phase-Lock Techniques," *Proc. of the 11th Annual Symp. on Frequency Control*, U. S. Signal Corps, Fort Monmouth, N. J., pp. 335-336; May, 1957.

<sup>8</sup> I. L. Bershtein and V. L. Sibiriakov, "Phase stabilization of microwave generators," *Radiotekhn. i Elektron.*, vol. 2, pp. 944-945; July, 1957.

Further possibilities include:

- 6) A source of FM centered on the reference frequency (Section III G)
- 7) A phase or frequency discriminator (Sections III, D and IV, B).

The object of this paper is the preparation of a design basis in terms of system parameters.

Section II deals with a filterless system to exemplify such basic subjects as phase pull-in, asynchronous degeneration, and the effects of small perturbations at lock.

Section III establishes the equivalent circuit that allows for a filter in the control system. Design equations (19) and (22) follow by optimization with regard to detector noise. Different criteria hold when phase perturbations are considered (Section III, D and E). Section III concludes with the pull-out problem and with self-maintaining FM in the locked state.

Section IV hinges on the demonstration of the asynchronous limit cycle. Its degenerative properties allow  $(\hat{\Omega}/K)$  to be determined (Section IV-C), and hence, to be compared with experimental data (Section IV-D). Agreement is satisfactory, as is the result that pull-in range  $\hat{\Omega}$  and noise bandwidth  $B$  are roughly equal in a system optimized with regard to  $B$ .

Section V reviews some complications.

B. Analytical

Let

- $\sin(\omega_s t + \pi/2)$  = the time dependence of the reference signal,
- $-\sin(\omega_s t + \phi)$  = the time dependence of the oscillation.

Then their first-order beat has the form

$$V = -\hat{V} \sin \phi. \tag{1}$$

The modulator control voltage  $v$  is the output of the filter  $N$  fed with  $V$ , and determines the instantaneous angular frequency

$$\dot{\phi} = \Omega + Kv/\hat{V}. \tag{2}$$

where  $\dot{\phi} = d\phi/dt$ ,  $\Omega$  = open-loop tuning error, and the modulation sensitivity  $K/\hat{V}$  is regarded as a constant.

Since exact analysis is precluded by the nonlinearity of (1), previous theory of the asynchronous state has been confined mainly to numerical or graphical analysis with regard to the phase plane. The present treatment is based on three observations:

1) The closed system tends toward a steady state or limit cycle wherein the control voltage approaches a harmonic series.

2) The dc and the fundamental component of the control voltage suffice for an approximate analysis of two important cases:

- a) the synchronous state,

b) the steady asynchronous state, including that which corresponds to a tuning error at the pull-in limit ( $\Omega = \hat{\Omega}$ ).

3) Operational methods can be applied readily to case a), but not to case b).

II. THE FILTERLESS CASE

The analysis is simplified if the filter passes the beat of (1) without modification while rejecting all other components in the detector output; then  $v = V$  and

$$\dot{\phi} = \Omega - K \sin \phi, \tag{3a}$$

$$= K(\sin \phi_\infty - \sin \phi), \tag{3b}$$

where

$$\phi_\infty = \arcsin \Omega / K,$$

$$|\phi_\infty| < \pi/2 \text{ and } \phi \text{ is real if } |\Omega| < K. \tag{4}$$

The circle diagram of Fig. 4 illustrates the differential equation, and suggests a driven pendulum subjected to a driving torque ( $\Omega$ ), to gravity ( $K \sin \phi$ ) and to viscous damping ( $\dot{\phi}$ ); the inertia is negligible in the absence of a filter [but see (23a)].

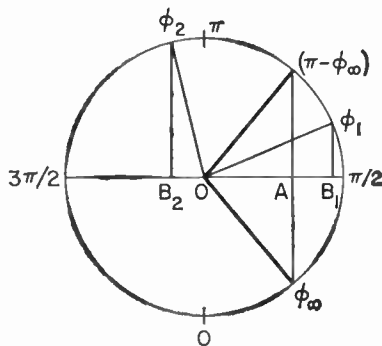


Fig. 4—Phase regions.

When  $|\Omega| < K$ , the “velocity”  $\dot{\phi}$  is proportional to  $(OA - OB)$ , where  $A$  and  $B$  are the projections on the diameter through  $(\pi/2)$  of  $\phi_\infty$  and  $\phi$ , respectively. Thus,

1)  $\dot{\phi}$  is negative when  $\phi (= \phi_1)$  is on the short arc between  $\phi_\infty$  and  $(\pi - \phi_\infty)$ ;

2)  $\dot{\phi}$  is positive when  $\phi (= \phi_2)$  is on the long arc between  $\phi_\infty$  and  $(\pi - \phi_\infty)$ .

Since  $\dot{\phi} = 0$  only when  $\phi = \phi_\infty$  or  $(\pi - \phi_\infty)$ , equilibrium is stable at  $\phi_\infty$  but unstable at  $(\pi - \phi_\infty)$ . The phase cannot pass through the equilibrium values, and must reach  $\phi_\infty$  with a total phase change  $< 2(\pi - \phi_\infty)$  from anywhere; this process of initial stabilization is called “phase pull-in.” The exact integral of (3b) is considered in the Appendix, but can be approximated by linearization; thus

$$\sin \phi \sim \phi \text{ for } -\pi/2 < \phi < \pi/2,$$

then

$$(\phi - \phi_\infty) \sim \phi_0 \exp(-KT),$$

then

$$\sin \phi \sim (\pi - \phi) \text{ for } \pi/2 < \phi < 3\pi/2,$$

$$(\phi - \phi_\infty) \sim \phi_0 \exp KT. \tag{5}$$

The decay or growth is roughly exponential with time constant  $1/K$ . However,  $\phi$  is not discontinuous at  $\pm \pi/2$ , although the approximation suggests it.

The case  $\Omega > K$  merits attention. The system is then asynchronous, of course, but the average frequency error is less than  $\Omega$ . Eq. (3a) in the form

$$\dot{\phi} = K \left( \frac{\Omega}{K} - \sin \phi \right)$$

shows that

$$0 < \dot{\phi} < \Omega \text{ where } \phi = \pi/2,$$

$$\Omega < \dot{\phi} \text{ where } \phi = -\pi/2.$$

Hence,  $\phi$  dwells longer on the arc from 0 to  $\pi$  than on the supplementary arc,  $\sin \phi$  has a positive mean, and the control signal  $-\dot{V} \sin \phi$  has a dc component of the correct polarity for reducing the tuning error. The asynchronous state can be said to have degenerative properties.

It will now be shown that the locked system is described by a forward transfer function

$$G = K/iv \tag{6}$$

and a feedback function

$$\cos \phi_\infty = \sqrt{1 - \Omega^2/K^2} \tag{7}$$

with reference to the perturbation  $\varphi$  of the controlled phase that results from a small voltage disturbance

$$E = A \dot{V} \exp ivt, \quad |A| \ll 1.$$

The proof is as follows. When the loop is opened between detector and modulator, and  $E$  together with the lock-maintaining bias  $-\dot{V} \sin \phi_\infty$  is applied to the latter, the oscillation phase is perturbed by

$$\varphi_0 = \frac{K}{iv} \frac{E}{\dot{V}}.$$

The perfect integration is due to FM, and (6) follows on taking  $V\varphi_0$  as the output. However, the detector output is

$$-\dot{V} \sin(\phi_\infty + \varphi_0) \sim -\dot{V} \sin \phi_\infty - \dot{V} \varphi_0 \cos \phi_\infty$$

$$\text{if } |\varphi_0| \ll 1, \tag{8}$$

and reveals the feedback function of (7) that depends on tuning error but not on the perturbing frequency.

A sudden perturbation  $\varphi_0$  of the oscillation phase is easily shown to decay as

$$\varphi = \varphi_0 \exp(-Kt \cos \phi_\infty). \tag{9}$$

Locked system properties are considered further in the next section.

### III. THE SYNCHRONOUS STATE

#### A. The Stable State

The low-pass filter will be described by the transfer function

$$N(\omega) = N_\omega \exp[-i\psi_\omega]. \quad N_\omega \text{ and } \psi_\omega \text{ real, } N(0) = 1. \tag{10}$$

In the case of the locked loop, allowance for the filter is made by modifying the forward function to  $NG$ ; the over-all transfer function  $NG \cos \phi_\infty$  must satisfy Nyquist's criterion for stability. (Evidently  $NG$  and  $\cos \phi_\infty$  play the parts of the "μ" and "β" of feedback theory.) The stably locked system is a form of regulator; with regard to small perturbations, it is represented by an equivalent circuit comprising linear transfer functions and a differencing element (Fig. 5). The signal  $E$  injected into the filter perturbs the oscillation phase by the amount

$$\varphi = YE/\hat{V},$$

where  $Y$  is the transfer function

$$Y = NG/(1 + NG \cos \phi_\infty). \tag{11}$$

In many instances, the stability condition is related to the frequency  $\nu$  at which the filter has a 90° lag through

$$\frac{K}{\nu} N_\nu \cos \phi_\infty < 1 \quad \text{where } \psi_\nu = \frac{\pi}{2}. \tag{12}$$

The static phase error  $\phi_\infty$  of (4) is not affected by  $N$  if the system is stable.

#### B. RC Filter with Compensation

A particularly suitable filter has the configuration of Fig. 6 and the transfer function

$$N(\omega) = \frac{1 + i\omega a\tau}{1 + i\omega\tau}, \quad 0 \leq a \leq 1; \tag{13}$$

the limit  $a=0$  corresponds to a simple RC filter, and the limit  $a=1$  corresponds to no filter. By substituting in (11),

$$Y = K \frac{1 + i\nu a\tau}{K \cos \phi_\infty + i\nu(1 + aK\tau \cos \phi_\infty) - \nu^2\tau}, \tag{14a}$$

or

$$Y = \frac{1 + i\nu(2\zeta K/\omega_n)}{1 + i\nu(2\zeta/\omega_n) - (\nu/\omega_n)^2} \sec \phi_\infty, \tag{14b}$$

where

$$\omega_n^2 = \frac{K}{\tau} \cos \phi_\infty, \quad 2\zeta = (K\tau \cos \phi_\infty)^{-1/2} + a(K\tau \cos \phi_\infty)^{1/2},$$

$$k = \frac{aK\tau \cos \phi_\infty}{1 + aK\tau \cos \phi_\infty}, \quad 2\zeta\omega_n = \frac{1}{\tau} + aK \cos \phi_\infty, \tag{15a}$$

or conversely,

$$K \cos \phi_\infty = \frac{\omega_n}{2\zeta(1-k)}, \quad \frac{1}{\tau} = 2\zeta\omega_n(1-k),$$

$$a = 4\zeta^2 k(1-k). \tag{15b}$$

Now, a stable linear feedback system can be represented by a passive circuit; corresponding to the locked system with the compensated RC filter is the LRC circuit of Fig. 7. It has resonant frequency  $\omega_n$ , and damping ratio  $\zeta$ ; the output terminals 1, 3 are across  $C_{eq}$  and  $kR_{eq}$  in series, and deliver the output  $\varphi \hat{V} \cos \phi_\infty$  rather than  $\varphi \hat{V}$ .

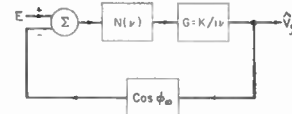


Fig. 5—Locked system equivalent circuit.

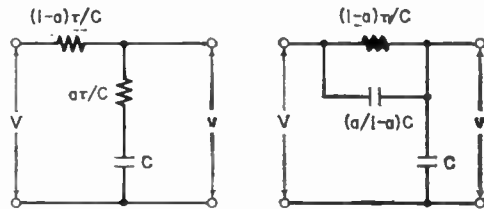


Fig. 6—Filters with transfer function  $(1+i\omega a\tau)/(1+i\omega\tau)$ .

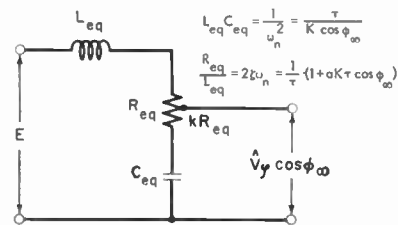


Fig. 7—Equivalent passive circuit with filter of Fig. 6.

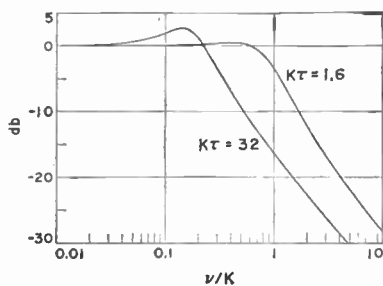
If  $E$  is a small step at time  $t=0$ , the subsequent phase perturbation follows from (15b) as

$$\varphi = \frac{E}{\hat{V}} \sec \phi_\infty [1 - g(t)],$$

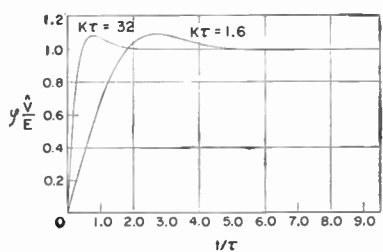
$$g(t) = (\exp - \zeta\omega_n t) \left[ \cos \sqrt{1 - \zeta^2}\omega_n t - \frac{(2k-1)\zeta}{\sqrt{1 - \zeta^2}} \sin \sqrt{1 - \zeta^2}\omega_n t \right]. \tag{16}$$

The cases  $K\tau=1.6$  and  $32$ ,  $\Omega=0$ , and  $a$  chosen according to (21a), are illustrated for both the sinusoidal and step responses by Fig. 8.

A certain design criterion will now be discussed.



(a)



(b)

Fig. 8—Optimized transfer functions of locked system; (a) sinusoidal response and (b) step response.

C. The Noise Bandwidth

Let white noise of mean square (MS) value  $\overline{\delta e^2} = \overline{A^2 V^2 \delta \nu}$  per unit bandwidth be injected into the detector output. The resultant phase perturbation is random, with MS value

$$\overline{\varphi^2} = \overline{A^2} B, \tag{17a}$$

where (the lower limit of integration being  $-\infty$  for noise at the detector input)

$$B = \int_0^\infty |Y|^2 d\nu. \tag{17b}$$

If  $\overline{\varphi^2}$  is small, clipping caused by nonlinearity is unimportant; (17a) then shows the relative contribution of injected noise to the oscillation spectrum, and can be expressed in the form

$$\text{in-band spurious contribution} = 10 \log_{10} \overline{A^2} B \text{ db.} \tag{17c}$$

The “integrated noise bandwidth”  $B$  is an index of noise performance; the spectral distribution of  $\varphi$  is  $|Y|$ , of course, and the 3-db bandwidth is found from (14a), e.g., as

$$K \cos \phi_\infty \text{ for } a = 1,$$

and as

$$\omega_n \{ 1 - 2\zeta^2 + [1 + (1 - 2\zeta^2)^2]^{1/2} \}^{1/2} \text{ for } a = 0.$$

The value of  $B$  for a system without filter or with a simple RC filter is, with (14) for  $a=0$  or  $1$  and on integrating (17b) by partial fractions or in the complex plane,

$$B = \pi K / 2 \sqrt{1 - \Omega^2 / K^2}. \tag{18a}$$

At the edge of the control range  $\Omega=K$ , the feedback vanishes,  $B$  is infinite, and operation is unstable because of noise;  $B$  has its least value  $\pi K / 2$  when  $\Omega=0$ . Given  $\Omega=\Omega_0$ , the corresponding  $B$  is minimized on taking

$$K = \sqrt{2}\Omega_0;$$

then

$$B = \pi\Omega_0 (= \pi K / \sqrt{2}). \tag{18b}$$

The time constant  $\tau$  affects  $B$  only indirectly, by precluding pull-in if  $\Omega$  exceeds  $\hat{\Omega}$  (Fig. 3). A system with simple RC filter is then optimized with regard to detector and predetector noise by

$$K = \sqrt{2}\Omega_0, \quad K\tau = 2.6, \tag{19}$$

on using (35) and  $\Omega_0 = \hat{\Omega}$ . As  $\Omega$  drifts towards  $K$ ,  $B$  is doubled when  $\Omega \sim 1.33\Omega_0$ ; for greater drifts, it is necessary to increase  $K$  and  $K\tau$  beyond the above values.

In the case of a system with compensated RC filter, (18a) is replaced by

$$B = \left( \frac{1 + a^2 K \tau \cos \phi_\infty}{1 + a K \tau \cos \phi_\infty} \right) \frac{\pi K}{2} \sec \phi_\infty \tag{20a}$$

$$= \left( \frac{1}{2\zeta} + 2k\zeta \right) \frac{\pi \omega_n}{2} \sec^2 \phi_\infty. \tag{20b}$$

It is readily shown<sup>2</sup> that  $B$  has a broad minimum if

$$\zeta = \frac{1}{2} \sqrt{1 + (\omega_n / K \cos \phi_\infty)^2}$$

so that

$$B = \pi \omega_n \text{ if } \zeta = 1/2 \text{ and } \omega_n \ll K.$$

The last condition entails a low pull-in ratio (Section IV, C), ensures a small static phase error in the absence of drift and corresponds to the lead parameter

$$a = (\sqrt{K\tau} - 1) / K\tau.$$

The increase of  $B$  with the tuning error is evident from (20a). However,  $B$  is minimized by the lead parameter  $a$  if

$$(1/a) = 1 + \sqrt{1 + K\tau \cos \phi_\infty}, \tag{21a}$$

so that

$$B_{\min} = (\pi/\tau) (\sqrt{1 + K\tau \cos \phi_\infty} - 1) \sec^2 \phi_\infty. \tag{21b}$$

The lowest curve of Fig. 9 represents (21a) if the abscissae are read as  $K\tau \cos \phi_\infty$ . Eq. (21b) is also shown there, normalized with regard to  $a=0$  on dividing by  $(\pi K/2 \cos \phi_\infty)$ ; the middle curve is valid for  $\phi_\infty=0$ . The slight improvement for  $K\tau \sim 1$  becomes more marked as  $K\tau$  increases; it is somewhat less at tuning errors for which  $B$  is not optimized, as indicated by the upper curve that has been computed from (20a) and (21a) on taking  $\Omega = \sqrt{3}K/2$  for  $B$  but  $\Omega=0$  for  $a$ .

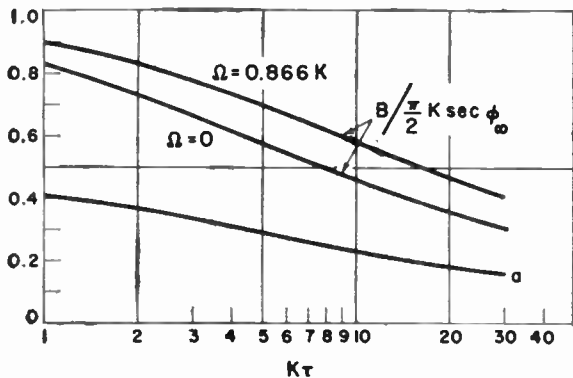


Fig. 9—Normalized noise bandwidth and  $a$  for  $a=(1+\sqrt{1+K\tau})^{-1}$ .

Given  $\Omega = \Omega_0$ , the system is optimized further by differentiating (21a) with respect to  $K$ , and substituting

$$K = \sqrt{2\Omega_0} \sqrt{1 + \epsilon}.$$

The resulting equation

$$\epsilon = (\Omega_0\tau/4)(1 - \epsilon)^2 \sqrt{1 + 2\epsilon};$$

is solved approximately by

$$3\epsilon = [\sqrt{(1 + 4/\Omega_0\tau)^2 + 6} - (1 + 4/\Omega_0\tau)];$$

clearly,

$$\sqrt{2} \leq (K/\Omega_0) < 1.8,$$

the upper limit being approached when  $\Omega\tau_0 \gg 4$ .

System optimization is thus complicated by the effect of the lead parameter  $a$  on both  $B$  and  $\hat{\Omega}/K$ . Two limiting cases are of interest,  $K\tau \gg 1$  [see the paragraph following (20b) above], and  $K\tau < 10$ , say. In the latter case,  $\phi_\infty$  can be appreciable so that  $a$  may be chosen for  $\cos \phi_\infty = 1/\sqrt{2}$  and  $K$  from (19). Also, in view of (35), nearly optimal relations are

$$K = \sqrt{2}\Omega_0, \quad K\tau = 6.7, \quad a = 0.39. \quad (22)$$

The remarks following (19) still apply with regard to drift.

#### D. Perturbations of the Reference Phase

A small signal  $E$  injected into the filter is equivalent to the perturbation  $\epsilon$  of the reference phase ( $\omega_s t + \pi/2$ ), if

$$E = \epsilon \hat{V} \cos \phi.$$

In the closed loop, the detector output is then

$$E/(1 + NG \cos \phi_\infty),$$

and the oscillation phase perturbation is

$$\varphi = \epsilon \cdot Y \cos \phi_\infty,$$

where  $Y$  is defined by (11); the perturbation vanishes where  $\Omega = K$ , i.e., where  $B$  is infinite.

The effects of changes in the reference frequency are of interest; it will be shown that the controlled frequency settles at the correct value if the reference frequency suffers a small impulse or step; however, the response to the ramp  $\dot{\omega}_s$  tends to the error limit  $\dot{\omega}_s/K \cos \phi_\infty$ .

A small step  $\Omega_s$  at time  $t=0$  of the reference frequency  $\omega_s$  is identical with the ramp function of phase

$$\epsilon = \Omega_s t, \quad t \geq 0.$$

The controlled frequency is then subjected to an evanescent error that follows from (16) as

$$-\ddot{\varphi} + \Omega_s = \Omega_s g(t);$$

the change  $\varphi$  of the controlled phase has the steady-state component  $(\Omega_s/K \cos \phi_\infty)$ , as can be shown by integration or by static considerations alone.

If the reference frequency changes at the constant rate  $\dot{\omega}_s (=d\omega/dt)$ , then

$$\epsilon = \dot{\omega}_s t^2/2, \quad t \geq 0,$$

so that

$$\dot{\varphi} - \dot{\omega}_s = -\dot{\omega}_s g(t),$$

i.e., the rate of following the frequency tends towards its correct value. However, steady error components are given by

$$(-\dot{\varphi} + \dot{\omega}_s) \rightarrow \dot{\omega}_s/K \cos \phi_\infty$$

for the frequency, and by

$$\left(-\varphi + \frac{\dot{\omega}_s t^2}{2}\right) \rightarrow \frac{\dot{\omega}_s t}{K \cos \phi_\infty} - \omega_s \frac{\zeta^2 - 2k}{\omega_n^2}$$

for the phase. The situation is complicated if  $\varphi$  or noise is substantial.<sup>4</sup>

#### E. Inherent Perturbations

Small phase perturbations arising within the oscillator (Section V, B) are modified by the factor  $(1 + NG \cos \phi_\infty)^{-1}$ .

In the case of the compensated RC filter, reductions occur at perturbation frequencies below

$$\omega_c = \{K \cos \phi_\infty / \tau [2(1 - a) - a^2 K \tau \cos \phi_\infty]\}^{1/2}$$

if  $\omega_c$  is real, or at all frequencies if

$$(2/a) < 1 + \sqrt{1 + 2K\tau \cos \phi_\infty}.$$

When  $\omega$  is given by (21a), the cutoff frequency equals the resonance frequency  $\omega_n$  of (15a). The closed-loop perturbation  $\varphi$  is related to the open-loop perturbation  $\varphi_{o.l.}$  by the equivalent circuit of Fig. 7 if  $\hat{V}\varphi_{o.l.}$  is applied between terminals 1, 2 and  $\hat{V}\varphi$  is measured across terminals 1 and 3.

The integrated effect of the loop depends upon the nature of the uncontrolled oscillation spectrum. For random phase perturbations confined to the band  $(\omega_a, \omega_b)$  with spectral power distribution  $\omega^{-2}$ , the uncontrolled MS deviation of phase  $\overline{\varphi_{o.l.}^2}$  and frequency  $\overline{\omega^2}$  are related through

$$\overline{\varphi_{o.l.}^2} = \overline{\omega^2} / \omega_a \omega_b.$$

The normalized MS deviation in the closed loop is then given by

$$\frac{\overline{\varphi^2}}{\overline{\varphi_{o.l.}^2}} = \frac{\omega_a \omega_b}{\omega_b - \omega_a} \int_a^b \frac{(1 + \omega^2 \tau^2) d\omega}{[(K \cos \phi_\infty - \omega^2 \tau)^2 + \omega^2 (1 + aK\tau \cos \phi_\infty)^2]}$$

where  $\omega_a < \omega_b$ . The deviation is least for no filter ( $a=1$ ), and  $(K/\tau) > \omega^2$  is desirable.

#### F. Pull-Out

The perturbations considered so far were assumed to be too small to destroy the locked state. An example of another type is the following:

The error  $\Omega_0$  is corrected by  $\phi_0 = \arcsin \Omega_0/K$  when the additional error  $\Omega_1$  is applied suddenly (e.g., owing to a step voltage  $\hat{V}\Omega_1/K$  at the frequency modulator); what is the greatest value  $\hat{\Omega}_1$  that will not throw the system out of synchronism? The condition  $|\Omega| \leq K$  (where  $\Omega = \Omega_0 + \hat{\Omega}_1$ ) is implied, of course.

On allowing for the compensated RC filter that has the differential equation

$$v + \tau \dot{v} = V + a\tau \dot{V},$$

and combining with (1), (2) and (4), the system equation is

$$\ddot{\phi} + \dot{\phi} \left( \frac{1}{\tau} + aK \cos \phi \right) + \frac{K}{\tau} \sin \phi = \frac{\Omega}{\tau}. \quad (23a)$$

In the filterless case ( $a=1$ ), Section II shows that the new equilibrium

$$\phi_\infty = \sin^{-1} \frac{(\Omega_0 + \Omega_1)}{K}$$

is reached without overshoot, and the static condition  $|\Omega| = K$  answers the problem.

This is not so if  $a=0$ . The problem is then identical with that of the pull-out torque for synchronous motors; (23a) is the torque equation if  $\ddot{\phi}$  is due to inertia,  $(\dot{\phi}/\tau)$  arises from the slip between the cage and the ro-

tating field,  $(K/\tau) \sin \phi$  is due to the angle between the fields of rotor and armature, and  $(\Omega/\tau)$  represents the torque load.

An apparent approach is to linearize as in Section II, D; (23a) then becomes

$$\ddot{\phi} + 2\omega_n \dot{\phi} + \omega_n^2 \phi = \omega_n^2 \tan \phi_\infty \quad (23b)$$

which can be solved for  $\phi$  in terms of the initial values  $\phi = \phi_0$ ,  $\dot{\phi}_0 = \Omega_1$ . Since  $\phi_\infty$  is a point of stable equilibrium, it is obvious that if  $|\phi - \phi_\infty|$  is never appreciable, the system will settle at  $\phi_\infty$ . However, the linearized equation does not provide the solution  $\hat{\Omega}_1$ .

The two equilibria  $\phi_\infty$  and  $(\pi - \phi_\infty)$  were found in Section II;  $(\pi - \phi_\infty)$  is unstable also in the presence of a filter, although either point can then be traversed, in general. If the perturbations are such that  $(\pi - \phi_\infty)$  is not traversed, there can be no pullout; the critical condition follows as

$$\ddot{\phi} = \dot{\phi} = 0 \quad \text{where} \quad \phi = \pi - \phi_\infty. \quad (24)$$

Since

$$\ddot{\phi} = \frac{d\dot{\phi}}{dt} = \dot{\phi} \frac{d\dot{\phi}}{d\phi},$$

(23a) can be rewritten as a relation between the variables  $\phi$  and  $\dot{\phi}$ . This leads to the "phase plane" concept of Nonlinear Mechanics, i.e., the graph of  $\dot{\phi}$  vs  $\phi$ . Methods of constructing and interpreting such trajectories are well known.<sup>9-11</sup> Clearly, when  $\dot{\phi} > 0$ , the representative point  $(\dot{\phi}, \phi)$  is in the upper half plane and moves to the right as time increases; conversely for  $\dot{\phi} < 0$ . The pull-out problem is represented by Fig. 10(a);<sup>9</sup> the critical trajectory passes through  $\phi_0$  with infinite slope and cuts the abscissa again at  $(\pi - \phi_\infty)$ . Since equilibrium is unstable there,  $\dot{\phi}$  increases again and the system pulls out into the asynchronous limit cycle for  $(\Omega_0 + \Omega_1)$  (see Section IV, B); alternatively,  $\dot{\phi}$  reverses sign and the system settles at the stable equilibrium point  $\phi_\infty$ .

The case  $a=0$  has been treated by numerical approximation<sup>11</sup> and, more extensively, by integragraph<sup>12</sup> solution of (23a). The result depends upon both  $\Omega_0$  and the damping term  $(K\tau)^{-1/2}$ . The lowest value

$$\frac{\Omega_0 + \Omega_1}{K} \sim 0.72$$

was obtained for  $\Omega_0 = 0$ ,  $1/K\tau = 0$ ; the static limit unity is obtained with sufficient damping ( $1/\sqrt{K\tau} > 0.11$ ).

<sup>9</sup> Z. Jelonek, O. Celinski and R. Syski, "Pulling effect in synchronized systems," *Proc. IEE*, vol. 101, pt. 4, pp. 108-117; November, 1953.

<sup>10</sup> Z. Jelonek and C. I. Cowan, "Synchronized systems with time delay in the loop," *Proc. IEE*, Monograph No. 229R, March, 1957, or vol. 104C, pp. 388-397; September, 1957.

<sup>11</sup> J. J. Stoker, "Nonlinear Vibrations," Interscience Publishers, Inc., New York, N. Y., pp. 70-98; 1950.

<sup>12</sup> W. V. Lyon and H. E. Edgerton, "Transient torque-angle characteristics," *Trans. AIEE*, vol. 49, pp. 686-699; April, 1930.

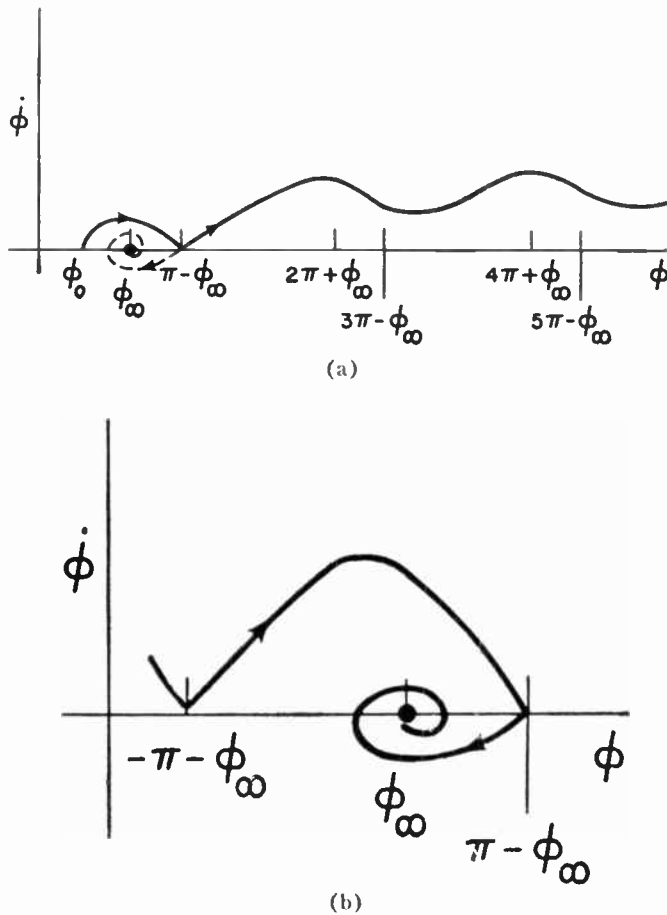


Fig. 10—(a) Pull-out trajectory. (b) Pull-in trajectory.

As  $a > 0$  increases the damping term, the situation for  $0 < a < 1$  is intermediate between that for  $a = 0$  and  $a = 1$ .

G. Instability

The existence of the locked state is compatible with a violation of the stability condition (12). Self-maintained oscillations then occur in the loop and modulate the phase. The oscillations are limited by nonlinearity and are almost sinusoidal when their amplitude is small. A suitable form of the phase is

$$\phi = \phi_\infty + \mu \sin \theta, \quad \dot{\theta} = \nu, \quad (25)$$

where the oscillation frequency  $\nu$  and the deviation index  $\mu$  will be determined with the aid of (1) and (2), and the Fourier-Bessel series

$$\exp(i\mu \sin \theta) = J_0(\mu) + 2iJ_1(\mu) \sin \theta + 2J_2(\mu) \cos 2\theta + \text{terms in } 3\theta \text{ etc.};$$

the control voltage  $V$  follows as the output of the filter  $N$  fed with  $-\dot{V} \sin \phi$ , as

$$\frac{-v}{\hat{V}} = a_0 + b_1 \sin(\theta - \psi_\nu) + a_2 \cos(2\theta - \psi_{2\nu}) + \dots$$

where

$$\begin{aligned} a_0 &= J_0(\mu) \sin \phi_\infty, & b_1 &= 2J_1(\mu) \cos \phi_\infty N_\nu, \\ a_2 &= 2J_2(\mu) \sin \phi_\infty N_{2\nu}, & \dots & \end{aligned} \quad (26)$$

Combining with (2) but ignoring terms of frequency  $2\nu$  etc., then

$$\begin{aligned} \nu \mu \cos \theta &= \Omega - KJ_0(\mu) \sin \phi_\infty \\ &\quad - KN_\nu 2 \cos \phi_\infty J_1(\mu) \sin(\theta - \psi_\nu). \end{aligned}$$

Assuming  $\nu$  and  $\mu$  to be constant, this equation is satisfied separately by the dc and by the coefficients of  $\sin \theta$  and  $\cos \theta$  if

$$\begin{aligned} \sin \phi_\infty &= \frac{\Omega}{KJ_0(\mu)} \cos \psi_\nu = 0, \\ \mu &= -\frac{K}{\nu} N_\nu \cos \phi_\infty 2J_1(\mu). \end{aligned} \quad (27)$$

Thus, if the criterion (12) is violated, synchronism is subject to periodic FM of frequency  $\nu$  and deviation index  $\mu$  such that

$$\frac{\mu^2}{8} \sim 1 - \frac{\nu}{N_\nu K \cos \phi_\infty} \quad \text{if } \mu^2 \ll 1. \quad (28)$$

The gravest of the suppressed terms in (26) has frequency  $2\nu$  and relative amplitude

$$\frac{a_2}{b_1} = \frac{J_1(\mu)}{J_2(\mu)} \tan \phi_\infty \frac{N_{2\nu}}{N_\nu}.$$

Now  $N_{2\nu} < N_\nu$  and  $(J_1/J_2) \sim (\mu/4)$  if  $\mu$  is small; then if  $|\phi_\infty| < \pi/4$ , the ignored term is slight and can be allowed for, e.g., by a variable part of  $\mu$  of frequency  $3\nu$ . Such higher approximations will not be considered further.

IV. NONSYNCHRONOUS STATES

A. The Hysteresis Effect

Hysteresis occurs if the boundary between the locked and the unlocked state depends upon the approach (Fig. 3). In the locked state,  $\Omega$  can drift slowly through the interval  $\pm K$ . However, it is well known that in the asynchronous state,  $|\Omega|$  can fall well below  $K$  before lock occurs. The effect can be estimated as follows: When the loop is opened at the frequency modulator, the filter output is AC of frequency  $\Omega$  and peak amplitude  $\hat{V} N_\omega$  as distinct from the direct  $p-d$  ( $\Omega/K$ )  $\hat{V}$  at lock. Hence, the equality

$$\hat{\Omega} = KN_{\hat{\Omega}}$$

defines a first approximation to the locking ratio  $\hat{\Omega}/K$ ; for a simple RC filter, this is equivalent to

$$\frac{\hat{\Omega}}{K} \sqrt{K\tau} \sim \left[ \left( 1 + \frac{1}{4K^2\tau^2} \right)^{1/2} - \frac{1}{2K\tau} \right].$$

The better approximations derived in Sec. IV-C yield somewhat higher values by allowing for asynchronous degeneration in the closed loop.

### B. Steady Asynchronism

In the asynchronous state, the phase  $\phi$  differs from the open-loop value  $\Omega$  because of modulation by the control voltage. An expression to be considered is

$$\phi = \theta + \gamma + \mu \sin \theta, \quad \dot{\theta} = \omega \quad (29)$$

where  $\gamma$  is a phase angle and  $\mu$  is a deviation index.

A steady asynchronous state is described by  $\omega = \text{constant}$ , while  $\gamma$  and  $\mu$  are constant or harmonic with period  $2\pi/\omega$  (or a multiple thereof). Eq. (29) then includes a  $\phi$  component that grows linearly with time, but assigns purely periodic forms to  $\sin \phi$  and the derivatives  $\dot{\phi} - \omega, \ddot{\phi}$  etc. Since these, and not  $\phi$ , enter into the system equation [e.g., (23)], it follows that (29) is in the nature of a particular solution. On using it, instead of (25) for a harmonic balance as in Section III-G:

$$\begin{aligned} \omega &= \Omega + KN_1(\mu) \sin \gamma \\ \mu \omega \sin \psi_\omega &= +KN_\omega [J_0(\mu) - J_2(\mu)] \cos \gamma \\ \mu \omega \cos \psi_\omega &= -KN_\omega [J_0(\mu) + J_2(\mu)] \sin \gamma. \end{aligned} \quad (30)$$

For a very small deviation index, these relations simplify to

$$\begin{aligned} \omega &\sim \frac{\Omega}{2} \left( 1 \begin{matrix} + \\ - \end{matrix} \sqrt{1 - \frac{2K^2}{\Omega^2} (N \cos \psi)_\omega} \right), \\ |\mu \omega| &\sim KN_\omega, \quad \gamma \sim \psi_\omega \begin{matrix} (- \\ + \end{matrix} \frac{\pi}{2}. \end{aligned} \quad (31)$$

The upper signs are chosen for continuity with the properties of the filterless case (Section II); thus, when  $\Omega > K$ , then  $\omega > 0$ ,  $\mu > 0$  and  $\phi$  is a minimum when

$$\theta = \pi, \quad \phi = \pi + \gamma \sim \frac{\pi}{2} + \psi_\omega;$$

when  $\Omega < -K$ , then  $\omega < 0$ ,  $\mu < 0$  and  $|\phi|$  is a minimum when

$$\theta = 0, \quad \phi = \gamma \sim -\frac{\pi}{2} + \psi_\omega. \quad (31a)$$

The control voltage has the mean value  $[(\omega - \Omega)/K] \hat{V}$  here, compared with  $(-\Omega/K) \hat{V}$  at lock; the relation is reminiscent of a frequency discriminator.

### C. Pull-In

The pull-in problem can be stated as follows: Given the asynchronous state for  $\Omega > K$ ,  $\Omega$  is reduced very slowly; at what value  $\Omega = \hat{\Omega}$  does synchronism occur?

The answer depends on the nature of the system. For the filterless case, the identity  $\hat{\Omega} = K$  was found (Section II). A more general result is suggested by the condition that the control voltage should just reach the required value  $-\hat{V} \hat{\Omega}/K$ . This is consistent with the determination of the critical limit cycle, that is, the unstable

asynchronous state that is reached as  $\mu$  grows very slowly.

In view of (29), the stationary condition

$$\dot{\phi} = \ddot{\phi} = 0$$

is attained when

$$\mu = 1, \quad \theta = \pi; \quad (32)$$

implied stationary conditions are

$$\dot{\mu} = \dot{\gamma} = \dot{\omega} = 0. \quad (33)$$

When the system equation is of the second order, the stationary conditions imply the phase<sup>13</sup>  $(\pi - \phi_\infty)$  and an asynchronous state that is critical since  $(\pi - \phi_\infty)$  is a point of unstable equilibrium. The plot [Fig. 10(b)] of  $\dot{\phi}$  vs  $\phi$  touches the abscissae in cusps at  $[(2n+1)\pi - \phi_\infty]$ ;  $\dot{\phi}$  fluctuates between 0 and  $2\omega_t$ , where  $\omega_t$  denotes the value of  $\omega$  for  $m=1$ .

Eq. (24) was introduced by the pull-out problem (Section III, F) where it represents a transient condition that terminates in either  $\phi_\infty$  or in the stable asynchronism described by (29) for  $|\mu| < 1$ .

In the context of the slow approach to  $|\mu| = 1$  from stable asynchronous states with  $|\mu| < 1$ , (24) defines a critical limit cycle that is nearly attained over many complete cycles of  $\phi$  until a slight perturbation launches the phase transient that terminates in  $\phi_\infty$  [Fig. 10(b)].

The pull-out frequency is never less than the pull-in frequency, in accordance with the practice of running synchronous motors up to speed on no-load.

On solving (30) for  $\mu=1$  (and writing  $N_{\omega_t} = N_t$ , etc.),

$$\frac{\omega_t}{KN_t} = \frac{0.965}{\sqrt{2.202 - \cos^2 \psi_t}} \quad (34a)$$

and

$$\frac{\hat{\Omega}}{\omega_t} = 1 + \frac{\cos \psi_t}{2N_t}, \quad (34b)$$

providing that  $|\Omega/K| < 1$ .

The first equation allows  $\omega_t$  to be computed, given the value of  $K$  and the function  $N$ . Its nature usually requires a numerical method of solution; the pull-in ratio  $\hat{\Omega}/K$  then follows from (34b).

This has been computed for the system with the RC filter of Fig. 6 for  $(1/a) = 1 + \sqrt{1 + K\tau}$ , and plotted in Fig. 11(a) against the independent variable  $K\tau$ . Hysteresis is seen to set in when  $K\tau \sim 1.65$  and corresponds to  $\phi_K = 0.46$ ; the pull-in ratio falls as  $K\tau$  increases further, as was to be expected. The corresponding ratio<sup>14</sup>  $B_{\min}/\hat{\Omega}$  has also been entered in Fig. 11(a), and appears to be fairly constant. The ratio  $K\sqrt{2(N \cos \psi)_\Omega}/\hat{\Omega}$  [see (31)] is shown as well, and lies between the limits

<sup>13</sup> Actually, (31a) only indicates that the phase is in the quadrant of  $(\pi - \phi_\infty)$  when  $\phi$  is a minimum.

<sup>14</sup> This  $B_{\min}$  has been both optimized and computed for  $\Omega=0$ .

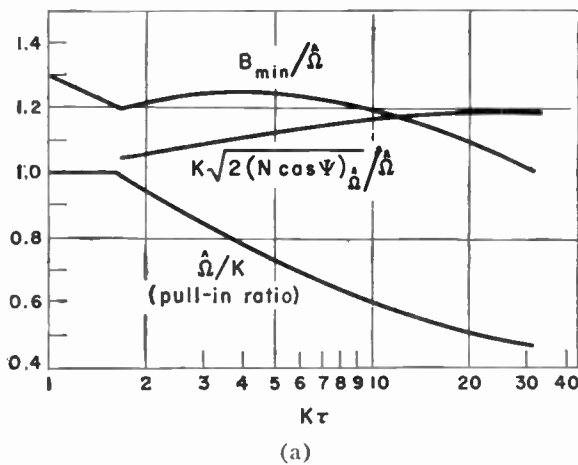
1.05 and 1.19. The ratio  $\hat{\Omega}/K$  is shown in Fig. 11(b) for  $(1/a) = 1 + \sqrt{1 + 2^{-1/2}K\tau}$ .

Noise depresses the ratio near unity since lock is unstable where  $\Omega = K$ , and raises it somewhat where damping is small ( $K\tau \gg 1$ ) and random perturbations of the asynchronous state modify the unperturbed values of  $\phi$  and  $\dot{\phi}$ .

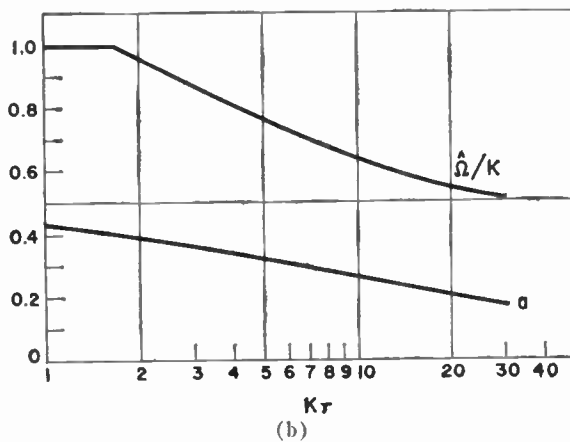
The ratio  $\hat{\Omega}/K$  can be increased artificially by increasing the in-phase component of the filter transfer function transiently, e.g., by short circuiting the top arm of the filter of Fig. 6, by shunting this arm with two diodes connected back to back, or by rocking the tuning capacitor; an equivalent of the latter expedient is the injection of low-frequency ac into the modulator, the resulting deviation being reduced drastically when the system locks. However, these expedients are questionable if they tend to make  $\Omega = K$  or to introduce spurious signals.

For the system with a simple RC filter, (34) reduces to the explicit form

$$(\omega_l\tau)^2 = \sqrt{0.423(K\tau)^2 + 0.075} - 0.273, \quad \hat{\Omega} = 1.5\omega_l, \quad (35)$$



(a)



(b)

Fig. 11—(a) Pull-in ratio, approximate criterion and  $B/\hat{\Omega}$  for  $a = (1 + \sqrt{1 + K\tau})^{-1}$ . (b) Pull-in ratio and  $a$  for  $a = (1 + \sqrt{1 + 2^{-1/2}K\tau})^{-1}$ .

$$\frac{\hat{\Omega}}{K} \sqrt{K\tau} \sim 1.21 \sqrt{1 - \frac{0.446}{K\tau}} \quad \text{if } K\tau \gg 1.$$

D. Experimental Verification

Fig. 12 presents a plot of (35) and the results<sup>9</sup> of experiment and of graphical analysis.

Hysteresis sets in where  $K\tau \sim 0.95$ ,  $\psi_{\hat{\Omega}} = 0.77$ . The quantity

$$\frac{K}{\hat{\Omega}} \sqrt{2(N\cos\Psi)_{\hat{\Omega}}} = \frac{K}{\hat{\Omega}} \sqrt{\frac{2}{1 + \hat{\Omega}^2\tau^2}}$$

is also plotted, and lies between 1.02 and 0.97. Agreement between theory and experiment is good; the discrepancies at great values of  $K\tau$  are attributed to experimental error by the experimenters.<sup>9</sup>

For the system with the filter of Fig. 6 in which  $\zeta = 0.5$ , (34) has been computed for independent variable  $\omega_n/K$ , using (15). This is plotted in Fig. 13, together with the results<sup>2</sup> of experiment and of graphical analysis. Quantity  $K\sqrt{2(N\cos\Psi)_{\hat{\Omega}}}/\hat{\Omega}$  is also plotted, and lies between 0.75 and 1.19. It should be noted that, since  $\zeta = 0.5$ , the abscissa  $\omega_n/K = 1$  implies  $a = 0$ ,  $K\tau = 1$ ; then  $\hat{\Omega}/K \sim 0.96$  agrees with this point of Fig. 12, as it should.

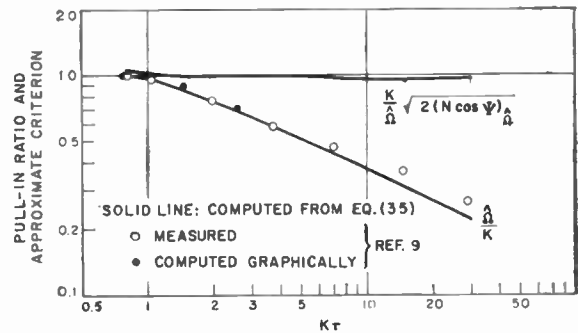


Fig. 12—Pull-in ratio of system with simple RC filter.

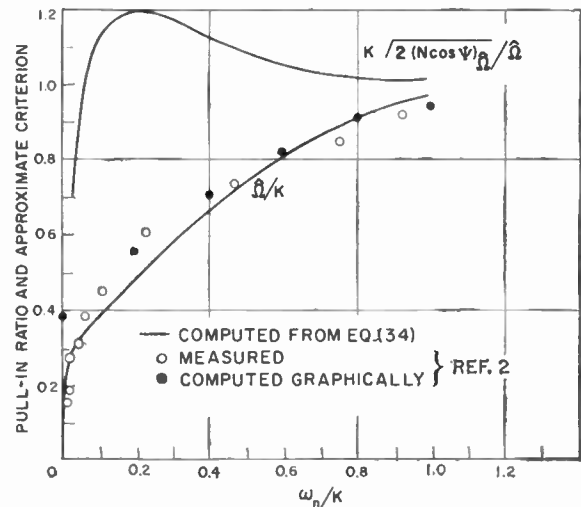


Fig. 13—Pull-in ratio for  $\zeta = 0.5$ .

An approximation to the pull-in ratio is suggested by the vanishing of the surd in (31):

$$\frac{K}{\hat{\Omega}} \sqrt{2(N \cos \psi) \hat{\Omega}} = 1. \tag{36}$$

Agreement with (34) is excellent for the system with a simple RC filter. However, the computations for other systems (Figs. 11 and 13) show that (36) provides only a rough estimate there.

Experience with systems containing a simple RC filter and a delay line, respectively, has led to the conjecture<sup>10</sup> that hysteresis sets in where  $\psi_K \sim \pi/4$ , but this conflicts with the value 0.46 in the case illustrated by Fig. 11(a). Moreover, the present theory must be modified when  $N$  is a delay line, perhaps to allow for the term of frequency  $2\omega$  in the  $\sin \phi$  series. The results of applying (34) to this case differ significantly from the experimental data (Fig. 14).

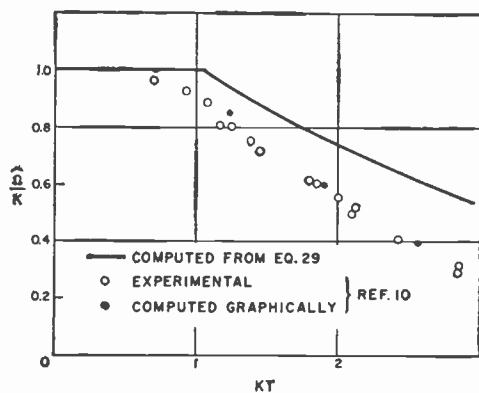


Fig. 14—Pull-in ratio for system with delay  $T$  in the loop.

Finally, it should be noted that APC circuits will synchronize at tuning errors  $\hat{\Omega}$  such that

$$\hat{\Omega} < |\Omega| < K$$

when the loop is first closed, if the initial conditions happen to be more favorable than those considered in Section III, C.

V. IMPERFECTIONS

A. The Detector

The specification of a physical APC system in terms of  $K$  and  $N$  is usually incomplete, though effects that are represented by linear transfer functions can be absorbed in  $N$ ; e.g., if there is a time constant  $\tau_1$  in addition to the filter function of (13), the locked system remains stable if

$$\frac{K\tau_1}{1 + \tau_1/\tau} < 1 + aK\tau. \tag{37}$$

However, the representation of the detector as a source of the beat signal is often complicated by the fact that dc is generated when the frequency of the weaker signal is equal to that of the stronger or to one of its harmonics. The detector then acts as a sampler, and a plurality of synchronous states is inherent in the system. Stability is limited by an inequality of type

$$K < \omega_s/\pi, \tag{38}$$

where  $\omega_s$  now denotes the frequency of the stronger signal. However, if both  $\Omega$  and  $K$  are small compared with  $\omega_s$ , the sampling aspect is significant only with regard to the noise bandwidth  $B$  in relation to the pre-detector bandwidth  $B_p$ , let us say. The predetector noise spectrum is folded into the low-frequency band by beating with the harmonics of the strong signal, and magnifies the contribution of  $B_p$  to the  $B$  as defined in Section III, C by a factor of order

$$B_p / \frac{\omega_s}{2} \tag{39}$$

if this is large.

The subject of APC with pulse reference will be considered at another time.

B. Inherent Noise

Spurious modulation also occurs at power-line frequency and its harmonics, e.g., by leakage to the diode cathodes where these are ac heated.

It was shown in Section III, E that inherent phase noise is reduced only to a limited extent by APC; this can convert incoherent amplitude noise into phase noise. Inherent oscillator noise depends partly on the response to injected ac; the relation between this and the output of an oscillator with APC is interesting, and will be considered in a further paper. However, synchronization by APC and by injection are very different processes. The advantage of APC is that the oscillator and the control circuit may be designed quite independently; the quality factor  $Q$  of the elements that determine the oscillation frequency when the APC loop is open does not affect the ease of automatic tuning.

APPENDIX—SOLUTIONS OF (3)

Approximate solutions of the synchronization equation in the filterless case have been presented above [(5) and (9)]. Periodic solutions are best approximated by (29). Since  $N(\omega) \equiv 1$ , (30) simplifies to

$$\gamma = -\frac{\pi}{2}, \quad \frac{\omega}{K} = \frac{J_0(\mu) + J_2(\mu)}{\mu}, \quad \frac{\Omega}{K} = \frac{\omega}{K} + J_1(\mu). \tag{40}$$

The example  $\mu = 0.8$ , i.e.,  $\Omega/K = 1.521$ , has been computed and is presented in Fig. 15(a), in normalized form. The ordinates  $-\sin \phi$  represent the instantaneous beat frequency or control signal outside synchronism.

The exact solution of (3) is obtained by separating the variables and integrating with the aid of the successive substitutions

$$x = \tan \frac{\phi}{2}, \quad \zeta^2 = \left(x - \frac{K}{\Omega}\right)^2 / \left(1 - \frac{K^2}{\Omega^2}\right),$$

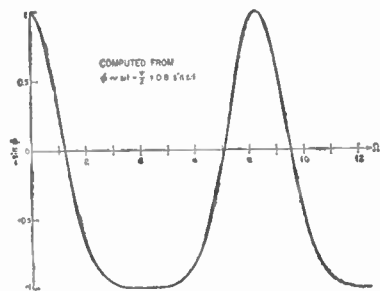
or by using tables (e.g., Dwight, 436.00). The solutions have the indefinite forms

$$\frac{\sqrt{K^2 - \Omega^2}}{2} t = \frac{1}{2} \ln \left( \frac{\sqrt{K^2 - \Omega^2} - K + \Omega \tan \phi/2}{\sqrt{K^2 - \Omega^2} + K - \Omega \tan \phi/2} \right) \quad \text{for } \Omega < K; \quad (41)$$

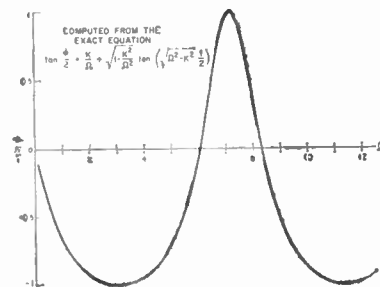
or

$$\frac{\sqrt{\Omega^2 - K^2}}{2} t = \arctan \left( \frac{\Omega \tan (\phi/2) - K}{\sqrt{\Omega^2 - K^2}} \right) \quad \text{for } K < \Omega. \quad (42)$$

The last equation is illustrated by Fig. 15(b) for  $\Omega/K=1.521$ . Both the approximate and the exact solutions demonstrate asynchronous degeneration, the beat periods being  $1.33 \ 2\pi/\Omega$  and  $1.31 \ 2\pi/\Omega$ , respectively.



(a)



(b)

Fig. 15—Asynchronous control  $p-d$  (normalized); (a) approximate, (b) exact.

## CORRECTION

Harold T. McAleer, author of "A New Look at the Phase-Locked Oscillator," which appeared on pages 1137-1143 of the June, 1959, issue of PROCEEDINGS, has pointed out the following to the *Editor*.

In Appendix I in the section titled "Capture Range" (page 1142), (14) and (17), while correct, are improperly derived. The section should be rewritten to read:

**Capture Range:** For a system with a simple RC filter ( $t_2=0$ ) and a balanced cosine phase-detector, several authors<sup>2,6,12</sup> have shown that the capture range  $|\Delta\omega|$  is approximately proportional to the crossover frequency  $\omega_n$ . Expressed as a "capture ratio," the relation becomes:

$$\left| \frac{\Delta\omega}{K} \right| = \frac{\text{capture range}}{\text{lock range}} \approx A \frac{\omega_n}{K}.$$

The value of the multiplying constant  $A$  has been variously estimated at values ranging from 0.7 to 1.2.

For a system with an optimized lag network, the capture ratio becomes:<sup>4,5,12</sup>

$$\frac{\text{capture range}}{\text{lock range}} \approx B \sqrt{\frac{\omega_n}{K}}.$$

For the region ( $\omega_n/K \ll 1$ ), the multiplying constant  $B$  has been estimated as 1.4.<sup>4,12</sup>

The value  $B=1$  gives a useful approximation for the entire range of values of  $\omega_n/K$ .

<sup>12</sup> W. E. Ingham, "The Design of an A.P.C. Synchronizing Loop," E.M.I. Res. Labs., Ltd., Hayes, Middlesex, Eng., Rept. No. RW/8; April, 1956.

# IRE Standards on Solid-State Devices: Definitions of Semiconductor Terms, 1960\*

## 60 IRE 28. S1

### Committee Personnel

#### Subcommittee on Semiconductor Diode Definitions

C. H. KNOWLES, *Chairman 1957*

A. C. SHECKLER, *Chairman 1956-1957*

L. D. Armstrong  
D. C. Dickson

B. Jacobs  
J. D. Johnson  
A. C. Sheckler

R. P. Lyons  
R. H. Rediker

#### Subcommittee on Semiconductor Devices 1959-1960

J. M. EARLY, *Chairman (IRE)*

G. Abraham  
J. B. Angell  
E. N. Clarke  
A. Coblenz  
S. K. Ghandi

J. M. Goldey  
B. Jacobs  
J. D. Johnson  
C. H. Knowles  
R. P. Lyon

A. C. SHECKLER, *Chairman (AIEE)*

R. Morrison  
C. W. Mueller  
M. B. Prince  
R. L. Pritchard  
B. J. Rothlein

H. N. Sachar  
A. P. Stern  
R. L. Trent  
R. Ure

#### Committee on Solid State Devices 1959-1960

R. L. PRITCHARD, *Chairman*

E. O. JOHNSON, *Vice-Chairman*

V. P. MATHIS, *Secretary*

J. B. Angell  
S. J. Angello  
J. S. Blakemore  
A. Coblenz  
W. C. Dunlap, Jr.

J. M. Early  
H. J. Evans  
P. A. Fleming  
J. R. Hyneman  
B. Kazan

N. R. Kornfield  
A. W. Lampe  
E. E. Loebner  
R. H. Rediker  
J. R. Roeder

B. J. Rothlein  
S. Sherr  
A. E. Slade  
B. N. Slade  
W. M. Webster

#### Committee on Standards 1959-1960

R. F. SHEA, *Chairman*

J. G. KREER, JR., *Vice-Chairman*

J. Avins  
W. F. Bailey  
M. W. Baldwin, Jr.  
J. T. Bangert  
W. R. Bennett  
J. G. Brainerd  
P. S. Carter  
A. G. Clavier  
S. Doba, Jr.  
R. D. Elbourn  
P. Elias

G. A. Espersen  
R. J. Farber  
D. G. Fink  
G. L. Fredendall  
E. A. Gerber  
A. B. Glenn  
V. M. Graham  
R. A. Hackbusch  
R. T. Haviland  
A. G. Jensen  
R. W. Johnston

C. H. PAGE, *Vice-Chairman*

L. G. CUMMING, *Vice-Chairman*

I. Kerney  
A. E. Kerwien  
G. S. Ley  
W. Mason  
D. E. Maxwell  
P. Mertz  
H. I. Metz  
H. R. Mimno  
E. Mittelman  
L. H. Montgomery, Jr.  
G. A. Morton

R. C. Moyer  
J. H. Mulligan, Jr.  
A. A. Oliner  
M. L. Phillips  
R. L. Pritchard  
P. A. Redhead  
R. Serrell  
W. A. Shipman  
H. R. Terhune  
E. Weber  
R. B. Wilcox

W. T. Wintringham

#### Definitions Coordinator

C. H. PAGE

\* Approved by the IRE Standards Committee, September 10, 1959. Reprints of this Standard, 60 IRE 28. S1, may be purchased while available from the Institute of Radio Engineers, 1 East 79th Street, New York, N. Y., at \$0.50 per copy. A 20 per cent discount will be allowed for 100 or more copies mailed to one address.

**Acceptor (in a Semiconductor).** See *Impurity, Acceptor*.

**Anode Terminal (of a Semiconductor Diode).** The *terminal* which is positive with respect to the other *terminal* when the *diode* is biased in the *forward* direction.

**Avalanche Breakdown (of a Semiconductor Device).** A *breakdown* that is caused by the cumulative multiplication of *charge carriers* through field-induced impact ionization.

**Avalanche Impedance.** Obsolete, see *Breakdown Impedance*.

**Base (of a Transistor).** A *region* which lies between an *emitter* and a *collector* of a *transistor* and into which *minority carriers* are injected.

**Boundary, P-N.** A surface in the transition region between *P-type* and *N-type* material at which the *donor* and *acceptor* concentrations are equal.

**Breakdown (of a Semiconductor Diode).** A phenomenon occurring in a *reverse* biased *semiconductor diode*, the initiation of which is observed as a transition from a region of high dynamic resistance to a region of substantially lower dynamic resistance for increasing magnitude of *reverse current*.

**Breakdown Impedance (of a Semiconductor Diode).** The small-signal impedance at a specified direct current in the *breakdown region*.

**Breakdown Region (of a Semiconductor-Diode Characteristic).** That entire region of the volt-ampere characteristic beyond the initiation of *breakdown* for increasing magnitude of *reverse current*.

**Breakdown Voltage (of a Semiconductor Diode).** The voltage measured at a specified current in the *breakdown region*.

**Capacitance (of a Semiconductor Diode).** The small-signal capacitance measured between the *terminals* of the *diode* under specified conditions of bias and frequency.

**Cathode Terminal (of a Semiconductor Diode).** The *terminal* which is negative with respect to the other *terminal* when the *diode* is biased in the *forward direction*.

**Charge Carrier (of a Semiconductor).** A mobile *conduction electron* or mobile *hole*.

**Collector (of a Transistor).** A *region* through which a primary flow of *charge carriers* leaves the *base*.

**Conduction Band.** A range of states in the energy spectrum of a solid in which electrons can move freely.

**Conductivity Modulation (of a Semiconductor).** The variation of the conductivity of a semiconductor by variation of the *charge-carrier* concentration.

**Conductivity, N-Type.** The conductivity associated with *conduction electrons* in a semiconductor.

**Conductivity, P-Type.** The conductivity associated with *holes* in a *semiconductor*.

**Contact, High Recombination Rate.** A semiconductor-semiconductor or metal-semiconductor contact at which thermal equilibrium *charge-carrier* concentrations are maintained substantially independent of current density.

**Depletion Layer (in a Semiconductor).** A region in which the *charge-carrier* charge density is insufficient to neutralize the net fixed charge density of *donors* and *acceptors*.

**Diffusion Capacitance (of a Semiconductor Junction).** The rate of change of stored *minority-carrier* charge with the voltage across the *junction*.

**Diffusion Constant, Charge Carrier.** In a homogeneous semiconductor, the magnitude of the quotient of diffusion current density by the *charge-carrier* charge concentration gradient.

**Diffusion Length, Charge-Carrier.** In a homogeneous *semiconductor*, the average distance to which *minority carriers* diffuse between generation and recombination.

*Note:* The diffusion length is equal to the square root of the product of the *charge-carrier diffusion constant* and the *volume lifetime*.

**Diode, Semiconductor.** A *semiconductor device* having two *terminals* and exhibiting a nonlinear voltage-current characteristic; in more restricted usage, a *semiconductor device* which has the asymmetrical voltage-current characteristic exemplified by a single *p-n junction*.

**Donor (in a Semiconductor).** See *Impurity Donor*.

**Doping.** Addition of an *impurity* to a *semiconductor*, or production of a deviation from stoichiometric composition, to achieve a desired characteristic.

**Drift Mobility (in a Homogeneous Semiconductor).** The ensemble average of the drift velocities of the *charge carriers* per unit electric field.

*Note:* In general, the mobilities of *electrons* and *holes* are different.

**Electrode (of a Semiconductor Device).** An electrical and mechanical contact to a region of a *semiconductor device*.

**Electrons, Conduction.** The *electrons* in the *conduction band* of a solid, which are free to move under the influence of an electric field.

**Element (of a Semiconductor Device).** Any integral part of the *semiconductor device* that contributes to its operation.

**Emitter (of a Transistor).** A region from which *charge carriers* that are *minority carriers* in the *base* are injected into the *base*.

**Energy Gap (of a Semiconductor).** The energy range between the bottom of the *conduction band* and the top of the *valence band*.

**Extrinsic Properties (of a Semiconductor).** The properties of a *semiconductor* as modified by *impurities* or *imperfections* within the crystal.

**Forward Direction (of a Semiconductor Diode).** The direction of lower resistance to the flow of steady direct current.

**Generation Rate (in a Semiconductor).** The time rate of creation of *electron-hole* pairs.

**Hall Coefficient (of an Electrical Conductor).** The constant of proportionality  $R$  in the relation

$$E_h = R[J \times B]$$

where

$E_h$  = transverse electric field (Hall Field),

$J$  = current density,

$B$  = magnetic flux density.

*Note:* The sign of the *majority carrier* can be inferred from the sign of the Hall Coefficient.

**Hole.** A vacancy in the electronic band structure of a *semiconductor* which acts like a positive electronic charge with a positive mass.

**Imperfection (of a Crystalline Solid).** Any deviation in structure from that of a perfect crystal.

**Impurity.** An *imperfection* that is chemically foreign to the perfect crystal.

**Impurity, Acceptor (in a Semiconductor).** An *impurity* that may act as a source of mobile *holes*.

**Impurity, Donor (in a Semiconductor).** An *impurity* that may act as a source of *conduction electrons*.

**Impurity, Stoichiometric.** A crystalline *imperfection* arising from a deviation from stoichiometric composition.

**Intrinsic Properties (of a Semiconductor).** The properties of a *semiconductor* that are characteristic of the ideal crystal.

**Intrinsic Temperature Range (in a Semiconductor).** The temperature range in which the *charge-carrier* concentration of a *semiconductor* is substantially the same as that of an ideal crystal.

**Junction (in a Semiconductor Device).** A region of transition between *semiconductor* regions of different electrical properties (e.g., *n-n+*, *p-n*, *p-p+* semiconductors), or between a metal and a *semiconductor*.

**Junction, Collector (of a Transistor).** A *junction* normally biased in the high-resistance direction, the current through which can be controlled by the introduction of *minority carriers*.

**Junction, Emitter (of a Transistor).** A *junction* normally biased in the low-resistance direction to inject *minority carriers* into a *base*.

**Junction (Semiconductor), Diffused.** A *junction* which has been formed by the diffusion of an *impurity* within a *semiconductor* crystal.

**Junction (Semiconductor), Doped.** A *junction* produced by the addition of an *impurity* to the melt during crystal growth.

**Junction, Fused (or Alloy) (in a Semiconductor).** A *junction* formed by recrystallization on a *base crystal* from a liquid phase of one or more components and the *semiconductor*.

**Junction (Semiconductor) Grown.** A *junction* produced during growth of a crystal from a melt.

**Junction (Semiconductor), Rate-Grown.** A *grown junction* produced by varying the rate of crystal growth.

**Lifetime, Volume.** The average time interval between the generation and recombination of *minority carriers* in a homogeneous *semiconductor*.

**Majority Carrier (in a Semiconductor).** The type of *charge carrier* constituting more than one half the total *charge-carrier* concentration.

**Minority Carrier (in a Semiconductor).** The type of *charge carrier* constituting less than one half the total *charge-carrier* concentration.

**Mobility.** See *Drift Mobility*.

**Mobility, Hall (of an Electrical Conductor).** The quantity  $\mu_H$  in the relation  $\mu_H = R\sigma$ , where  $R$  = *Hall Coefficient* and  $\sigma$  = conductivity.

**Ohmic Contact.** A purely resistive contact; *i.e.*, one which has a linear voltage-current characteristic throughout its entire operating range.

**PIV (Peak Inverse Voltage).** The maximum instantaneous anode-to-cathode voltage in the *reverse direction* which is actually applied to the diode in an operating circuit.

*Note:* This is an applications term not to be confused with *Breakdown Voltage* which is a property of the device.

**PIV, Maximum Rated (of a Semiconductor Diode).** The recommended maximum instantaneous anode-to-cathode voltage which may be applied in the *reverse direction*.

**Point Contact.** Pressure contact between a *semiconductor* body and a metallic point.

**Recombination Velocity (on a Semiconductor Surface).** The quotient of the normal component of the *electron (hole)* current density at the surface by the excess *electron (hole)* charge density at the surface.

**Reverse Current (of a Semiconductor Diode).** The total current flowing through a *semiconductor diode* in the *reverse direction*.

**Reverse Direction (of a Semiconductor Diode).** The direction of higher resistance to the flow of steady direct current.

**Saturation Current (of a Semiconductor Diode).** That portion of the steady-state *reverse-current* which flows as a result of the transport across the *junction of minority carriers* thermally generated within the regions adjacent to the *junction*.

**Semiconductor.** An electronic conductor with resistivity usually in the range between metals and insulators in which the electrical *charge-carrier* concentration increases with increasing temperature over some temperature range.

**Semiconductor, Compensated.** A *semiconductor* in which one type of *impurity or imperfection* (e.g., *donor*) partially cancels the electrical effects of the other type of *impurity or imperfection* (e.g., *acceptor*).

**Semiconductor Device.** An electron device in which the characteristic distinguishing electronic conduction takes place within a *semiconductor*.

**Semiconductor, Extrinsic.** A *semiconductor* with *charge-carrier* concentration dependent upon impurities.

**Semiconductor, Intrinsic.** A *semiconductor* whose *charge-carrier* concentration is substantially the same as that of the ideal crystal.

**Semiconductor, N-Type.** An *extrinsic semiconductor* in which the *conduction electron* concentration exceeds the mobile *hole* concentration.

*Note:* It is implied that the net ionized *impurity* concentration is *donor type*.

**Semiconductor, N+-Type.** An *n-type semiconductor* in which the excess *conduction electron* concentration is very large.

**Semiconductor, P-Type.** An *extrinsic semiconductor* in which the mobile *hole* concentration exceeds the *conduction electron* concentration.

*Note:* It is implied that the net ionized *impurity* concentration is *acceptor type*.

**Semiconductor, P+-Type.** A *p-type semiconductor* in which the excess mobile *hole* concentration is very large.

**Space-Charge Region (of a Semiconductor Device).** A region in which the net charge density is significantly different from zero. See also *Depletion Layer*.

**Terminal (of a Semiconductor Device).** The externally available point of connection to one or more *electrodes*.

**Thermal Resistance, Effective (of a Semiconductor Device).** The effective temperature rise per unit power dissipation of a designated *junction* above the temperature of a stated external reference point under conditions of thermal equilibrium.

**Thermistor.** An electron device which makes use of the change of resistivity of a *semiconductor* with change in temperature.

**Transistor.** An active *semiconductor device* with three or more *terminals*.

**Transistor, Conductivity Modulation.** A *transistor* in which the active properties are derived from *minority-carrier* modulation of the bulk resistivity of a *semiconductor*.

**Transistor, Filamentary.** A *conductivity modulation transistor* with a length much greater than its transverse dimensions.

**Transistor, Junction.** A *transistor* having a *base* and two or more *junctions*.

**Transistor, Point-Contact.** A *transistor* having a *base* and two or more *point-contacts*.

**Transistor, Unipolar.** A *transistor* which utilizes *charge carriers* of only one polarity.

**Valence Band.** The range of energy states in the spectrum of a solid crystal in which lie the energies of the valence electrons which bind the crystal together.

**Varistor.** A two-terminal *semiconductor device* having a voltage-dependent nonlinear resistance.

**Zener Breakdown (of a Semiconductor Device).** A *breakdown* that is caused by the field emission of *charge carriers* in the *depletion layer*.

**Zener Impedance.** Obsolete, see *Breakdown Impedance*.

**Zener Voltage.** Obsolete, see *Breakdown Voltage*.

# Correspondence

## Esaki Diode Oscillators from 3 to 40 KMC\*

Esaki diode oscillators operating at microwave frequencies of 10 kmc and below have been reported in the literature.<sup>1-5</sup> Fundamental power up to 40 kmc in frequency has now been obtained from Esaki diode oscillators, with appreciable harmonic output up to about 63 kmc. The microwave power at all wavelengths has been sufficient to be detected and displayed by the simplest video methods. Although small-area junction diodes of both gallium arsenide and germanium have provided substantial power below 10 kmc, the highest frequencies were obtained with gallium-arsenide units.

Junctions were formed by alloying tin to zinc-diffused gallium arsenide, and aluminum to germanium doped with arsenic. Alloying took place when an electric current was passed through a point of the appropriate metal which had been brought in contact with the semiconductor. Peak currents of the resulting Esaki diodes ranged from less than 100  $\mu$ a to more than 30 ma, depending upon the forming conditions. Peak-to-valley current ratios exceeded 2:1 and were commonly 6:1. The impurity concentration in the germanium was approximately  $6 \times 10^{19}$ , and, although the carrier concentration in the gallium arsenide was not measured, the resistivity was 0.0015 ohm-cm.

Fig. 1(a) shows the current-voltage characteristic of a gallium-arsenide Esaki diode in an oscillating circuit. The *s*-shaped deviation from the expected static characteristic indicates oscillation. Except for the voltage scale, this characteristic was typical of those obtained with germanium as well as with gallium arsenide.

Oscillations ranging in frequency from 2.7 to 33.4 kmc have been obtained in cylindrical cavities. A diode of either gallium arsenide or germanium shunted each cavity at the apex of a re-entrant cone, as shown in Fig. 2. The cavity resonances occurred at frequencies for which the radius equaled approximately an odd integral number of quarter wavelengths, altered by the diode loading. The circuit of Fig. 2 is resonant near odd-order harmonics, and power at these frequencies was coupled out of the cavity through the loop. Odd harmonics through the seventh have easily been detected from a germanium unit having a fundamental frequency of 2.7 kmc. Low-order harmonics of much higher fundamental frequencies

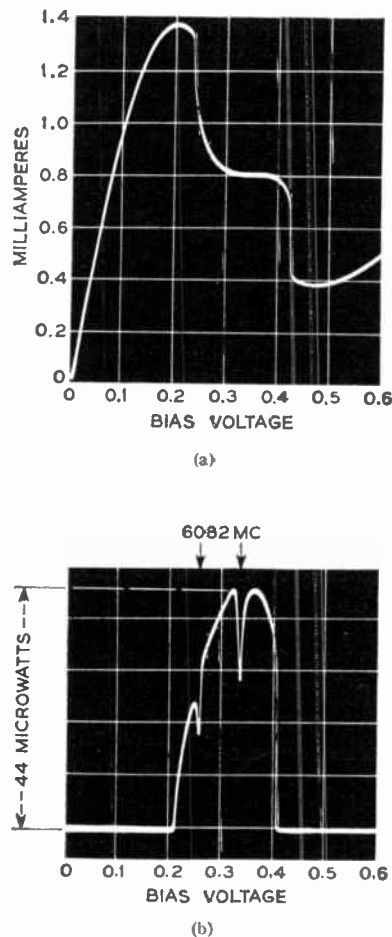


Fig. 1—(a) Current-voltage characteristic of a gallium-arsenide Esaki diode oscillating at 6 kmc in a cavity. (b) Detected power output from the cavity oscillator. The sharp dips are absorptions from a wavemeter set to 6082 mc.

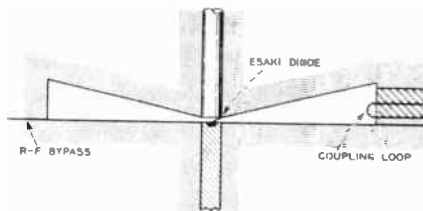


Fig. 2—Section of a cavity oscillator.

were easily attained with gallium arsenide diodes.

Oscillations can occur in higher order cavity modes. Gallium arsenide units have oscillated at fundamental frequencies which were three times the resonant frequency of the dominant cavity mode. In contrast, germanium units could be made to oscillate only in the lowest-order mode.

Fundamental oscillation in a higher-order cavity mode can be confused with a harmonic of an oscillation in the lowest-order mode, since adjustments in the coupling loop and external loading can shift operation from one mode to the other. A ferrimagnetic resonance phenomenon was employed to differentiate between these possibilities. A small yttrium iron garnet sphere was placed within the cavity diametrically opposite the coupling loop, and was biased with an external magnetic field along the axis of the cavity. With fields near resonance at either a fundamental or a low-order harmonic present within the cavity, the output was altered drastically in power and frequency. Thus, the fundamental frequency of oscillation could be inferred from the magnetic field and the known relationship between magnetic field and frequency for the sphere.

Waveguide circuits consisted of gallium-arsenide diodes mounted directly across the center of relatively low impedance waveguide, with a movable piston in one end of the waveguide. Oscillations were readily obtained with the other end of the waveguide feeding directly into a detector, or into an isolator or attenuator. The fundamental frequencies were often three or four times the waveguide cutoff frequencies.

The circuit operation of Esaki diodes may be classified somewhat arbitrarily as either weakly or strongly oscillating. The static characteristics of both kinds of operation show an *s*-shaped oscillatory region which, for weakly oscillating circuits, is less pronounced and extends over a smaller bias range than for strong oscillators. Fundamental microwave power has been observed at frequencies from 14.5 to 39.9 kmc in various weakly oscillating circuits, using diodes having peak currents in the 300-700- $\mu$ amp range. The maximum power measured was 3.5  $\mu$ w in the 17-25-kmc region, falling off to about 0.2  $\mu$ w at 37 kmc. Movement of the piston behind the diode could be used to tune the frequency of a given circuit 300 to 500 mc, or to suppress the oscillation. Diodes having peak currents from 1 to 3 ma oscillated more strongly in the same circuits, and the oscillations were less readily controlled by the piston. Fundamental frequencies of high-current diode oscillators were, in general, not as high as those for lower-current units operating in the same circuits. The maximum fundamental power observed with strongly oscillating circuits was 50  $\mu$ w at 16.7 kmc. Appreciable harmonic output was observed at frequencies to 62.7 kmc, where the SNR of the detected output displayed on an oscilloscope was as high as 20:1.

Because both the negative resistance and capacitance of a diode varies with voltage, the frequency of oscillation depends somewhat upon bias, and the voltage tuning range may be as much as several per cent of the center frequency. As the bias voltage is increased, the frequency of weakly oscillating circuits decreases monotonically. For large amplitudes of oscillation, however, the frequency may go through a minimum or maximum or both. Fig. 1(b) shows the

\* Received by the IRE, July 14, 1960.

<sup>1</sup> H. S. Sommers, Jr., "Tunnel diodes as high frequency devices," *Proc. IRE*, vol. 47, pp. 1201-1206; July, 1959.

<sup>2</sup> R. F. Rutz, "A 3000-mc lumped parameter oscillator using an Esaki negative-resistance diode," *IBM J. Res. & Dev.*, vol. 3, pp. 372-374; October, 1959.

<sup>3</sup> R. N. Hall, "Tunnel diodes," *IRE TRANS. ON ELECTRON DEVICES*, vol. ED-7, pp. 1-9; January, 1960.

<sup>4</sup> R. L. Batdorf, G. C. Dacey, R. L. Wallace, and D. J. Walsh, "Esaki diode in InSb," *J. Appl. Phys.* vol. 31, pp. 613-614; March, 1960.

<sup>5</sup> J. K. Puffer, "Voltage tuning in tunnel diode oscillators," *Proc. IRE*, vol. 48, p. 1155; June, 1960.

detected power output of the diode of Fig. 1(a) and is an example of a strongly oscillating circuit. The two sharp dips in power are absorptions by a wavemeter at 6082 mc. The peak power output was 44 microwatts with an efficiency of 15 per cent.

Very strongly oscillating circuits are much more complicated in behavior, and are characteristic of high peak-current units. Deviations from the non-oscillating characteristic curves are no longer s-shaped, but show multiple breaks which are accompanied by a power output very different in shape from a parabola. The frequency behavior is far from simple, and the harmonic content is strong enough to give sizable power output well into the millimeter wavelength region.

We found the performance of gallium-arsenide diodes to be superior at high frequencies to that of diodes made from the most highly doped germanium available to us. Gallium-arsenide diodes loaded a cavity resonant at 4 kmc almost imperceptibly, but the best germanium units in the same circuit oscillated barely in excess of 2.8 kmc. The higher fundamental frequencies and harmonics have been obtained with gallium-arsenide units. It appears that these gallium-arsenide diodes have a lower barrier capacitance than germanium units of the same negative resistance, and show promise for application in amplifiers and oscillators well into the millimeter wavelength regions.

Although the circuits employed here are probably far from optimum, high-frequency microwave power sufficient for certain applications has been generated at relatively high efficiencies with Esaki diodes. Power as low as 50  $\mu$ w can be used, if necessary, for a local oscillator in heterodyne detection, and even less power will suffice for simple microwave measurements. As an illustration, Fig. 3 shows an oscilloscope display of the detected output of a frequency swept Esaki diode oscillator in waveguide having a peak power of about 0.2  $\mu$ w; the absorption dip at 36.85 kmc is the ferrimagnetic resonance curve of an yttrium iron garnet sphere.

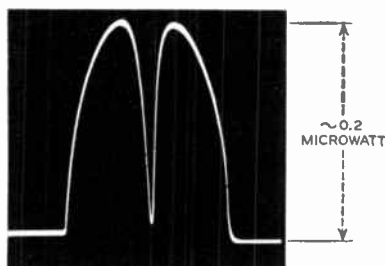


Fig. 3—Detected output of a frequency swept Esaki diode oscillator in waveguide. The peak power was about 0.2  $\mu$ w. The absorption dip is the ferrimagnetic resonance curve of a YIG sphere at 36.85 kmc, and the frequency range covered was 120 mc.

We should like to thank W. M. Sharpless for helpful discussions.

R. TRAMBARULO  
C. A. BURRUS  
Bell Telephone Labs.  
Holmdel, N. J.

## The Emitter Diffusion Capacitance of Drift Transistors\*

The emitter diffusion capacitance of drift transistors with exponential impurity distributions was calculated by Krömer<sup>1</sup> for high built-in fields as:

$$C_{DE} = \frac{qI_E W^2}{kT D} \frac{1}{\eta^2} \quad (1)$$

where:

$I_E$  = emitter current,

$kT/q$  = thermal voltage,

$W$  = base width,

$D$  = diffusion constant of minority carriers (holes),

$$\eta = \frac{q}{kT} E_b W$$

$$= \ln \left( \frac{\text{impurity conc. at the emitter}}{\text{impurity conc. at } W} \right),$$

$E_b$  = built-in field.

For convenience,  $p$ - $n$ - $p$  transistors are considered.

Eq. (1) was obtained by solving the input admittance,  $y_{11}$ , for low frequencies and high  $\eta$ . In an attempt to calculate the diffusion capacitance in the common base configuration

$$C_{DE} = \frac{dQ}{dV_E} \quad (2)$$

we shall use the integrated hole concentration as the stored charge  $Q$ . The hole distribution may be obtained from the expression for the hole current density:

$$J = q\mu E_b P - qD \frac{dP}{dx} \quad (3)$$

where  $\mu$  = mobility of holes,  $P$  = the hole concentration.

The solution of (3) leads to:

$$P = \frac{JW}{qD} \frac{1 - \exp \left[ -\eta \left( 1 - \frac{x}{W} \right) \right]}{\eta}$$

$$= P_{EO} \frac{1 - \exp \left[ -\eta \left( 1 - \frac{x}{W} \right) \right]}{\eta} \quad (4)$$

where  $P_{EO}$  is the concentration of holes at the emitter in the diffusion transistor. The total stored charge is obtained as:

$$Q = qA \int_0^W P dx = \frac{W^2}{D} I_E \frac{\eta - 1 + e^{-\eta}}{\eta^2} \quad (5)$$

Using this charge in (2) (neglecting the equilibrium concentration and volume recombination), and considering that  $dI_E/dV_E = qI_E/kT$  is independent of  $\eta$ , we obtain:

$$C_D = \frac{qI_E W^2}{kT D} \frac{\eta - 1 + e^{-\eta}}{\eta^2} \quad (6)$$

Eq. (6) gives the correct results for the diffusion transistor ( $\eta = 0$ ):

\* Received by the IRE, July 5, 1960.  
<sup>1</sup> H. Krömer, "The Drift Transistor"; *Transistors I*, RCA Labs., Princeton, N. J., 1956.

$$C_{DE} (\text{diffusion}) = \frac{qI_E W^2}{kT} \frac{1}{2D} \quad (7)$$

However, for large built-in fields (large  $\eta$ ), (6) results in a  $1/\eta$  dependence instead of the  $1/\eta^2$  dependence obtained from  $y_{11}$ , *i.e.*, (1).

The discrepancy between the diffusion capacitance derived from the total stored charge, (6), and the diffusion capacitance derived from the emitter admittance, (1), is resolved by multiplying the emitter current in (6) by a factor  $\Gamma$ . The factor equals the ratio of the diffusion current by holes averaged over the base layer divided by the total hole current, *i.e.*,

$$\Gamma = \frac{I_E (\text{average diffusion})}{I_E (\text{total})}$$

The average diffusion current over the base region is  $qADP_E/W$ , and the total current may be obtained from (3).  $\Gamma$  may then be written as:

$$\Gamma = \frac{P_E/W}{\eta P_E/W + (-P')_{x=0}} = \frac{P_E}{\eta P_E + P_{EO}e^{-\eta}} \quad (8)$$

where  $P'(x=0)$  has been substituted from (4), and  $P_E$  is the concentration of holes at the emitter for any  $\eta$ . From (4) we may write:

$$P_E = P_{EO} \frac{1 - e^{-\eta}}{\eta} \quad (9)$$

Setting (9) into (8):

$$\Gamma = \frac{1 - e^{-\eta}}{\eta} \quad (10)$$

The necessity of multiplying by this factor can be interpreted by saying that only the diffusion current of holes contributes to the diffusion capacitance. In other words, only the stored charges carried by diffusion can be reclaimed by the emitter lead. This may also be seen if we write the input admittance

$$\left( \frac{\partial I_E}{\partial V_E} \right)_{v_{c=0}} = \frac{\partial}{\partial V_E} (\text{drift current } (x=0) + \text{diffusion current } (x=0)).$$

Since the drift term depends only on the emitter boundary of the base region, the term will remain real and will not contribute to the diffusion capacitance.

The emitter diffusion capacitance in the common base configuration,  $C_{DE}$ , is therefore  $\Gamma C_D$ , or

$$C_{DE} = \frac{qI_E W^2}{kT D} \left( \frac{\eta - 1 + e^{-\eta}}{\eta^2} \cdot \frac{1 - e^{-\eta}}{\eta} \right) \quad (11)$$

For  $\eta = 0$  this expression returns to the diffusion transistor case in (7). For large  $\eta$  it gives the correct  $1/\eta^2$  dependence. Fig. 1 shows the variance of the factor in parentheses with  $\eta$ .

Measurement of the diffusion capacitance supplies information about the built-in field of a drift transistor. Such a measurement is difficult in the common base configuration due to the small parallel resistance  $\approx kT/qI_E$ . In the common emitter configuration, however, the ohmic part is approximately  $\beta_0 kT/qI_E$ ; where  $\beta_0$  is the common emitter current amplification factor. Such a basic measuring circuit is shown in Fig. 2. In the case of diffusion transistors,

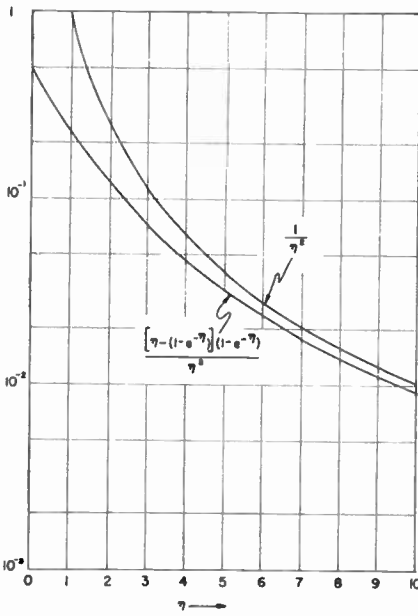


Fig. 1—The factor appearing in the emitter diffusion capacitance. Krömer's approximation by  $1/\eta^2$  is also shown.

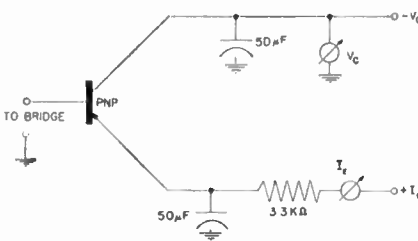


Fig. 2—Circuit for measurement of the diffusion capacitance in common emitter. Bridge provides the bias path for the base.

the capacitance measured in this manner is  $C_{DE}$ . However, for drift transistors it will differ.

From four-pole theory, the input admittance in common emitter,  $y_{11E}$ , is:

$$y_{11E} = y_{11B} + y_{12B} + y_{21B} + y_{22B} \approx y_{11B} + y_{21B} \quad (12)$$

$y_{12B}$  and  $y_{22B}$  can be neglected, since they are much smaller than  $y_{21B}$  and  $y_{11B}$ . From (12) one can write:

$$y_{11Ei} = y_{11Bi} + y_{21Bi} \quad (13)$$

where the subscript  $i$  refers to the imaginary parts. Considering that

$$y_{21B} = -\alpha y_{11B} \quad (14)$$

where  $\alpha$  is the current transport factor,

$$y_{21Bi} = \alpha_i y_{11Bi} - y_{11Bi} \alpha_r \quad (15)$$

where the subscript  $r$  refers to the real part. Since  $\alpha_r \approx 1$  for low frequencies, combining (13) and (15):

$$y_{11Ei} = \alpha_i y_{11Bi} = \alpha_i \frac{qI_E}{kT} \quad (16)$$

For low frequencies, the measured input capacitance in common emitter is then:

$$C_m = \frac{\alpha_i}{\omega} \frac{qI_E}{kT} \quad (17)$$

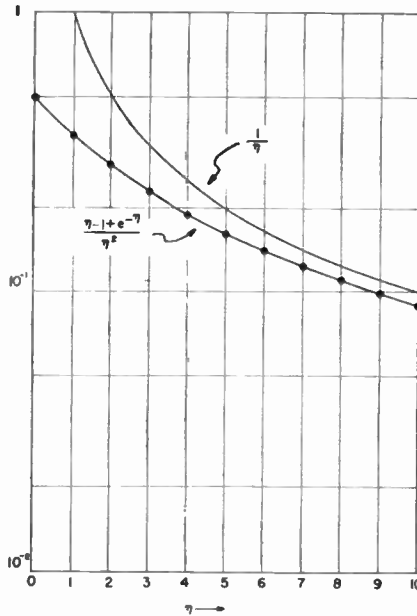


Fig. 3—The factor appearing in the measured capacitance. A  $1/\eta$  approximation is also shown.

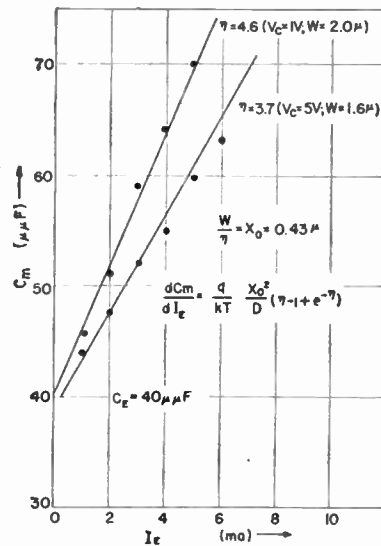


Fig. 4—Measured input capacitance for a  $p-n-p$  drift transistor for two collector voltages. The measured points are indicated by dots and the calculated slopes are drawn through them.  $C_E$  is the depletion layer capacitance.

Therefore, the capacitance which is measured is the imaginary part of the transport factor and not  $C_{DE}$ . By computing the imaginary part of the transport factor<sup>2</sup> for low frequencies and fitting an analytical expression to the result, we obtain

$$\frac{\alpha_i}{\omega} \frac{D}{W^2} = \frac{\eta - 1 + e^{-\eta}}{\eta^2} \quad (18)$$

Therefore,

$$C_m = \frac{qI_E}{kT} \frac{W^2}{D} \left( \frac{\eta - 1 + e^{-\eta}}{\eta^2} \right) \quad (19)$$

<sup>2</sup> D. Thomas and J. Moll, "Junction transistor short-circuit current gain and phase determination," *Proc. IRE*, vol. 46, pp. 1177-1184; June, 1958. ( $L = x_0$ .)

Fig. 3 shows the factor in parentheses as a function of  $\eta$ . It also shows points computed from the full analytical expression for the alpha transfer function, [left-hand side of (18)], and a crude approximation by the factor  $1/\eta$ .

The capacitance measured in the common emitter configuration is the same as calculated for  $C_D$  in (6). This is expected if we consider that the emitter and collector leads are strapped together for ac in the common emitter configuration. In this case, for the  $\delta V_E$  change the total  $\delta Q$  (drift and diffusion components), can be reclaimed by the input terminals. Therefore  $C_m = C_D$ .

In the case of the diffusion transistor  $C_m = C_{DE}$ , but for drift transistors  $C_m$  is larger than  $C_{DE}$  by the factor  $\eta/(1 - e^{-\eta})$ .

Fig. 4 shows the measured capacitance,  $C_m$ , for the  $p-n-p$  drift transistor with an impurity distribution closely resembling

$$N = N_0 \exp \left( -\frac{x}{x_0} \right) \quad (20)$$

with  $x_0 = 0.43 \mu$ . The slopes expected from (19) agree with the measured values and justify the equation for  $C_m$ .

The authors are grateful for the advice of Dr. Kurt Lehovc of the Sprague Electric Company.

J. LINDMAVER  
C. WRIGLEY  
Sprague Electric Co.  
North Adams, Mass.

### Bomb-Excited "Whistlers"\*

Theoretical and experimental studies of "whistler" or "magneto-ionic" modes, which allow the propagation of low-frequency electromagnetic waves through the ionosphere, have shown that these modes can be excited by lightning strokes<sup>1</sup> or by low-frequency radio transmitters.<sup>2</sup> In this note, we wish, first, to point out that these modes can also be excited by nuclear explosions, and second, to discuss some of the characteristics of the signals to be expected.

The information we require, relating to the electromagnetic characteristics of whistlers and of nuclear explosions, is all available in the unclassified literature.<sup>1-3</sup> The pertinent facts fall into two groups which describe the electromagnetic properties associated with the whistler modes and nuclear explosions, respectively.

Regarding the whistlers, it is known<sup>1,2</sup> that the propagation of electromagnetic waves through the ionosphere is qualitatively changed by the presence of the earth's magnetic field. If the earth's field were ab-

\* Received by the IRE, May 31, 1960.

<sup>1</sup> R. O. Storey, "An investigation of whistling atmospherics," *Phil. Trans. Roy. Soc. (London) A*, vol. 246, pp. 113-141; July, 1953.

<sup>2</sup> R. A. Helliwell and E. Gehrels, "Observations of magneto-ionic duct propagation using man-made signals of very low frequency," *Proc. IRE*, vol. 46, pp. 785-787; April, 1958.

<sup>3</sup> J. C. Mark, "The detection of nuclear explosions," *Nucleonics*, vol. 17, pp. 64-73; August, 1959.

sent, electromagnetic waves of frequency lower than the plasma frequency would be totally reflected by the ionosphere. However, the earth's magnetic field introduces an anisotropy into an otherwise isotropic medium. This anisotropy has the effect of permitting the wave belonging to the extraordinary mode to penetrate the ionosphere, if the frequency is less than the gyrofrequency of the region. However, not all low-frequency waves are transmitted, but only those pulses, or wave-packets, that correspond to rays traveling at angles less than about  $20^\circ$  with the direction of the magnetic field. As a result, the low-frequency components of the wave-packet radiated by an impulsive disturbance move in a direction (the ray direction) that lies fairly close to the direction of a line of force of the earth's magnetic field.

The lateral spreading of the whistler mode structure is small; as a matter of practical experience, it is found<sup>1</sup> that lightning strokes will produce whistlers only when they occur within about 2000 km of the point of observation. Attenuation within the whistler mode is also small; measurements of the relation between the direct (ground-wave) signal produced by a radio transmitter and the signal produced by excitation of a whistler mode<sup>2</sup> have shown that propagation by the whistler mode is down only about 10 to 30 db from the direct signal. The signal received by the whistler mode is delayed about 1 second, since it propagates along a line of force of the earth's magnetic field. Finally, since the line of force passes much of the way through a dispersive medium, the original sharp pulse becomes diffuse, the component of frequency  $f$  arriving at a time proportional to  $f^{-1/2}$ .

Turning now to nuclear explosions, according to a recent account,<sup>3</sup> electromagnetic field strengths of tens of mv per meter have been recorded thousands of km from the burst point of a 1-kiloton bomb. The signal produced varies as the logarithm of the yield. At large distances, it is composed of low frequencies only, the high frequencies attenuating rapidly as the distance from the explosion increases.

Combining these two sets of facts, we conclude:

- 1) Nuclear explosions in the kiloton range can reasonably be expected to excite whistler modes. The corresponding electromagnetic signal propagates along a line of force of the earth's field, can penetrate the ionosphere, and consists of a pulse or wave-packet of low-frequency components dispersed according to the law that the time of arrival goes as  $f^{-1/2}$ . If the signal is sufficiently strong, pulses will be observed, caused by reflections of the wave at the points where the line of forces meets the surface of the earth. The successive pulses will be progressively more dispersed and their times of arrival will obey the integral relationships observed for whistlers.<sup>1,2</sup>
- 2) The whistler signal produced by a nuclear explosion will be localized in the neighborhood of the line of force along which the signal is propagating.

The lateral spread about the line of force will be about 2000 km. Thus, on the surface of the earth, there will be two regions of detectability for each whistler, one where the line of force penetrates the earth near the burst point, and another at the conjugate point in the other hemisphere. The strength of the signal transmitted by the whistler mode will be about 10 to 30 db below the direct signal. Roughly, kiloton explosions will produce signals of hundredths or tenths of mv per meter at the conjugate point. The signal will be logarithmically dependent on the yield of the bomb.

- 3) A spherically symmetric system of charges and currents, in a spherically symmetric medium, cannot radiate electromagnetically because the electromagnetic field at large distances is a transverse, vector field and requires a unique direction of polarization to be defined, a condition that is incompatible with the assumed spherical symmetry of the sources and their surroundings. If, then, the earth's magnetic field is neglected, nuclear explosions can be expected to produce electromagnetic signals only at the top or the bottom of the atmosphere, where the properties of the medium change rapidly in a mean free path of the current-producing radiation emitted by the bomb. The middle region of the atmosphere, in particular, constitutes a "dead spot" for the generation of electromagnetic signals if the earth's field is ignored. Thus, we see that the anisotropy introduced by the earth's magnetic field has two effects. First, by impairing the spherical symmetry otherwise present in the middle atmosphere, it makes possible the generation of electromagnetic signals in this region, and this may explain why the signals observed from bursts in this region have not been as small as expected;<sup>3</sup> second, and more important, the earth's field sets up the conditions required for the presence of whistler modes, which we would expect to be excited by bomb bursts at *any altitude and on either side of the ionosphere*, though the influence of the Van Allen belts on whistlers excited in outer space remains to be evaluated.
- 4) Finally, we note that because of the large natural background in the frequency range characteristic of whistler propagation—tens to hundreds of kc—we would not expect these signals to be of primary interest in detecting nuclear explosions, but we would expect that they can furnish important secondary information regarding explosions in either the atmosphere or in outer space.

B. A. LIPPMANN  
Lawrence Rad. Lab.  
Livermore, Calif.  
Consultant, Physics Section  
Convair-San Diego  
San Diego, Calif.

## A Ferromagnetic Amplifier Using Dielectric Loading\*

Since Suhl's original paper<sup>1</sup> proposing the ferromagnetic parametric amplifier, a number of experimental amplifiers have been built and tested. Until recently, most of these required rather high pumping powers compared with parametric amplifiers using diodes as variable-reactance elements. Considerable reductions in pumping powers became possible with the use of narrow linewidth materials such as single-crystal yttrium iron garnets. Further improvements were reported when use was made of the larger filling factors achievable by operating the amplifier in a modified semistatic mode<sup>2</sup> or in a completely magnetostatic manner.<sup>3</sup>

Preliminary experimental work at Syracuse University<sup>4</sup> indicates that further improvement may be possible by the use of dielectric-loaded cavities. A rectangular cavity of internal dimensions  $0.618 \times 0.384 \times 0.210$  inch was constructed and filled completely (except for the yttrium iron garnet sample) with Stycast Hy K dielectric, of dielectric constant 10. The cavity dimensions were chosen to make the cavity resonant in the  $TE_{012}$  mode at the pump frequency of approximately 9300 megacycles per second, and in the  $TE_{101}$  mode at the signal frequency of 5900 megacycles per second. (See Fig. 1.) The pump mode was excited from the end wall of a standard X-band guide in the X-Z plane of the cavity. The signal mode was excited by a probe terminating coaxial line in the opposite cavity wall. A disc-shaped sample of 0.132 inch diameter and 0.027 inch thickness was cut from a single crystal of yttrium iron garnet and located at a position of maximum pump and signal fields as shown in Fig. 1.

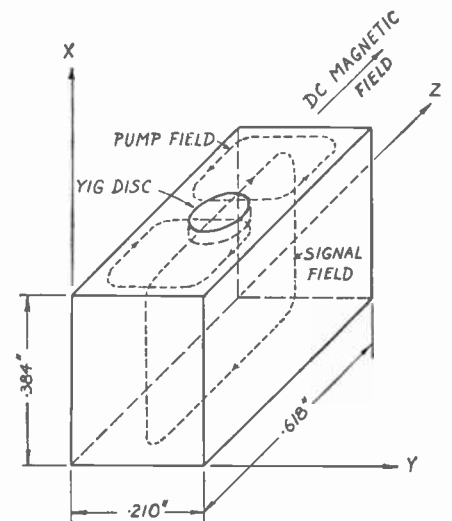


Fig. 1.

\* Received by the IRE, July 8, 1960.

<sup>1</sup> J. Suhl, "Theory of the ferromagnetic microwave amplifier," *J. Appl. Phys.*, vol. 28, pp. 1225-1236, November, 1957.

<sup>2</sup> A. D. Berk, L. Kleinman and C. E. Nelson, "Modified semistatic ferrite amplifier," 1958 WESCON CONVENTION RECORD, pt. 3, pp. 9-12.

<sup>3</sup> R. T. Denton, "A ferromagnetic amplifier using longitudinal pumping," *Proc. IRE*, vol. 48, pp. 937-938, May, 1960.

<sup>4</sup> This work is sponsored by the Rome Air Dev. Center, under Contract No. AF 30(602)-1627.

A dc magnetic field was supplied parallel to the RF signal field at the sample.

Amplification has been observed at dc fields of 700 and 1600 oersteds. The first of these is the field required for resonance of the uniform precessional mode in the sample at the idler frequency, *i.e.*, the difference between pump and signal frequency. The higher field value presumably corresponds to another magnetostatic mode. Pumping powers of a few watts peak were required in the first tests, but theoretical estimates indicate that improvement by at least a factor of ten should be possible. Most of the discrepancy can be ascribed to a poor quality (large line-width) crystal sample.

The uniform precessional mode was identified from observations of the magnetostatic mode spectrum of the disk at the pump frequency. Tests were made with the dc field parallel and normal to the disk. In each case more than 50 resonances were observed as a function of the applied dc field. The uniform precessional mode was most strongly excited in each case. The dc fields required for resonance of the uniform mode in each case, the spread of the spectrum, and the upper and lower bounds of the spectrum were reasonably consistent with the values computed from Kittel's formula and Walker's analysis<sup>5</sup> when use was made of the normally quoted saturation magnetization (1750 oersteds) and gyromagnetic ratio (2.8 megacycles/oersted) of yttrium iron garnet and a demagnetization factor of 0.76 normal to the disk.<sup>6</sup>

Based upon the above preliminary results, it is felt that dielectric loading of the cavity may eventually lead to a practical low-noise ferromagnetic amplifier. The large effective filling factors obtained this way should make it possible to reduce pumping powers to a small fraction of a watt. Furthermore, the small cavity size makes possible the use of small-airgap permanent magnets in the microwave frequency range in which these amplifiers appear to be most useful at present.

HARRY GRUENBERG  
Dept. of Elec. Engrg.  
Syracuse University  
Syracuse, N. Y.

<sup>5</sup> L. R. Walker, "Magnetostatic modes in ferromagnetic resonance," *Phys. Rev.*, vol. 105, pp. 390-399; January, 1957.

<sup>6</sup> J. A. Osborne, "Demagnetizing factors of the general ellipsoid," *Phys. Rev.*, vol. 67, pp. 351-357; June, 1945.

### Low Reverse Leakage Gallium-Arsenide Diodes\*

Gallium-arsenide diffused diodes have been reported whose operation as high-Q variable capacitors and as computer diodes

\* Received by the IRE, July 5, 1960. This work was supported by the U. S. Army, Navy and Air Force.

compared favorably with the best commercially available of germanium and silicon.<sup>1-3</sup> It is the purpose of this note to describe high-speed gallium-arsenide diffused diodes which, because of their reverse leakage currents between  $10^{-12}$  and  $5 \times 10^{-11}$  amperes and rectification ratios above  $10^{10}$ , have replaced vacuum diodes in applications requiring extremely low reverse leakage and/or high rectification ratios.

The current-voltage characteristics of two such devices are plotted to semi-logarithmic scale in Figs. 1 and 2. At 2 volts the rectification ratios for the two diodes are  $1.3 \times 10^{10}$  and  $2.5 \times 10^{11}$ . The forward current in both devices shows an  $\exp(qv/2kT)$  voltage dependence over a relatively large range of voltage. If this portion of the characteristic is extrapolated to zero volts, a space charge generated saturation current of about  $2 \times 10^{-11}$  amperes is predicted. If one uses the theory of Sah, Noyce, and Shockley<sup>4</sup> and combines this space charge generated saturation current with the diode area and diode zero bias capacitance, one obtains a value for the carrier lifetime  $(\tau_{no}\tau_{po})^{1/2}$  of the order of  $1 \times 10^{-9}$  seconds assuming the trap level to be at the Fermi level for intrinsic material,  $E_i$ . This lifetime should be compared with the value of  $\tau_{po}$  of about  $6 \times 10^{-9}$  seconds determined from hole storage measurements on these diodes.<sup>5</sup>

Preliminary measurements have been made on the I-V characteristics of these devices as a function of ambient and temperature in order to try to understand the mechanisms which contribute to the current in the diodes. The lowest reverse currents have been obtained in dry nitrogen or in vacuum. Exposure to dry oxygen increases the reverse current by an order of magnitude, exposure to wet nitrogen increases it by three to four orders of magnitude. The original low reverse currents can be restored by vacuum baking. The reverse characteristic of many of the diodes exhibits the shape shown in Fig. 2. The current at the higher reverse biases ( $\sim 7$  volts to breakdown voltage) increases relatively slowly (by a factor of 2 for a 60°C temperature rise) with increasing temperature, while at the lower biases the increase is from one to two orders of magnitude for the same temperature rise and is more closely that expected from the increase in the intrinsic carrier concentration  $n_i$ . The preliminary ambient and temperature measurements which have been made give promise that further work may lead to even lower reverse currents.

The above devices and others with similar I-V characteristics were fabricated using vertically-pulled single-crystal gallium-arsenide. This material had net impurity densi-

<sup>1</sup> J. Lowen and R. H. Rediker, "Gallium-arsenide diffused diodes," *J. Electrochem. Soc.*, vol. 107, pp. 26-29; January, 1960.

<sup>2</sup> J. Halpern, J. Lowen and R. H. Rediker, "Gallium-Arsenide Diffused Diodes," presented at the Fifth Annual Electron Devices Conference, Washington, D. C.; October 29-30, 1959.

<sup>3</sup> R. I. Walker, F. A. Cunnell, C. H. Gooch and J. J. Low, "A gallium arsenide switching diode," *J. Electronics Control*, vol. 7, pp. 268-269; September, 1959 (published February, 1960).

<sup>4</sup> C. T. Sah, R. N. Noyce and W. Shockley, "Carrier generation and recombination in *p-n* junctions and *p-n* junction characteristics," *Proc. IRE*, vol. 42, pp. 1228-1243; September, 1957.

<sup>5</sup> R. H. Kingston, "Switching time in junction diodes and junction transistors," *Proc. IRE*, vol. 42, pp. 829-834; May, 1954.

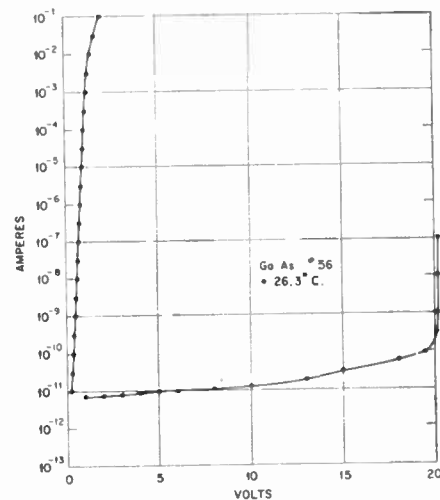


Fig. 1—Current-voltage characteristic (in vacuum) of diode GaAs 56.

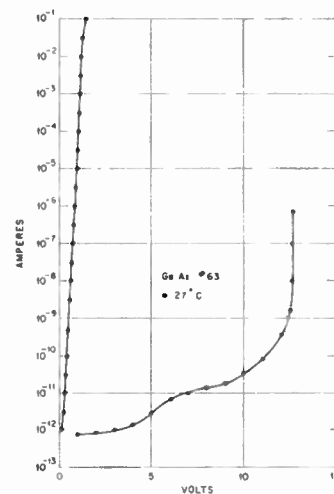


Fig. 2—Current-voltage characteristic (in vacuum) of diode GaAs 63.

ties  $N_D - N_A = 5 \times 10^{16}$  to  $2 \times 10^{17} \text{ cm}^{-3}$ , room temperature mobilities  $\mu \approx 3000$  to  $3800 \text{ cm}^2 \text{ volt}^{-1} \text{ sec}^{-1}$  and dislocation densities 5000 to  $20,000 \text{ cm}^{-2}$ . Diodes have been made from this single crystal material with very high yield and excellent reproducibility. The devices were fabricated by diffusing zinc into wafers of (100) oriented *n*-type starting material to produce a *p*-type region of depth 3-6 microns. The difference in breakdown voltage between the diodes of Figs. 1 and 2 is due to different diffusion temperatures and hence a shallower gradient in one device than in the other. Both devices were made from the same starting material. After diffusion the wafers were diced and the dice lapped to 3-mils thickness. Ohmic contact to the *n*-type bulk was made by alloying to a gold-antimony plated kovar stud. Ohmic contact to the *p*-diffused region was made by alloying a 0.002-inch diameter sphere of 90 per cent Pb and 10 per cent In into this region. Leads were attached and the device was then etched both to form a mesa defining the diode area ( $\text{HNO}_3$ , HF, HAc; 2:2:3) and to clean up the junction (HAc,  $\text{H}_2\text{O}_2$ ;

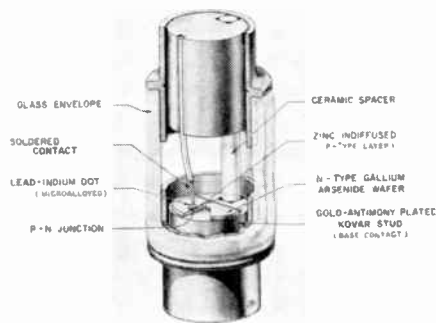


Fig. 3—Artist's representation (not to scale) of a low-leakage gallium-arsenide diode.

3:1). An artist's representation of a completed unit is shown in Fig. 3.

The authors wish to thank T. J. Rey for pointing out important circuit applications of these very low leakage diodes and T. M. Quist for helping in the design of the circuitry to measure the very low currents. They also wish to thank J. Lowen for helpful discussions regarding the fabrication of the devices and especially for developing the etches used, F. M. Sullivan for help in fabricating the diodes, and P. L. Moody for supplying us with the single crystal GaAs.

J. HALPERN  
R. H. REDIKER  
Lincoln Lab.  
Mass. Inst. Tech.  
Lexington, Mass.

### Scattering by a Spherical Satellite\*

In a recent paper,<sup>1</sup> Vea, Day, and Smith discuss the scattering of electromagnetic waves by a conducting sphere whose radius is large compared to the wavelength. Since the purpose of the paper is to provide information necessary for carrying out imminent propagation experiments, it should be pointed out that the results obtained by these authors are seriously in error. In particular, they deduce a dipole-type scattering pattern for a large sphere, which is at variance with the well-known result that a large, smooth, totally reflecting sphere scatters light by reflection isotropically, while the diffracted light contributes an intense, narrow lobe in the forward direction. The fact that the intensity of the reflected radiation is independent of direction follows easily from geometrical optics, and it can also be derived from the rigorous Mie solution of the electromagnetic problem, as given, for example, by Vea, Day, and Smith's (4) to (6). Indeed, it is the isotropic scattering characteristic of large spheres that makes them such useful standards for monostatic as well as bistatic echo area measurements.

\* Received by the IRE, May 26, 1960.

T. H. Vea, J. B. Day, and R. T. Smith, "The use of a passive spherical satellite for communication and propagation experiments," *Proc. IRE*, vol. 48, pp. 620-624; April, 1960.

In the paper under discussion, a perfectly conducting sphere of radius  $a$  is illuminated by a plane, linearly polarized electromagnetic wave of wavelength  $\lambda$  ( $\lambda \ll a$ ) and maximum electric intensity  $E_0$ . The incident wave is traveling in the positive  $z$ -direction ( $\theta=0$ ) and is polarized with the electric field parallel to the  $x$ -axis ( $\phi=0$ ). This choice of axes corresponds to (1) and (2) of the paper, although Fig. 1 shows the incident wave traveling in the negative  $z$ -direction. In terms of bistatic radar cross section, (9) and (17) yield, when a missing factor of  $r^2$  is supplied in the latter equation,

$$\sigma = 4\pi a^2(1 - \sin^2\theta \cos^2\phi).$$

This formula gives a backscattering cross section (echo area) of  $4\pi a^2$ , which is four times the geometrical cross section and just four times too large. A more serious discrepancy is the completely spurious scattering null which is predicted in the equatorial plane at  $\theta=\pi/2$ ,  $\phi=0$  and  $\pi$ .

A correct treatment of the problem of electromagnetic scattering by a perfectly conducting sphere has been given in many places, but an unusually thorough discussion may be found in a recent book by van de Hulst.<sup>2</sup>

In the coordinate system introduced above, the scattered field at a great distance may be written in the form<sup>3</sup>

$$V_\theta = \frac{-iE_0}{kr} e^{i\omega t - ikr} \cos\phi S_2(\theta),$$

$$E_\phi = \frac{iE_0}{kr} e^{i\omega t - ikr} \sin\phi S_1(\theta),$$

where  $k=2\pi/\lambda$ , and the amplitude functions  $S_1(\theta)$  and  $S_2(\theta)$  are series of associated Legendre functions with coefficients involving spherical Bessel functions. On the other hand, for a sphere large compared to the wavelength the functions  $S_1(\theta)$  and  $S_2(\theta)$  may be computed simply by geometrical optics,<sup>4</sup> and turn out to be

$$-S_1(\theta) = S_2(\theta) = \frac{1}{2}ika e^{2ika} \sin(\theta/2).$$

These equations together imply isotropic power scattering by the large sphere, with a scattering cross section

$$\sigma = \pi a^2$$

independent of direction.

It has been shown, both analytically and by numerical computation, that as  $ka$  increases the series expressions for  $S_1(\theta)$  and  $S_2(\theta)$  approach the geometrical optics limit, except of course near the forward scattering direction  $\theta=0$ , where the Fraunhofer diffraction pattern is superposed on the part of the scattering pattern which is due to reflection. At  $\theta=0$  the total scattered field has a large forward lobe, and in the  $E$ -plane ( $\phi=0$  and  $\pi$ ) there is a pronounced dip at an angle which gets closer to  $\theta=0$  as  $a/\lambda$  increases. The uniform part of the scattered

field can be approximated by geometrical optics, while physical optics will also indicate the dip and the large forward scattering.<sup>5</sup> Numerical summation<sup>6,7</sup> of the Mie series shows these effects developing as the value of  $ka$  increases. An extensive bibliography of calculations which have been made using the Mie theory is given by van de Hulst.

The analytical problem of showing that the series for  $S_1(\theta)$  and  $S_2(\theta)$  approach the geometrical optics limit as  $ka \rightarrow \infty$  (provided  $\theta \neq 0$ ) was essentially solved by Debye<sup>8</sup> 50 years ago. Vea, Day, and Smith attempted to carry out the limiting process from their (4) and (6), but they appear to have gone astray in replacing the spherical Hankel function  $h_n(ka)$  by the first term of its expression in powers of  $1/ka$ , as given by their (18). This approximation breaks down completely if  $n$  and  $ka$  are both large and approximately equal, whereas it is well known that important contributions to the sum of the Mie series are made by the terms with  $n \approx ka$ . Readers interested in the correct analysis will find an account of it in van de Hulst.<sup>9</sup>

As a minor point, we are unable to follow the reasoning in Section C of Vea, Day, and Smith's appendix, where the equivalent gain of the sphere over an isotropic scatterer is said to be computed from the pattern volume. The volume of a three-dimensional radiation pattern, where the radius is proportional either to field strength or to power density, has no simple relationship to the total radiated power. If the authors are trying to compute the gain of the dipole-type pattern given by (9), this is well known to be equal to 3/2. In any case, the dipole pattern is irrelevant to the problem at hand.

In summary, the scattering by a conducting spherical satellite which is over 20 wavelengths in diameter can unquestionably be considered isotropic at all aspects of interest for passive satellite reflectors. The calculated variation is less than 1 db for scattering angles greater than 80° if the diameter of the sphere is even as large as  $20/\pi$  wavelengths. Furthermore, the choice of polarization will have little effect upon the available scattered power insofar as the satellite reflection properties are concerned.

E. M. KENNAUGH  
Antenna Lab.  
The Ohio State University  
Columbus, O.  
S. P. MORGAN  
Bell Telephone Labs., Inc.  
Murray Hill, N. J.  
H. WEIL  
Radiation Lab.  
Electrical Engineering Dept.  
University of Michigan  
Ann Arbor, Mich.

<sup>1</sup> K. M. Siegel, H. A. Alperin, R. R. Bonkowski, J. W. Crispin, A. L. Moffett, C. E. Schensted, and I. V. Schensted, "Bistatic radar cross sections of surfaces of revolution," *J. Appl. Phys.*, vol. 26, pp. 297-305; March, 1955.

<sup>2</sup> Van de Hulst, *op. cit.*, p. 163.

<sup>3</sup> R. W. P. King and T. T. Wu, "The Scattering and Diffraction of Waves," Harvard University Press, Cambridge, Mass., pp. 205-213; 1959.

<sup>4</sup> P. Debye, "Der Lichtdruck auf Kugeln von beliebigem Material," *Ann. Phys.*, Ser. 4, vol. 30, pp. 57-136; August, 1909.

<sup>5</sup> Van de Hulst, *op. cit.*, pp. 208-214.

<sup>6</sup> H. C. van de Hulst, "Light Scattering by Small Particles," John Wiley and Sons, Inc., New York, N. Y.; 1957.

<sup>7</sup> Van de Hulst, *op. cit.*, pp. 124-125.

<sup>8</sup> Van de Hulst, *op. cit.*, p. 223.

**Scattering Properties of Large Spheres\***

If the plane wave  $E_i = E_0 \hat{x} \exp [i(kz + \omega t)]$  illuminates a perfectly conducting sphere of radius  $a$ , the secondary field at a large distance from the sphere is, according to geometrical optics, given by

$$E_s \xrightarrow{r \rightarrow \infty} (-\cos \phi \hat{\theta} + \sin \phi \hat{\phi}) \frac{a}{2r} \cdot \exp \left[ i \left( 2ka \cos \frac{\theta}{2} - kr + \omega t \right) \right]$$

In a recent paper, Vea, Day, and Smith<sup>1</sup> have started from the exact solution

$$E_s = \frac{1}{ik} \sum_{n=1}^{\infty} \frac{2n+1}{n(n+1)} i^n \left[ \frac{\psi_n(ka)}{\xi_n^{(2)}(ka)} \cdot \text{curl curl} [r h_n^{(2)}(kr) P_n^1(\cos \theta) \cos \phi] + \frac{\psi_n(ka)}{\xi_n^{(2)}(ka)} \cdot \text{curl} [r h_n^{(2)}(kr) P_n^1(\cos \theta) \cos \phi] \right]$$

$$\psi_n(x) = x j_n(x) = \sqrt{\frac{\pi x}{2}} J_{n+1/2}(x),$$

$$\xi_n^{(2)}(x) = x h_n^{(2)}(x) = \sqrt{\frac{\pi x}{2}} H_{n+1/2}^{(2)}(x)$$

and have arrived at the erroneous result

$$E_s \xrightarrow{r \rightarrow \infty} (-\cos \theta \cos \phi \hat{\theta} + \sin \phi \hat{\phi}) \frac{a}{r} \cdot \exp [i(ka \cos \theta + ka - kr + \omega t)].$$

These authors have erred in using the asymptotic estimate

$$\xi_n^{(2)}(x) \sim i \exp \left[ -ix + in \frac{\pi}{2} \right], \quad x = ka$$

for all values of  $n$ , although it is actually valid only for  $n \ll ka$ . The objections to the use of this estimate for all values of  $n$  has a long history.

Rayleigh<sup>2</sup> discussed its use in his 1872 paper on diffraction of sound by a sphere. In 1903, Macdonald<sup>3</sup> made this error in a study of diffraction of radio waves around a sphere and was immediately criticized by both Rayleigh<sup>4</sup> and Poincaré.<sup>5</sup> Macdonald<sup>6</sup> conceded his mistake, and for several years the mathematical physicists were unable to show that the exact solutions for the diffraction of waves by spheres and cylinders are consistent with geometrical optics when the radius greatly exceeds the wavelength. In 1908, Debye<sup>7</sup> showed how to obtain an asymptotic estimate to the exact solution of the cylinder problem which is identical with

the result predicted by geometrical optics. The exact solution for the sphere problem has been shown to lead to the optics result by Nicholson,<sup>8,9</sup> Bromwich,<sup>10</sup> and White.<sup>11</sup>

In a report which is now in preparation,<sup>12</sup> we will show that the estimates obtained from geometrical optics are the leading terms in asymptotic expansions of the form

$$\begin{aligned} \hat{\theta} \cdot E_s \xrightarrow[r \rightarrow \infty]{ka \ll r} -\cos \phi \frac{a}{2r} \exp \left[ i \left( 2ka \cos \frac{\theta}{2} - kr + \omega t \right) \right] & \left[ 1 + i \frac{1}{2(ka) \cos^3 \frac{\theta}{2}} - \frac{7 \sin^2 \frac{\theta}{2}}{4(ka)^2 \cos^6 \frac{\theta}{2}} \right. \\ & \left. - i \frac{79 \sin^2 \frac{\theta}{2} + 33 \sin^4 \frac{\theta}{2}}{8(ka)^3 \cos^9 \frac{\theta}{2}} + \frac{8 + 1076 \sin^2 \frac{\theta}{2} + 1401 \sin^4 \frac{\theta}{2} + 210 \sin^6 \frac{\theta}{2}}{16(ka)^4 \cos^{12} \frac{\theta}{2}} + \dots \right] \\ \hat{\phi} \cdot E_s \xrightarrow[r \rightarrow \infty]{ka \ll r} \sin \phi \frac{a}{2r} \exp \left[ i \left( 2ka \cos \frac{\theta}{2} - kr + \omega t \right) \right] & \left[ 1 + i \frac{1 - 2 \sin^2 \frac{\theta}{2}}{2(ka) \cos^3 \frac{\theta}{2}} + \frac{7 \sin^2 \frac{\theta}{2} - 2 \sin^4 \frac{\theta}{2}}{4(ka)^2 \cos^6 \frac{\theta}{2}} \right. \\ & \left. + i \frac{63 \sin^2 \frac{\theta}{2} + 7 \sin^4 \frac{\theta}{2}}{8(ka)^3 \cos^9 \frac{\theta}{2}} + \frac{8 - 836 \sin^2 \frac{\theta}{2} - 683 \sin^4 \frac{\theta}{2} - 84 \sin^6 \frac{\theta}{2}}{16(ka)^4 \cos^{12} \frac{\theta}{2}} + \dots \right] \end{aligned}$$

Care must be exercised in using these asymptotic expansions because they describe only the wave reflected from the sphere. The wave diffracted around the sphere (sometimes called a creeping wave) is generally important if

$$\left( \frac{ka}{2} \right)^{1/3} (\pi - \theta) < 8.$$

It is a curious fact that the introduction of the improper asymptotic estimate for  $\xi_n^{(2)}(ka)$  when studying large perfectly conducting spheres leads to patterns for the scattered energy which are identical with the Rayleigh scattering patterns for small dielectric spheres. If  $m$  denotes the index of refraction, the Rayleigh scattering law is

$$E_s \xrightarrow[r \rightarrow \infty]{ka \ll r} -(\cos \theta \cos \phi \hat{\theta} + \sin \phi \hat{\phi}) \cdot \frac{a}{r} \left[ (ka)^2 \frac{m^2 - 1}{m^2 + 2} \right] \exp [i(-kr + \omega t)].$$

The corresponding result for Rayleigh scattering by small conducting spheres is

$$\hat{\theta} \cdot E_s \xrightarrow[r \rightarrow \infty]{ka \ll r} \frac{a}{r} (ka)^2 \left[ \cos \theta + \frac{1}{2} \right] \cos \phi \cdot \exp [-ikr + i\omega t]$$

$$\hat{\phi} \cdot E_s \xrightarrow[r \rightarrow \infty]{ka \ll r} -\frac{a}{r} (ka)^2 \left[ \frac{\cos \theta}{2} + 1 \right] \sin \phi \cdot \exp [-ikr + i\omega t]$$

and therefore cannot be obtained from the dielectric result by merely letting  $m$  tend to infinity.

In view of the above remarks, we must conclude that the results of Vea, Day, and Smith do not describe the reflection properties of large conducting spheres and no useful results are contained in their article.

N. A. LOGAN  
Lockheed Missiles and Space Div.  
Sunnyvale, Calif.

**WWV and WWVH Standard Frequency and Time Transmissions\***

The frequencies of the National Bureau of Standards radio stations WWV and WWVH are kept in agreement with respect to each other and have been maintained as constant as possible with respect to an improved United States Frequency Standard (USFS) since December 1, 1957.

The nominal broadcast frequencies should, for the purpose of highly accurate scientific measurements, or of establishing high uniformity among frequencies, or for removing unavoidable variations in the broadcast frequencies, be corrected to the value of the USFS, as indicated in the table below.

The characteristics of the USFS, and its relation to time scales such as ET and UT2, have been described in a previous issue,<sup>1</sup> to which the reader is referred for a complete discussion.

\* Received by the IRE, August 29, 1960.

<sup>1</sup> Refer to "United States National Standards of Time and Frequency," Proc. IRE, vol. 48, pp. 105-106; January, 1960.

\* Received by the IRE, June 21, 1960.

<sup>1</sup> T. H. Vea, J. B. Day, and R. T. Smith, "The use of a passive spherical satellite for communication and propagation experiments," Proc. IRE, vol. 48, pp. 620-624; April, 1960.

<sup>2</sup> Lord Rayleigh, "Investigation of the disturbance produced by a spherical obstacle on the waves of sound," Proc. London Math. Soc., vol. 4, pp. 253-283; 1872.

<sup>3</sup> H. M. Macdonald, "The bending of electric waves round a spherical obstacle," Proc. Roy. Soc. (London) A, vol. 71, pp. 251-258; 1903.

<sup>4</sup> Lord Rayleigh, "On the bending of waves round a spherical obstacle," Proc. Roy. Soc. (London) A, vol. 72, pp. 40-41; 1903. ("Scientific Papers," Cambridge University Press, New York, N. Y., vol. 5, pp. 112-114; 1912.)

<sup>5</sup> H. Poincaré, "L'upon the diffraction of electric waves; upon a paper of Macdonald," Proc. Roy. Soc. (London) A, vol. 72, pp. 42-52; 1903.

<sup>6</sup> H. M. Macdonald, "The bending of electric waves round a conducting obstacle: amended result," Proc. Roy. Soc. (London) A, vol. 72, pp. 59-68; 1903.

<sup>7</sup> P. Debye, "The electromagnetic field surrounding a cylinder, and the theory of the rainbow," Physik Z., vol. 9, pp. 775-778; 1908.

<sup>8</sup> J. W. Nicholson, "The scattering of light by a large conducting sphere," Proc. London Math. Soc., vol. 9, pp. 67-80; 1910.

<sup>9</sup> J. W. Nicholson, "The scattering of light by a large conducting sphere (second paper)," Proc. London Math. Soc., vol. 11, pp. 277-284; 1912.

<sup>10</sup> T. Bromwich, "The scattering of plane electric waves by spheres," Phil. Trans. Roy. Soc. (London) A, vol. 220, pp. 189-206; 1920.

<sup>11</sup> F. P. White, "The diffraction of plane electromagnetic waves by a perfectly reflecting sphere," Proc. Roy. Soc. (London) A, vol. 100, pp. 505-525; 1922.

<sup>12</sup> N. A. Logan, "General Research in Diffraction Theory III. Asymptotic Expansions of Exact Solutions for Diffraction by Cylinders and Spheres," Lockheed Missile Systems Div., Sunnyvale, Calif., Tech. Rept. No. LMSD 288089, in preparation.

The WWV and WWVH time signals are also kept in agreement with each other. Also they are locked to the nominal frequency of the transmissions and consequently may depart continuously from UT2. Corrections are determined and published by the U. S. Naval Observatory. The broadcast signals are maintained in close agreement with UT2 by properly offsetting the broadcast frequency from the USFS at the beginning of each year when necessary. This new system was commenced on January 1, 1960. The last time adjustment was a retardation adjustment of 0.02 s on December 16, 1959.

WWV FREQUENCY WITH RESPECT TO U. S. FREQUENCY STANDARD

1960 July 1600 UT	Parts in 10 <sup>10</sup> †
1	-147
2	-148
3	-148
4	-148
5	-148
6	-148
7	-149
8	-149
9	-149
10	-149
11	-149
12	-149
13	-149
14	-149
15	-149
16	-149
17	-149
18	-149
19	-149
20	-149
21	-149
22	-148
23	-148
24	-148
25	-148
26	-147
27	-147
28	-147
29	-147
30	-147
31	-147

† A minus sign indicates that the broadcast frequency was low.

National Bureau of Standards  
Boulder, Colo.

**Correction to "Direct Reading Noise Figure Measuring Device"**

George Bruck, author of the above, which appeared on page 1342 of the July, 1960, issue of PROCEEDINGS, has been advised of the following by W. W. Mumford of Bell Telephone Laboratories, Whippany, N. J.

In the third column, second to the last paragraph, the formula for the noise figure appears. The text following this formula should read "where  $F_0$  is the excess noise ratio of the noise source. . . ."

The excess noise ratio of the noise source is the ratio of the excess power of the noise source to the thermal power at 290° K.

**Correction to "Absolutely Stable Hybrid Coupled Tunnel Diode Amplifier"**\*

John J. Sie, author of the above Correspondence, which appeared on page 1321 of the July, 1960 issue of PROCEEDINGS, has advised the Editor of the following.

Eq. (2) should read:

$$|S_{21}|^2 = \frac{\left(1 + \frac{G}{G_0} - \frac{G_1}{G_0}\right)^2 + B^2}{\left(1 - \frac{G}{G_0} + \frac{G_1}{G_0}\right)^2 + B^2}$$

In (3),

$$F = 1 + \frac{G_1 + 20I_0}{G_0} \eta + \frac{|S_{22}|^2}{|S_{21}|^2}$$

and

$$\eta = \frac{4}{\left(1 + \frac{G}{G_0} - \frac{G_1}{G_0}\right)^2 + B^2}$$

where  $B$  is the normalized susceptance of the shunt circuit.

\* Received by the IRE, July 25, 1960.

**Some Results on Diode Parametric Amplifiers\***

Parametric amplifiers at  $S$  and  $X$  band have been studied at room temperature with the following results:

*S Band*

- $f_s = 3$  kmc
- $f_p = 11.9$  kmc
- Gain = 17 db
- Bandwidth = 50 mc
- Noise Figure = 1.6 db  $\pm$  0.2 db
- Diode MA450F-R  $f_c = 80$  kmc
- Pump Power = 10 mw
- Calculated NF = 1.74 db,

*X Band*

- $f_s = 9900$  mc
- $f_p = 19,800$  mc
- Gain = 20 db
- Bandwidth = 25 mc
- Noise Figure = 1.2 db  $\pm$  0.5 db
- Diode MA450H-R  $f_c = 100$  kmc
- Radar Noise Figure = 4.2 db  $\pm$  0.5 db
- Pump Power = 120 mw
- Calculated NF = 1.2 db

The relationship of Penfield<sup>1</sup> was used to check theoretically these results for single sideband operation. The noise figure is

$$F = 1 + \frac{\omega_s}{\omega_i} \left[ \frac{m^2 \omega_c^2 + \gamma \omega_i^2}{m^2 \omega_c^2 - \omega_i \omega_s} \right]$$

\* Received by the IRE, April 18, 1960.

<sup>1</sup> P. Penfield, Jr., private communication.

where

- $\omega_c$  = Cutoff frequency of the diode based on  $C_{min}$
- $\omega_i$  = Idler frequency
- $m$  = Modulation ratio =  $|S_1|/S_{max}$
- $|S_1|$  = Pump frequency component of elastance
- $S_{max}$  = Maximum varactor elastance
- $\gamma = (R_i + R_s)/R_s$
- $R_s$  = Varactor series resistance
- $R_i$  = Real part of the external idler terminating impedance.

For the case under consideration,

- $m = 0.2$
- $\gamma = 1.$

I. GOLDSTEIN  
J. ZORZY  
Raytheon Co.  
Missile System Div.  
Bedford, Mass.

**Some Parametric Amplifier Circuit Configurations and Results\***

The application of two techniques, well known to the microwave engineer, have been applied to parametric amplifiers. These are quarter-wave-coupled filter techniques and the cascading of the amplifiers. First, a simple circuit configuration for the parametric amplifier was selected and this was a Hewlett-Packard 440A crystal mount which makes a good degenerate amplifier at  $S$  band. I call the filter type an active quarter-wave-coupled filter as compared to a passive one. A schematic of the circuit is shown in Fig. 1. The cold characteristic of this circuit is shown in Fig. 2.

The active characteristic is shown in Fig. 3.

In the reverse direction the gain characteristic is shown in Fig. 4.

The reverse characteristics actually indicated gain off frequency for given settings of the amplifier tuning stubs. The results are summarized in Table I.

This amplifier with adjustment was also operated in a nondegenerate mode with the following characteristics:

- Gain = 10 db,
- BW = 17 db,
- $f_s = 2600$  mc,
- $f_p = 10,800$  mc,
- Pump power = 500 mw.

In the backward wave mode of operation, a very narrow band-pass of 1 mc at a gain of 10 db was observed which was tunable over a 15-mc band by varying pump frequency and amplitude. The signal and pump frequencies were the same as in the forward wave mode.

\* Received by the IRE, April 15, 1960.

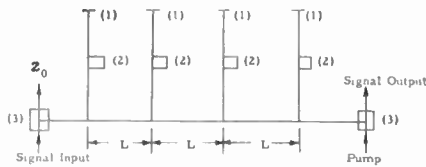


Fig. 1—1) Tuning stub; 2) Varactor; 3) Diplexer;  $l=0.5 \lambda$  signal;  $L=0.7 \lambda$  signal.

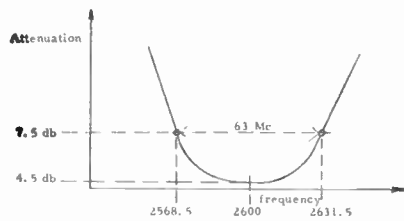


Fig. 2.

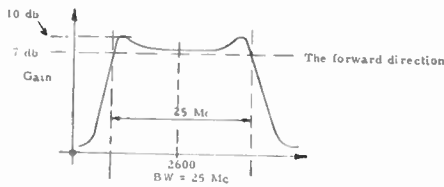


Fig. 3.

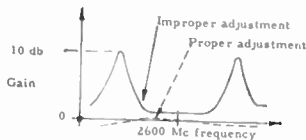


Fig. 4.

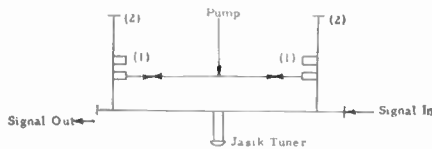


Fig. 5—1) Diode; 2) Tuning stub.

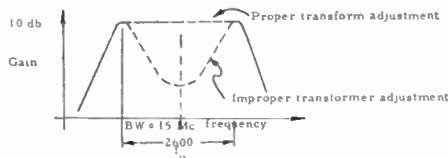


Fig. 6.

TABLE I

Pump	Direction	Gain	Bandwidth
On	Input to Output	10 db	25 mc
On	Output to Input	0 to -1.5 db	25 mc
Off	Input to Output	4.5 db	63 mc

$f_p=2600$  mc.  
 $f_s=5200$  mc.  
 Pump power=100 mw.  
 NF=5 db, double-sideband.

CASCADING RESULTS

The basic circuit used in this experiment is shown in Fig. 5. With adjustment of the amplifiers and Jaski tuner, the following data were obtained:

Gain = 10 db,  
 BW = 15 mc,  
 $f_p = 5200$ ,  
 $f_s = 2600$ ,

Pump power = 6 mw.

The coupling between the amplifier circuits is shown in Fig. 6.

In summary, two techniques have been experimentally demonstrated to show that increased gain bandwidth can be obtained.

I. GOLDSTEIN  
 Raytheon Co.  
 Missile Systems Div.  
 Bedford, Mass.

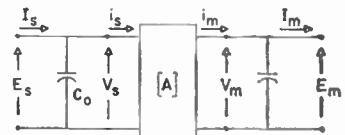


Fig. 1.

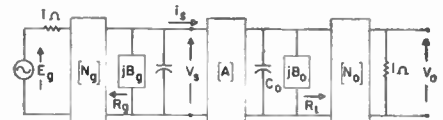


Fig. 2.

Let the amplifier have the form as shown in Fig. 2.  $[N_\theta]$  and  $[N_0]$  are coupling networks matching the amplifier to the source and load.  $[N_\theta]$  and  $[N_0]$  may be represented as

$$[N_\theta] = \begin{vmatrix} 1/\sqrt{R_\theta} & 0 \\ 0 & \sqrt{R_\theta} \end{vmatrix}$$

and

$$[N_0] = \begin{vmatrix} \sqrt{R_L} & \\ 0 & 1/\sqrt{R_L} \end{vmatrix}$$

where  $R_\theta$  and  $R_L$  are the transformed source and load impedances. We will assume single frequency operation such that the capacitances  $C_0$  at the input and output are tuned out by the susceptances  $jB_\theta$  and  $jB_0$ .

The transfer matrix for the amplifier can be written as

$$[T] = [N_\theta][A][N_0] = \begin{vmatrix} T_{11} & T_{12} \\ T_{21} & T_{22} \end{vmatrix} = \begin{vmatrix} 0 & j \frac{1}{\sqrt{\omega_s \omega_m} |C_p| \sqrt{R_L R_\theta}} \\ \sqrt{\frac{\omega_s C_p^*}{\omega_m C_p}} & j \sqrt{\omega_m \omega_s} |C_p| \sqrt{R_L R_\theta} \end{vmatrix} \quad (1)$$

It is the purpose of this note to offer a first-order explanation of this phenomenon and suggest ways to improve the performance of these amplifiers.

Assume that a lossless parametric diode may be represented, in ABCD matrix form, by the equivalent circuit as shown in Fig. 1.

$E_s, I_s$  are signal frequency components at  $\omega_s$ ;

$E_m, I_m$  are upper sideband components at  $\omega_m$ ;

$$[A] = \begin{vmatrix} \sqrt{\frac{\omega_s C_p^*}{\omega_m C_p}} & \\ j |C_p| \sqrt{\omega_m \omega_s} & 0 \end{vmatrix};$$

$C_p = C_1 v_p$ , where  $C_1$  is the nonlinear term in the diode capacitance expansion;  $C = C_0 + C_1 v$ , and  $v_p = V_p e^{j\theta p}$  is the pump voltage.

Assuming that  $R_\theta = R_L = R$ ,

$$[T] = \begin{vmatrix} \sqrt{\frac{\omega_s C_p^*}{\omega_m C_p}} & \\ 0 & j \frac{1}{\sqrt{\omega_s \omega_m} |C_p| R} \end{vmatrix} \cdot \begin{vmatrix} 0 & j \frac{1}{\sqrt{\omega_s \omega_m} |C_p| R} \\ j \sqrt{\omega_m \omega_s} |C_p| R & 0 \end{vmatrix} \quad (2)$$

The power gain may be expressed<sup>1</sup> as

$$G_p = \frac{P_m}{P_p} = \frac{4 \left( \frac{\omega_m}{\omega_s} \right)}{\left| \sum_{ij} T_{ij} \right|^2} \quad (3)$$

Thus

$$G_p = \frac{4 \frac{\omega_m}{\omega_s}}{2 + \omega_m \omega_s R^2 |C_p|^2 + \frac{1}{\omega_m \omega_s R^2 |C_p|^2}} \quad (4)$$

<sup>1</sup> H. Seidel and G. Herrmann, "Circuit aspects of parametric amplifiers," 1959 IRE WESCON CONVENTION RECORD, pt. 2, pp. 83-90.

\* Received by the IRE, April 4, 1960.



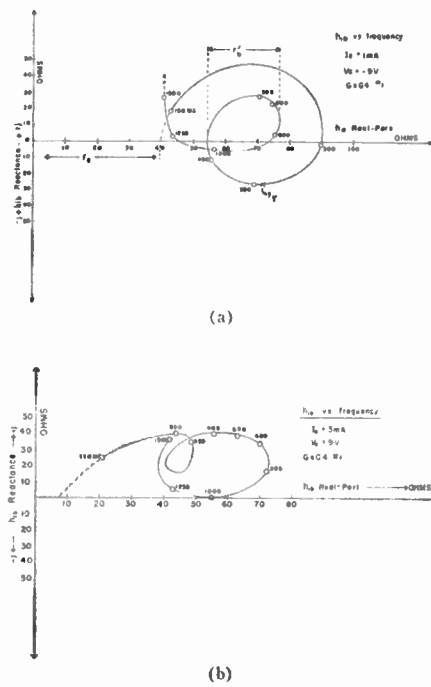


Fig. 2—(a) Complex input impedance  $h_{ib}$  measurement with frequency as variable for a Hughes G4G4 transistor. Bias condition: emitter current  $I_e = 1$  ma, collector voltage  $V_c = -9$  v. (b) Complex input impedance  $h_{ib}$  measurement as for (a) but at  $I_e = 3$  ma.

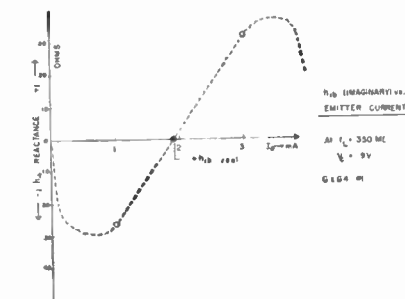


Fig. 3—Plot of imaginary part of the input impedance  $h_{ib}$  vs emitter current at a fixed frequency, e.g., 350 mc.

the current is 2 ma. Furthermore, it is conclusive that, for a particular frequency, the input impedance of a certain transistor can be made real for a specific current. Accomplishing this is referred to as current tuning. Considering the dc bias arrangement in Fig. 1, the current tuning for a fixed oscillating frequency  $f_L$  can be performed by adjusting  $R_1$ . The effectiveness of this procedure can be seen in Fig. 4(a), where conversion gain is plotted as a function of emitter current. To meet the condition of tuning requires continuation of oscillation. This is not easily met in all existing high-frequency transistors, but can be designed into the device. The amount of feedback can be adjusted at will and one can obtain stable gains for desirable settings by avoiding disturbance of current tuning, and matching conditions for  $L_s$ .

The excellent gain performance is due not only to variable reactance behavior of the input impedance, but also to the feed-

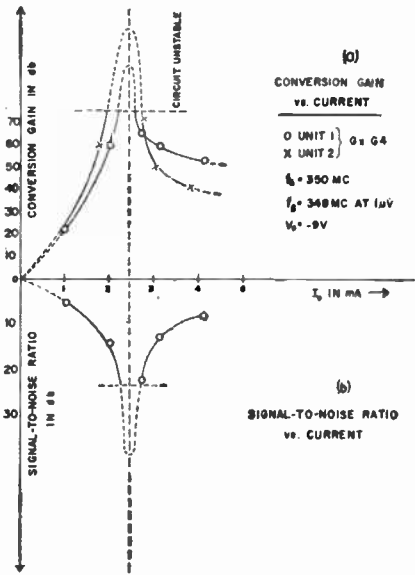


Fig. 4—(a) Conversion gain, measured in circuit of Fig. 1 for a G4G4 transistor vs emitter current at collector voltage of  $V_c = -9$  v. (b) Signal-to-noise ratio of the same transistor under the test conditions of a versus current at a bandwidth of approximately 20 kc.

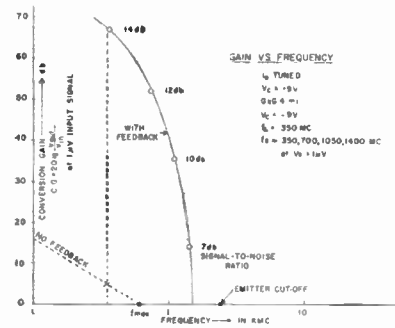


Fig. 5—Conversion gain vs frequency with and without feedback, including signal frequencies in multiples of the oscillator frequency, e.g., harmonics.

back amplifier properties<sup>2</sup> of the circuit, even under oscillatory conditions. These advantages are evidenced from results presented in Figs. 4(a), 4(b) and Fig. 5 and they are

- 1) increase in frequency gain bandwidth,
- 2) noise reduction,
- 3) reduction in the influence of transistor parameter variations upon gain, which increases stability since now external circuitry elements determine the performance.

The coordination of circuit development and device design produced maximum conversion gains of the fundamental frequency of operation of 90 db with a signal-to-noise ratio of 30 db. The best performance at harmonics of the fundamental oscillation frequency occurred at 1.4 mc with 14 db conversion gain and a signal-to-noise ratio of 7 db at a bandwidth of 150 kc. The true noise

performance during this measurement reveals a noise figure of 2-3 db above ambient. The measurements at multiples of the fundamental oscillation frequency are given in Fig. 5. From the maximum frequency of oscillation for that particular transistor, only 5 db gain can be predicted at 350 mc. With feedback operation and current tuning in the new mode, the conversion gain was 66 db. Without feedback we assumed the 6 db per octave slope. The slope or falloff of gain with applied feedback vs frequency is not understood at the present writing and extrapolations of the measurements to produce ultimate performances are subject to speculation. However, it is reasonable to believe that the emitter cutoff frequency alone in present devices will limit the performance to frequencies of the order of approximately 2.4 mc. In regard to performance it may be said that under present circumstances the matching conditions in the test circuits are not perfected and proper transistor designs are not fully explored so that the possibilities of extending the useful frequency range in transistors into the microwave region of 5-10 mc is most likely in the near future.

Although the theoretical development is not yet completed, enough quantitative experimental evidence has been presented to manifest the existence of a parametric-amplifier transistor. The up-conversion mode of operation has been verified experimentally and a detailed analysis of the nonlinear elements which produce the conversion gain has been initiated in regard to harmonic power generation. The results will be published as soon as the work is completed.

The authors are indebted to both managements and are especially grateful to Dr. R. A. Gudmundsen and G. M. Løbedeff for their valuable time devoted to discussions on this matter.

R. ZULEG  
Hughes Aircraft Co.  
Semiconductor Div.  
Newport Beach, Calif.  
V. W. VONICKA  
Lenkurt Electric Company, Inc.  
General Telephone and  
Electronics Corp  
San Carlos, Calif

### The Electron Content and Distribution in the Ionosphere\*

In a recent letter,<sup>1</sup> results were given of electron content measurements determined from the Faraday rotation rate of transmissions from the satellite 1958<sub>2</sub>. From this data and estimates of the electron content below the maximum of the  $F_2$  layer, the ratio of the number of electrons above the  $F_2$  maximum to that below was estimated.

\* Received by the IRE, April 22, 1960.  
<sup>1</sup> T. G. Hame and W. D. Stuart, "The electron content and distribution in the ionosphere," Proc. IRE, vol. 48, pp. 364; March, 1960.

<sup>2</sup> R. I. Shea, "Principles of Transistor Circuits," John Wiley and Sons, Inc., New York, N. Y., 1953.

More exact data<sup>2</sup> have since been received concerning the electron content below the  $F_2$  maximum and indicates that the estimated nighttime value of the electron distribution ratio was too low. Fig. 1 shows the electron content to the satellite height, the electron content below the  $F_2$  maximum and the electron distribution ratio during the pre-dawn period for May 4-11, 1959. The distribution ratio is between 3.1 and 4.7, which is consistent with the results given by Bauer, Daniels<sup>3</sup> and Evans.<sup>4,5</sup> The electron distribution ratio during the daytime has also been determined for the period March 4 to April 20, 1959. Excluding measurements during periods of high geomagnetic activity, a mean value of 2.3 was obtained.

To illustrate the variations in observed electron content measurements, the electron content is plotted in Fig. 2(a) as a function of increasing date and local time for the period March 21 to April 13, 1959. If this data is compared with the  $N_{max}F_2$  values<sup>6</sup> shown in Fig. 2(b) it is found that similar variations occur. Relating these observations to the geomagnetic and solar activity shown in Fig. 2(c), it is found that two of the major deviations in electron content are accounted for by the magnetic storms occurring on March 26-30 and April 9-10. However, the low value of electron content and  $N_{max}F_2$  observed on April 3 does not appear to correlate with any unusual geomagnetic activity.

### Maximum Avalanche Multiplication in $p-n$ Junctions\*

It has been shown that the rate of build-up of current in avalanche devices (avalanche transistors, 4-layer diodes, etc.) depends upon the value of the multiplication factor in the junctions exhibiting avalanche multiplication.<sup>1-3</sup> To obtain a rapid build-up of current, it is necessary to bias the junction so that  $M$  is as large as possible, where

$$M = 1/[1 - (V/V_B)^n],$$

- $V$  the reverse voltage across the junction,
- $V_B$  the breakdown voltage,
- $n$  a number (approximately 3) depending upon the type of material and the impurity concentration.<sup>4</sup>

It is therefore important to know whether there is a limit to the value of  $M$  which can be obtained in a practical situation, and what bias conditions are necessary to obtain the maximum  $M$ .

The purpose of this note is to obtain, from thermal considerations alone,<sup>5</sup> the following:

- 1)  $M_{max}$ , the maximum value of  $M$  that can be realized for a given  $p-n$  junction, and
- 2)  $I_{opt}$ , the bias current which should be used to obtain  $M_{max}$ .

The results of the analysis show that

- 1) at a given ambient temperature  $I_{opt}$  varies inversely with the breakdown voltage  $V_B$ , and
- 2)  $M_{max}$  is proportional to the ratio of optimum bias current to thermally generated current with the junction temperature equal to the ambient temperature.

For example, a germanium junction with a breakdown voltage of 42 volts, a thermally generated current of 5 microamperes at the ambient temperature, and a temperature coefficient of  $0.5 \times 10^8$  degrees  $C/watt$ , has  $M_{max}$  of approximately 40 and  $I_{opt}$  of approximately 0.54 ma.

A simplified biasing scheme is shown in Fig. 1. In this case, the  $p-n$  junction might be the collector junction of an avalanche transistor in a pulse circuit. The reverse bias current is considered to be the result, in the junction, of the avalanche multiplication of thermally generated carrier pairs. Thus,  $M = I/I_s$ , where  $I_s$  is the thermally generated current. Qualitatively, the following

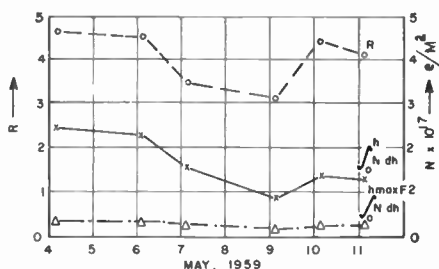


Fig. 1—Electron content, electron content below  $h_{max}F_2$  and electron distribution ratio during the pre-dawn period.

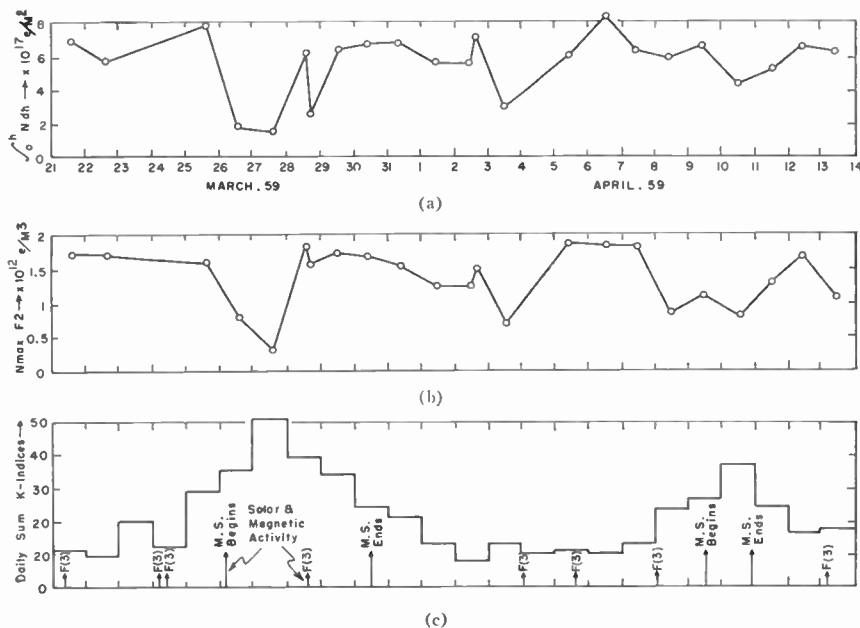


Fig. 2—Correlation of electron content and  $N_{max}F_2$  with solar and magnetic activity. (a) Electron content. (b)  $N_{max}F_2$  electron density. (c) Daily sum K-indices and solar flares.

<sup>2</sup> "Electron Integral to  $h_{max}$ ." Soundings Research, Sun-Earth Relationships Section, Radio Propagation Physics Div., Nat'l. Bur. Standards, Boulder, Colo. (Private communication.)

<sup>3</sup> S. J. Bauer and F. B. Daniels, "Ionospheric parameters deduced from the Faraday rotation of lunar radio reflections," *J. Geophys. Res.* vol. 60, p. 439; 1958.

<sup>4</sup> J. V. Evans, "The measurement of the electron content of the ionosphere by the lunar radio echo method," *Proc. Phys. Soc. (London)*, vol. 69, pp. 963; 1956.

<sup>5</sup> J. V. Evans, "The electron content of the ionosphere," *J. Atmos. Terr. Phys.*, vol. 11, p. 259; 1957.

<sup>6</sup> "Detailed Values of Ionospheric Characteristics and  $F_2$ -plots for Washington," Central Radio Propagation Lab., Nat'l. Bur. Standards, Boulder, Colo.; March and April, 1959.

T. G. HAME  
W. D. STUART  
Antenna Lab.  
Dept. of Elec. Engrg.  
Ohio State University  
Columbus Ohio

\* Received by the IRE, February 23, 1960; revised manuscript received, April 13, 1960.

This work was done at Stanford Electronics Labs., Stanford, Calif., under Contract Nonr 225(24), NR 373 360.

<sup>1</sup> W. Shockley and J. Gibbons, "Current build-up in semiconductor devices," *Proc. IRE*, vol. 46, pp. 1947-1949; December, 1958.

<sup>2</sup> W. Shockley and J. Gibbons, "Theory of Transient Build-up in Avalanche Transistors," presented at AIEE Conference, Pittsburgh, Pa. Paper No. 58-1249; September 10, 1958.

<sup>3</sup> D. J. Hamilton, J. Gibbons, and W. Shockley, "Physical principles of avalanche transistor pulse circuits," *Proc. IRE*, vol. 47, pp. 1102-1109; June, 1959.

<sup>4</sup> S. L. Miller, "Avalanche breakdown in germanium," *Phys. Rev.*, vol. 99, pp. 1234-1241; August 15, 1955.

<sup>5</sup> D. J. Hamilton, "A Theory for the Transient Analysis of Avalanche Transistor Pulse Circuits," Stanford Electronics Labs., Stanford, Calif., Tech. Rept. No. 1701-1; June 15, 1959.

reasoning is helpful in visualizing the existence of a maximum value of  $M$ :

As the bias current  $I$  is increased from zero, the device dissipation will at first be very small, and  $I_s$  will remain essentially constant at its ambient temperature value. The multiplication  $M$  thus increases with  $I$ . As  $I$  is made still larger, the dissipation becomes important because  $I_s$  begins to increase. Finally the percentage increase of  $I$  is even less than the percentage increase caused in  $I_s$  by the rise of junction temperature due to dissipation. A further increase of  $I$  causes a reduction of  $M$ .

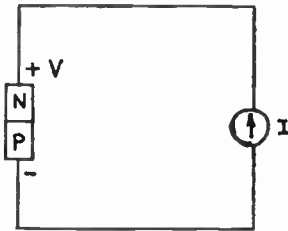


Fig. 1—Equivalent biasing circuit for p-n junction in avalanche operation.

To obtain a quantitative estimate of  $M_{max}$  and  $I_{opt}$ , the following approximations are made:

- 1) All of the current through the junction results from the avalanche multiplication of thermally generated current in the junction. (This precludes surface and other extraneous leakage currents.)
- 2) It is assumed for convenience that  $M_{max}$  will be greater than 10. Thus, for values of  $n \geq 3$ , the reverse voltage will be within a few per cent of  $V_B$ . The power dissipation of the junction is then approximated by  $V_B I$ .
- 3) The junction temperature rise above ambient is  $C$  degrees centigrade per watt dissipation.

The thermally generated current in a junction is

$$I_s = F \exp(-E_G/kT)$$

where  $E_G$  is the energy gap between conduction and valence bands,  $k$  is Boltzmann's constant, and  $T$  is the junction temperature in degrees Kelvin. In reality,  $F$  is a function of temperature, but we shall assume that the temperature variation of  $\exp(-E_G/kT)$  masks that of  $F$  so that in the temperature range of interest,  $F$  may be considered constant.

Denoting the ambient temperature by  $T_a$ , we may write

$$T = T_a + CV_B I$$

and

$$F = I_{ta} \exp(E_G/kT_a)$$

where  $I_{ta}$  is the thermally generated current with the junction temperature equal to the ambient temperature. Thus

$$I_s = I_{ta} \exp \left[ \frac{E_G}{kT_a[(T_a/CV_B I) + 1]} \right]$$

We make the additional approximation that  $(T_a/CV_B I) \gg 1$ . The multiplication factor is then given by

$$M = (I/I_s) = \frac{I}{I_{ta} \exp(E_G CV_B I / kT_a^2)}$$

Setting  $\partial M / \partial I = 0$ , we obtain

$$I_{opt} = (kT_a^2) / (E_G CV_B) \tag{1}$$

and

$$M_{max} = (I_{opt}) / (I_{ta} \exp 1) \tag{2}$$

It should be emphasized that this analysis was based on the assumption that there were no currents other than the avalanche-multiplied, thermally generated current in the junction. If other currents exist which contribute to the dissipation but not to the avalanche process, the value of  $M_{max}$  will be decreased.

DOUGLAS J. HAMILTON  
Applied Research Laboratory  
University of Arizona  
Tucson, Ariz.

The characteristic function of  $f_i(X)$  is  $\phi_i(t)$ , where

$$\phi_i(t) = \frac{1}{A_i} \left[ \frac{1}{jt} - \frac{e^{-j t A_i}}{jt} \right]$$

Here the characteristic function is defined, just as the Fourier transform. The characteristic function of output density function

$$\begin{aligned} \phi(t) &= \frac{1}{A_1 A_2 \cdots A_n} \left[ \frac{1}{jt} - \frac{e^{-j t A_1}}{jt} \right] \\ &\quad \cdot \left[ \frac{1}{jt} - \frac{e^{-j t A_2}}{jt} \right] \cdots \left[ \frac{1}{jt} - \frac{e^{-j t A_n}}{jt} \right] \\ &= \frac{1}{A_1 A_2 \cdots A_n} \frac{1}{(jt)^n} + \cdots \\ &\quad + C_i \frac{1}{(jt)^n} e^{-j t X_i} \cdots \end{aligned}$$

where  $X_i = \sum A_i$ , are taken one, two, three . . . etc., at a time and arranged in increasing order of magnitude.

The characteristic function of cumulative density function is

$$\begin{aligned} \phi(T) &= \frac{1}{A_1 A_2 \cdots A_n} \left[ \frac{1}{(jt)^{n+1}} \right. \\ &\quad \left. + \cdots + C_i \frac{1}{(jt)^{n+1}} e^{-j t X_i} \cdots \right] \end{aligned}$$

The probability of output being between extreme end value and a limiting percentage value  $X_p$  is given by

$$P(X \leq X_p) = \frac{1}{A_1 A_2 \cdots A_n} \frac{1}{(n)!} [(X_p)^n + \cdots + C_i (X_p - X_i)^n + \cdots + C_k (X_p - X_k)^n]$$

where  $X_{k+1} \leq X_p \leq X_k$ .

K. G. ASHAR  
IBM Corp  
Product Dev. Lab  
Poughkeepsie, N. Y

### An Improvement in the Use of "Piecewise Approximations to Reliability and Statistical Design"

When a functional relation  $T = T(X_1; X_2, X_3, \dots, X_n)$  is given,<sup>1</sup> and if one is interested in finding the probability of the output  $T$  at its near extreme value, then instead of expanding the function near central value by Taylor series, more accurate results will be given if the expansion is carried out at the end point. This amounts to calculating  $a_1, a_2, \dots, a_n$  by substituting the values of  $(X_{1e}, X_{2e}, X_{3e}, \dots, X_{ne})$  which give the extreme value of  $T$ , say  $T_e$ .

The value of  $b_i$  should be obtained from

$$b_i = \frac{a_i X_{ie}}{T_e}$$

The percentages which are normally expressed with respect to mean value  $X_{ie}$  should now be modified with respect to  $X_{ie}$ . They will be denoted by  $p_i$ .

In relation

$$\xi = \xi_1 + \xi_2 + \cdots + \xi_n,$$

$\xi_1, \xi_2, \dots, \xi_n$  and  $\xi$  are all distributed from 0 value.

If the variables are uniformly distributed, then the density function of  $\xi_i$  is  $f_i(X)$ , where

$$\begin{aligned} f_i(X) &= 0 & X < 0 \\ f_i(X) &= \frac{1}{A_i} & 0 \leq X \leq A_i \\ A_i &= p_i \times b_i \end{aligned}$$

\* Received by the IRE, November 23, 1959.  
<sup>1</sup> H. J. Gray, Jr., "An application of piecewise approximations to reliability and statistical design," Proc. IRE, vol. 47, pp. 1226-1231; July, 1959.

\* Received by the IRE, April 6, 1960. This work has been carried out under the auspices of the Scientific Department, Ministry of Defense, Israel.

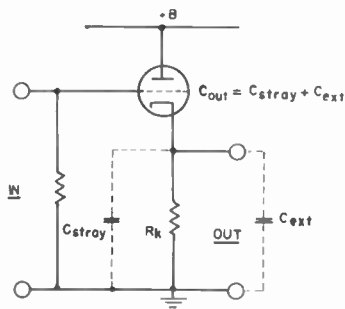


Fig. 1—Conventional cathode follower.

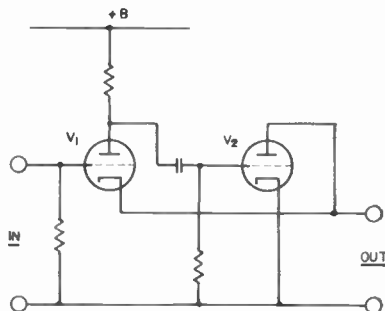


Fig. 2—Simplified White cathode follower.

being approximately  $(1/g_m)C_{out}$ . The discharge of  $C_{out}$  depends solely on the cathode resistor  $R_K$  and is accordingly considerably slower.

The "White Cathode Follower (WCF)" (Fig. 2) provides a well-known solution to this problem.<sup>1</sup> It is essentially a class AB push-pull stage with unity gain, providing  $C_{out}$  with a charging path through  $V_1$  and a discharging path through  $V_2$ . However, the WCF has its drawbacks:

- 1) It requires an additional valve.
- 2) Means have to be provided to prevent  $V_1$  from bottoming when it draws heavily on the HT, at large input pulses.<sup>2</sup>
- 3) Its transfer function exhibits two poles in the complex frequency plane, as compared with the single pole of the conventional cathode follower. Thus, special measures have to be taken to maintain monotonic response if one wishes to include the WCF into the feedback loop of an amplifier.<sup>3</sup>

A simple way of providing  $C_{out}$  with a discharge path and at the same time avoiding the above enumerated drawbacks is described below. Fig. 3 shows the simplified circuit diagram of a 3-valve feedback loop which is being used in the Model 302A linear

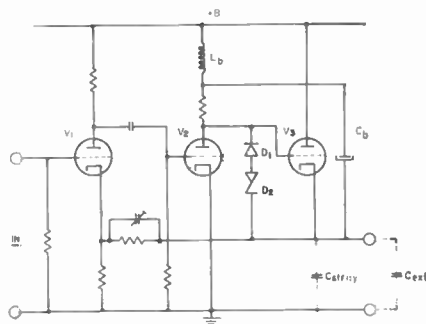


Fig. 3—Three-valve feedback loop.  $L_b$  and  $C_b$  are a bootstrapping arrangement.<sup>2</sup>

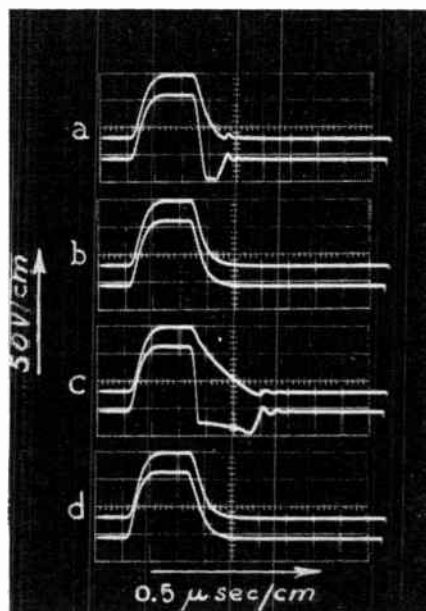


Fig. 4—Wave shapes in amplifier of Fig. 3. Upper traces—output; lower traces—anode of  $V_2$ . (a) and (c) before modification, (b) and (d) after modification.

amplifier.<sup>3</sup> The modification introduced is the addition of a Zener diode ( $D_2$ ) and a high-voltage silicon diode ( $D_1$ ) in series between the plate of  $V_2$  and the cathode of  $V_3$ .

Fig. 4 illustrates the operation of the amplifier under four different conditions, by showing the pulse shapes at the output (upper trace) and at the anode of  $V_2$  (lower trace), for positive input pulses of  $0.2\text{-}\mu\text{sec}$  leading and trailing edges. At rise times of this order of magnitude, the detrimental effect of the output capacitance on the negative edge of the output pulse is already considerable.

The operation prior to modification and without external loading is explained with the aid of Fig. 4(a). The slow discharge of the output capacitance causes  $V_3$  to be driven into cutoff and prevents the waveform at the anode of  $V_2$  from being fed back to the cathode of  $V_1$ , thereby opening the feedback loop. The ensuing high forward gain causes  $V_2$  to draw current heavily and to lower its anode potential sharply, thereby driving  $V_3$  further into cutoff. After  $C_{out}$  discharges suf-

ficiently to allow  $V_3$  to conduct, the feedback loop closes again. However, because of the low  $g_m$  of the valve near cutoff, the output time constant  $[(1/g_m)C_{out}]$  is considerably larger than under normal conditions. The resulting increased phase lag is the cause of the non-monotonic transient observed at the end of the pulse.

The influence of additional external loading is evident from Fig. 4(c). The larger time constant  $C_{out}R_K$  considerably lengthens the discharge time, and hence the cutoff period.

This analysis emphasizes the need to discharge  $C_{out}$  quickly, as well as to maintain the  $g_m$  of  $V_3$  above the minimum value which is required for monotonic response. A review of the operation of the amplifier brings out the point that during the time  $C_{out}$  is to be discharged,  $V_2$  draws a heavy current. Now, introduction of a Zener diode ( $D_2$ ) as indicated in Fig. 3, enables  $C_{out}$  to discharge through  $V_2$  as soon as the Zener diode breaks down because of the inability of the cathode voltage to follow the sharp drop in the grid voltage.

During the breakdown period of the Zener diode, the output capacitance is effectively parallel to the one at the anode of  $V_2$ , so that the number of poles at the feedback loop in the complex frequency plane is decreased by one (their number would be increased by one were a WCF used for improvement of the performance). This fact insures monotony of response during the breakdown period.

A proper choice of the breakdown voltage of the Zener diode will limit the grid cathode voltage of  $V_3$  to such a value that its  $g_m$  will be sufficiently high to maintain monotonic response after the Zener diode recovers from conduction.

Fig. 4, (b) and (d) are the replicas of (a) and (c), respectively, after modification. The negative edges of the pulses are quite similar to the positive ones. The heavy capacitive loading, shown in Fig. 4(d), causes only very slight lengthening of the rise times of both edges.

The power rating of the Zener diode should be adequate to cope with the discharge currents under the highest PRF's expected.

The high-voltage silicon diode ( $D_1$ ) decreases the effective capacitance of the Zener diode and protects the latter from occasional high forward current surges which may be caused by on-off switching or by pulling out  $V_2$  or  $V_3$ .

### CONCLUSION

Pulse amplifiers of the type shown in Fig. 3 may be easily modified to provide a better negative edge response, at the cost of two diodes. In case RC coupling is used, it should first be replaced by direct coupling. For large capacitive loads, it might be advisable to use, for both  $V_2$  and  $V_3$ , a power valve in order to equate the maximum available charging and discharging currents.

I. BAR-DAVID  
Scientific Dept.  
Ministry of Defence  
Israel

<sup>1</sup> Moody, Howell, and Taplin, "The Chalk River pulse amplitude analyzer," *Rev. Sci. Instr.*, vol. 22, pp. 555-558; August, 1951.

<sup>2</sup> E. Fairstain, "Nonblocking double line linear pulse amplifier," *Rev. Sci. Instr.*, vol. 27, pp. 472-482; July, 1956.

<sup>3</sup> A. F. Fischmann-Arbel and I. Bar-David, "A method of linear pulse amplifier design," to be published in *Nuclear Instruments and Methods*.

## A Proposed Technique for $F_2$ -Layer Scatter Propagation\*

The continuing need for reliable radio circuits over great distances is becoming ever more acute. The purpose of this note is to suggest a method that may be useful in providing reliable ionospheric circuits at frequencies above the classical  $F_2$  MUF.

In what follows, the term  $F_2$  MUF will be used to specify the conventionally calculated maximum usable frequency of the  $F_2$  region of the ionosphere. It is equal, numerically, to the critical frequency at vertical incidence multiplied by the secant of the angle between an incident ray and the normal to the ionosphere.<sup>1</sup>

Since the technique to be described attempts to make use of frequencies above the  $F_2$  MUF, it may be considered in one sense a form of " $F_2$ -layer scatter" propagation. Unfortunately, the term "scatter" has been used in recent years to describe a multiplicity of apparently unrelated physical phenomena. For this reason, a brief description is presented below of the scattering mechanism to be considered in this paper.

A physical model, first proposed by M. L. Phillips,<sup>2,3</sup> can be used to represent the reflection, either total or partial, of radio waves by the ionosphere. It is hypothesized that the ionosphere is made up of a vast number of irregularly ionized volumes. Each of these innumerable volumes will have associated with it a value of MUF corresponding to the electron density within the volume. It would be reasonable to assume, then, that the distribution of MUF values would vary in a Gaussian manner about the conventionally calculated MUF, i.e., the value used in the operation of ordinary ionospheric circuits. The true distribution, of course, is somewhat skewed, but since the present discussion deals only with frequencies above the MUF (the modal value of the distribution), the lower percentiles are of little interest. It is practicable, therefore, to consider that the distribution of elemental MUF's follows a true Gaussian distribution. Fig. 1 represents such a distribution.

The conventionally calculated path MUF is represented by the vertical line intersecting the central value of the distribution. The curve represents the distribution of actual elemental MUF's above and below that value. The frequency designated by  $F_1$  represents a typical operating frequency of a high-frequency, point-to-point circuit. Such a frequency is lower than most of the elemental MUF values of the  $F_2$  region. Consequently, most of the ionized volumes will be effective in reflecting the signal back to earth. Frequency  $F_2$ , on the other hand, is higher in frequency than most of the MUF values, and only a small percentage of these are capable of reflecting the incident energy

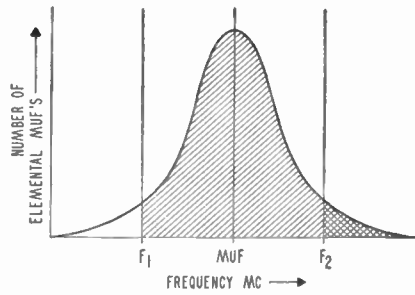


Fig. 1—Assumed distribution of elemental MUF values as a function of frequency.

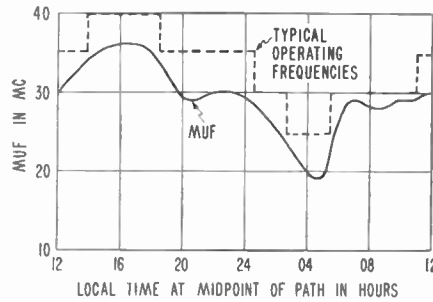


Fig. 2—Typical frequency changes required to employ the  $F_2$ -layer scatter mechanism.

back to earth. It is only necessary, then, to determine the standard deviation  $\sigma$  of the distribution, in order to relate this physical model to  $F_2$ -layer reflection phenomena at frequencies above the  $F_2$  MUF.

A curve has been developed<sup>2</sup> experimentally which relates the scatter loss  $L$  to  $X/\sigma$  where  $X$  represents the number of megacycles by which the operating frequency exceeds the  $F_2$  MUF, and  $\sigma$  (in megacycles) is defined as above. A few corresponding values are given below to illustrate orders of magnitude.

$X/\sigma$	$L$ (decibels)
0	3
1	8
2	17
3	29
4	45
5	66
6	89

The values of  $L$  given above must be added to the path loss that would be encountered if the system were operating at an optimum frequency slightly below the MUF.

Phillips has deduced values of  $\sigma$  from 1 to 2 mc for ionospherically quiet conditions in the eastern part of the United States. Values to perhaps 4 mc pertain to ionospherically-disturbed conditions.

With this information in hand, it occurred to the authors that a practicable radio circuit might be established between two points at frequencies above the conventional  $F_2$  MUF. Because of the diurnal, seasonal, and cyclical variation of the MUF, however, any such technique would require a frequency changing capability in order to prevent the operating frequency from exceeding the MUF by too great a margin. On the other hand, it would also be necessary to change frequencies so that the system would never encroach upon other systems in use below the MUF. The dashed line of Fig. 2 illustrates the way in which the operating frequency might be varied diurnally in

order to make use of the  $F_2$ -layer scatter mechanism.

The system would operate much the same as a conventional below-the-MUF system, except for the operating frequency, which would always exceed the  $F_2$  MUF. In this way, a new group of frequencies would become available for ionospheric propagation without the inherent disadvantages associated with  $D/E$ -layer systems.

An  $F_2$ -layer system, for example, should not be susceptible to interference (or bandwidth limitations) from the motion of ionized meteor trails. It is well known<sup>4</sup> that such trails occur at heights from 80 to 120 km above the earth, heights corresponding roughly to the  $E$  layer. The incidence of ionized meteor trails is negligible at  $F_2$ -layer heights.

Another factor which might affect the bandwidth of an  $F_2$ -layer scatter system is the motion of charges existing within the ionosphere itself. It has been shown<sup>5</sup> that the fast fading rate of an ionospheric signal increases by a factor of 4 or 5 at the transition from "normal layer" to  $F_2$ -layer scatter propagation. This phenomenon might be attributable to a more rapid rate of drift or diffusion of the electrons in the ionosphere. It is known<sup>6</sup> that this velocity is of the order of 2 or 3 msec at the lower HF frequencies. It will be somewhat higher for scatter signals, but it is not likely that the velocity would approach the many thousands of meters per second necessary to produce interference to frequency division multiplex systems.

In the system design of an  $F_2$ -layer scatter circuit, the path should be chosen to have a length near the maximum limit of single-hop propagation. The MUF for such a path is near the highest possible value. This permits the use of frequencies well above the range that is useful for conventional point-to-point circuits at any given time, in any particular part of the world.

It should be pointed out, of course, that the appropriate values of  $\sigma$  may vary considerably with geomagnetic latitude, longitude, time of day, period in the sunspot cycle, etc. Considerable work must be done to determine that suitable values do, in fact, exist for a particular path. In this regard, the prevalence of spread- $F$  conditions in equatorial regions will result in higher values of  $\sigma$  for a large fraction of the time, especially during the period of low early morning MUF's during the low portion of the sunspot cycle. During 1944, for example, the Maui and Christmas Island ionograms recorded severe spread  $F$  to exist over 50 per cent of the time during the hours in question. As a result,  $\sigma$  would have relatively high values when the  $F_2$  MUF is lowest, permitting the use of relatively higher operating frequencies at such times.

W. C. VERGARA  
J. L. LEVATICH  
Advanced Res. Dept.  
Bendix Radio Div.  
The Bendix Corp.  
Towson, Md.

\* Received by the IRE, April 6, 1960.  
1. J. A. Ratcliffe, "The Magneto-Ionic Theory and Its Applications to the Ionosphere," Cambridge University Press, Cambridge, Eng., p. 160; 1959.

2. M. L. Phillips, "F-Layer Radio Transmissions on Frequencies Above the Conventionally Calculated MUF," a portion of "Project Earmuf, Final Report," Signal Corps Contract DA-36-029-SC-72802, pp. 138-162; September, 1958.

3. M. L. Phillips, M.I.T. Lincoln Lab., Lexington, Mass.; report now in preparation.

4. B. Lovell and J. A. Clegg, "Radio Astronomy," John Wiley and Sons, Inc., New York, N. Y., ch. 10; 1952.

5. R. W. E. McNicol, "Fading of radio waves of medium and high frequencies," *Proc. IEE*, vol. 96, pt. III, pp. 517-524; October, 1949.

# Contributors

Kent D. Broadbent was born in Provo, Utah, on June 19, 1926. He received the B.S. degree in physics from Brigham Young University, Provo, in 1949 and the M.S. degree in physics from Case Institute of Technology, Cleveland, Ohio, in 1951.



K. D. BROADBENT

From 1951 to 1954, he was a Research Fellow at the University of Utah, Salt Lake City, engaged in nuclear reactor instrumentation studies. He joined Hughes Aircraft Company, Culver City, Calif., in 1954, to do research on advanced computer components; and at the time of leaving, early in 1960, he was head of the Subsystems, Devices, and Components Section of the Information Processing Research Department at Hughes Research Laboratories. He is currently with American Systems Inc., Inglewood, Calif., where he heads a research effort into thin film devices and advanced information processing subsystems.

Mr. Broadbent is a member of Sigma Xi, Sigma Pi Sigma, and RESA.



H. J. Carlin (M'47-SM'50-F'56) was born in New York, N. Y., on May 1, 1917. He received the B.S. and M.S. degrees in 1938 and 1940, respectively, from Columbia University, New York, N. Y., and the D.E.E. degree in 1947 from Polytechnic Institute of Brooklyn, Brooklyn, N. Y.



H. J. CARLIN

He was with Westinghouse Electric Company from 1940-1945. In the latter part of 1945, he joined the Polytechnic Institute of Brooklyn, where he now holds the position of Research Professor and Associate Director of the Microwave Research Institute. His major work has been in the fields of microwave devices and network theory.

Dr. Carlin is a member of the AAAS, Tau Beta Pi, Sigma Xi, and Eta Kappa Nu.



Thomas J. Rey (SM'56) was born on January 31, 1918 in Berlin, Germany. He was educated at the Collège Français in Berlin, and at the University of London,

England, where he received the B.Sc. degree in engineering in 1938, the B.A. degree in mathematics in 1947, and the M.S. degree in mathematics in 1950.



T. J. REY

He was a Development Engineer at Murphy Radio, and at the United Insulator Company, London, between 1939 and 1941. From 1941 to 1944, he trained Radio Engineers and Officers under the Hankey Scheme at Northampton Polytechnic, London. During the period of 1944 to 1948, he investigated spark discharges at the laboratories of the British Electrical Research Association in Middlesex. As a Senior Engineer at E.M.I. ("His Master's Voice") in Hayes, Middlesex, from 1948 to 1955, he worked on circuits, digital computers, microwave plumbing, and classified projects. He came to this country in October, 1955, and joined Westinghouse Electric Corporation in Baltimore, Md., where he was concerned with methods of frequency control and microwave problems. He has been doing similar work since joining the staff of Lincoln Laboratory, M.I.T., Lexington, Mass., in May, 1957.

Mr. Rey is a Corporate Member of the IEE.



August W. Rihaczek (M'59) was born in Bruenn, Czechoslovakia, on August 25, 1929. In 1953, he received the Diploma in



A. W. RIHACZEK

Electrical Engineering from the Technische Hochschule Muenchen, Germany, and the degree of Doctor of Engineering from the same school in 1957. From 1950 to 1951, he held a scholarship at the University of Rhode Island, Kingston, sponsored by the Institute of International Education. He was scientific assistant at the Institute for High-Frequency Techniques of the Technische Hochschule Muenchen from 1953 to 1958. Among other projects, he was at this time working on the development of a bandwidth conservation system for the transmission of radar displays. In 1958, he accepted a position at the White Sands Missile Range, Las Cruces, N. M., where he was assigned to the improvement and further development of missile trajectory measuring systems and related range instrumentation. Recently he joined the Space

Technology Laboratories, Inc., Los Angeles, Calif.

As a student in Germany, Dr. Rihaczek was a member of the Studienstiftung des deutschen Volkes. He has published articles in German periodicals and handbooks, and has been granted several patents, having others still pending.



Bruno Schneider was born on August 6, 1929, in Zürich, Switzerland. He studied electrical engineering at the Swiss Federal



B. SCHNEIDER

Institute of Technology, Zürich, from 1950 to 1954, and received the M.S. degree in 1954. Since that time, he has been an assistant, and later Research Fellow, in the Department of Advanced Electrical Engineering, Swiss Federal Institute of Technology, and received the D. Techn. Sc. degree in 1959.

Dr. Schneider worked on a variety of transistor circuit problems, and has done research on junction diode and transistor noise. He has published several papers on temperature and other stabilization of transistor circuits, and on semiconductor noise.



Anthony E. Siegman (S'54-M'56) was born in Detroit, Mich., on November 23, 1931. After receiving the B.A. degree from



A. E. SIEGMAN

Harvard University, Cambridge, Mass., in 1952, he joined the Hughes Aircraft Company, Culver City, Calif., from 1952 to 1954. During this period, he also studied at the University of California at Los Angeles, under the Hughes Cooperative Plan, receiving the M.S. degree in applied physics in 1954. He received the Ph.D. degree in electrical engineering from Stanford University, Stanford, Calif., in 1957, and is now assistant professor in that subject at Stanford. He has worked on helix circuits for traveling-wave tubes, noise fluctuations in electron beams, and solid-state masers.

Dr. Siegman is a member of Phi Beta Kappa and Sigma Xi.

John J. Sparkes was born in London, England, on December 4, 1924. He received the B.Sc. degree with honors in physics from Manchester University, England, in 1947.



J. J. SPARKES

During World War II, he was with the Admiralty Signal Establishment, Haslemere, England, and after graduating, was employed for two years in Hospital Physics at St. Mary's and the Middlesex Hospitals, London.

After a period of three years spent in teaching school, he entered British Telecommunications Research Ltd., Taplow, England, and was appointed Head of the Physics Section in 1954. He has been engaged primarily in the study of transistors and related semi-conductor devices and of the properties of copper-clad laminates.

Mr. Sparkes is an associate member of the Institute of Physics.



Max J. O. Strutt (SM'46-F'56) was born on October 2, 1903, in Surakarta, Java. He attended the University of Munich, Germany, and the Institute of Technology at Munich, and received the M.Sc. degree in electrical engineering and the Doctor of Tech.Sc. degree (cum laude) in 1926 and 1927, respectively, from the Institute of Technology at Delft, The Netherlands.



M. J. O. STRUTT

He was a research engineer at the Phillips Company, Ltd., Eindhoven, The Netherlands, from 1927 to 1948. Since 1948, he has been professor and director of the Department of Advanced Electrical Engineering, Swiss Federal Institute of Technology, Zürich, and since 1958, chairman of the Division of Electrical Engineering.

Dr. Strutt holds more than sixty U. S. patents on electron tubes and circuits, especially at VHF and UHF. Among his awards are the Doctor Honoris Causa (1950) conferred by the Institute of Technology, Karlsruhe, Germany, and the Carl Friedrich Gauss Medal (1954) of the Society of Sciences, Brunswick, Germany. In 1955 he was elected an honorary member of that Society. He is a member of the Swiss Society of Electrical Engineers, the German Society of Electrical Engineers, the Swiss Society of Sciences at Berne, the German Physical Society, the Swiss Mathematical Society, and the Zürich Physical Society.



Takuo Sugano (M'59) was born in Tokyo, Japan, on August 25, 1931. He received the B.Eng. degree in electrical engineering in



T. SUGANO

1954 from the University of Tokyo. In 1956 he received the M.Eng. degree, and in 1959 the D.Eng. degree, both in electrical engineering, from the University of Tokyo.

He has been engaged in the research of transistors and other associated semiconductor devices for the past five years. He is now an assistant professor in the electronic engineering department in the University of Tokyo.

Dr. Sugano is a member of the Institute of Electrical Engineers of Japan and of the Institute of Electrical Communication Engineers of Japan.



Wilhelm H. von Aulock (A'54) was born in Pirna, Germany, on January 24, 1915. He received the Dipl.Ing. degree from the Technische Hochschule, Berlin, in 1937 and the Dr.Ing. degree from the Technische Hochschule, Stuttgart, in 1953.

From 1938 to 1942, he worked in Berlin for the AEG Kablewerk; and from 1942 to 1945, he worked for Torpedoversuchsanstalt in Gotenhafen (Gdynia).



W. H. VON AULOCK

In 1947, he accepted an invitation to work for the U. S. Navy, Bureau of Ships in Washington, D. C. where he was involved in work on torpedo countermeasures and studies of electromagnetic fields in sea water. Dr. von Aulock joined the Bell Telephone Laboratories, Whippany, N. J., in 1954. Since then, he has been principally engaged in analytical and experimental studies of ferrite devices for microwave applications and in the development of electronically scanned antennas.



Hisayoshi Yanai (M'57) was born in Okayama, Japan, on May 19, 1920. From 1940 to 1942, he studied electrical engineering at the University of Tokyo, where he received the D.Eng. degree for research on measurements of dielectric properties in dm wave region in 1953.



H. YANAI

After three years of military service, he joined the staff of the electrical engineering department at the University of Tokyo as an instructor in 1945. In 1947, he became an assistant professor, and is now a professor at the University, where he is currently concerned with microwave components and high frequency semiconductor devices. From 1954 to 1955, he studied at the Institute of Technology at Munich, Germany.

Dr. Yanai is a member of the Institute of Electrical Engineers of Japan, the Institute of Electrical Communication Engineers of Japan, and the German Society of Electrical Engineers.

## Books

### Fixed and Variable Capacitors, by G. W. A. Dummer and Harold M. Nordenberg

Published (1960) by McGraw-Hill Book Co., Inc., 330 W. 42 St., N. Y., 36, N. Y. 257 pages+6 index pages+ix pages+22 bibliography pages. Illus. 6½×9½. \$10.00.

This book is an excellent contribution to the literature on capacitors and fills a long-felt need for a generalized handbook on the subject. There has been no general text of this type available in recent years which includes all of the modern structures of importance.

This text is definitely not intended for the more sophisticated capacitor engineer or for the research scientist working in this field. It should be valuable to the components engineer or the apparatus designer faced with a choice of capacitor constructions and needing information on the properties of the various types and on methods of measurement. The measurement section of the book, though highly simplified, is very good. This work should be particularly valuable to the newer generation of electronics engineers who have had little or no exposure to capacitors.

The general excellence of the work must relegate criticism to the area of detailed faultfinding, yet this reviewer must make certain criticisms, if only to suggest constructive improvement for future editions.

In view of the excellent technical treatment of the many capacitor types covered, it was unnecessary for the authors to base their descriptive text on military specification items. This will lead to unnecessary dating of the material, which is sufficiently general to endure beyond the content of military specifications.

On pages 32 and 97, the treatment of metalized paper capacitors gives the impression that it is satisfactory to tolerate sparking of metalized paper capacitors during operation within rated voltage, or that the so-called "self healing" property may be relied on as a safety factor. This is a fallacy which leads to unreliability.

It should be pointed out on page 35 that the degradation rate of molded mica capacitors in high humidity is a function of the molding material and processing of the casing.

The statement is made on page 40 that Mylar capacitors must be hermetically sealed due to moisture sensitivity of Mylar. This statement needs modification as there are many satisfactory constructions which are not hermetically sealed.

On pages 46 and 47, the solid tantalum capacitor exposition leaves something to be desired, but it is recognized that the book was written while this construction was in a highly evolutionary state. Wider temperature ranges than are given in the book are available. Capacitors of this type should still be completely sealed to protect them against moisture.

The statement is made on page 95 that the maximum ac voltage per section of capacitors applied to ac should not exceed 350 volts. This is not correct. Good standard

engineering practice on ac section design, based on currently available dielectrics, is 800 volts per section.

On page 96, the discussion of the behavior of paper dielectric capacitors at radio frequencies makes no distinction between the extended foil construction and the tab construction, and makes no mention of the special duct and "ThruPass" designs which have been developed for RF use.

On pages 159 and 160, the discussion on the etching method used on aluminum foil includes only the acid etch and makes no mention of the more modern electrochemical etch technique.

While it is by no means complete, the book contains a most excellent bibliography of the more recent and significant literature in the electronic capacitor field published since 1924. There is a good index. The book is a valuable addition to the working literature of the electronics engineer.

It is hoped the above small corrections will be made by the authors in future editions.

LEON PODOLSKY  
Sprague Electric Co.  
North Adams, Mass.

### Infrared Radiation, by Henry L. Hackforth

Published (1960) by McGraw-Hill Book Co., Inc., 330 W. 42 St., N. Y., 36, N. Y. 285 pages+10 index pages+xii pages+bibliography by chapter+3 appendix pages. Illus. 6½×9½. \$10.00.

This book is the first of what we can confidently expect to be a rapidly increasing number of texts in the field of Infrared Radiation techniques. The large number of workers in the field and the expanding interest in the military, industrial, and scientific applications justify this literary attention.

However, since this present text is the first to appear in the United States (England, Germany, and the Soviet Union have already published monographs in the field, by Smith, Jones, and Chasmar; Brugel; and Margolin, respectively) it will have to serve either as a target for criticism or else win common acceptance. I rather think that it will be mainly the latter, since the style and organization of the material is such that Hackforth's "Infrared Radiation" can be a highly useful reference for introducing technical workers to recent advances and the scientific literature in IR.

Attention is given to the major divisions of the field; namely, Radiation Sources, Atmospheric Transmission, Optical Components and Systems, Infrared Detectors, and System Design Considerations. In addition, Part II is concerned with the applications of infrared to instruments for measurement, as a tool for Physics, Chemistry, Biology, and Astronomy, and in Industry and Space Technology.

The book does not purport to be a definitive work in any of these areas, since the design is more in the direction of collating

information from other less readily available references in the periodical literature (including numerous references to the *Classified Journal of IRIS*!), than in developing any of the material from more basic principles. Of necessity, much is "lost in translation" from these more specialized and extensive references, and it is hoped that the reader will, wherever possible, be led to a study of these other works to check the facts, see the context and broaden his knowledge.

In summary, "Infrared Radiation" must be considered only an introduction. However, in providing this, Mr. Hackforth has performed a very useful service because heretofore no real starting point in IR was available in the unclassified literature.

For those desiring a more detailed coverage of the more technical aspects of this field, members of the IRE are reminded of the special issue on Infrared of the PROCEEDINGS (vol. 47, September, 1959).

SIDNEY PASSMAN  
The RAND Corp.  
Santa Monica, Calif.

### Advanced Engineering Mathematics, 2nd Ed., by G. R. Wylie, Jr.

Published (1960) by McGraw-Hill Book Co., Inc., 330 W. 42 St., N. Y., 36, N. Y. 658 pages+10 index pages+28 answer pages+xi pages. Illus. 6½×9½. \$9.00.

For this second edition, the author has completely rewritten and rearranged his text. Several new chapters have been added, as well as additional advanced subject matter, while some of the earlier material has been displaced in favor of material of greater general interest. The resulting changes have added some 50 pages to the size of the book.

The book is divided into fifteen chapters as follows: Determinants and matrices, three chapters on ordinary differential equations, finite differences, applications to mechanical and electrical circuits, Fourier series and integrals, the Laplace transformation, partial differential equations, Bessel functions and Legendre polynomials, vector analysis, and four chapters (over 120 pages) on functions of a complex variable.

The author writes in an especially clear style, and carries out the derivations in considerable detail, so that the reader rarely will need to ponder over intervening steps. This style makes the book very easy to use, although the increased space required necessarily means that a wider coverage of subject matter is sacrificed. The author makes liberal use of examples and exercises to illustrate and clarify the presentation. There are over 1000 exercises, the answers to the odd-numbered ones being given at the end of the book.

Professor Wylie's book should appeal especially to those desiring a textbook for self-study.

MARTIN KATZIN  
Electromagnetic Research Corp.  
Washington, D.C.

### Introduction to Modern Network Synthesis, by M. E. Van Valkenburg

Published (1960) by John Wiley and Sons, Inc., 400 Fourth Ave., New York 16, N. Y. 490 pages+5 index pages+xii pages+2 bibliography pages. Illus. 6×9½. \$11.75.

Professor Van Valkenburg's book is a welcome addition to the literature of network synthesis. It is intended to serve as a textbook for a senior undergraduate or a first-year graduate course, and the selection of topics covered in the book has been governed by what the author feels a student should know about synthesis if he has had only a single course in this area. The author's judgment is excellent.

The prerequisites for use of the book and the contents are clearly summarized in the preface:

"The reader of this book should have the usual undergraduate knowledge of network analysis and the Laplace transformation. Some of this assumed background is reviewed in the first two chapters. Other material of these chapters, network function definitions and frequency and magnitude scaling, for example, may be new to the reader and in this case should be mastered for later use.

The order in which the remaining topics appear is that found most successful in several experiments in teaching the subject from preliminary notes. Positive real functions are the foundation of network synthesis and are studied first. Elementary synthesis procedures are covered for the LC, RC and RL, and RLC cases. The related topics of approximation and the relationship of the parts of network functions help complete a study of one terminal-pair network synthesis by Chapter 9. It should be noted that the approximation methods of Chapter 9 are suited for 'rough' approximation as in automatic control applications. Precision approximation procedures, often identified with telephone industry applications, are postponed until Chapter 13.

Chapter 10 introduces the subject of two terminal-pair synthesis with the Cauer ladder development. This chapter and the four that follow describe the major modern methods of two terminal-pair synthesis and also enumerate the important properties of the network functions that describe these networks. The last chapter of the book covers synthesis from image parameters. Although this topic is often excluded from 'modern' methods, I strongly recommend that it be studied and understood in relationship to the other competitive methods of Chapters 14 and 15."

There are the inevitable errors and omissions. For example, the footnote on page 65 is in error, and in his discussion of the Bott and Duffin method of synthesis on page 175, the author omits a proof that a real and positive  $k$  which allows the synthesis to proceed does indeed exist. However, these are minor points, and they do not detract seriously from the worth of the book as a whole.

For a course in which the students have had an introduction to the theory of functions of a complex variable, it might be desirable to supplement the book with additional material from function theory. For example, the students in such a course would profit from a proof of Richards' theorem.

The presentation is concise and clear, and the book is self-contained. These facts, combined with the numerous problems and references for more advanced and detailed studies at the end of each chapter, make this book exceptionally well-suited to serve the purpose for which it was intended.

THOMAS R. WILLIAMS  
Princeton Univ.  
Princeton, N. J.

### Introduction to Operations Research, by C. West Churchman, Russell L. Ackoff, and E. Leonard Arnoff.

Published (1957) by John Wiley and Sons, Inc., 440 Fourth Ave., N. Y. 16, N. Y. 635 pages+9 index pages+x pages+bibliography by chapter. Illus. 9½×5½. \$12.00.

"Introduction to Operations Research," as the title indicates, is an introduction to a growing field of scientific research. The book was developed from lecture material at the Case Institute of Technology, Cleveland, Ohio. It provides the prospective consumer of Operations Research a basis for evaluating the field and for understanding its potentials and how Operations Research is accomplished. The book presents an excellent survey of the field. It provides a good background for launching into advanced methods and techniques of Operations Research. The technical information is presented simply and without distortion and gives a general coverage of many methods useful in Operations Research. Methods and Models are clearly illustrated by case examples to point up important implications.

C. L. ENGLEMAN  
Engleman & Co., Inc.  
Washington, D. C.

### Electron Tube Life Factors, Craig Walsh and T. C. Tsao, Eds.

Published (1960) by Engineering Publishers, Elizabeth, N. J. 172 pages+1 appendix page+ix pages. Illus. 8¼×11¼. \$9.50.

The authors and editors present a series of charts and tables containing valuable information on the behavior characteristics of electron tubes, derived from six million electrical measurements made on 35,000 tubes tested under multiple-level stress conditions, over 5000 hours of life-test. Effects of the different levels of environmental stress are portrayed in tabular and chart form for easy interpretation and applications by design engineers. Chapter 5 demonstrates the utility of the data for solving circuit design problems where *reliability* is an important parameter of the system. If the designer knows the requirement for electrical stability in his circuit, understands the deleterious effects of detrimental properties on circuit performance, and has determined the permissible failure rate for his circuit consistent with the reliability requirement imposed on the design, he can make direct use of this excellent source of data to adjust circuit conditions and application stresses to yield a reliable design.

The data were derived from life-test experience with miniature tubes, (JAN Types 5654, 6005, 5726, 5670, 6j6W, 5814A,

6AG7, 6AN5, 7AK7, 12AT7, 5687, and 5963) many of which should no longer be considered acceptable in the design of new equipment. However, the general similarity in behavior characteristics as a function of environmental stress, among tube-types within specific classes (miniature and sub-miniature, alike) does permit at least a qualitative extrapolation to design problems involving subminiature types, pending breadboard verification of design reliability—which the designer must do in any event.

To those of us who have spent the better part of the past ten years attempting to develop application notes and design "guide lines" for designers of military electronic equipment, this book represents a masterpiece of test-design, data analysis, and editorial digestion! It is of course regrettable that such an informative treatise of electron tube "Life Factors" could not have been made available to designers years ago, through a MIL Specification requirement for multiple-level life tests, by which to have generated the necessary data automatically. Nevertheless, electron tubes are still being designed into many of our future systems, where the need for design guidance is just as evident today as it was ten years ago. The book is therefore still "timely," and an important contribution to the designer's kit of reliability tools.

The book serves another purpose of perhaps even more long-range importance; it very dramatically proves that the life-behavior of electronic parts *can be* and *should be* quantitatively described in terms readily applicable to design problems having a quantitative reliability requirement to fulfill. It sets a standard, both in analysis and presentation of engineering data, for the guidance of future (and sorely needed) work on transistors, special purpose and microwave tubes, and other parts in general.

G. T. BIRD  
ARINC Res. Corp.  
Washington, D. C.

### Photoconductivity of Solids, by Richard H. Bube

Published (1960) by John Wiley and Sons, Inc., 440 Fourth Ave., N. Y. 16, N. Y. 433 pages+5 index pages+xix pages+21 bibliography pages. Illus. 6×9½. \$14.75.

The purpose of this book, in the author's words, is "to present a unified picture and interpretation of photoconductivity phenomena, drawing examples from many different kinds of materials, and to show the correlation between photoconductivity and other related photophenomena in insulators and semiconductors."

The book begins with an historical survey and an introduction to electron processes in crystals. The basic concepts and parameters of photoconductivity are then discussed, followed by chapters devoted to preparation of photoconductors, and electrode effects. The important subject of impurity photoconductivity is then discussed, and is followed by four chapters devoted to specific processes important to photoconductivity. These include excitation transitions, free carrier mobility, trapping, and recombination. The next-to-last chapter deals

with theoretical viewpoints on photoconductivity, and the last covers related topics, such as the photovoltaic effect, photoelectromagnetic effect, organic photoconductors, photodielectric effect, and others. There is an appendix which presents a short survey of uses of photoconductors.

The subject matter is chosen to be of use to graduate students and research workers in allied fields, and also to provide more detailed treatments for more advanced readers.

One feature which distinguishes this book and makes it a valuable contribution is the fact that it is the first extensive treatment of the complex subject of photoconductivity. It is further distinguished by the manner of presentation. The relationships between photoconductivity and luminescence are emphasized throughout, and the chapters devoted to excitation mechanisms, carrier mobility, trapping, and recombination demonstrate the usefulness of photoconductivity as a tool for the study of the electronic properties of solids.

The reader who is interested in applications of photoconductors might wish to find in this book more detailed discussion of the performance of practical photoconductor systems, such as plastic embedded CdS powder, or chemically deposited PbS layers. Such information might have been located in the Appendix as a part of an expanded

survey of photoconductor uses.

This book is highly recommended to all those who have been awaiting a comprehensive treatment of photoconductivity, both as an important phenomenon in its own right, and as an adjunct to other solid state phenomena.

M. S. WASSERMAN

General Telephone & Electronics Labs., Inc.  
Bayside, N. Y.

#### **A Primer of Programming for Digital Computers, by Marshall H. Wrubel**

Published (1959) by McGraw-Hill Book Co., Inc., 330 W. 42 St., N. Y. 36, N. Y. 217 pages+6 index pages+xv pages+5 glossary pages. Illus. 6 X 9. \$7.50.

As a "primer" for scientific and engineering types of problems to be solved by a computer, this book assumes the reader knows little or nothing about programming. The author, using the IBM 650 (basic configuration) instruction codes, leads the reader from the simplest of problems through various programming techniques, to the use of assembly routines.

Part I of the book introduces the reader to the computer and covers what the author calls "Elementary Programming." First are shown some simple sample problems which can be handled by straightforward coding.

Following these are the looping and branching techniques of solving more complex mathematical situations. At this point, the basic ideas of coding have been established, and the author proceeds into the methods of depicting a problem symbolically in the form of flow diagrams. Storage of previously written programs and subroutines in a permanent library is discussed.

Since practically all programs as first written have errors (bugs) in them, testing and debugging methods are fully explained. Automatic programming, which minimizes the number of bugs, provides a relatively easy way for a beginner to build a program. The fairly long treatment of this subject should be of great assistance to the reader.

Part II of the book is entitled "Advanced Programming." An introductory section provides information about the internal hardware operation of the computer, and some of the peculiarities arising when using it. Following this introduction, the remainder of the book is a detailed explanation of the use of SOAP, an assembly system for the IBM 650.

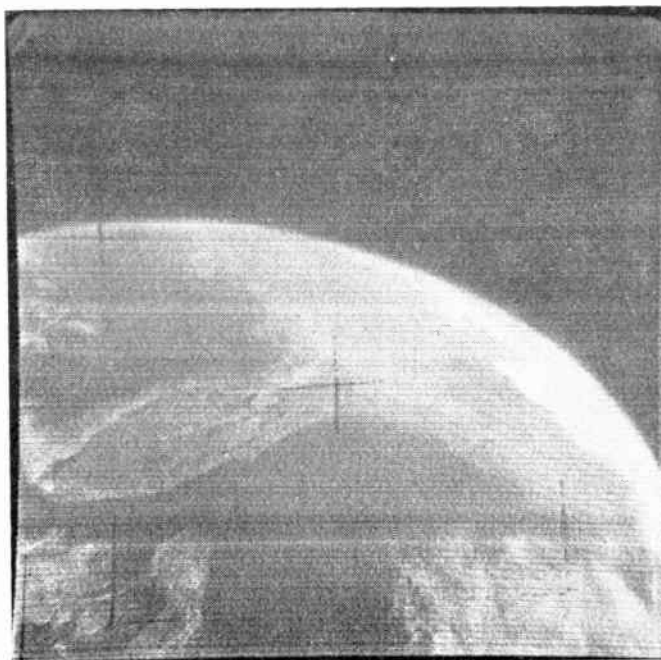
For the scientist or engineer who desires to use a computer as a research tool, this book will give a good insight into the solution of his problems.

MALCOLM D. SMITH  
Remington Rand Univac  
Div. of Sperry Rand Corp.  
Philadelphia 29, Pa.

## Scanning the Transactions

**The U. S. Army in space.** The unusual picture at right was taken last April by the TIROS I meteorological satellite from an altitude of about 450 miles. It shows the entire Florida peninsula, the extending coastline up to the Carolinas on the right, and a major portion of the Gulf of Mexico on the upper left. It is one of many interesting features contained in a special issue of the IRE TRANSACTIONS ON MILITARY ELECTRONICS devoted to the U. S. Army role in space, complementing two earlier issues concerning the U. S. Air Force and Navy space programs. When one considers the modest beginnings of the Army's space activities in 1946—assembling captured components of V-2's in the hangars of White Sands Proving Ground—one cannot help but be impressed by the fact it now requires 49 papers and over 300 pages to describe current Army space activities. The issue, which ranges over the Juno projects, communication satellites, satellite and space probe tracking, and other space activities, is a tribute to the progress that has been made in a little over a decade. (U. S. Army Space Issue, IRE TRANS. ON MILITARY ELECTRONICS, April-July, 1960.)

**A new tricolor camera tube** is under development which for some applications may make unnecessary the three separate tubes found in most present-day color TV cameras. The new tube features a multiple-electrode target structure having three interlocking groups of color-sensitive strips con-



nected to separate output terminals for each primary color. In this way only a single compact tube is required, instead of the usual three, to obtain three color signals. The performance of laboratory models constructed to date, although not equal to broadcast quality, indicates that the tube is potentially useful for industrial and scientific purposes where sufficient light is available and structural defects do not obscure the information desired. (P. K. Weimer, *et al.*, "A developmental tricolor vidicon having a multiple-electrode target," IRE TRANS. ON ELECTRON DEVICES, July, 1960.)

The rapid application of basic discoveries is one of the most significant characteristics of the present era and has contributed greatly to the acceleration of technical developments. Indeed, we have now reached the point where the elapsed time from an initial discovery to a commercial product has essentially disappeared. This is strikingly illustrated by selecting a few significant developments and examining the number of years of applied research and engineering between the basic discovery and a commercial product.

Photography	(1729-1839)	112 years
Telephone	(1820-1876)	56 years
Radio	(1867-1902)	35 years
Radar	(1925-1940)	15 years
Television	(1922-1934)	12 years
Atomic Bomb	(1939-1945)	6 years
Transistors	(1948-1953)	5 years
Solid State Masers	(1956-1958)	2 years

(M. R. Donaldson, "On the sponsorship of tutorial work by the Professional Group," IRE TRANS. ON COMMUNICATIONS SYSTEMS, June, 1960.)

A class of superconducting devices has been suggested by the results of studies of the contact formed by two crossed

superconducting wires. Investigations have shown that the contact itself is superconducting. This makes possible a form of device in which the critical current flows through the contact and is modulated by a current flowing along one or both of the crossed superconductors. Moreover, the area of contact can be made microscopically small so that the transitions between normal and superconducting states may be actuated at high speed and by very small currents. A superconducting contact of this sort offers a variety of possibilities as a switch or modulator. For instance, it might be used to switch between two values of reactances and thus prove useful in phase-locked oscillators or in parametric amplifiers. (J. I. Pankove, "Superconducting contacts," IRE TRANS. ON ELECTRON DEVICES, July, 1960.)

A recent development in bandwidth utilization techniques has extended the usable portion of the available bandwidth from one-half to as much as nine-tenths the carrier frequency. In narrow band transmission of television or radar over telephone lines, it is necessary to use a carrier system to avoid phase distortion normally present at the lower end of the transmission band. Using ordinary modulation and demodulation techniques, the usable video bandwidth is limited to one-half the carrier frequency. In the limiting case in which the carrier is placed at the extreme upper end of the band, this is one-half the total available bandwidth. A new modulation-demodulation system has been developed which is basically amplitude modulation but which is not subject to the normal two-to-one limitation. Using this system, it is possible to use a video frequency of as much as nine-tenths that of the carrier. For example, one may use a video frequency of 3.2 kc on a 3.5 kc carrier. (A. G. Gatfield, "Maximum Bandwidth Utilization Demodulator," IRE TRANS. ON COMMUNICATIONS SYSTEMS, June, 1960.)

## Abstracts of IRE Transactions

The following issues of TRANSACTIONS have recently been published, and are now available from the Institute of Radio Engineers, Inc., 1 East 79th Street, New York 21, N.Y. at the following prices. The contents of each issue and, where available, abstracts of technical papers are given below.

Sponsoring Group	Publication	Group Members	IRE Members	Non Members*
Aeronautical and Navigational Electronics Communications Systems	ANE-7, No. 2	\$1.35	\$2.05	\$4.05
Electron Devices	CS-8, No. 2	1.65	2.50	4.95
Electronic Computers	ED-7, No. 3	1.55	2.35	4.65
Engineering Writing and Speech	EC-9, No. 2	1.80	2.70	5.40
Medical Electronics	EWS-3, No. 2	1.50	2.55	4.50
Microwave Theory and Techniques	ME-7, No. 3	2.65	3.95	7.95
Military Electronics	MTT-8, No. 4	1.65	2.45	4.95
	MIL-4, Nos. 2-3	5.75	8.60	17.25

\* Libraries and colleges may purchase copies at IRE Member rates.

### Aeronautical and Navigational Electronics

VOL. ANE-7, NO. 2, JUNE, 1960

The Editor Reports (p. 26)

1960 Pioneer Awards (p. 27)

Prizes for Progress—R. I. Colin (p. 31)

A Flush-Mounted Runway Antenna for Use with the FAA Directional Glide-Path System—J. R. Baechle and R. H. McFarland (p. 32)

A flush-mounted airport runway antenna has been designed, built, and tested which will allow glide-path signals for instrument landings to be radiated directly from the touchdown point on the runway. Empirical and simplified analytical design procedures are discussed together with a comparison of desirable and measured antenna characteristics. Sufficient low-elevation angle directivity has been obtained from a prototype antenna to provide a path which extends well beyond 5 miles, the approximate distance at which the glide is intercepted in practice.

**Radio Collision-Avoidance Systems for Aircraft**—R. T. Fitzgerald, H. C. Brown, and M. D. Reed (p. 40)

Several cooperative radio systems for avoiding aircraft collisions are considered from the standpoints of technical requirements, feasibility, and cost. The system with the broadest potential application is selected. In basic form, the selected system utilizes the upper UHF region to communicate altitude and heading information, and vertical maneuvers are defined by the altitude information. In expanded form this system determines relative bearing and heading, to predict collision hazard in both the vertical and horizontal planes. Potentially, a reduction in unintentional collisions of 100:1 can be achieved with the selected approach. The applicability of this system to collision avoidance problems of military, commercial, and private aircraft, and to related problems of navigation and air traffic control is outlined.

**Multiple Pulse and Phase Code Modulation in the Loran-C System**—Robert L. Frank (p. 55)

Transmission of a group of closely spaced pulses increases the duty cycle and consequently the range of the Loran-C (formerly called Cytac) 100-kc pulsed hyperbolic radio navigation system while retaining the advantages of time sharing. Phase coding by carrier phase reversal, coupled with synchronous detection, facilitates automatic master and slave identification and search, and prevents multihop skywave interference. Instrumentation for simple and complex pulse patterns is considered. The phase codes used are characterized by lack of spurious responses associated with other bipolar codes.

Abstracts (p. 62)

PGANE News (p. 63)

Contributors (p. 65)

Suggestions to Authors (p. 66)

Roster of PGANE Members (p. 67)

## Communications Systems

VOL. CS-8, JUNE, 1960, No. 2

Frontispiece and Editorial (p. 79)

**Recording Type Direction Finder**—K. Miya and S. Matsushita (p. 81)

**Maximum Bandwidth Utilization Demodulator**—Allen G. Gatfield (p. 83)

In narrow band transmission of television or radar over telephone lines it is necessary to use a carrier system to avoid phase distortion normally present at the lower end of the transmission band. Using ordinary modulation and demodulation techniques, the usable video bandwidth is limited to one-half the carrier frequency. In the limiting case in which the carrier is placed at the extreme upper end of the band, this is one-half the total available bandwidth. A new modulation-demodulation system has been developed which is basically amplitude modulation but which is not subject to the normal two-to-one limitation. Using this system, it is possible to use a video frequency of as much as nine-tenths that of the carrier. For example, one may use a video frequency of 3.2 kc on a 3.5-kc carrier.

**Coded Binary Decision-Feedback Communication Systems**—J. J. Metzner and K. C. Morgan (p. 101)

The problem of nonconservation of message length in a decision-feedback system arises as a result of noise in the feedback channel. A system is considered which avoids this by requiring all corrections to be transmitted during specified intervals. The decision mechanism of the receiver is based on the structure of a modified Slepian code, and several final decision schemes are analyzed and compared. Comparisons are also made with unidirectional systems and ideal decision-feedback systems, and it is found that much of the theoretical advantage of a decision-feedback system over a unidirectional system is retained.

**Air-to-Ground Meteoric Scatter Communication System**—A. J. Hannum, G. L. Evans, J. T. Chambers, and K. Otten (p. 113)

Several point-to-point systems have demonstrated successful communications while employing propagation via meteor trail reflections at very high frequencies. However, few systems have been able to control the output error rate in the presence of sporadic *E* and auroral phenomenon. Nevertheless, early results clearly indicated the strong potential of the meteor mode for extremely reliable communications over ranges (1300 miles) far in excess of existing military airborne UHF equipment.

A test system is described which has been developed at Hughes Aircraft Company, Culver City, Calif., under Air Force contract AF33(616)5674. This system has been designed specifically to operate at fixed frequency (50 mc) through rapidly changing propagation conditions by whatever path exists. Thus, sporadic *E*, or other scatter modes, as well as meteoric scatter are effectively utilized to transmit high quantities of data. Test results described in the paper, however, rule out all modes other than the meteor mode in order to determine minimum performance characteristics.

The system employs high speed, automatic control circuits to govern duplex transmission on a single frequency. The fixed length message block is coded for single error correction and even error detection on each of 11 blockettes. Messages containing uncorrectable errors are automatically repeated until successful. The code was sufficient to guarantee an output error rate of less than 0.6 per cent under all conditions encountered on an initial point-to-point test. The results of this test have indicated that the air/ground application will be a successful one in spite of the limitations imposed by the aircraft environment.

Extension of basic system concepts in combination with further improvements predict a performance capability well in excess of the present successful results.

**Measured Performance of the Sebit-25 Data System Over Wire Line Facilities at 2500 Bits per Second**—James L. Hollis (p. 134)

This paper discusses the actual performance of a 2500 bit per second data modem under simulated conditions in the laboratory and actual conditions on 27 different voice frequency wire lines.

Under simulated conditions, it was determined that an error rate of one in  $10^6$  can be maintained with a signal-to-white noise of 14.5 db. On actual line tests for over 200 hours, the error rate was approximately two hits per hour.

The paper includes seven curves illustrating measured results.

Contributors (p. 138)

## Electron Devices

VOL. 7, JULY, 1960, No. 3

**Prediction of Optimum Performance of Vacuum-Diode Configuration of Thermionic Engines**—G. N. Hatsopoulos, J. Kaye, and E. Langberg (p. 117)

A basic analysis is given of the close-spaced vacuum diode operating as a direct converter of heat to electricity. This analysis is arranged to yield the characteristics of this engine when operating at maximum efficiency. Values of the various parameters are chosen to produce conservative design charts. For a fixed collector temperature and fixed collector work function, two representation design charts are given. These charts permit the designer to estimate very rapidly the optimum performance characteristics, such as efficiency, power to load, current, voltage, conductance of load, etc., as a function of emitter temperature, over a range from 1200° to 1700°K.

**Behavior of Traveling-Wave Tubes Near Circuit Cutoff**—Daniel G. Dow (p. 123)

A theory is developed which explains the operation of a traveling-wave tube when operated near the cutoff frequency of the slow-wave circuit, including the effect of two circuit waves instead of the usual one. The theory is normalized in a manner analogous to that used in more conventional analyses and a first-order expansion about the cutoff frequency is used, making a relatively small number of curves applicable to a large number of cases. The relationship between this theory and the three-wave theory usually used in traveling-wave-tube analysis is shown, and they are in agreement when the system is operated far from the cutoff frequency. Numerical results are given for a range of parameters which might be useful in traveling-wave-tube design, and an excellent agreement with published experimental results is shown.

**Design Consideration for a Germanium P-N-P-N Switching Device with Three Contacts and a "Sandwich" Structure**—George Wertwijn (p. 132)

The current  $I_{off}$  through a germanium *p-n-p-n* switch in the OFF state is described as a simple function of the control current  $I_c$  in its third contact. The device is of a so-called "sandwich" structure, the third contact being the outer edge of the middle *p* layer. The voltages considered are sufficiently small so that avalanche multiplication can be neglected.

It is derived that:

$$I_{off} = \frac{1}{2} \left\{ (a + I_c) - \sqrt{(a + I_c)^2 - 4(b - cI_c)} \right\};$$

*a*, *b* and *c* are device parameters determined by the physical and geometrical structure. The conditions for switching into the ON state are given and the temperature dependence of the parameters is predicted. The experimental results are found to be in good agreement with the design theory.

**Superconducting Contacts**—Jacques I. Pankove (p. 137)

The microscopic size of the contact between two crossed superconducting wires offers a practical way to make a class of superconducting devices which are operated at high speed by very small currents. The critical current through the contact can be modulated by a current flowing along one or both of the crossed superconductors.

Several device possibilities are presented.

**New Helix-Support Method for Traveling-Wave Tubes**—D. J. Blattner and F. E. Vaccaro (p. 142)

Traveling-wave tube helices can be supported at every turn by shrinking a nonprecision glass envelope directly on to the wires. Contact of glass and wire can occur continuously or at discrete flutes. The glass-shrinking procedure and the equipment used are described in detail.

**High Current Grid-Controlled Electron Multiplier Tube**—G. L. Stambach, W. J. Graham, and T. E. Hanley (p. 143)

A grid-controlled secondary-emission electron multiplier amplifier tube has been designed and built which can deliver an output pulse of five amperes into a load impedance of 100 ohms, with a rise time of less than 10  $\mu$ sec and a transit time of less than 20  $\mu$ sec. The measured transconductance of the tube is 600,000  $\mu$ mbos, and it can provide a positive output pulse with a positive grid input.

The tube is constructed as a series of concentric cylinders, with the grid and cathode structure of a 6AG7 pentode serving as a controlled emitter source. Outside the last grid, a series of four louvered, concentric dynodes are placed, with the first dynode serving as the missing pentode plate. Outside the last dynode are a screen-mesh collector and a fifth dynode. From the fifth dynode, a solid cylinder, the output pulse is taken. The concentric geometry has several advantages. Space-charge dif-

facilities are decreased because the current gain at each dynode may be kept at a high level without increasing the current density in proportion. Furthermore, the geometry is suited to a coaxial input and output for obtaining optimum rise-time characteristics.

**A Developmental Tricolor Vidicon Having a Multiple-Electrode Target**—P. K. Weimer, S. Gray, C. W. Beadle, H. Borkan, S. A. Ochs, and H. C. Thompson (p. 147)

Color television cameras which are now widely used require three separate camera tubes to supply the simultaneous primary color information transmitted by the compatible system. This paper describes a developmental tricolor camera tube of the vidicon type for use in a single-tube color camera. The ability to generate the three simultaneous signals is achieved in the tricolor vidicon by means of a multiple-electrode target structure having three interlocking groups of color-sensitive strips connected to separate output terminals for each primary color. A single low-velocity electron beam scans the photoconductive target. No special requirements are made on the beam with respect to focus or scanning accuracy. Registry of the three signals is inherent in the design of the target.

The performance of the developmental cameras which have been constructed to date does not equal the three-tube image orthicon camera from the standpoint of sensitivity, color fidelity and uniformity. In its present state, the tube is potentially useful for industrial and scientific purposes where sufficient light is available and structural defects do not obscure the information desired. To extend its range of application, the development of more sensitive photoconductors and improved methods of fabrication are required.

**Some Calculations on the Large Signal Energy Exchange Mechanisms in Linear Beam Tubes**—S. E. Webber (p. 154)

The large signal energy exchange process both with and without space charge are studied by extending techniques used to compute multiple-cavity klystron bunching. The mechanics of this interaction at a klystron gap and in a traveling-wave type of system are examined in detail and the effects of space charge and of velocity spreading on efficiency are discussed.

**A Small-Signal Field Theory Analysis of Crossed-Field Amplifiers Applicable to Thick Beams**—Bernard Hershenov (p. 163)

Various authors have presented analyses of crossed-field amplifiers. Generally, these analyses have dealt with very thin electron beams in the presence of crossed-fields or with beams in which the bulk or charge density within the beam has been neglected. It is the purpose of this paper to develop a field-theory analysis which is applicable to both thick or thin beams and which includes the effect of space charge. In place of the usual approximate match at the input boundary plane, a rigorous variational technique is presented, which considers the effect of the cutoff waves on the amplitudes of the propagating waves. This enables one to solve the input boundary problem for the first time insofar as the amplitudes of the propagating waves are concerned, without determining the individual amplitudes of the cutoff waves implicitly. As opposed to the usual approximate match, which is only valid for a thin, unmodulated entering electron stream, this variational method is valid for both thick and thin beams, as well as unmodulated or modulated beams entering a crossed-field slow-wave interaction region or entering a crossed-field drift region.

The paper presents propagation constants obtained for thick beams based on the author's model. The variational procedure, which is a valid technique for other models as well as other types of beam devices, has been applied to one numerical case involving a thin beam and the results are compared with the results of

the usual approximate match. A modification of the complex amplitudes of the excited waves, even in the case of thin beams, is noted.

**Noise Reduction in Electron Beams**—A. Zacharias and L. D. Smullin (p. 172)

Direct measurements were made of the electron-beam noise parameters using a modified Currie-type gun. The noise parameters were measured as a function of the electric field in the vicinity of the cathode. The  $S$  parameter was found to be strongly influenced by this field in the Currie-type gun, but the parameter  $\pi/s$  is relatively unaffected.

**Transient Operation of Transistor With Inductive Load**—H. C. Lin, A. R. Illavacek, and B. H. White (p. 174)

A transistor operating with an inductive load may develop a collector-emitter short circuit when the transistor is suddenly turned off. The secondary breakdown of the collector characteristics determines the susceptibility to this type of failure. The secondary breakdown is greatly influenced by the reverse base current. The reverse base bias voltage and impedance affect the reverse base current in a predictable manner. The failure mechanism can be explained in terms of the characteristics of a four-layer device. Transistor requirements and design considerations are examined.

For safe operation, the secondary breakdown current should be greater than the maximum operating current. When the reverse base current is minimized, the transistor is also protected. Several circuits which prevent the flow of reverse base current are presented.

**A Design Method for Crossed-Field Electron Guns**—G. S. Kino (p. 179)

A design method for crossed-field guns based on a space-charge flow solution in crossed fields is given. By using the method of analytic continuation in the complex plane, it is shown that it is possible to find the exact form of the electrodes required. The design results in a gun similar to the French "short gun" with the great advantage that the current emitted from the gun and the current density at the cathode can be predicted. It is also shown that by making certain approximations to the exact space-charge-flow solution, a new type of gun can be designed, a "long gun" which can have extremely high convergence. The theory for this latter gun is extremely simple and the electrode shapes can be given entirely in analytic form.

**Experimental Notes and Techniques** (p. 185)

Contributors (p. 187)

## Electronic Computers

VOL. EC-9, JUNE, 1960, NO. 2

**Sequence Detection Using All-Magnetic Circuits**—H. D. Crane (p. 155)

A technique is described for detecting specific sequences of pulses occurring on a net of input lines. This technique lends itself to realization in all-magnetic networks by the use of multi-aperture magnetic devices (MAD's). The resulting circuits are remarkably simple and reliable. Processing rates in excess of 100,000 characters per second may be achieved. Examples are given of systems using arrays of such detectors. One example involves a system for detecting handwritten characters which makes use of a special pen having the property of generating specific sequences of pulses as symbols are written. The second example relates to the problem of monitoring text for the detection of specific words (letter sequences) and phrases (series of sequences).

**Comparison of Saturated and Unsaturated Switching Circuit Techniques**—G. H. Goldstick (p. 161)

The concept that the junction transistor is a charge-controlled current source is reviewed. Saturated operation and non-saturated operation are defined on the basis of minority and majority carrier distributions in the base

region. Several common emitter switching circuits are analyzed. The switching efficiency, a figure of merit based on the charge storage properties of the transistor, is introduced. Saturated and nonsaturated operation are compared on the basis of switching efficiency, transient waveforms, stability of the voltage levels, power dissipation, noise rejection and suppression ability, and circuit complexity. Currently-used antisaturation techniques are discussed.

**Comparative Performance of Saturating and Current-Clamped High-Frequency Pulse Circuits (Abstract)**—V. P. Mathis, H. Raillard, and J. J. Suran (p. 175)

**A New Core Switch for Magnetic Matrix Stores and Other Purposes**—I. P. V. Carter (p. 176)

This paper analyzes the conventional uses of magnetic switch cores to drive matrix stores in both current-driven and voltage-driven modes. A new method of using switch cores is proposed and analyzed which offers, at the cost of replacing in every selection line the usual switch-core and terminating resistor by two smaller cores, intrinsic pulse shaping and amplitude regulation, and much reduced power dissipation, particularly in the driving stages. Constructional details of an application of the new method to drive a store  $100 \times 80 \times 10$  are given, and waveforms for this store are shown. All address decoding and driving are performed by 34 transistors. A model of a multiple coincidence store  $101 \times 101$  with a cycle time of  $1 \mu\text{sec}$  has also been constructed; details are given.

**Submicrosecond Core Memories Using Multiple Coincidence**—H. P. Schlaepfli and I. P. V. Carter (p. 192)

Memories using toroidal ferrite cores with cycle times less than a microsecond are described; the selection ratio is increased by the use of biasing and the multiple coincidence principles of Minnick and Ashenburt. It is shown that this mode of operation leads to important changes in the structure of the store; in particular, the classical core switch does not fulfill the new requirements. The "two-core switch" is then briefly described; it permits an elegant and economic solution of the problems arising at high selection ratios. Details of the design and operation of memories embodying these ideas are given; it is shown, for example, that standard core memory matrices can be used very efficiently at a selection ratio of 3:1 to achieve a cycle time of 2 microseconds. Further illustrations are given from a model of a  $100 \times 100$  store operated at 4:1 and 7:1 selection ratios, and it is shown that a store of 10,000 8-bit characters with a cycle time of 0.25 microsecond is feasible.

**Magnetic Fields of Twistors Represented by Confocal Hollow Prolate Spheroids**—H. Chang and A. G. Milnes (p. 199)

A twistor is an anisotropic ferromagnetic cylindrical wire with nonmagnetic core. The intrinsic magnetization flux curls in helical sense in the wire and has an air return path. Many field problems must be solved for their successful use as information storage elements. For instance, the demagnetizing field in the wire causes instability of storage and therefore must be reduced by suitable geometry of the twistor. The flux lines emanating from a bit link neighboring windings and also impose a magnetic field intensity in neighboring bits. The interactions, although undesirable in packing bits in a memory array, can be used to advantage as operating forces in logical devices.

This paper analyzes the demagnetizing field in a twistor bit, based on the geometrical model of a confocal hollow prolate spheroid and the magnetic characterization of the material by  $\vec{B} = \mu_0(H + M)$  where  $\vec{M}$  is the intrinsic magnetization, constant in magnitude, but oriented by the external field.

Demagnetizing factors for confocal hollow

prolate spheroids are plotted against length-to-diameter ratio and wall thickness. Expressions for field intensities outside a twistor bit are given. Analogies between twistors and thin film are examined.

**The Design of a General-Purpose Microprogram-Controlled Computer with Elementary Structure**—Thomas W. Kampe (p. 208)

This paper presents the design of a parallel digital computer utilizing a 20- $\mu$ sec core memory and a diode storage microprogram unit. The machine is intended as an on-line controller and is organized for ease of maintenance.

A word length of 19 bits provides 31 orders referring to memory locations. Fourteen bits are used for addressing, 12 for base address, one for index control, and one for indirect addressing. A 32nd order permits the address bits to be decoded to generate special functions which require no address.

The logic of the machine is resistor-transistor; the arithmetic unit is a bus structure which permits many variants of order structure.

In order to make logical decisions, a "general-purpose" logic unit has been incorporated so that the microcoder has as much freedom in this area as in the arithmetic unit.

**An Evaluation of Several Two-Summand Binary Adders**—J. Sklansky (p. 213)

Five fairly representative members of the class of two-summand binary adders are described and evaluated. Hopefully, this will help the development of more general approaches to computer subsystems evaluation. The adders are evaluated on the basis of three quantities: the number of two-input AND gates and OR gates,  $G$ ; the gate-normalized addition time,  $\tau$ ; and the number of bits,  $n$ , in each summand. Three plausible formulas for computational efficiency,  $\eta$ , are postulated, and plotted vs  $n$  for the five adders. Based on a comparison of the resulting curves, the following efficiency formula seems preferable:

$$\eta = \frac{n}{\tau \log_2 G}$$

Of the five adders considered, the new "conditional-sum adder" is best by the above formula when  $n \geq 3$ . Other adders, however, are shown to be superior when the assumptions underlying the evaluation of  $G$  and  $\tau$  are changed. The evaluation is found to have several limitations; these are discussed. Curves of  $G$  and  $\tau$  vs  $n$  are given. It is suggested that these curves can serve as raw data for other evaluations, so that various evaluation methods may be compared.

**Conditional-Sum Addition Logic**—J. Sklansky (p. 226)

Conditional-sum addition is a new mechanism for parallel, high-speed addition of digitally-represented numbers. Its design is based on the computation of "conditional" sums and carries that result from the assumption of all the possible distributions of carries for various groups of columns.

A rapid-sequence mode of operation provides an addition rate that is invariant with the lengths of the summands. Another advantage is the possibility of realizing the adder with "integrated devices" or "modules."

The logic of conditional-sum addition is applicable to all positive radices, as well as to multisummand operation.

In a companion paper, a comparison of several adders shows that, within a set of stated assumptions, conditional-sum addition is superior in certain respects, including processing speed.

**Constant-Weight Counters and Decoding Trees**—William H. Kautz (p. 231)

A class of counters is described in which the number of 1's in the flip-flops or register stages composing the counter remains constant as the counter advances from state to state. Simple digital circuit arrangements are described for the design of such counters, which may be used

with a particular type of decoding tree as economical ring-type counters, to provide a separate output lead for each state. Some interesting theoretical questions concerning the minimization of these decoding trees are raised and partially answered. Finally, the costs of these counters are compared with one another, and with those of other types of counters, over a continuous range of values of the flip-flop/gate-input cost ratio.

**Determination of the Irredundant Normal Forms of a Truth Function by Iterated Consensus of the Prime Implicants**—Thomas H. Mott, Jr. (p. 245)

This paper describes a new algebraic way of determining irredundant forms from the prime implicants. The method does not require using the developed normal form, and it makes novel application of Quine's technique of iterative consensus-taking. Thus, by applying repeatedly the rule of consensus to the prime implicants, it is possible to derive a list of implication relations that express the necessary and sufficient conditions of eliminability of the prime implicants in terms of which the irredundant normal forms can be computed. The extension of Quine's technique to this phase of simplification serves to shorten considerably the logical machinery needed for complete solution of the simplification problem. By the same token, it renders the method suitable for use with a digital computer.

**A Precision Amplitude-Distribution Amplifier**—W. F. Caldwell, G. A. Korn, V. R. Latorre, and G. R. Peterson (p. 252)

A new electronic slicer circuit produces output pulses whenever a random input voltage  $x(t)$  is between two slicing levels  $X - \Delta x/2$  and  $X + \Delta x/2$ . The slicer pulses gate a counter to produce a direct digital readout count equal to the estimated first-order probability density of the input signal. The system was designed for random process studies with conventional electronic analog computers and has compatible accuracy.

**A Pulse Position Modulation Analog Computer**—E. V. Bohn (p. 256)

An important field of application for computers is in real-time systems simulation. This requires the generation of nonlinear functions, obtaining the sums and products of these functions and solving systems of nonlinear differential equations. A new type of analog computer suitable for systems simulation is described which combines the desirable features of the digital and analog computers in its mode of operation. Variables are represented by the time interval between pulses. Utilizing a few basic components, it is possible to carry out the operations of addition, subtraction, multiplication and function generation to 0.1 per cent accuracy.

**Correction to "The Determination of Carry Propagation Length for Binary Addition,"** by George W. Reitwiesner (p. 261)

Correspondence (p. 262)

Contributors (p. 268)

**Abstracts of Current Computer Literature** (p. 275)

PGEW News and Notices (Start on p. 293)

**Reviews of Books and Papers in the Computer Field** (p. 270)

scribed, including script writing, shooting, planning, editing and methods of animation.

**A Note on the Writing of Scientific Papers**—W. Hume-Rothery (p. 43)

The structure of scientific papers is discussed, with the aim of making the manuscript as interesting, clear, and concise as possible without loss of subject matter. Some suggestions are given for increasing clarity of language presenting sequences or comparisons, citing numerical values, using appropriate illustrations, and clarifying experimental diagrams.

**The Editorial Function in Scientific Organization**—J. D. Chapline (p. 48)

An analysis is made of the true functions of a good technical editor. In addition to giving his attention to language rules and conventions, an editor must be alert to the ambiguities and weak points in the draft copies of manuscripts. An editor should minimize the distortions that may appear in the communication process. When properly applied, the editorial function can actually give direction and focus to scientific pursuits.

**More Effective Engineering Proposals—One Key to Success**—Frank W. Evans, Jr. (p. 54)

A review is made of the importance and significance of the technical communication in engineering R & D contract proposals. This paper shows what the Services are seeking in contracts with engineering firms and outlines the basic elements that the proposal should contain. Procedures for evaluating finished proposals are discussed, and a number of specific reasons are given for rejecting proposals. General recommendations are given for effectively shaping the material in an engineering proposal.

**Communication: Art or Science**—G. F. Paskusz (p. 59)

This paper discusses the problem of teaching technical communications to engineering students and of how an engineering college can increase the quality of communications. First, students lacking prerequisites in basic English should be screened from such communications courses; the program should then consist of systematic instruction in technical writing and speaking principles augmented by continued exercise. An outline is given of the technical communications program at UCLA.

**Notes Toward Improving Technical Reports**—Sol Cohen (p. 62)

Technical reports can be improved only through the understanding of their use and of their readers. Reports should show what was done and why, what is considered most significant and why, and what action is recommended. Organization and format are considered less important than understanding the needs and interests of the actual readers and of applying this information to the ideas in the report.

**PGEWS 1960 International Symposium** (p. 66)

The Authors (p. 67)

## Medical Electronics

VOL. ME-7, JULY, 1960, No. 3

**Editorial**—John E. Jacobs (p. 118)  
**Papers from the Twelfth Annual Conference on Electrical Techniques in Medicine and Biology**

**Some General Problems of Absorption Measurements in the Cell**—B. Thorell (p. 119)

The physical, chemical, and optical properties of various substances in the living cell, fundamental for their microspectrographic analysis, will be described. Some limits of the present techniques will be discussed.

**The Application of Ultraviolet Absorbance Measurements to Problems in Cell Biology**—George T. Rudkin (p. 122)

## Engineering Writing and Speech

VOL. EWS-3, JULY, 1960, No. 2

The Cover (p. 34)

PGEWS Officers, 1960-1961 (p. 35)

**Technical Motion Pictures in Science and Engineering**—Steve E. Strem (p. 36)

Unlike business and industrial films, the technical motion picture primarily serves the purpose of communication. This paper reviews the merits and disadvantages of using technical films as a medium for scientific and engineering information. Production techniques are de-

Ultraviolet (UV) absorption spectra of intracellular structures are an aid in the interpretation of the biological effects of UV radiation and are useful for the identification of the substances localized in the structures. Microassays of the total amount of a UV absorbing compound in a structure enable a study of the metabolism of that compound to be made in reference to the function of the structure. Both types of analysis are possible in the spectral range between 230 and 300  $m\mu$  where the absorption peaks of the biologically important nucleic acids (260  $m\mu$ ) and proteins (280 and less than 250  $m\mu$ ) lie. The components of a microspectrophotometer, source of radiation, monochromator, microscope optics, and detector are discussed with reference to the UV. The main restriction on the design of an instrument is imposed by the necessity to measure the absorption of an extremely small area (of the order of one micron in diameter) in the specimen. High intensity sources, optical components with high transmission values, and sensitive detectors are required. The application of the method to a study of nucleic acid metabolism in chromosomes is outlined. The total amount of UV absorbing material in an intrachromosomal structure was measured by scanning a photomicrograph and integrating the absorbencies over the structure. Nucleic acid was determined by the difference between the total amount of material found before and after extraction with nucleases. The identity of the extracted material with nucleic acid was checked by measuring the absorption spectra with a photoelectric device before and after the extraction and obtaining the spectrum of the extracted material by difference. As a result of the study it was shown that nucleic acid metabolism varies from place to place along a chromosome and with time at any one place, a finding that has significance with respect to the variety of functions in heredity associated with different regions of a single chromosome. It is suggested that the future use of the method will be enhanced by the development of rapid scanning techniques and of auxiliary chemical and physical methods on a micro scale.

#### Biographical Effects of Ultraviolet Radiation—M. R. Zelle (p. 130)

Except for the studies of partial cell irradiation by ultraviolet microbeams, most of the data concerning the biological effects of ultraviolet irradiation have been obtained in studies utilizing relatively simple and inexpensive apparatus. As more sophisticated instruments such as the microbeam combined with monochromatic light sources and the flying spot microscopes are perfected, even more critical biological analyses should be forthcoming. The few examples of the contributions of ultraviolet radiobiological studies to the analysis of complex biological problems briefly discussed in this paper serve only as indicators of the future progress which will result as these radiobiological techniques are applied to an even wider range of biological problems.

#### The Use of Television and Scanning Techniques for Ultraviolet Irradiation Studies of Living Cells—P. O'B. Montgomery and L. L. Hundley (p. 135)

The Ultraviolet Flying-Spot Television Microscope is a new tool for the study of living cells. The original development of the technique has been described by the authors elsewhere.

One of the major uses of this technique is the study of ultraviolet irradiation damage in living cells. Recent advances in the technique now enable one to perform experiments designed to elucidate the relationship between total cellular damage and cellular component damage. This paper describes the methods for the simultaneous utilization of two wavelengths of light for the illumination of different portions of a single living cell. This technical advance now makes it possible to produce

ultraviolet irradiation damage in any area of the cell while illuminating the remainder of the cell with nondamaging visible light purely for image production purposes.

#### Television Spectroscopy of Biological Fluorescence—S. S. West, C. N. Loesner, and M. D. Schoenberg (p. 138)

Fluorescence emission spectra were obtained from single unfixed ascites tumor cells stained at  $3.3 \times 10^{-7}$  M to  $3.3 \times 10^{-4}$  M concentrations of the vital fluorochrome, acridine orange. The new RCA Intensifier Image Orthicon television camera tube was used as the light detector and afforded approximately a one-hundredfold increase in sensitivity over a standard image orthicon in this application.

The light from the microscope was dispersed by a Leitz "High Power" Monochromator (exit slit removed) and the spectrum focused on the faceplate of the Intensifier Image Orthicon. Spectral curves were obtained by applying appropriate corrections to recordings of line selected oscilloscope traces. These curves show two emission peaks which indicate the presence of two molecular species in close agreement with *in vitro* data. Advantages of the technique and some implications of the results are discussed.

#### Infrared and Microwave Effects on Skin Heating and Temperature Sensation—E. Hendler and J. D. Hardy (p. 143)

In order to study the physiological mechanisms of temperature sensation, the forehead area of seven subjects was exposed to controlled heating while the skin temperature was radiometrically measured and recorded. Continuous exposure to variations in far infrared radiation produced temperature sensations which could best be correlated with rates of change of skin temperature. Warmth threshold was accompanied by a rate of rise of skin temperature of  $0.001^\circ\text{C}/\text{second}$ ; cool threshold was accompanied by a rate of fall of skin temperature of  $0.005^\circ$  to  $0.006^\circ\text{C}/\text{second}$ . Reports of temperature sensation continued to be given when no changes in skin temperature could be measured. Small, rapid fluctuations in skin temperature, exceeding the rates of rise and fall just given, evoked no reports of sensation. It was postulated that the temperature changes involved were confined to the most superficial layers of the skin, and therefore did not stimulate the cutaneous temperature receptors. The same sequence of sensation reports resulted from preliminarily heating up or cooling down the skin, and then allowing it to return spontaneously to its normal temperature level. Cool sensations accompanying rapidly rising skin temperature change rates were believed to be due to simultaneous inhibition of warmth receptors and excitation of cold receptors. Exposure of blackened and unblackened forehead skin to various pulse duration-intensity combinations of near infrared radiation sufficient to evoke threshold warmth sensation, permitted intracutaneous temperature changes to be calculated. All such changes producing a threshold warmth sensation caused a temperature rise of about  $0.02^\circ\text{C}$  at a depth of 150–200 microns below the skin surface. Exposure of the skin to free-field, 3-cm microwave radiation produced initial changes in skin temperature compatible with primary heating of the tissues by the absorbed energy. Response times to onset and offset of stimuli were characterized by their variability. Persistence of warmth sensation of microwave irradiation was a consistent finding. Stimulation of warmth receptors by slowly dissipated heat retained in the tissues was believed responsible. Analysis of the above findings in terms of known temperature receptor discharge activity was made on the basis of change in temperature at the receptor level, as indicated above. In order to explain the observations made, neither the temporal nor spatial dependence of the temperature change was

required. Only a very small change in the discharge activity of any given sensory unit appears to be necessary for a threshold temperature sensation.

#### Opacities in the Lens of the Eye Experimentally Induced by Exposure to Microwave Radiation—R. L. Carpenter, D. K. Biddle, and C. A. Van Ummersen (p. 152)

Lens opacities result from exposure of the rabbit eye to 2450-mc continuous wave radiation. Threshold for a single damaging exposure is determined by power density and duration. Opacities may also result as a cumulative effect of repeated subthreshold exposures. Intraocular temperature increases during irradiation, the extent and rate of increase being related to power density. Inasmuch as a particular temperature critical for opacity induction cannot be identified, it is suggested that the intraocular thermal response may be coincident with, rather than the cause of, induction of opacities. Lens damage may result from irradiation at power levels not sufficient to cause discomfort to nonanesthetized animals. Pulsed radiation with high peak intensities appears to be more potent in inducing lens opacities than continuous wave radiation of equal average power. Since ocular temperature is related to average rather than to peak power, these findings further suggest the possibility of a non-thermal biological effect of microwave radiation.

#### The Mechanism of the Absorption of Ultrasound in Biological Materials—Edwin L. Carstensen (p. 158)

1) Absorption of sound in solutions of macromolecules has been found to be comparable in magnitude and similar in frequency dependence to that of tissues and blood. The absorption has been shown to arise through a relaxation process. Several experimental observations suggest that the relaxation may be related to the protein-water interactions. 2) The absorption of sound in normal blood, although predominately a molecular process, has in addition a component arising from the relative motion between the cells and the plasma. 3) In certain tissues, the experimental evidence points out again the importance of direct molecular absorption. This may be modified to some extent in inhomogeneous tissues where there is the possibility of selective absorption arising at macroscopic discontinuities.

#### Ultrasonically-Induced Movements in Cells and Cell Models—H. J. Dyer and W. L. Nyborg (p. 163)

Normal- and high-speed cinemicrographs of events resulting from highly localized 25-kc vibration of small regions of an individual cell wall in *Elodea* leaf cells and in plastic cell models are discussed. In plant cells, complex patterns of ordered agitation are set up, similar to parts of the patterns observed in model cells. In models containing Newtonian fluids, steady circulation results with streamline positions and directions being functions of viscosity and the vibration pattern of the wall, the general features being accounted for by the theory of acoustic streaming. In models containing weak agar gels, a combination of plastic and fluid behavior is observed as setting ensues; immediately after vibration begins, suspended particles "flow" for a short distance following the streamlines of a viscous fluid, with displacement vectors distributed like the velocity vectors in acoustic streaming, but, as the sound ceases, return slowly almost to their original positions.

#### Fundamental Neurological Research and Human Neurosurgery Using Intense Ultrasound—W. J. Fry and F. J. Fry (p. 166)

Focused high intensity ultrasound can be used, under accurately controlled dosage conditions, to produce either temporary or permanent changes in practically any desired brain structure. Volumes of tissue smaller than one tenth of a cubic millimeter can be affected in

deep brain structures of experimental animals (cats and monkeys), and regions as large as desired can be changed by moving the focal spot of the ultrasonic beams through an appropriately chosen path. The changes can be induced without adversely affecting intervening brain structure and without interrupting the vascular system even within the site in which irreversible or permanent changes in the neural components are produced. The selectivity and absence of effects on the intervening tissue make focused ultrasound a tool of considerable power for investigating basic brain mechanisms. It is now being used in an extensive experimental animal program involving neuro-anatomical, behavioral and physiological studies. It is also being used to study and modify the symptoms of various neurological disorders in humans. The signs and symptoms which have been and are under investigation in human patients at the present time include abnormal movements (tremor and nonpatterned), muscular rigidity, intractable pain (following amputations, cerebral vascular accidents, the acute phase of herpes zoster) and hypersensitivity to stimulation of the body surface.

This paper includes brief descriptions of the instrumentation which has been developed for this type of fundamental neurological research and medical applications, the techniques of preparation and irradiation of the experimental animal and human patient, the types of research results which are obtained from experimental animal studies in which the ultrasonic dosage parameters are chosen for producing either irreversible or reversible changes, the results obtained from producing arrays of ultrasonic lesions in deep brain structures of patients suffering from various neurological disorders, and the present status of investigations of the physical mechanism of the action of the intense sound on the tissue.

**Penetration of Corneal Opacities by Infra-red Electronics**—Joel Friedman (p. 182)

Some areas of application of the infrared image converted to diagnostic procedures in cases of corneal opacification are presented. Further extension of areas of usefulness will be paced by technical advances in infrared optics, quality of screen image, and simplification of design to facilitate the adaptation of the tube as an auxiliary for direct ophthalmic examination.

**Monitoring the Arrival in the Cerebral Hemispheres of Intravenously Injected Radioisotope (Cerebral Radiorheography)**—W. H. Oldendorf (p. 184)

A preliminary study has been carried out to establish the usefulness of a simple clinical technique for evaluating the relative cerebral blood flow in each hemisphere.

The theory of the test is to monitor the arrival in the head of intravenously injected radioisotope. Two collimated detectors monitor the two cerebral hemispheres for 60 seconds. The test is simple to administer and extremely safe since a rapidly excreted radioisotope is used. Preliminary study suggests it may be of considerable clinical value in view of its simplicity and safety.

**An Electrical Method to Determine Hemocrits**—R. H. Okada and H. P. Schwan (p. 188)

It has been determined that the electrical conductance of whole blood is a very accurate index of its hematocrit. The new instrument described here fills a need for a quick, accurate portable hematocrit meter. This meter can be used at the patient's side for an instantaneous determination, and wherever a portable instrument is required.

The advantages of this new instrument are its speed of operation, direct reading, small sample of blood required, and the inherent accuracy of the electrical determination. The last fact could well result in greater clinical significance of the hematocrit measurement.

**A Miniature Versatile Dosimeter**—S. J. Malsky, C. G. Amato, and C. Reid (p. 193)

A miniature glass dosimetry system is described that, when employed with a gold shield of suitable wall thickness and "softer energy" portals, is energy independent over a specified photon energy spectrum. A brief review of the characteristics that this dosimeter must meet before its use as a clinical *in vivo* dosimeter is included. Various physical characteristics relating to range, integration of daily dose, and orientation with respect to the source of radiation, etc., are also considered. Its clinical applications are reviewed as well as its use with radium and other discrete sources as implants. A brief review is made of its possible use in the detection of gamma radiation in the presence of neutrons. The applications of this dosimeter, as the authors indicate, are not limited to any specific field; rather, its use is determined if one wants the daily and/or total dosage of radiation delivered to a specific point. A separate electronic reader is required to read the dosimeter.

**The Television Eye Marker as a Recording and Control Mechanism**—E. Lewellyn-Thomas N. H. Mackworth, and M. R. Howat (p. 196)

The Television Eye Marker utilizes the reflection of a light from the cornea to record the position of a man's gaze upon a picture of the scene at which he is looking. This corneal reflection is viewed under magnification by a television camera while the scene is viewed by a second television camera and the outputs of the two cameras are combined. The resultant picture on the monitor television screen shows the scene with a bright spot superimposed, indicating the position and movements of the subject's gaze. This can be photographed by a motion picture camera. The bright spot is called the Eye Marker. Photocells are mounted against the monitor television screen and are thus activated when the Eye Marker passes beneath them. The position of each photocell is correlated with a position in the scene so that when the subject looks at a point in the scene, the corresponding photocell is activated. The photocell output is used to record the positions of visual fixation, and also to control the visual or other information presented to the subject.

A method of converting the photocell output into signals in the teletype code is described.

**Contributions**

**Some Unsolved Problems in Bio-Medical Electronics**—Lee B. Lusted (p. 201)

**The Bioelectric Field Pattern in the Salamander and Its Simulation by an Electronic Analog**—Robert O. Becker (p. 202)

The dc field potential has been determined on the surface of the intact salamander, *Triturus viridescens*. A complex field was found which did not correspond to a simple dipole. The field was found to vary in a dynamic fashion with changes in the level of anesthesia. The spatial organization of the field correlated well with the anatomical organization of the central nervous system of the animal, in that areas of nerve cell aggregations within the central nervous system appeared to serve as both sources and sinks of the potential, with transmission of the steady potential along major nerve trunks. An analog model of the central nervous system was constructed utilizing several bimetallic junctions and a conducting network. This model produced a field in a modified electrolytic tank which corresponded well with the field found in the intact animal. It was concluded that the dc bioelectric potential in organisms may be generated within and conducted by portions of the central nervous system. The possibility that this is a means of data transmission and/or control (in addition to the usual action potential system) is being evaluated.

**A Gas-Hemoglobin Diffusion Photometer**—F. Kreuzer and L. Garceau (p. 207)

A double-beam photometer is described which employs a single photocell and motor-driven shutter synchronized with alternately energized screens in a gated amplifier. The equipment is used for indicating and recording monochromatic light absorption changes by a thin layer of hemoglobin-containing media exposed to diffusion of various gases.

**A Blood Flowmeter for Use in Coronary Heart Disease Research**—Francis A. Giori (p. 211)

In connection with research on coronary heart diseases, the need arose to measure extremely low blood flows in uncannulated vessels in the immediate vicinity of the heart in a living animal. Measurement of blood flow in this instance is complicated by the typically small flow rates, the requirement to transmit faithfully the pulsating components of the flow, and the large interfering cardiac voltages in the vicinity of the implanted vessel. Nearly all of the development effort described in this paper was devoted to extending the range of the electromagnetic type of flowmeter. Critical system parameters in this particular application were found to be the input impedance level and coupling methods of the preamplifier, phase accuracy of the timing voltages, and common-mode rejection of the carrier amplifier. Significant but relatively less important factors are the coil-drive method, the waveshape of the coil-drive current, and the noise level of the gating system. The blood flowmeter described in this paper has been in daily use at the Buffalo Veterans' Administration Hospital since mid-June 1959. During most of this period, medical personnel have been operating the instrument and have performed the electrical adjustments which occasionally are needed to maintain the instrument at a suitable performance level.

**Diagnostic Decisions by Machine**—Keeve Brodman (p. 216)

A data-processing machine, programmed to simulate what is postulated to be the operation of a physician's mind when he makes a diagnostic decision, interprets patients' medical histories with such discrimination that it identifies the patient's disease as often as does a physician who interprets the same data. Although the diagnostic decisions made by the machine could not be distinguished from those made by the physician, it cannot be said that the machine is an analog of the human mind, which remains a black box of unknown operation.

**Program for a Diagnostic Model**—Adrianus J. Van Woerkom (p. 220)

**A Portable, Self-Contained Electronic Cardiometer for the Medical Research Profession Evolved by a Unique Group of Engineers**—L. J. Ryan (p. 221)

The medical research groups have been somewhat at a disadvantage in securing certain instrumentation for their various projects because usually they must rely upon large established engineering organizations where close liaison is rather difficult. A group of volunteer engineers at the Illinois Bell Telephone Company, in their own spare time, have been able to produce instrumentation for a number of these projects in a unique manner. This paper describes the SAVE (Service Activities of Volunteer Engineers) operation and one of their projects, the portable (3-ounce) self-contained, cumulative heartbeat recorder.

**Fluorocinematographic and Manometric Studies of Esophageal Motility in Patients with Achalasia**—G. Chejfec, H. A. Danemann, J. Milewski, E. C. Texter, Jr., and C. J. Barborka (p. 225)

Achalasia is a neuromuscular disorder of the esophagus with typical motility, X ray, and intraluminal pressure patterns. In the past, diagnostic and therapeutic procedures in this disease involved the use of fluoroscopy and

"spot" filming. With the introduction of fluorocinematography (General Electric TV-X), it has become feasible to perform prolonged studies and more accurate therapy with simultaneous filming of all these events. The motor phenomena could then be studied in detail with frame by frame analysis of the film. At the same time the radiation hazard to the patient and the observer has been greatly reduced.

Although at the moment certain technical problems have tended to limit the usefulness of this procedure to the esophagus and adjacent structures, it is felt that the entire gastrointestinal tract will ultimately be amenable to such detailed methods of study.

**A Simple Method for Recording the Electrocardiogram, Phonocardiogram, or Pressure Tracing on the Cineangiogram**—J. G. Mudd and R. Loeffel (p. 228)

A method is presented for simultaneous recording of the electrocardiogram on the cineangiogram. A system for direct visualization of the stylus recording has been designed. Simultaneous recording is helpful in determining the exact timing of the blood flow through intracardiac shunts.

**Abstracts of Current Bio-Medical Research Projects** (p. 229)

**Correction to "Television X-Ray Movies: Dose and Contrast Factors,"** by R. Stuart Mackay (p. 230)

## Microwave Theory and Techniques

### VOL. MTT-8, JULY, 1960, NO. 4

**Report of Advances in Microwave Theory and Techniques in Great Britain—1959**—John Brown (p. 382)

**Report of Advances in Microwave Theory and Techniques in Western Europe—1959**—Georges Goudet (p. 387)

**Report of Advances in Microwave Theory and Techniques in Japan—1959**—Kiyoshi Morita (p. 395)

**The Design and Measurement of Two Broad-band Coaxial Phase Shifters**—C. F. Augustine and J. Cheal (p. 398)

Two mechanical (servo-driven) phase shifters were developed in response to systems requirements of low torque, compactness, octave bandwidth, and linear relation between mechanical motion and phase shift. One phase shifter relies upon the axial motion of a dielectric slug through a helix wound from modified miniature rigid coaxial cable. The second design consists of a 3-db coupler with ganged movable shorts on two ports. The helix design displayed phase shift of 720 degrees at 3 kmc and linearity to within  $\pm 3$  degrees. The coupler design is capable of achieving 720 degrees phase shift at 3 kmc and linearity within  $\pm 2$  degrees. A precision measuring facility (phase bridge) was developed for the purpose of determining the electrical performance of the phase shifters. A brief analysis is included to illustrate the prediction of maximum possible errors in the phase bridge and the phase shifters, in terms of transmission line parameters.

**A Dielectric Resonator Method of Measuring Inductive Capacities in the Millimeter Range**—B. W. Hakki and P. D. Coleman (p. 402)

A novel technique for the measurement of dielectric and magnetic properties of a homogeneous isotropic medium in the range of approximately 3 to 100 kmc is described. An accuracy of  $\mp 0.1$  per cent is possible in the determination of permittivity or permeability in those cases where the loss tangent is sufficiently small. The measuring structure is a resonator made up of a right circular cylindrical dielectric rod placed between two parallel conducting plates. For measurement of permittivity two or more resonant  $TE_{0nl}$  mode frequencies are determined whereas for the measurement of

permeability two or more resonant  $TM_{0nl}$  mode frequencies are determined. The dielectric or magnetic properties are computed from the resonance frequencies, structure dimensions, and unloaded  $Q$ . Since the loss tangent is inversely proportional to the unloaded  $Q$  of the structure, the precision to which  $Q$  is measured determines the accuracy of the loss tangent.

**Summary of Measurement Techniques of Parametric Amplifier and Mixer Noise Figure**—R. D. Haun, Jr. (p. 410)

Expressions are derived for the noise factor of a frequency mixing circuit under two different operating conditions: 1) single-sideband operation with input only in a band of frequencies at  $\omega_1$ ; and 2) double-sideband radiometer operation with incoherent inputs in the bands both at frequency  $\omega_1$  and at  $\omega_2 = \omega_3 - \omega_1$ . In both cases, the output is taken only at  $\omega_1$ .

It is shown that the noise figure for radiometer double-sideband operation is not always 3 db less than for single-sideband operation. It is also shown that it is possible to obtain an output signal-to-noise ratio which is greater than the input signal-to-noise ratio for coherent double-sideband operation.

Methods are analyzed for measuring the effective noise temperature of this circuit by using a broad-band noise source.

**Duplexing Systems at Microwave Frequencies**—A. F. Harvey (p. 415)

The paper reviews the various methods of duplexing at microwave frequencies. General principles, including the use of passive and solid-state devices, are first discussed. The characteristics of gaseous-discharge duplexing tubes of both self- and externally-excited types are examined and data for typical examples given. The various arrangements of discharge tube duplexers and methods of measuring their performance are described. The survey concludes with a bibliography.

**Impedances of an Elliptic Waveguide (For the  $eH_1$  Mode)**—G. R. Valenzuela (p. 431)

The power-voltage, power-current and voltage-current impedances for the elliptical waveguide for the fundamental mode ( $eH_1$  mode) are obtained by two different methods.

The first method consists of using the exact fields inside a perfectly conducting elliptical pipe. Numerical results were obtained by numerical integration of the integrals involving Mathieu functions by the Gaussian Quadratures method by a digital computer.

In the second method approximate fields which satisfy the boundary conditions were used. By this approximate method, actual expressions for the impedances are obtained as a function of minor to major diameter ratio with no need of numerical integration.

The actual expressions for the impedance obtained by the approximate method give the impedance for elliptical waveguide within six per cent. On the basis of comparison with the exact numerical solution the expressions for the approximate impedance give the impedance of elliptical waveguide within three per cent if they are scaled by 1.03.

**Analysis of a Transmission Cavity Wavemeter**—Leo Young (p. 436)

A section of transmission line partially closed off at each end constitutes a cavity wavemeter. If fixed in length, it may be used as a reference cavity; or if tunable, it may be used to determine frequency. Such a cavity is here treated systematically as a lossy transmission line, with the two end couplings either lossless or symmetrical. The analysis is by means of the transfer or wave matrix. Various expressions are derived which have previously not been obtained, or for which only approximate expressions have been derived from "equivalent circuits."

**Scattering of a Plane Wave on a Ferrite Cylinder at Normal Incidence**—W. H. Eggenmann (p. 440)

The scattered field is given as a series of cylinder functions. If the ferrite cylinder is magnetized along its axis the scattering pattern becomes asymmetrical about the direction of incidence. Approximation formulas for the thin cylinder and the far field zone are given. It is shown that in the first approximation the amplitude is an even function and the phase angle of the field is an odd function of the scattering angle. Exact numerical results have been obtained with a Univac digital computer. By a suitable arrangement of the ferrite cylinders, a unidirectional pattern can be obtained which is controlled by the applied magnetic dc field.

**Phase Adjustment Effects on Cascaded Reflex Klystron Amplifiers**—Koryu Ishii (p. 445)

Reflex klystrons (type 2K25) were used as regenerative amplifiers for the X-band. Two 2K25 reflex klystron amplifiers were cascaded with a coupling circuit which contained a variable phase shifter. The effect of the phase adjustment was investigated in comparison with another coupling scheme which did not contain the phase shifter. The phase adjustment in the coupling circuit gave the amplifier system high gain (more than 50 db max), and a reasonably low noise figure (8 db–17.5 db). High sensitivity was obtained. Proper phase adjustment of the two stage reflex klystron amplifier could give more than twice the gain in db of the single stage amplifier because of the regenerative feedback between stages. The linearity and dynamic range were considerably improved by the phase adjustment. But the frequency bandwidth became narrow (2 mc), and improvement in stability and directivity was not significant.

**TE Modes of the Dielectric Loaded Trough Line**—Marvin Cohn (p. 449)

The properties of TE modes on a dielectric loaded trough waveguide have been investigated. In the case of the dominant mode of this line ( $TE_{20}$ ), families of design curves giving the field distribution, guide wavelength, power handling capability, wall losses, and dielectric losses as a function of operating wavelength, waveguide dimensions and dielectric constant are presented. For a loosely bound wave, the losses are comparable to those of conventional rectangular waveguide and the power handling capability is an order of magnitude greater. The apparatus and procedure used to measure guide wavelength, rate of field decay in the transverse direction, and attenuation are described. The measured performance is in close agreement with the theoretically predicted characteristics.

**Coupling of Modes in Uniform, Composite Waveguides**—L. C. Bahiana and L. D. Smullin (p. 454)

The principle of coupling of modes is used to compute the phase constant in a uniform waveguide filled with two different dielectric materials. The natural modes of two hypothetical waveguides filled with the different dielectrics are computed. The propagation of the combined system is computed by considering the coupling between the two sets of modes. Comparison is made between the approximate theory and an exact theory.

**Correction to "Design of Linear Double Tapers in Rectangular Waveguides,"** by R. C. Johnson (p. 458)

**Correspondence** (p. 459)

**Contributors** (p. 468)

**PGMTT News** (p. 471)

## Military Electronics

VOL. MIL-4, APRIL-JULY,  
1960, NOS. 2-3

U. S. Army Space Issue

### Automatic Meteorological Data Collecting System—R. Thomas and M. McLardie (p. 234)

The automatic data collecting system, as designed, permits automatic sensing and logging of 64 meteorological parameters measured on a 220-foot tower. The design permits simultaneous measurements of all parameters at all levels, with response of the instruments on the order of a few seconds. There is a resultant increase in data accuracy and acquisition, flexibility of observation periods, ease of maintenance and simplicity of operation. With those capabilities, studies requiring large volumes of data on a continuing basis are feasible with existing manpower.

### Rocket Sounding of High Atmosphere Meteorological Parameters—K. R. Jenkins, W. L. Webb, and G. Q. Clark (p. 238)

The need for systematic data collection pertaining to meteorological parameters in the high atmosphere has led to the development of several relatively economical meteorological rocket vehicles and uncomplicated rocket payloads. The progress toward an optimum system has been encouraging during the past two years, but the over-all state of the sensor development has lagged behind rocket performance. The complexity of the atmosphere in the area of interest indicates a need for extensive theoretical study in the application of sensors and corrective techniques applied to empirical data obtained during rocket flights.

The Signal Corps has been active in the development and testing of rocket vehicles and sensors as well as telemetry systems for recovery of the measured data. Over one hundred and fifty rounds have been fired at White Sands Missile Range in testing of hardware and techniques and in training personnel and perfecting launching techniques for application in a more comprehensive observations system.

The Loki meteorological sounding rocket has proven to be the first reliable vehicle to be used in large numbers. It can be fired under almost all conditions, but is restricted in payload to the simplest sensors. So far, only wind measurements have been made, using a small parachute below 150,000 feet and chaff above that level to 280,000 feet. The Arcas has considerably increased the capability of the system by providing telemetry for other sensors as payload on a 15-foot diameter parachute.

An effort toward the installation of a permanent synoptic meteorological rocket sounding network has been made with the initiation of a one-year series of soundings in October, 1959 and a planned schedule of daily firings for one month of each season during 1960. Rocket payloads compatible with the monetary and physical limitations of the initial series of soundings are discussed.

### Automatic Rocket Impact Predictor—Louis D. Duncan (p. 243)

The ARIP was designed to improve rocket impact predictions. Previous procedures involved lag time in wind measuring which could not be fully accounted for in an  $x$ -time firing decision. This lag time assumes an importance in direct proportion to the magnitude of the wind weighting factors, which with some free flight rockets could be as large as 50 per cent of the total wind effect.

Five Aerovane anemometer sensors distributed in the first 100-foot layer provide the data via mechanical and electronic coupling to a computer which has been preset for the ballistic values of a particular rocket. The computer output then activates an  $X$ - $Y$  plotter which has been previously zeroed for all other cumulative displacement effects.

### The Satellite Vanguard II: Cloud Cover Experiment—R. A. Hanel, J. Licht, W. Nordberg, R. A. Stampf, and W. G. Stroud (p. 245)

Artificial satellites promise means of completing precise surveys of the world and of ac-

quiring world-wide photographic coverage for the production of topographic maps. The applicability of satellites to the field of geodesy is covered, and problem areas associated with map compilation serve to emphasize a critical research area.

### TIROS—The System and Its Evolution—H. I. Butler and S. Sternberg (p. 248)

At 6:40 A.M. on April 1, 1960, the TIROS I Satellite was launched, went into its planned orbit, and demonstrated full capability of operation. The cloud pictures returned to earth not only fulfilled all the expectations of the satellite designers from a technical standpoint, but also proved to be informative and of practical value to meteorologists. The effects of the space environment on the satellite itself remained well within the design extremes. Ground operations also went according to plan, with the highly-automated equipment successfully programming the satellite, and then reconstructing the received pictures and their identification coding for photographic reproduction. One of the photographs taken by the wide-angle camera is shown in Fig. 1.

The following paper describes the satellite and ground data-acquisition system. A brief history tracing the evolution of the project from its earliest concepts is included, as well as a discussion of the major factors, both technical and managerial, which affected the final design.

### Surveying and Mapping from Space—Charles S. Spooner, Jr. (p. 256)

This paper contains a summary of the launch and performance of the first meteorological satellite, Vanguard II. A brief description of its instrumentation is given.

### Radio Interferometry Applied to Geodesy—Werner D. Kahn (p. 259)

Mark II Minitrack, a basic type of radio interferometer, is used to obtain observational data from artificial earth satellites. It is assumed that the antenna field pattern can be approximated by a family of coaxial cones whose common apex is the electrical center of the system. The mathematical theory of calibrating the system with stellar radio sources and the reduction of satellite observational data is given, with an error analysis of the system.

### Application of Electronic Distance Measuring Equipment in Surveying—Thelma A. Robinson (p. 263)

Recent improvements in electronic distance-measuring equipment have made it possible to obtain higher degrees of accuracy in surveys for mapping. Electronic equipment has therefore become a far-reaching and powerful tool when used for establishing geodetic control in remote areas, between distant triangulation stations, over impassable terrain, and through intervening vegetation, where it is impossible to connect stations by visual methods. As a result of this broader coverage made possible by electronic measurements, more extensive geodetic connections are provided for the determination of the size and shape of the earth and consequent mapping of paths of missiles and of satellites.

This paper gives an up-to-date account of these geodetic applications of HIRAN, LORAC, tellurometers, geodimeters, as well as flares, and includes a brief description of the systems. Some of the limitations and problems encountered with these instruments are described and the accuracies which have been obtained from specific field surveys are noted.

### Semi-active Correlation Radar Employing Satellite Borne Illumination—O. E. Rittenbach and W. Fishbein (p. 268)

This paper describes a semi-active radar system in which the transmitter is carried in a satellite. The satellite transmits a randomly modulated signal. On the ground the radar has two antennas and receivers. One antenna points at the satellite, the other at the target. The signal from the satellite oriented receiver

is delayed and correlated with the satellite signal reflected from the target. The delay corresponding to the peak of the correlation function is used to determine range. It is planned to test this system with various communications satellites.

### Artificial Ionospheres for Communications—F. F. Marmo and A. Engleman (p. 270)

This paper suggests the utilization of an artificial ionosphere (artificial electron cloud) for RF communication. For convenience the presentation is given in two major parts. The first part is concerned with the general considerations associated with the generation, dynamics and other physical characteristics of the artificial ionospheres. It presents a general survey of the data and analysis from several experiments designed and performed expressly for obtaining critical engineering parameters required for the systematic development of these clouds as a propagation medium. These parameters include 1) chemical yield of contaminant, 2) thermal ionization efficiency, 3) upper atmosphere wind velocities, 4) wind shear, 5) ambipolar diffusion, 6) neutral diffusion, 7) solar photoionization probabilities, and 8) several decay processes including mutual neutralization, chemical consumption, electron attachment, recombination, etc. The effect of these processes upon the propagation capabilities of electron clouds is emphasized. Finally, some suggested improvements are offered for optimizing the artificial ionosphere propagation capability.

The analytical model for cloud reflection, which is discussed in detail, is the spherically symmetric Gaussian electron distribution cloud. Cross-sectional cloud values as a function of time, including the maximum case, are discussed for this model. Calculations of cloud effectiveness for other reflective cases assuming various distribution functions, as well as one refractive case, are also presented. For the model discussed, the RF communications capability of the artificially generated ionosphere is presented. Since it is of first-order importance, the geometrical limitation of cloud generation altitude as a function of system communications range is considered. The altitude requirements for the limiting case of world-wide communications will be noted. In addition, the electronic system parameters, *e.g.*, antenna gains, transmitter power, carrier frequency, bandwidth, etc., that are required to perform certain communications functions are presented in detail. Finally, the utility of existing UHF troposcatter communications equipment for optimum electron cloud communications will be demonstrated.

### Basic Research Efforts in Astrobiology—R. S. Young and J. L. Johnson (p. 284)

The special problems involved in performing basic biological experiments in space vehicles are described, emphasizing the need for unique types of instrumentation. Some of the techniques used in preliminary experiments in recoverable nose cones of Army ballistic missiles are explained in detail. The reasons for doing this type of research in these vehicles are included.

### Bio-Telemetry in the Nose Cones of U. S. Army Jupiter Missiles—S. J. Gerathwohl, S. W. Downs, Jr., G. A. Champlin, and E. S. Wilbarger (p. 288)

On December 1, 1958, a South American squirrel monkey, and on May 28, 1959, a rhesus and a squirrel monkey, were launched in the nose cones of two U. S. Army Jupiter missiles. The experiments were done by scientists of the Army and Navy medical departments, and personnel of the Army Ballistic Missile Agency. They were done on a noninterference basis with the main mission of the missile.

The primary objective of the bio-flights was to demonstrate that animals can survive ballistic flights unharmed, if an adequate life

support is provided. The secondary aim was to design, construct and test such a system, to develop countdown and launching procedures, and to recover the specimen after flight. Moreover, technical and scientific information on the physiologic and behavior status of the animal was to be gained through telemetry.

Although the first animal was lost, valuable data were obtained on the functioning of the bio-package during flight. They served to improve the second experiment, which added substantially to the understanding of the biomedical requirements for space flight. Moreover, Able and Baker were the first primates recovered unharmed from an operational IRBM nose cone after re-entering the earth's atmosphere.

**Recovery System Development**—R. M. Barraza and W. G. Huber (p. 303)

The design and development of a recovery system involves extensive studies and tests to determine the best configuration for each specific application. Thought should be given to using off-the-shelf, well proven components where applicable in any new recovery system design. This will reduce the development cost and yield higher system reliability. In discussing the design and development of recovery systems, the over-all problem can be broken down to include considerations of structural integrity of the vehicle, *i.e.*, deceleration loads it can safely withstand, re-entry heating, practical end conditions of velocity and altitude at which recovery system sequence can be initiated with reliable operation, efficiency of system; *i.e.*, weight and space requirements of the system for the amount of braking force developed, flotation equipment if required, and locating devices.

This paper discusses these considerations in detail and their application to present and future booster and payload recovery systems being developed by the U. S. Army Ballistic Missile Agency.

**Electronic Components for Space Instrumentation**—James P. McNaul (p. 308)

The advent of the space age has placed unique requirements on the design and application of electronic components. Not only has a rigorous environment been imposed on components, but the system demands have often exceeded the state of the art of component development. From all indications these system demands will greatly increase over the next few years.

This paper briefly describes some of the Research and Development programs which have been accomplished at USASRD in meeting the space age system and environmental requirements. Based on future system requirements, some programs now in existence, as well as some which are planned, are discussed, and some general conclusions are presented on the work that must be done if the proper electronic components are to be available when needed.

**Power Sources Designed for Space**—W. Shorr, D. Linden, and A. F. Daniel (p. 313)

New, improved and more reliable power sources will have to be developed if anticipated, space-oriented, requirements for higher power and longer life are to be satisfied. Conversion systems employing chemical, solar and nuclear energies are described and their prospects for further improvement discussed.

**Launching Procedures for Space Vehicles**—Daniel D. Collins (p. 317)

Operations conducted at a launching site on any space vehicle program are a result of all contributions to the launching operation team from the many sources of origin concerned with the vehicle. Recognizably, therefore, these contributions vary from contractor to contractor.

The paper is based on the general launching techniques developed and followed by one of the contractors at the Atlantic Missile Range.

Launching procedures are the recommended methods and operations necessary in testing, checking and preparing a space vehicle for flight. They are the culmination of all previous experiences, studies and tests formed into a written chronological schedule to check and test each critical flight component and operation in proper sequence. The procedures are accomplished by a group of engineers, technicians and various other specialists organized into a well coordinated team.

**From an Early Sputnik Diary**—Harold A. Zahl (p. 320)

Like almost everyone else in the world, personnel of the U. S. Army Signal Research and Development Laboratory (USASRD), Fort Monmouth, N. J. were caught by surprise when the USSR successfully launched earth satellites in October and November, 1957. The narrative portrays some of the happenings in our environment when the BEEP-BEEPS descended upon us. I should mention, however, that any humor the reader may see in the latter-day remarks which constitute this diary was certainly nonexistent during the long, dreary 40 days and 40 nights when, in the wilderness of the outer space, we were "wrestling" with these electronic invaders. It is only in retrospect that we can now smile.

**Army Participation in Project Vanguard**—W. E. Smitherman (p. 323)

The Army was responsible for the design and construction of the Minitrack stations for Project Vanguard. In addition, the Army responsibility included the electrical tracking of the artificial satellites.

This article outlines the actions taken by the Army in fulfilling these responsibilities.

**The Signal Corps Astro-Observation Center, Fort Monmouth, N. J.**—L. H. Manamon and A. S. Gross (p. 327)

Many months of active participation in the satellite and missile observation program have resulted in a number of new and improved concepts which have been put to practical use in the establishment of the U. S. Army Signal Research and Development Laboratory's Astro-Observation Center, Fort Monmouth, N. J.

This paper will describe the capabilities of the Research and Development station and several of the instrumentation techniques in use, including the use of phase-locked audio-frequency tracking filters, and high speed digital readout equipment for precision Doppler measurements.

The extreme flexibility of frequency coverage of the station has been of exceptional value in the rapid acquisition of signals transmitted from foreign satellites and space probes.

**Tracking in Space by DOPLOC**—L. G. DeBey (p. 332)

A satellite and space vehicle tracking system of the Doppler type, known as DOPLOC, is described. The characteristics of the heart of the system, a phase-locked tracking filter, are discussed from the viewpoints of bandwidth, signal-to-noise ratio, and accuracy of Doppler frequency measurement. System sensitivity to low energy signals is shown to be  $2 \times 10^{-20}$  watts at a bandwidth of 1 cps. Tracking ranges vs frequency are given for constant gain and constant aperture antennas. The advantages of DOPLOC in satellite tracking programs are briefly discussed.

**Orbit Determination from Single Pass Doppler Observations**—R. B. Patton, Jr. (p. 336)

This paper presents a method for determining the orbit of a satellite by observing, in the course of a single pass, the Doppler shift in the frequency of a CW signal transmitted from the ground and reflected by the satellite to one or more ground-based receivers at remote sites. The method is sufficiently general that, with minor modification, it may be applied to any type of satellite or ICBM tracking measure-

ments. The computation consists of improving approximations for initial position and velocity components by successive differential corrections which are obtained from a least squares treatment of an over-determined system of condition equations while imposing elliptic motion as a constraint. Methods for obtaining approximations for the initial position and velocity components are likewise discussed. Results are presented for computations with typical input data.

**Comparison of Precalculated Orbital Elements of the Army Explorer Satellites with the Actual Elements Derived from Observations**—H. G. L. Krause and R. N. DeWitt (p. 344)

Based on precalculated data for the position and velocity vector of the injection point for the Explorers I through V, orbital elements are derived, and compared with the actual orbital elements at injection time, calculated from position and velocity data obtained from radar measurements. Calculations were also made for the different orbital periods of a satellite perturbed by the Earth's oblateness.

**Tracking Experiments with Pioneer IV**—T. A. Barr and C. A. Lundquist (p. 353)

Several organizations, including ABMA, participated in a world-wide program for testing receiver techniques used in tracking the low power transmitters carried on the space probe Pioneer IV. A meeting was held and presentations were made on each system tested.

This paper presents a summary and comparison of the results of the receiving techniques used to track the Pioneer IV. It also gives a brief description of the transmitters and antennas used on Pioneer IV.

**Review of USASRD Satellite Propagation Studies**—P. R. Arendt (p. 357)

The U. S. Army Signal Research and Development Laboratory has been engaged in a series of analyses of satellite radio propagation. Some examples of the observations and their interpretation are given. Details have been published elsewhere in individual reports.

**Analysis of Satellite Motion from Radio Reception**—Friedrich O. Vonbun (p. 359)

This paper presents an analysis of a radio signal originating from a tumbling and rotating earth satellite. An equation is derived for the relative motion of the unit position vector pointing from the observer to the satellite with respect to the satellite coordinate system. From this, the amplitude variation of the ground received radio signal is calculated. It is further shown how a recording of this amplitude variation can be used to calculate the tumbling angle of the satellite in space. A simple example is given in which this angle between the normal of the plane of a satellite turnstile antenna system and a fixed axis in space is determined with the help of AGC recording. These recordings can be made either with linear or circular polarized receiving antenna. For future stabilized satellites, these derived equations can be used as an easy check of the operational condition of the stabilization system itself.

**World-Wide Clock Synchronization**—F. H. Reder and G. M. R. Winkler (p. 364)

To satisfy already existing needs for higher precision in various time measurements, a world-wide system of synchronized clocks is required.

One possible method for accomplishing such a system, the transportation of operating precision clocks, is discussed. Particular consideration is given to the use of atomic clocks in this connection, and methods of maintenance of synchronization by means of phase tracking of a central master clock via VLF transmissions are reviewed. Project WOSAC, a Signal Corps project of world-wide synchronization of atomic clocks based upon the principles discussed, is outlined and results already achieved are described.

**Contributors** (p. 375)

# Abstracts and References

Compiled by the Radio Research Organization of the Department of Scientific and Industrial Research, London, England, and Published by Arrangement with that Department and *Electronic Technology* (incorporating *Wireless Engineer* and *Electronic and Radio Engineer*) London, England

NOTE: The Institute of Radio Engineers does not have available copies of the publications mentioned in these pages, nor does it have reprints of the articles abstracted. Correspondence regarding these articles and requests for their procurement should be addressed to the individual publications, not to the IRE.

Acoustics and Audio Frequencies.....	1805
Antennas and Transmission Lines.....	1806
Automatic Computers.....	1807
Circuits and Circuit Elements.....	1807
General Physics.....	1808
Geophysical and Extraterrestrial Phenomena.....	1809
Location and Aids to Navigation.....	1811
Materials and Subsidiary Techniques.....	1811
Mathematics.....	1815
Measurements and Test Gear.....	1815
Other Applications of Radio and Electronics.....	1815
Propagation of Waves.....	1815
Reception.....	1816
Stations and Communication Systems.....	1816
Subsidiary Apparatus.....	1817
Television and Phototelegraphy.....	1817
Tubes and Thermionics.....	1818
Miscellaneous.....	1819

The number in heavy type at the upper left of each Abstract is its Universal Decimal Classification number. The number in heavy type at the top right is the serial number of the Abstract. DC numbers marked with a dagger (†) must be regarded as provisional.

## UDC NUMBERS

Certain changes and extensions in UDC numbers, as published in PE Notes up to and including PE 666, will be introduced in this and subsequent issues. The main changes are:

Artificial satellites:	551.507.362.2	(PE 657)
Semiconductor devices:	621.382	(PE 657)
Velocity-control tubes, klystrons, etc.:	621.385.6	(PE 634)
Quality of received signal, propagation conditions, etc.:	621.391.8	(PE 651)
Color television:	621.397.132	(PE 650)

The "Extensions and Corrections to the UDC," Ser. 3, No. 6, August, 1959, contains details of PE Notes 598-658. This and other UDC publications, including individual PE Notes, are obtainable from The International Federation for Documentation, Willem Witsenplein 6, The Hague, Netherlands, or from The British Standards Institution, 2 Park Street, London, W. 1., England.

## ACOUSTICS AND AUDIO FREQUENCIES

**534.1-14:538.6** 2962  
**Sound Pulses in a Conducting Medium**—F. G. Friedlander. (*Proc. Camb. Phil. Soc.*, vol. 55, pt. 4, pp. 341-367; October, 1959.) Theoretical treatment of the propagation of small disturbances in a compressible conducting fluid in a magnetic field.

A list of organizations which have available English translations of Russian journals in the electronics and allied fields appears at the end of the Abstracts and References section.

The Index to the Abstracts and References published in the PROC. IRE from February, 1959 through January, 1960 is published by the PROC. IRE, June, 1960, Part II. It is also published by *Electronic Technology* (incorporating *Wireless Engineer* and *Electronic and Radio Engineer*) and included in the April, 1960 issue of that Journal. Included with the Index is a selected list of journals scanned for abstracting with publishers' addresses.

**534.2+538.566** 2963  
**Propagation of Acoustic and Electromagnetic Waves in a Half-Space**—Khaskind. (See 3059.)

**534.21-14** 2964  
**Experimental Investigation of Waveguide Sound Propagation in Layered Inhomogeneous Media**—A. N. Barkhatov and I. I. Shmelev. (*Akust. Zh.*, vol. 5, no. 4, pp. 403-407; 1959.) Laboratory investigation of sound propagation in media in which the axis of the waveguide is located (a) on the surface and (b) below the surface of an inhomogeneous liquid.

**534.21-14:534.88** 2965  
**Some Phenomena associated with Sound Propagation in the Sea**—A. L. Sosedova. (*Akust. Zh.*, vol. 5, no. 4, pp. 445-449; 1959.) Experimental investigation of sound propagation with velocity distribution in depth. Results are compared with theoretical curves showing the variation of sound intensity with distance. Focusing effects are discussed.

**534.213.4+621.372.823** 2966  
**On the Field Structure in Cylindrical Waveguide with Complex Cross-Section**—Merkulov. (See 2987.)

**534.22-14:534.88** 2967  
**Some Effects of Velocity Structure on Low-Frequency Propagation in Shallow Water**—A. O. Williams, Jr. (*J. Acoust. Soc. Am.*, vol. 32, pp. 363-371; March, 1960.)

**534.26+[538.566:535.43]** 2968  
**Second Approximation in the Method of Small Perturbations**—Shirokova. (See 3063.)

**534.26+[538.566:535.43]** 2969  
**The Scattering of a Plane Wave by a Row of Small Cylinders**—R. F. Miller. (*Canad. J. Phys.*, vol. 38, pp. 272-289; February, 1960.) A perturbation method is applied to two-dimensional problems associated with "hard" and "soft" scatterers. Far fields and scattering cross sections are calculated, and special cases are considered.

**534.26-14:534.88** 2970  
**Side Scattering of Sound in Shallow Water**—R. J. Urlick. (*J. Acoust. Soc. Amer.*, vol. 32, pp. 351-355; March, 1960.) Using two submerged transducers  $1\frac{1}{2}$  miles apart, the intensity of scattering was measured at 22 kc for different angular orientations of the two beams. The results indicate a bottom scattering strength between -30 and -40 db, having no appreci-

able dependence on angle between the two beams: isotropic bottom scattering may be assumed at these frequencies.

**534.286:534.6** 2971  
**A Simple Instrument for the Determination of the Flow Resistance of Acoustically Absorbent Materials**—L. Müller. (*Rundfunktech. Mitt.*, vol. 3, pp. 153-156; June, 1959.) A portable material tester is described.

**534.414** 2972  
**Conductivity of a Group of Holes**—V. S. Nesterov. (*Akust. Zh.*, vol. 5, no. 4, pp. 440-444; 1959.) The Fock equation is applied to arrangements of single holes in an acoustic baffle in a circular tube, and to an array of several holes. Results of measurements on air resonators agree with theory.

**534.52** 2973  
**Method of Calculating the Amplification Factor of Converging Sound Beams**—B. D. Tartakovskii. (*Akust. Zh.*, vol. 5, no. 4, pp. 450-458; 1959.) An approximate method is described, and graphs are given for determining the amplification factor of a focusing system in terms of the focusing action of a nonuniformity in the amplitude distribution along the wave front in conjunction with phase aberration.

**534.52** 2974  
**Scattering of Sound by Sound**—J. L. S. Bellin and R. T. Beyer. (*J. Acoust. Soc. Amer.*, vol. 32, pp. 339-341; March, 1960.) A report of experiments to determine the presence of scattering resulting from the nonlinear interaction of two finite-amplitude sources operating in water. Results indicate no scattered sound above the noise level of the detection system: this is in agreement with Westervelt (2657 of 1957) but contrary to the predictions of Ingard and Pridmore-Brown (2939 of 1956).

**534.61-8:621.395.616** 2975  
**Condenser Microphones with Plastic Diaphragms for Airborne Ultrasonics: Pt. 2**—K. Matsuzawa. (*J. Phys. Soc. Japan*, vol. 15, pp. 167-174; January, 1960.) Formulas for the resonance frequency, capacitance, and low-frequency sensitivity obtained theoretically are in agreement with experiment. Part 1: 2448 of 1959. See also 905 of 1955 (Kuhl, et al.).

**534.76:681.84.087.7** 2976  
**Stereophonic and Quasi-stereophonic Reproduction**—J. P. A. Lochner and W. de V. Keet. (*J. Acoust. Soc. Amer.*, vol. 32, pp. 393-401; March, 1960.) Results are given of sub-

jective tests to compare true stereophonic systems with single-channel systems in which delayed reflections or echoes are introduced.

534.88:534.417 2977

**General Theory for the Synthesis of Hydrophone Arrays**—H. S. Heape. (*J. Acoust. Soc. Amer.*, vol. 32, pp. 356-363; March, 1960.) A determination of the optimum spatial distribution of hydrophone elements and the optimum linear combination of their outputs, by means of amplification and time delay, for obtaining a high signal-to-noise ratio.

621.395.612.4 2978

**New Microphone has Unique Directivity**—H. S. Mawby. (*Audio*, vol. 44, pp. 26-28, 74; April, 1960.) Description of the construction and mode of operation of a combined slotted acoustic line and pressure-gradient microphone. Above 3 kc the acceptance angle is approximately  $\pm 45^\circ$ .

621.395.616.089.6 2979

**Accurate Coupler Pressure Calibration of Condenser Microphones at Middle Frequencies**—T. F. W. Embleton and I. R. Dagg. (*J. Acoust. Soc. Amer.*, vol. 32, pp. 320-326; March, 1960.) An improved form of the reciprocity technique for determining pressure sensitivities is described. Sensitivities are measured in terms of the volume of a cavity, a fixed capacitance, and the variable setting of an accurate potentiometer. Accuracy of measurement is within  $\pm 0.05$  db on an absolute scale.

621.395.623.7:389.6 2980

**Recent Progress in the Standardization of Loudspeakers**—R. Lehmann. (*Onde élect.*, vol. 40, pp. 207-211; February, 1960.)

#### ANTENNAS AND TRANSMISSION LINES

621.315.212:621.372.62 2981

**An  $n$ -Way Hybrid Power Divider**—E. J. Wilkinson. (*IRE TRANS. ON MICROWAVE THEORY AND TECHNIQUES*, vol. MTT-8, pp. 116-118; January, 1960. Abstract, *PROC. IRE*, vol. 48, p. 972; May, 1960.)

621.372.029.6 2982

**Periodic and Guiding Structures at Microwave Frequencies**—A. F. Harvey. (*IRE TRANS. ON MICROWAVE THEORY AND TECHNIQUES*, vol. MTT-8, pp. 30-61; January, 1960. Abstract, *PROC. IRE*, vol. 48, p. 972; May, 1960.)

621.372.2+621.372.8 2983

**A Simple General Equation for Attenuation**—D. K. Gannett and Z. Szekely. (*PROC. IRE*, vol. 48, pt. 1, pp. 1161-1162; June, 1960.) When em waves are guided by conductors, the attenuation per unit length can be expressed by separate coefficients representing the intrinsic properties of the media used and the configuration and scale of the cross section of the system. The equation is given, and values of the constants for different types of transmission line are tabulated.

621.372.2 2984

**Design of the Optimum Smooth Transition**—A. L. Fel'dshteyn. (*Radiotekhnika*, vol. 14, pp. 40-46; March, 1959.) Design formulas are given for a modified "bell shaped" transition between homogeneous transmission lines of different characteristic impedance. Improved matching characteristics are obtained.

621.372.2 2985

**Higher-Order Modes in Coupled Helices**—R. E. Hayes. (*IRE TRANS. ON MICROWAVE THEORY AND TECHNIQUES*, vol. MTT-8, pp. 119-120; January, 1960.) The general determinantal equation is derived from which the propagation constants for all modes may be calculated.

621.372.2:621.374.5 2986

**The Properties of a Symmetrical Delay System with Three Channels**—L. N. Deryugin and N. V. Trunova. (*Radiotekhnika*, vol. 14, pp. 28-39; March, 1959.) A delay system with two rows of combs situated between parallel planes or in a rectangular waveguide is examined. The influence of the middle and outer channels on the dispersion characteristics, coupling resistance and the position of the nodes of the electric field is investigated.

621.372.823+534.213.4 2987

**On the Field Structure in Cylindrical Waveguide with Complex Cross-Section**—V. V. Merkulov. (*Akust. Zh.*, vol. 5, no. 4, pp. 428-431; 1959.) The wave equation for a two-dimensional region with complex boundaries is simplified by conformal transformation and integrated using perturbation theory. As an example, the field of an  $E_{11}$  wave in a rectangular waveguide with a concave upper wall is calculated.

621.372.823:621.372.852.21 2988

**A Dispersionless Dielectric Quarter-Wave Plate in Circular Waveguide**—R. D. Tompkins. (*PROC. IRE*, vol. 48, pt. 1, pp. 1171-1172; June, 1960.) Design of a plate which generates a circularly polarized wave with an axial ratio  $< 0.2$  db over the frequency band 8.5-9.6 kMc.

621.372.824:621.382.832.6 2989

**Theory of the Slotted-Tube Hybrid Junction**—S. W. Conning. (*Proc. IRE (Australia)*, vol. 21, pp. 248-252; April, 1960.) Conditions for matching with either one- or two-section  $\lambda/4$  transformers are obtained in terms of the characteristic impedances of the TEM modes of the shielded slotted coaxial line.

621.372.825:621.385.633 2990

**A Simple Method for Predicting the Characteristics of Tape Structures**—J. Allison. (*Proc. IEE*, vol. 107, pt. B., pp. 295-300; May, 1960.) The dispersion characteristics and coupling impedance of a Karp type slow-wave structure (2647 of 1957) are calculated using an approximate theory. Measurements confirm the results.

621.372.837.3 2991

**The Tetrahedral Junction as a Waveguide Switch**—J. A. Weiss. (*IRE TRANS. ON MICROWAVE THEORY AND TECHNIQUES*, vol. MTT-8, pp. 120-121; January 1960.) A junction of two rectangular waveguides which are mutually crosspolarized becomes a magnetically controlled reactive switch when properly loaded by a ferrite rod magnetized longitudinally; characteristic properties are given.

621.372.85 2992

**Equivalent Circuits for Small Symmetrical Longitudinal Apertures and Obstacles**—A. A. Oliner. (*IRE TRANS. ON MICROWAVE THEORY AND TECHNIQUES*, vol. MTT-8, pp. 72-80; January, 1960. Abstract, *PROC. IRE*, vol. 48, p. 972; May, 1960.)

621.372.852 2993

**A Nonreciprocal, TEM-Mode Structure for Wide-Band Gyator and Isolator Applications**—E. M. T. Jones, G. L. Matthaei, and S. B. Cohn. (*IRE TRANS. ON MICROWAVE THEORY AND TECHNIQUES*, vol. MTT-7, pp. 453-460; October, 1959. Abstract, *PROC. IRE*, vol. 48, p. 272; February, 1960.)

621.372.852 2994

**Bounds on the Elements of the Equivalent Network for Scattering in Waveguides: Pt. 1—Theory**—L. Spruch and R. Bartram. (*J. Appl. Phys.*, vol. 31, pp. 905-913; May, 1960.) An approach devised by T. Kato (*Progr. Theor. Phys.*, vol. 6, pp. 394-407; June 3, 1951) is ap-

plied to variational techniques for solving scattering problems caused by three-dimensional obstacles in waveguides. The bounds on the values of the equivalent-circuit elements can be evaluated where symmetry exists about a plane perpendicular to the waveguide axis.

621.372.852.21 2995

**Bounds on the Elements of the Equivalent Network for Scattering in Waveguides: Pt. 2—Application to Dielectric Obstacles**—R. Bartram and L. Spruch. (*J. Appl. Phys.*, vol. 31, pp. 913-917; May, 1960.) The exact solution for a dielectric slab of finite length extending to the conducting boundaries of the waveguide and completely enclosing the obstacle is considered as a convenient trial function.

621.372.825.5 2996

**Design of Mode Transducers**—L. Solymar and C. C. Eaglesfield. (*IRE TRANS. ON MICROWAVE THEORY AND TECHNIQUES*, vol. MTT-8, pp. 61-65; January, 1960. Abstract, *PROC. IRE*, vol. 48, p. 972; May, 1960.)

621.372.853 2997

**On the  $TE_{n0}$  Modes of a Ferrite-Slab-Loaded Rectangular Waveguide and the Associated Thermodynamic Paradox**—A. D. Biesler. (*IRE TRANS. ON MICROWAVE THEORY AND TECHNIQUES*, vol. MTT-8, pp. 81-95; January, 1960. Abstract, *PROC. IRE*, vol. 48, p. 972; May, 1960.)

621.372.853 2998

**The Block-Loaded Guide as a Slow-Wave Structure**—W. B. Mims. (*PROC. IRE*, vol. 48, pt. 1, pp. 1176-1177; June, 1960.) Construction and performance details are given for a waveguide loaded with spaced copper blocks and dielectric.

621.396.67 2999

**The Correct Design of the Feed Point of Wide-Band Aerials**—H. Meinke. (*Nachrichtentech. Z.*, vol. 12, pp. 286-290; June, 1959.) The influence of the shape of the region near the feed point on the input impedance of an antenna is considered. The design of a reflection-free feed arrangement for wide-band antennas is discussed; tests on a spherical radiator show that the input impedance remains constant over a wide frequency range.

621.396.67 3000

**V.H.F. and Television Transmitter Aerials for Omnidirectional and Directional Radiation which use the Surface of a Tubular Mast as Reflector**—R. Becker. (*Telefunken Ztg.*, vol. 32, pp. 83-92; June, 1959. English summary, p. 137.) Some practical antenna installations are illustrated, and their characteristics are discussed. Costs are considerably reduced by the use of the mast as a reflector, as the individual reflectors for each antenna element can be omitted and omnidirectional radiation can be achieved with fewer elements.

621.396.674.2:621.375.9:621.372.44 3001

**Parametric-Amplifier Antenna**—A. D. Frost. (*PROC. IRE*, vol. 48, pt. 1, pp. 1163-1164; June, 1960.) A particular parametric amplifier circuit can be built in a balanced form and incorporated inside a half-wave dipole. 22 db gain at 220 Mc has been achieved.

621.396.677:523.164 3002

**Response of a Square Aperture to a Thermal Point Source of Radiation**—M. S. Wheeler. (*PROC. IRE*, vol. 48, pt. 1, pp. 1170-1171; June, 1960.) Gives figures for the power received with different bandwidths.

621.396.677:621.397.6 3003

**Determining the Operational Patterns of Directional TV Antennas**—F. G. Kear and

S. W. Kershner. (PROC. IRE, vol. 48, pt. 1, pp. 1088-1097; June, 1960.) It was found that propagation conditions did not materially affect the directivity of the array, even at distances where the scatter fields were of an appreciable magnitude.

**621.396.677.3** 3004  
**Reduction of Side-Lobe Level and Beam Width for Receiving Antennas**—O. R. Price. (PROC. IRE, vol. 48, pt. 1, pp. 1177-1178; June, 1960.) A new technique which improves the conventional Dolph-Tchebycheff antenna pattern is presented.

**621.396.677.3:396.965** 3005  
**Ground-Mapping Antennas with Frequency Scanning**—A. Bystrom, R. V. Hill, and R. E. Metter. (Electronics, vol. 33, pp. 70-73; May 6, 1960.) Frequency scanning as a technique of electronically steering antenna beams is explained. Its application in two practical antenna systems for use in high-speed aircraft is described.

**621.396.677.833:523.164** 3006  
**Design Considerations and Electrical Measurements on the Aerial of the Radio Observatory Stockert**—E. Schüttlöffel. (Telefunken Ztg., vol. 32, pp. 93-98; June, 1959. English summary, pp. 137-138.) Design calculations for the 25-meter parabolic reflector [1737 of 1957 (Pederzani)] and tests on a 4-meter model are described. For tests on the completed antenna using astronomical RF sources, see 3007 below.

**621.396.677.833:523.164** 3007  
**The Calibration of Large Parabolic Reflectors in the Microwave Region by Radio-Astronomical Means**—P. G. Mezger. (Telefunken Ztg., vol. 32, pp. 99-108; June, 1959. English summary, p. 138.) The difficulties of measuring the gain of large parabolic antennas with the accuracy required for astronomical applications are discussed. The measurement of the main lobe of the 25-meter antenna of the Stockert observatory (see also 835 of March), using the Cassiopeia A RF source, is described. Radiation from the sun was used to determine the stray factor of the antenna.

#### AUTOMATIC COMPUTERS

**681.142** 3008  
**Small Universal Computing Machine with Magnetic (Ferrite) Elements LEM-1**—Yu. A. Makhmudov. (Radiotekhnika, vol. 14, pp. 47-57; March, 1959.) Description of the development and operation of a digital computer using contactless ferrite-core storage and logic elements and a capacitive permanent store.

**681.142:538.221:539.23** 3009  
**Chemically Deposited NiCo Layers as High-Speed Storage Elements**—Heritage and Walker. (See 3208.)

**681.142:621.317.7** 3010  
**Direct Metering for a Transformer Analogue Computer**—J. F. Young. (Electronic Engrg., vol. 32, pp. 280-288; May, 1960.) Descriptions are given of the phase-shift and combining networks of the Witton Network Analyzer (WINA).

**621.142:621.382.2/.3** 3011  
**Procedure for Designing Reciprocal Computer Circuits**—A. Gill. (Electronics, vol. 33, pp. 92-93; May 20, 1960.) Circuits with outputs which are approximately inversely proportional to their inputs can be constructed with diodes, resistors, and dc supplies.

#### CIRCUITS AND CIRCUIT ELEMENTS

**621.3.049.7:621.382** 3012  
**Semiconductor Networks for Microelectronics**—J. W. Lathrop, R. E. Lee, and C. H. Phipps. (Electronics, vol. 33, pp. 69-78; May 13, 1960.) Both active and passive components are fabricated in a single-crystal semiconductor wafer. The development from a circuit diagram by combining oxide masking, diffusion, metal deposition, alloying, and surface shaping is described.

**621.3.049.7:621.382** 3013  
**Inductive Elements for Solid-State Circuits**—M. Scholler and W. W. Gärtner. (Electronics, vol. 33, pp. 60-61; April 22, 1960.) A resonant circuit is described in which a Ge diffused-base transistor with an open circuit base connection functions as a negative resistance diode with an effective inductance of 15  $\mu$ h. The low-frequency noise generated by the diode is attributed to avalanche multiplication occurring in localized nonstationary areas.

**621.314.2.012.8** 3014  
**Clear Method for the Determination of Transformer Equivalent-Circuit Diagrams**—H. Edelmann. (Arch. elekt. Übertragung, vol. 13, pp. 253-261; June, 1959.) The electrical equivalent circuits are directly derived from the magnetic equivalent circuit using principles of circuit duality.

**621.318.57:537.312.62** 3015  
**The Variation of Cryotron Current Amplification Factor with Temperature**—A. E. Brenne-mann. (IBM J. Res. & Dev., vol. 4, p. 197; April, 1960.) The factor increases as the penetration depth decreases, and there is probably a lower limit to the film thickness which can be used.

**621.318.57:621.3.087.4** 3016  
**Monitoring Multiple Inputs Simultaneously**—R. Kronlage. (Electronics, vol. 32, pp. 50-51; August 28, 1959.) Description of an electronic switch and sensing circuit which may be used for detecting a signal (or absence of signal) on one of many channels.

**621.372.413** 3017  
**U.H.F. Resonator with Linear Tuning**—B. H. Wadia and R. L. Sarda. (IRE TRANS. ON MICROWAVE THEORY AND TECHNIQUES, vol. MTT-8, pp. 66-72; January, 1960. Abstract, PROC. IRE, vol. 48, p. 972; May, 1960.)

**621.372.5** 3018  
**A Different Approach to the Approximation Problem**—S. Deutsch. (PROC. IRE, vol. 48, pt. 1, pp. 1175-1176; June, 1960.) An approximation method for the synthesis of network curves.

**621.372.5:621.317.716** 3019  
**A Constant-Resistance Network**—E. R. Wigan. (Electronic Engrg., vol. 32, pp. 289-293; May, 1960.) A modified bridged-T network of design impedance 1 kilohm is described. It can be adjusted in steps of 0.001 to give a maximum shunting ratio of 11.111/1.0.

**621.372.5:621.372.413** 3020  
**General Properties of the Propagation Constant of a Nonreciprocal Iterated Circuit**—R. N. Carlike. (PROC. IRE, vol. 48, pt. 1, pp. 1162-1163; June, 1960.) Formulas are given and the use of such circuits in traveling-wave tubes is considered.

**621.372.54** 3021  
**Method for Simplifying Filter Design**—K. Lichtenfeld. (Electronics, vol. 33, pp. 96-99; May 20, 1960.) Using Cauer parameters, Zobel filters may be simply designed, with a minimum number of elements.

**621.372.54** 3022  
**Narrow-Band Filtering of Random Signals**—S. P. Lloyd. (PROC. IRE, vol. 48, pt. 1, p. 1167; June, 1960.) Shows that the output of a narrow-band filter is not necessarily more Gaussian than the input.

**621.372.54:621.375.13** 3023  
**Selecting RC Values for Active Filters**—R. E. Bach, Jr. (Electronics, vol. 33, pp. 82-85; May 13, 1960.) The circuit configuration described facilitates the design of filters with zero transmission at either infinite or zero frequency. Component values are determined from the symmetry of the network voltage transfer function by the technique of coefficient matching.

**621.372.6** 3024  
**Theory of a Frequency-Synthesizing Network**—B. M. Wojciechowski. (Bell Sys. Tech. J., vol. 39, pp. 649-673; May, 1960.) By the introduction of "sideband algebra" and a frequency symbolic network, a formal method of designing frequency combining and selecting circuits is developed.

**621.372.6** 3025  
**General  $n$ -Port Synthesis with Negative Resistors**—H. J. Carlin. (PROC. IRE, vol. 48, pt. 1, pp. 1174-1175; June, 1960.)

**621.373.029.6:621.385.623** 3026  
**Noise Spectrum of Phase-Locked Oscillators**—M. W. P. Strandberg. (PROC. IRE, vol. 48, pt. 1, pp. 1168-1169; June, 1960.) With phase-locking equipment for klystrons in X band and K band, it was found that the noise level was 100 db below carrier per cps.

**621.373.029.63:621.382.23** 3027  
**Voltage Tuning in Tunnel-Diode Oscillators**—J. K. Pulfer. (PROC. IRE, vol. 48, pt. 1, p. 1155; June, 1960.) A voltage tuning range of 12 per cent has been achieved.

**621.373.029.64:621.382.23** 3028  
**High-Frequency Negative-Resistance Circuit Principles for Esaki Diode Applications**—Hines. (See 3305.)

**621.373.421** 3029  
**Phase-Shift Oscillator**—E. A. Freeman. (Electronic Tech., vol. 37, pp. 276-280; July, 1960.) An analysis based on the "describing-function" method for nonlinear control systems, which takes into account the nonlinear limiting process, and allows the oscillator to be designed to give specific values of harmonic distortion.

**621.374.3** 3030  
**A Voltage-Modulated Variable Pulse-Rate Generator**—E. J. C. Fowell and A. Cowley. (Electronic Engrg., vol. 32, pp. 304-306; May, 1960.) A pulse generator is described, the output frequency of which is a linear function of the input voltage. The circuit is a screen-coupled double-phantastron pulse circulating system with suitable modifications to improve the accuracy of transfer at low output frequencies. Four output frequency ranges are provided between 5 and 2500 pulses per second. A complete circuit diagram and performance data are given.

**621.374.3** 3031  
**Achieving Stable Discriminator Levels with a Biased Input Diode**—F. S. Goulding and L. B. Robinson. (Electronics, vol. 33, pp. 89-91; May 20, 1960.) A pulse height discriminator is described which is stable to within  $\pm 1 \mu$ a at a triggering level of 50  $\mu$ a, or within  $\pm 0.4$  mv at a level of 10 mv.

- 621.374.3:621.318.435 3032  
**Counting and Timing Circuits use Saturable Reactors**—J. S. Sicko. (*Electronics*, vol. 33, pp. 61-63; May 6, 1960.) A method of frequency division using a controlled rectifier and saturable reactor are described.
- 621.374.42:621.317.61 3033  
**The Application of Phase-Locking Techniques to the Design of Apparatus for Measuring Complex Transfer Functions**—G. Thirup. (*J. Brit. IRE*, vol. 20, pp. 387-396; May, 1960.) The principles of phase-lock synchronization are described, and details of two instruments for measuring complex voltage ratios and covering the frequency ranges 1-110 Mc and 30-700 Mc are given.
- 621.375.4.018.783 3034  
**Nonlinear Distortion including Cross-Modulation in High-Frequency Transistor Stages**—M. Akçin and M. J. O. Strutt. (*Arch. elekt. Übertragung*, vol. 13, pp. 227-242; June, 1959.) Harmonic distortion and cross modulation are calculated for the earthed-base transistor treated as a nonlinear quadripole and assuming low current densities. The solutions obtained are applied to the earthed-emitter configuration and experimental results of tests on earthed-emitter circuits confirm the theory, even for relatively high collector currents. An interpretation is given of a pronounced minimum in cross modulation depth as a function of collector current.
- 621.375.9:538.569.4 3035  
**Negative L and C in Solid-State Masers**—R. L. Kyhl. (*Proc. IRE*, vol. 48, pt. 1, p. 1157; June, 1960.) Gives an equivalent circuit for a maser which includes negative L and C components.
- 621.375.9:538.569.4 3036  
**Effect of Nuclear Polarization on the Behaviour of Solid-State Masers**—G. Makhov, L. G. Cross, R. W. Terhune, and J. Lambe. (*J. Appl. Phys.*, vol. 31, pp. 936-938; May, 1960.) An account is given of experiments conducted on a ruby sample placed in a doubly resonant microwave cavity. With Bloembergen stimulation, the application of RF power to a coil around the sample produced an increase in amplifier gain, the effect being greatest at the resonance frequency of the free Al nuclei.
- 621.375.9:538.569.4.029.65/.66 3037  
**Proposed Molecular Amplifier and Coherent Generator for Millimetre and Submillimetre Waves**—W. Gordy and M. Cowan. (*J. Appl. Phys.*, vol. 31, pp. 941-942; May, 1960.) The difficulties of obtaining maser action increase with frequency owing to the increasing number of energy sublevels, and to decreasing sensitivity of molecules to field gradients. A proposed method of avoiding these difficulties is to use special types of stimulated emitter, and to separate molecules with different energy levels by a combination of inhomogeneous and homogeneous fields, respectively, outside and inside the cell.
- 621.375.9:538.569.4.029.66 3038  
**Can the Landau Levels of Free Carriers be Utilized for a Submillimetre-Wave Semiconductor Maser?**—D. Geist. (*Z. Naturforsch.*, vol. 14, p. 752; August, 1959.) The proposal of Tager and Gladun (*Zh. Eksp. i Teoret. Fiz.*, vol. 35, pp. 808-809; September, 1958) of using cyclotron resonance in semiconductors for obtaining maser action is discussed. The difficulty of having signal and pumping frequencies of the same order can be overcome with the aid of the oscillatory magneto-absorption effect.
- 621.375.9:621.372.2 3039  
**Theory of a Negative-Resistance Transmission Line Amplifier with Distributed Noise Generators**—K. K. N. Chang. (*J. Appl. Phys.*, vol. 31, pp. 871-875; May, 1960.) "A transmission line with distributed positive and negative resistances as well as with distributed noise generators is treated. Gain and noise factor are derived as a function of boundary conditions, matching conditions and distributed noise. It is found that low-noise amplification can be achieved on such a line provided the line is characterized by high gain per unit length, high total gain, good matching, and low distributed noise. A distortionless active line for such low-noise amplifiers appears attractive."
- 621.375.9:621.372.44 3040  
**Comparison of Gain, Bandwidth and Noise Figure of Variable-Reactance Amplifiers and Converters**—J. D. Pearson and J. E. Hallett. (*Proc. IEE*, vol. 107, pt. B, pp. 305-310; May, 1960.) It is shown, theoretically and experimentally, that the converter has a greater bandwidth than the amplifier for the same gain and noise figure.
- 621.375.9:621.372.44:538.221 3041  
**Theoretical Limitations to Ferromagnetic Parametric Amplifier Performance**—R. W. Damon and J. R. Eshbach. (*IRE TRANS. ON MICROWAVE THEORY AND TECHNIQUES*, vol. MTT-8, pp. 4-9; January, 1960. Abstract. *Proc. IRE*, vol. 48, p. 971; May, 1960.)
- 621.375.9:621.372.44:621.382.2 3042  
**Microwave Parametric Amplifier using Silver-Bonded Diode**—S. Kita, B. Oguchi, T. Okajima and N. Inage. (*Rep. Elect. Commun. Lab. Japan*), vol. 7, pp. 366-371; October, 1959.) A gain of 16 db and a noise figure of 5 db are realized at 6 kMc.
- 621.375.9:621.382.23 3043  
**Operation of an Esaki Diode Microwave Amplifier**—A. Yariv, J. S. Cook, and P. E. Butzien. (*Proc. IRE*, vol. 48, pt. 1, p. 1155; June, 1960.) Performance formulas and data for operation at 4.5 kMc are given.
- 621.375.9:621.382.23 3044  
**A Technique for Cascading Tunnel-Diode Amplifiers**—P. N. Chirlian. (*Proc. IRE*, vol. 48, pt. 1, p. 1156; June, 1960.) The simple tunnel-diode amplifier does not readily lend itself to cascading, but the addition of a second tunnel diode, to each stage, gives an amplifier which can be cascaded easily.
- 621.375.9.121.2:621.372.44 3045  
**An Extension of the Mode Theory to Periodically Distributed Parametric Amplifiers with Losses**—K. Kurokawa and J. Hamasaki. (*IRE TRANS. ON MICROWAVE THEORY AND TECHNIQUES*, vol. MTT-8, pp. 10-18; January, 1960. Abstract, *Proc. IRE*, vol. 48, p. 972; May, 1960.)
- 621.376.223 3046  
**Rectifier Modulators with Frequency-Selective Terminations**—D. P. Howson and D. G. Tucker. (*Proc. IEE*, vol. 107, pt. B, pp. 261-272; May, 1960. Discussion, pp. 281-284.) The effects of even-order modulation products are examined, and the conditions for the elimination of such products determined. The theory is confirmed by experimental results.
- 621.376.223 3047  
**The Input Impedance of Rectifier Modulators**—D. G. Tucker. (*Proc. IEE*, vol. 107, pt. B, pp. 273-281; Discussion, pp. 281-284.) The impedances is calculated for a number of cases of shunt, series, and ring-type modulators.
- 621.376.54:621.382.333 3048  
**A Pulse-Width Modulator**—D. C. Brown and J. E. Baughen. (*Electronic Engrg.*, vol. 32, pp. 302-303; May, 1960.) Modulation is achieved, using the hole storage effect in a junction transistor.

## GENERAL PHYSICS

- 535.215+537.533 3049  
**On the Additivity of Photocurrent and Secondary-Electron Current**—E. Brinkmann and H. Deichsel. (*Z. Phys.*, vol. 156, pp. 159-162; September 10, 1959.) Measurements on Al provide confirmation of the existence of additivity as asserted by Ekertova (2401 of 1957) and contrary to the findings of Dember (*Z. Phys.*, vol. 33, no. 7, pp. 529-532; 1925) which may have been affected by an internal photoeffect in the oxide layer of the target.
- 537.311.31 3050  
**Nonlocal Current/Field Relationship in Metals**—J. L. Warren and R. A. Ferrell. (*Phys. Rev.*, vol. 117, pp. 1252-1256; March 1, 1960.) Chambers' analysis of the response of the conduction electrons in a metal to an internal electric field is extended to cover the case of longitudinal fields.
- 537.311.33 3051  
**The Theory of Elementary Excitations in Atomic Semiconductors**—A. G. Samoilovich and S. L. Korolyuk. (*Fiz. Tverdogo Tela*, vol. 1, pp. 1592-1599; October, 1959.) The simplest model of an atomic semiconductor is considered, in which every atom has a saturated valence shell with two electrons. Electrons, holes, ortho- and para-excitons are considered as elementary excitations, and the Hamiltonian describing the system is derived taking account of interaction between them.
- 537.525 3052  
**Charge-Localization on the Surface of Oxide-Coated Cathodes**—B. J. Hopkins and F. A. Vick. (*Brit. J. Appl. Phys.*, vol. 11, pp. 223-227; June, 1960.) Anomalous results obtained while using the Kelvin method of determining contact potential differences [see 2295 of July (Davies and Hopkins)] are investigated. Very high contact potential differences which occur, only after the passage of a discharge, are attributed to both positive ions and electrons which remain on the oxide surface for long periods; depending on the conductivity of the oxide.
- 537.56 3053  
**Plasma Stability and Boundary Conditions**—F. C. Hoh. (*Phys. Rev. Lett.*, vol. 4, pp. 559-561; June 1, 1960.)
- 537.56 3054  
**An Approximate Solution of a Problem concerning the Motion of a Conducting Plasma**—G. A. Skuridin and K. P. Stanyukovich. (*Dokl. Akad. Nauk SSSR*, vol. 130, pp. 1248-1251; February 21, 1960.) A new method for the asymptotic integration of linear differential equations with partial derivatives of the hyperbolic type has been applied to the integration of equations of plasma oscillations.
- 537.56:537.533 3055  
**Theory of Electron Oscillations in Nonuniform Plasmas**—M. Sumi. (*J. Phys. Soc. Japan*, vol. 15, pp. 120-127; January, 1960.) Deals with the case of an externally injected electron beam in a plasma.
- 537.56:538.56 3056  
**Excitation of Plasma Oscillations**—P. A. Sturrock. (*Phys. Rev.*, vol. 117, pp. 1426-1429; March 5, 1960.) The apparent paradox between the theory of Bohm and Gross (88 of 1950) and

the experiments of Looney and Brown (2371 of 1954) on the excitation of plasma oscillations by the two-stream mechanism is resolved.

537.56:538.566 3057

**Experimental Two-Beam Excitation of Electron Oscillations in a Plasma without Sheaths**—M. J. Kofoed. (*Phys. Rev. Lett.*, vol. 4, pp. 556–557; June 1, 1960.) Coherent standing waves of longitudinal electron oscillations have been excited in a plasma by two independent, oppositely directed electron beams, whose axes coincided. There were no sheaths on the electrodes from which the electron stream entered the plasma. Results of single-beam experiments [e.g., 2371 of 1954 (Looney and Brown)] using either equal or unequal sheaths are verified.

537.56:538.569.4.029.64 3058

**Influence of Negative Ions on Ambipolar Diffusion of Electrons**—H. J. Oskam and V. R. Mittlestadt. (*J. Appl. Phys.*, vol. 31, pp. 940–941; May, 1960.) A note on microwave measurements of the afterglow properties of plasmas in Ne-Ar mixtures. See 2203 of 1959 (Oskam).

538.566 + 534.2 3059

**Propagation of Acoustic and Electromagnetic Waves in a Half-Space**—M. D. Khaskind. (*Akust. Zh.*, vol. 5, pp. 464–471; 1959.) A half-space is considered, in which the impedance at the boundary is given in the form of an arbitrary complex number, and a general solution of the wave equation is formulated by introducing a function which reverts to zero at the boundary. Expressions for the acoustic and em potential are derived in terms of this function.

538.566:535.42 3060

**The Diffraction at Apertures in Nonplanar Screens**—W. Braunbek. (*Z. Phys.*, vol. 156, No. 1, pp. 66–77; August 24, 1959.) The approximation method, given in 2183 of 1950, is applied to the case of a circular aperture in a funnel shaped screen for a scalar plane wave, and for an em plane wave propagating in the axial direction.

538.566:535.42 3061

**Diffraction of Electromagnetic Waves according to Braunbek's Approximation**—W. E. Frahn. (*Z. Phys.*, vol. 156, pp. 78–98 and 99–116; August 24 and September 10, 1959.) Braunbek's approximation method (2183 of 1950) is applied to problems of em wave diffraction, in particular to that of a linearly polarized plane wave normally incident on a circular aperture in a perfectly conducting plane screen and on a perfectly conducting plane circular disk. The near-field distribution is calculated and compared with results of the rigorous method of solution and of Kirchhoff's approximation. Other approximation methods are discussed.

538.566:535.42 3062

**Diffraction by a Unidirectionally Conducting Half-Plane**—R. A. Hurd. (*Canad. J. Phys.*, vol. 38, pp. 168–175; February, 1960.) A solution is obtained by transform methods for diffraction of a plane em wave.

538.566:535.43 + 534.26] 3063

**Second Approximation in the Method of Small Perturbations**—T. A. Shirokova. (*Akust. Zh.*, vol. 5, no. 4, pp. 485–489; 1959.) The propagation of a plane wave in a medium containing random inhomogeneities is considered. A second approximation in the perturbation method is obtained by assuming that the correlation coefficient of refractive-index fluctuations is Gaussian. This is applied to determine the form of the normalizing factor in the wave equation.

538.566:535.43 + 534.26] 3064

**The Scattering of a Plane Wave by a Row of Small Cylinders**—Millar. (See 2969.)

538.566:537.56 3065

**Variational Method for the Propagation of Electromagnetic Waves in a Plasma**—L. Garbarre and L. Cairó. [*Compt. rend. acad. sci. (Paris)*], vol. 249, pp. 1750–1752; November 2, 1959.) Using a variation principle, a first approximation is obtained for the propagation constant of the TE<sub>10</sub> mode in a rectangular waveguide containing a thin layer of gyroelectric plasma.

538.567:621.375.9 3066

**Action of a Progressive Disturbance on a Guided Electromagnetic Wave**—J. C. Simon. (*IRE TRANS. ON MICROWAVE THEORY AND TECHNIQUES*, vol. MTT-8, pp. 18–29; January, 1960.) A method of approximations is applied to the investigation of the modes of action of a medium on a guided em wave. The results are discussed in relation to parametric amplification.

538.569.4 3067

**The Relation between the Polarization and the Magnetic Field Intensity in the Exciton Absorption Region**—A. F. Lubchenko. (*Fiz. Tverdogo Tela*, vol. 1, pp. 709–718; May, 1959.) Extension of Pekar's electromagnetic wave theory (3058 of 1958) to molecular crystals with a weak interaction between the exciton and the lattice vibrations.

539.2:538.2 3068

**Giant Spin Density Waves**—A. W. Overhauser. (*Phys. Rev. Lett.*, vol. 4, pp. 462–465; May 1, 1960.) An analytical treatment of energy states in an electron gas in which the lowest energy state is proved not to be the Hartree-Fock ground state but to have a spiral antiferromagnetic structure. Implications of this are discussed.

#### GEOPHYSICAL AND EXTRA-TERRESTRIAL PHENOMENA

523.152.3 + 551.510.536 3069

**Interplanetary Space and the Earth's Outermost Atmosphere**—S. Chapman. [*Proc. Roy. Soc. (London) A*], vol. 253, pp. 462–481; December 29, 1959.] See also 491 of February, 59 references.

523.164:061.3 3070

**Radar Astronomy Symposium Reports**—R. L. Leadabrand. (*J. Geophys. Res.*, vol. 65, pp. 1103–1118; April, 1960.) The subjects discussed were radar studies of the moon, the planets, the sun, meteors and auroras, and the exosphere and interplanetary medium.

523.164:551.507.362.2 3071

**Radio Astronomical Measurements from Earth Satellites**—A. C. B. Lovell. [*Proc. Roy. Soc. (London) A*], vol. 253, pp. 494–500; December 29, 1959.] Ionospheric and atmospheric absorption limit measurements made on earth. A summary is given of some of the problems whose solution can best be sought by measurements with apparatus mounted in earth satellites.

523.164.3 3072

**Polarization and Angular Extent of the 960-Mc/s Radiation from Jupiter**—V. Radhakrishnan and J. A. Roberts. (*Phys. Rev. Lett.*, vol. 4, pp. 493–494, May 15, 1960.) It is found that the source is strongly linearly polarized, especially in the outer regions, which extend to about three times the diameter of the planet.

523.164.32 3073

**On the Polarization of Sources of Solar Activity on 3 cm Wavelength**—M. R. Kundu

and J. L. Steinberg. (*J. Inst. Telecommun. Engrs, India*, vol. 6, pp. 23–30; December, 1959.) About 60 per cent of the bursts observed were polarized, the probability of observing a polarized burst being greater when the source had a small diameter. Great bursts associated with meter-wave bursts of type IV have been found in most cases to be polarized. For a description of the high-resolution interferometer used, and earlier results, see 2733 of 1957 (Alon, et al.).

523.164.32:523.165 3074

**Solar Radio Bursts and Cosmic Rays**—A. R. Thompson and A. Maxwell. (*Planetary Space Sci.*, vol. 2, pp. 104–109; April, 1960.) The correlations between the various types of bursts are discussed.

523.164.32:551.594.6 3075

**Periodicities in Solar Radio Noise Emission**—N. C. Gerson. (*Australian J. Phys.*, vol. 12, pp. 299–300; September, 1959.) Attention is drawn to the presence of sweeper trains [1625 of May (Gerson and Gossard)] in the work of Roberts (102 of 1959).

523.165 3076

**On the Theory of Protons Trapped in the Earth's Magnetic Field**—E. C. Ray. (*J. Geophys. Res.*, vol. 65, pp. 1125–1134; April, 1960.)

523.165 3077

**The Unusual Cosmic-Ray Events of July 17–18 1959**—B. G. Wilson, D. C. Rose, and M. A. Pomerantz. (*Canad. J. Phys.*, vol. 38, pp. 328–331; February, 1960.) Intensity variations recorded at six stations are discussed. See 475 of February (Carnichael and Steljes).

523.165:621.391.812.63 3078

**The Cosmic-Ray Increase of 17 July 1959**—D. K. Bailey and M. A. Pomerantz. (*Canad. J. Phys.*, vol. 38, pp. 332–333; February, 1960.) Variations in the intensity of ionospheric-scatter signals for the paths Iceland–England and Massachusetts–Labrador at about 38 Mc are plotted. Decreases in intensity starting at 0300 and 0800 UT indicate a large excess of ionizing particles with rigidities above geomagnetic cutoff at the path mid-points.

523.3:621.396.96 3079

**Roughness of the Moon as a Radar Reflector**—V. A. Hughes. (*Nature*, vol. 186, pp. 873–874; June 11, 1960.) Measurements have been made at a wavelength of 10 cm and pulse duration of 5  $\mu$ sec of the angular scattering properties of the moon's surface. From the results, a law of scattering has been obtained which is consistent with scattering from a rough surface which has irregularities much greater than a wavelength and a horizontal scale equivalent to about twenty times the vertical deviations.

523.5 3080

**Electric Discharges caused by Meteorites Moving in the Earth's Atmosphere**—V. P. Dokuchaev. (*Dokl. Akad. Nauk SSSR*, vol. 131, pp. 78–81; March 1, 1960.) The passage of meteorites through the atmosphere is followed by the formation of a trail of ionized gas about 10 km long and 5 meters in radius. Meteorites of the fifth magnitude have electron concentrations of about  $10^9/\text{cm}^3$  compared with  $2.5 \times 10^5/\text{cm}^3$  at the maximum of the E layer. The luminosity of the meteorite is attributed to a corona discharge in the front of the trail, and in the case of bright meteorites in strong electric fields, this discharge becomes a spark discharge of the lightning type.

550.385:550.375 3081

**Relations between the Electric and Magnetic Fields of Very Long Period Induced in a Medium of Variable Conductivity**—L. Bossy

- and A. De Vuyst. (*Geofs. pura appl.*, vol. 44, pp. 119-134; September-December, 1959. In French.) A model of ground conductivity distribution is derived which closely represents the conditions indicated by observations of geomagnetic and geoelectric pulsations [see also 1642 of 1955 (Scholte and Veldkamp)].
- 550.385.4:523.164** **3082**  
**Magnetic Storms and Cosmic Radio Noise on 25 Mc/s at Ahmedabad (23°02'N: 172°38'E)**—R. V. Bhonsle and K. R. Ramanathan. (*Planetary Space Sci.*, vol. 2, pp. 99-103; April, 1960.) In addition to changes in absorption caused by the D layer, and to the proximity of the F<sub>2</sub>-layer critical frequency, a storm-time variation was found the magnitude of which depends on local time.
- 550.385.4:523.75** **3083**  
**Solar Terrestrial Relationships**—K. D. Cole. (*Nature*, vol. 186, p. 874; June 11, 1960.) A note on the proton density in interplanetary space required to explain geomagnetic disturbances in terms of the hydro-magnetic-wave theory (2305 of July).
- 550.389.2** **3084**  
**Some Radio Aspects of the International Geophysical Year**—R. L. Smith-Rose. (*R.S.G.B. Bull.*, vol. 35, pp. 392-394; March, 1960.) A brief review of the results of investigations into long-distance radio propagation, polar regions of the ionosphere and rocket and satellite measurements of electron density in the upper atmosphere.
- 550.389.2:621.391.81** **3085**  
**Amateur Radio Participation in the I.G.Y.**—G. M. C. Stone. (*R.S.G.B. Bull.*, vol. 35, pp. 395-397; March, 1960.) Outline of the U.K. amateur program and a brief report of some results obtained from studies of auroral propagation in the 144-Mc sec band.
- 551.507.362.1:523.165** **3086**  
**Radiation Measurement during the Flight of the Second Cosmic Rocket**—S. N. Vernov, A. E. Chudakov, P. V. Vakulov, Yu. I. Logachev and A. G. Nikolaev. (*Dokl. Akad. Nauk SSSR*, vol. 130, pp. 517-520; January 21, 1960.) The equipment used consisted of six gas discharge counters and four scintillation counters. Measurements were carried out between 9000 and 120,000 km from the center of the earth and 40,000 km from the surface of the moon. Graphs show the trajectories of the first and second rocket in the earth's magnetic field. The space location of the radiation belt is examined, and the dependence of the radiation intensity on the distance from the earth considered. Maximum intensities were observed at 17,000 km and 27,000 km from the center of the earth. Electron beams of energies 20-50 keV were recorded with 10<sup>9</sup> particles 1 cm<sup>2</sup> sec. No increase in radiation was observed near the moon.
- 551.507.362.2** **3087**  
**Motion of a Satellite in the Earth's Gravitational Field**—G. V. Groves. [*Proc. Roy. Soc. (London) A*, vol. 254, pp. 48-65; January 19, 1960.] The equations of motion of a satellite are given in a general form taking account of the precession and nutation of the earth.
- 551.507.362.2** **3088**  
**Secular and Periodic Motions of the Node of an Artificial Earth Satellite**—L. Blitzer and D. G. King-Hele. (*Nature*, vol. 186, pp. 874-875; June 11, 1960.) Comment on 2233 of 1959, and author's reply.
- 551.507.362.2** **3089**  
**Analysis of the Orbits of the Russian Satellites**—D. G. King-Hele. [*Proc. Roy. Soc. (London) A*, vol. 253, pp. 529-538; December 29, 1959.] An analysis of orbital data for 1957β and 1958δ. See also 2723 of August (King-Hele and Walker) and back references.
- 551.507.362.2:523.165** **3090**  
**Experiments on Cosmic Radiation by means of Artificial Satellites**—C. F. Powell. [*Proc. Roy. Soc. (London) A*, vol. 253, pp. 482-487; December 29, 1959.] A review.
- 551.507.362.2:523.165** **3091**  
**Radiation Information from 1958δ**—R. P. Basler, R. N. DeWitt, and G. C. Reid. (*J. Geophys. Res.*, vol. 65, pp. 1135-1138; April, 1960.) The data indicate that the radiation intensity varies with altitude between heights of 250 and 500 km.
- 551.507.362.2:523.165** **3092**  
**Corpuscular Radiation Experiment of Satellite 1960 Iota (Explorer VII)**—G. H. Ludwig and W. A. Whelpley. (*J. Geophys. Res.*, vol. 65, pp. 1119-1124; April, 1960.) The equipment, including the calibration of the detectors, and the telemetry code are described, and samples of recordings are shown. International participation in recording the signals is invited.
- 551.507.362.2:551.510.535** **3093**  
**The Determination of Ionospheric Electron Content and Distribution from Satellite Observations: Parts 1 & 2**—O. K. Garriott. (*J. Geophys. Res.*, vol. 65, pp. 1139-1157; April, 1960.) The theory of the determination is given for measurements of total rotation of angle of polarization and also of its rate of rotation. Modifications to the simple theory, and sources of errors, are discussed. Observations made using Sputnik III have disclosed a diurnal variation in total electron content and data relating to the proportion of the total content which lies below the F<sub>2</sub> layer peak. The effect of magnetic disturbances is described.
- 551.510.52:551.510.62** **3094**  
**Statistical Consideration of the Structure of Atmospheric Refractive Index**—S. Ugai. (*Rep. Elec. Commun. Lab., Japan*, vol. 7, pp. 253-289; August, 1959.) Long-term meteorological measurements from a 300-meter tower and from radiosondes have been analyzed. Results show that the average gradient  $\alpha$  of an atmospheric layer  $\Delta H$  meters thick follows a normal distribution. Twice-daily measurements of  $\alpha$  are sufficient to represent statistically the mean monthly values of  $\alpha$  and the standard deviation  $\sigma\alpha$ . The vertical gradient of refractive index may be calculated from the expression  $\sigma\alpha^2\Delta H \approx \text{constant}$ .
- 551.510.535** **3095**  
**Artificial Electron Clouds: Part 5**—F. F. Marmo, J. Pressman, E. R. Manning, and L. Aschenbrand. (*Planetary Space Sci.*, vol. 2, pp. 174-186; April, 1960.) Values have been derived for diffusion coefficients, chemical yield, thermal ionization efficiency and wind velocity and shear. Part 4: 2732 of August (Pressman, et al.).
- 551.510.535** **3096**  
**The Origin of Nitrogen Ionization in the Upper Atmosphere**—J. W. Chamberlain and C. Sagan. (*Planetary Space Sci.*, vol. 2, pp. 157-164; April, 1960.)
- 551.510.535** **3097**  
**Some Problems concerning the Terrestrial Atmosphere above about the 100-km Level**—D. R. Bates. [*Proc. Roy. Soc. (London) A*, vol. 253, pp. 451-462; December 29, 1959.] Rocket and satellite data are considered in a survey concerned with the general structure of the thermosphere.
- 551.510.535** **3098**  
**Measurement of Positive Ion Density in the Ionosphere**—T. Ichimiya, K. Takayama, and Y. Aono. (*Rep. Ionos. Space Res. Japan*, vol. 13, pp. 155-176; September, 1959.) The design of a suitable rocket-borne probe is discussed, and a small meshed spherical type is adopted. Laboratory experiments designed to investigate the characteristics of such a probe are described.
- 551.510.535** **3099**  
**Vertical Transport of Electrons in the F Region of the Ionosphere**—S. Chandra, J. J. Gibbons, and E. R. Schmerling. (*J. Geophys. Res.*, vol. 64, pp. 1159-1175; April, 1960.) An expression is developed for the velocity, and can be evaluated using  $N(h)$  profiles. The results for equatorial stations show that the velocity is mainly downwards at night and upwards by day, and is roughly 25 meters/sec. The velocities agree with those deduced by  $S_q$  data using the dynamo theory.
- 551.510.535** **3100**  
**On the Question of the "Continental Effect," of the F<sub>2</sub> Layer**—R. Eyfrig. (*Geofs. pura appl.*, vol. 44, pp. 179-187; September-December, 1959. In German.) Analysis of  $f_0F_2$  data indicates an increase in daytime ionization during the summer months observed by USSR stations in Central Asia compared with data obtained by West European stations. The evening rise in  $f_0F_2$  appears much less pronounced for stations in Central Asia where the maximum usually occurs at local noon. This "continental effect" causes difficulties in the interpolation required for the preparation of MUF charts.
- 551.510.535** **3101**  
**Further Studies of "Spread-F" at Brisbane: Parts 1 & 2**—G. G. Bowman. (*Planetary Space Sci.*, vol. 2, pp. 133-156, April, 1960.) Vertical-incidence ionograms and directional measurements on oblique-incidence signals indicate that the spread F phenomenon is caused by large ripples with a wavelength of 20 to over 100 km. Seasonal and sunspot variations in the phenomenon are described. Model ionization distributions are constructed and ray paths drawn which may explain various types of spread F. The amplitude of the ripples seems to increase with the height of the F<sub>2</sub> layer. See also 119 of 1957 (McNicol, et al.).
- 551.510.535:523.164** **3102**  
**Ionospheric Absorption Investigations at Hawaii and Johnston Island**—A. Frederiksen and R. B. Dyce. (*J. Geophys. Res.*, vol. 65, pp. 1177-1181; April, 1960.) The absorption of cosmic noise at 30 mc varies in such a way as to suggest that the patches of absorption are less than 1000 km in size. The variations are not correlated with the spread F or with the sporadic E phenomena, but are correlated with  $f_0F_2$  suggesting partial reflection of the cosmic noise by the F<sub>2</sub> layer.
- 621.391.812.63:551.510.535** **3103**  
**Radio Wave Propagation Characteristics of a Simple Ionospheric Model based on Rocket Data**—Zhekulin. (See 3244.)
- 551.510.535:621.391.812.63** **3104**  
**The Reflexion of Radio Waves from a Stratified Ionosphere Modified by Weak Irregularities: Part 2**—Pittewar. (See 3245.)
- 551.510.535(98)** **3105**  
**Entry of High-Energy Particles into the Polar Ionosphere**—T. Obayashi. (*Rep. Ionos. Space Res. Japan*, vol. 13, pp. 201-219; September, 1959.) Shortened version of 2376 of July (Obayashi and Hakura).

- 551.510.535(98) 3106  
**The Height of F-Layer Irregularities in the Arctic Ionosphere**—H. F. Bates. (*J. Geophys. Res.*, vol. 65, p. 1304; April, 1960.) Correction to 515 of February.
- 551.510.536 3107  
**The Exploration of the Terrestrial Exosphere**—H. K. Paetzold. (*Z. angew. Phys.*, vol. 11, pp. 234–243; June, 1959.) A review of scientific investigations of the composition and structure of the exosphere dealing particularly with the observation of whistlers, and with results obtained from satellite and rocket measurements. 53 references.
- 551.510.536:523.165 3108  
**Properties of the Upper Atmosphere and their Relation to the Radiation Belts of the Earth**—S. F. Singer. (*Planetary Space Sci.*, vol. 2, pp. 165–173; April, 1960.) A new theory which gives the distribution of density with altitude for a planetary exosphere in the absence of thermodynamic equilibrium is outlined. The results differ considerably from those based on a hydrostatic equation.
- 551.594.2 3109  
**A Comparison of Intracloud and Cloud-to-Ground Lightning Discharges**—N. Kitagawa and M. Brook (*J. Geophys. Res.*, vol. 65, pp. 1189–1201; April, 1960.) Experimental results are discussed together with possible discharge mechanisms.
- 551.594.6:551.594.5 3110  
**Atmospherics on 20 kc/s at the Time of Local Aurorae**—E. Gherzi. (*Nature*, vol. 187, pp. 225–226; July 16, 1960.) Atmospherics have been recorded on each of the 30 occasions when a strong aurora has been observed. This enhancement is attributed to reflections from ionized strips associated with the auroras.
- LOCATION AND AIDS TO NAVIGATION**
- 621.396.962.3 3111  
**Precision Tracking with Monopulse Radar**—J. H. Dunn and D. D. Howard. (*Electronics*, vol. 33, pp. 51–56, April 22, 1960.) The principles of monopulse operation are explained, and its performance is compared with that of the conical-scan and sequential-lobing radar systems. See 1240 of April (Rhodes).
- MATERIALS AND SUBSIDIARY TECHNIQUES**
- 531.788.7 3112  
**Modulated Bayard-Alpert Gauge**—P. A. Redhead. (*Rev. Sci. Instr.*, vol. 31, pp. 343–344; March, 1960.) The true positive ion current at low pressures can be measured with the gauge to an accuracy within  $\pm 5$  per cent.
- 535.215:537.311.33 3113  
**Influence of Transverse Modes on Photoconductive Decay in Filaments**—J. S. Blake-more and K. C. Nomura. (*J. Appl. Phys.*, vol. 31, pp. 753–761; May, 1960.) The influence of high-order modes on excess-carrier decay in a semiconducting filament is discussed. Calculations show that, for typical generative procedures, the increased recombination rate is more serious than formerly supposed.
- 535.215:538.569.4 3114  
**Paramagnetic Resonance Detection of Trapping in a Photoconductor**—R. S. Title. (*Phys. Rev. Lett.*, vol. 4, pp. 502–503; May 15, 1960.) Experiments are described on trapping effects, luminescence, and photoconductivity in a sample of ZnS containing Gd. A proposed model for the structure is consistent with the observed effects.
- 535.215:546.47'48'221 3115  
**Photoconductivity of CdZnS Mixed Crystal**—M. Kikuchi and S. Iizima. (*J. Phys. Soc. Japan*, vol. 15, p. 357; February, 1960.) The energy-band gap is shown to be varied continuously and arbitrarily by adding ZnS to CdS.
- 535.215:546.48'221 3116  
**The Refractive Index of Cadmium Sulphide**—H. Gobrecht and A. Bartschat. (*Z. Phys.*, vol. 156, pp. 131–143; September 10, 1959.) Report of measurements of refractive index on CdS single crystals, 20–70  $\mu$  thick, for the extraordinary and ordinary rays in the wavelength range 5100–6500 Å at room temperature, and 4900–6500 Å at  $-180^\circ\text{C}$ . The influence of lattice disturbances on the refractive index is discussed.
- 535.215:546.48'221 3117  
**Photovoltaic Effects in CdS Crystals**—H. Kallmann, B. Kramer, J. Shain, and G. M. Spruch. (*Phys. Rev.*, vol. 117, pp. 1482–1486; March 15, 1960.) Photovoltages were obtained in CdS with inhomogeneous excitation. The effects were studied using different electrode arrangements.
- 535.215:546.48'221 3118  
**Electric-Field-Induced Light Absorption in CdS**—R. Williams. (*Phys. Rev.*, vol. 117, pp. 1487–1490; March 15, 1960.)
- 535.215:546.48'221 3119  
**Thermal Stability of Carbon Electrodes in Contact with Crystalline Layers of Cadmium Sulphide**—M. H. Boisot, G. Cohen-Solal, and F. Teissier du Gros. [*Compt. rend. acad. sci. (Paris)*], vol. 249, pp. 2184–2186; November 23, 1959.)
- 535.215:546.87:538.63 3120  
**Photoelectromagnetic Effect in Bismuth**—T. Young. (*Phys. Rev.*, vol. 117, p. 1244; March 1, 1960.) The photoelectromagnetic effect has been observed in Bi, and its dependence on the wavelength of the incident light and the magnetic field strength investigated.
- 535.37 3121  
**Vanadium-Activated Zinc and Cadmium Sulphide and Selenide Phosphors**—M. Avinor and G. Meijer. (*J. Phys. Chem. Solids*, vol. 12, pp. 211–215; February, 1960.) Vanadium activated ZnS, ZnSe, CdS and CdSe powders show a fluorescence at about  $2\mu$ . Addition of Cu and Ag as auxiliary activators enhances the vanadium emission without Cu and Ag emissions appearing.
- 535.37:546.281'26 3122  
**Polarized Edge Emission of SiC**—W. J. Choyke, D. R. Hamilton, and L. Patrick. (*Phys. Rev.*, vol. 117, pp. 1430–1438; March 15, 1960.) Mechanisms for producing polarized light are discussed; the most probable luminescence centers are donor-acceptor pairs.
- 535.37:546.281'26 3123  
**Polarization of the Luminescence of Donor-Acceptor Pairs**—L. Patrick. (*Phys. Rev.*, vol. 117, pp. 1439–1441; March 15, 1960.) The polarization is calculated for SiC. Certain degrees of polarization can be used to distinguish between donor-acceptor pairs and the iron group elements.
- 535.376:546.47'221 3124  
**Electroluminescence in Zinc Sulphide Single Crystals**—S. Narita. (*J. Phys. Soc. Japan*, vol. 15, pp. 128–135; January, 1960.) Experimental and theoretical investigation of the brightness waves and infrared quenching of electroluminescence of ZnS doped with Cu and Cl under pulse excitation.
- 537.226:621.319.2 3125  
**The Effect of an Alternating Electric Field on the Forming of Electrets**—F. I. Polovikov. (*Fiz. Tverdogo Tela*, vol. 1, pp. 783–788; May, 1959.) Treatment of the dielectric in an alternating and then in a constant field often results in an increase in stability of the polarized state and sometimes in a change in the direction of polarization.
- 537.226:621.396.677.85 3126  
**Microwave Properties of Metal-Flake Artificial Dielectrics**—Kishinaji and S. Swarup. (*J. Inst. Telecommun. Engrs., India*, vol. 6, pp. 38–46; December, 1959.)
- 537.227 3127  
**Dielectric Polarization of a Number of Complex Compounds**—G. A. Smolenskii and A. I. Agranovskaya. (*Fiz. Tverdogo Tela*, vol. 1, pp. 1562–1572; October, 1959.) The possibility of predicting the formation of complex compounds is considered with reference to oxygen compounds with perovskite structure. Experimental data on various synthesized polycrystalline materials are given including  $\text{PbNiNb}_2\text{O}_9$  and  $\text{Pb}_3\text{MgNb}_2\text{O}_9$ , which have a very high permittivity; the latter is piezoelectric.
- 537.227 3128  
**Ferroelectric Substitutional-Defect Solid Solutions**—G. A. Smolenskii, V. A. Supov, and A. I. Agranovskaya. (*Fiz. Tverdogo Tela*, vol. 1, pp. 1573–1582; October, 1959.) The solid solutions investigated can be classified in two groups according to the permittivity maximum at the Curie point is (a) retained, or (b) decreased, or increasing the concentration of the second component.
- 537.227 3129  
**Pyroelectricity, Internal Domains, and Interface Charges in Triglycine Sulphate**—A. G. Chynoweth. (*Phys. Rev.*, vol. 117, pp. 1235–1243; March 1, 1960.)
- 537.227 3130  
**Ferroelectric Transition in Rubidium Bisulphate**—R. Pepinsky and K. Vedam. (*Phys. Rev.*, vol. 117, pp. 1502–1503; March 15, 1960.)
- 537.227:546.431'824-31 3131  
**General Properties of Titanates of Barium near Stoichiometric Composition**—G. Lapluye, G. Morinet, and P. Palla. [*Compt. rend. acad. sci. (Paris)*], vol. 249, pp. 2172–2174; November 13, 1959.] Different ceramics with  $\text{TiO}_2/\text{BaO}$  ratio in the range 0.83–1.2 have been prepared from high-purity material; their principal dielectric and ferroelectric properties are given.
- 537.227:546.431'824-31 3132  
**Mechanism for the Sidewise Motion of  $180^\circ$  Domain Walls in Barium Titanate**—R. C. Miller and G. Weinreich. (*Phys. Rev.*, vol. 117, pp. 1460–1466; March 15, 1960.) Two possible mechanisms for the wall motion are discussed, one of which is shown to agree with experimental data.
- 537.227:547.476.3:539.12.04 3133  
**Some Properties of X-Ray-Damaged Rochelle Salt**—K. Okada. (*J. Phys. Soc. Japan*, vol. 15, pp. 363–364; February, 1960.)
- 537.228.1:534.133 3134  
**Infrared and Low-Temperature Acoustic Absorption in Synthetic Quartz**—J. C. King, D. L. Wood, and D. M. Dodd. (*Phys. Rev. Lett.*, vol. 4, pp. 500–501; May 15, 1960.)
- 537.228.1:534.133:538.566.029.64 3135  
**Excitation and Attenuation of Hypersonic Waves in Quartz**—H. E. Bömmel and K. Dransfeld. (*Phys. Rev.*, vol. 117, pp. 1245–1252; March 1, 1960.) Description of the technique of

generation and measurements of absorption of acoustic waves at frequencies above 1 kMc.

537.228.1:535.215 3136

**Piezoelectricity and Conductivity in ZnO and CdS**—A. R. Hutson. (*Phys. Rev. Lett.*, vol. 4, pp. 505-507; May 15, 1960.) The results of measurements of piezoelectric constants are given. They show that ZnO and CdS have electromechanical coupling constants much greater than that of quartz. Data on the piezoelectric scattering mobility are given and discussed.

537.311.31 + 535.376]:539.12.04 3137

**The Generation of Extremely High Lattice-Defect Concentrations by the Irradiation of Solids in Reactors**—N. Riehl and R. Sizmann. (*Z. angew. Phys.*, vol. 11, pp. 202-207; June, 1959.) Investigations were made on Cu foil and on a ZnS film whose luminescence properties were completely destroyed by radiation.

537.311.33 3138

**Theory of the Energy Levels of Donor-Acceptor Pairs**—F. E. Williams. (*J. Phys. Chem. Solids*, vol. 12, pp. 265-275; February, 1960.) An analysis in which the separate donors and acceptors are taken as point positive and negative charges which are bound by Coulomb forces to an electron and a positive hole, respectively. The theory is in qualitative agreement with experimental results for ZnS containing Group IIIB donors and Group IB acceptors.

537.311.33 3139

**Disintegration of an Exciton by Phonons in Atomic Semiconductors**—A. A. Lipnik. (*Fiz. Tverdого Tela*, vol. 1, pp. 726-733; May, 1959.) The probability of the disintegration of Mott's exciton into an electron and a hole is calculated and compared with the scattering probability.

537.311.33 3140

**The Recombination of Charge Carriers in Semiconductors for a Large Concentration of Traps**—V. D. Egorov. (*Fiz. Tverdого Tela*, vol. 1, pp. 832-833; May, 1959.)

537.311.33 3141

**The Determination of Effective Carrier Masses and Optical Constants of Semiconductors**—V. P. Silin. (*Fiz. Tverdого Tela*, vol. 1, pp. 705-708; May, 1959.) An application of Fermi fluid theory for the case of spherical Fermi surfaces to the determination of semiconductor characteristics.

537.311.33 3142

**Diffusion and Recombination during Measurements of Drift Mobility**—V. N. Dobrovolskii. (*Fiz. Tverdого Tela*, vol. 1, pp. 719-725; May, 1959.) The applicability of a simplified formula for calculating mobility in the case of one-, two-, and three-dimensional propagation of carriers is considered. The criterion formulated is checked experimentally.

537.311.33 3143

**Intervalley Scattering of Hot Electrons**—M. Shibuya and W. Sasaki. (*J. Phys. Soc. Japan*, vol. 15, pp. 207-208; January, 1960.) The results of a theoretical treatment of the problem are given and are compared with experimental data; in particular, for drift velocity.

537.311.33 3144

**Surface Conductivity allowing for the Scattering of Charge Carriers at the Surface with Slight Band Distortions**—H. Plietner. [*Ann. Phys. (Leipzig)*, vol. 3, pp. 396-413; July 2, 1959.] The conductivity of space-charge boundary layers parallel to the surface of a semiconductor, allowing for slight band distortion such as arises under field-effect conditions, is calculated. Curves of electron and hole

mobility and surface conductivity as a function of band distortion are plotted for Ge.

537.311.33 3145

**Direct Observation of Polarons and Phonons during Tunnelling in Groups III-V Semiconductor Junctions**—R. N. Hall, J. H. Racette, and H. Ehrenreich. (*Phys. Rev. Lett.*, vol. 4, pp. 456-458; May 1, 1960.) Conductive curves plotted as a function of bias voltage for a number of junctions at 4.2°K show distinct minima in the neighborhood of zero voltage, and further changes of slope at higher voltages. These measurements permit a direct experimental determination of the polar electron-phonon coupling constant, and the results imply that the tunnelling process takes place in a time short compared with the lattice relaxation time.

537.311.33 3146

**Investigation and Properties of the System AgSbTe<sub>2</sub>-PbTe**—H. Rodot. [*Compt. rend. acad. sci. (Paris)*, vol. 249, pp. 1872-1874; November 9, 1959.]

537.311.33:535.215 3147

**Theory of Current-Carrier Transport and Photoconductivity in Semiconductors with Trapping**—W. van Roosbroeck. (*Bell Sys. Tech. J.*, vol. 39, pp. 515-613; May, 1960.) Fundamental differential equations are derived taking into account diffusion, drift, recombination, and trapping. The general ambipolar theory is applied to investigate trapping in various connections. The theory and application of diffusion lengths, lifetime functions, the photomagnetic-electric effect, and photoconductivity are studied. 94 references.

537.311.33:535.215 3148

**The Determination of Doping Gradients from the Photo-e.m.f. and Photoconductivity of Semiconductors**—M. Zerbst and G. Winstel. (*Z. Naturforsch.*, vol. 14a, pp. 754-755; August, 1959.) Changes of impurity concentration along a specimen can be determined from measurements of photo-EMF and photoconductivity. Results obtained in this way are compared with those of conductivity measurements and good agreement is found.

537.311.33:535.215:539.23 3149

**Properties and Structure of Ternary Semiconductor Systems: Part 4—Electric and Photoelectric Properties of Films of the Sb<sub>2</sub>S<sub>3</sub>-Bi<sub>2</sub>S<sub>3</sub> System**—B. T. Kolomiets and V. M. Lyubin. (*Fiz. Tverdого Tela*, vol. 1, pp. 740-747; May, 1959.) Films have a resistivity which is higher by two to four orders of magnitude than that of the bulk material [Part 3: 2484 of 1957 (Goryunova, *et al.*)] and show a monotonic increase of resistivity and activation energy with increasing Sb<sub>2</sub>S<sub>3</sub> content. Spectral characteristics of photoconductivity are within the limits of those for the binary compounds.

537.311.33:537.312.9 3150

**The Piezoresistive Effect and its Applications**—L. E. Hollander, G. L. Vick and T. J. Diesel. (*Rev. Sci. Instr.*, vol. 31, pp. 323-327; March, 1960.) The magnitudes of the piezoresistive effect in semiconductors, particularly TiO<sub>2</sub> and PbTe, are tabulated and an analysis of the fourth-rank piezoresistive tensor for two crystal symmetries is presented. Design of devices based on the effect is discussed with reference to working models.

537.311.33:537.32 3151

**Effect of Charged Dislocation on the Thermoelectric Power of Semiconductors**—T. Ohta. (*J. Phys. Soc. Japan*, vol. 15, p. 197; January, 1960.) An edge dislocation in *n* type Ge gives rise to a cylinder of positive charge with an axis

of negative charge. The thermoelectric power of such material is calculated.

537.311.33:537.32:538.63 3152

**Phonon Relaxation Time and Magnetic Variation of Thermoelectric Power in Semiconductors**—J. Appel. (*Z. Naturforsch.*, vol. 14a, pp. 838-840; September, 1959.) Discussion of some of the assumptions restricting the validity of the theory given in 555 of February.

537.311.33:538.214 3153

**Magnetism of Interacting Donors**—E. Sonder and H. C. Schweinler. (*Phys. Rev.*, vol. 117, pp. 1216-1221; March 1, 1960.) The magnetic susceptibility of donor centers distributed at random in a semiconductor is calculated for the case of small, but not negligible, interactions between adjacent pairs of donors. Agreement with experiment is good.

537.311.33:538.63 3154

**Field-Effect Measurements in a Transverse Magnetic Field**—E. Aerts, S. Amelinck, and J. Vennik. (*J. Electronics Control*, vol. 7, pp. 497-504; December, 1959.) A description of some effects of a transverse magnetic field on the field effect and magnetoresistance of thin semiconductor samples.

537.311.33:539.23 3155

**Electrical Properties of Thin-Film Semiconductors**—F. S. Ham and D. C. Mattis. (*IBM J. Res. & Dev.*, vol. 4, pp. 143-151; April, 1960.) Metallic-film theory is extended to single-crystal films of nondegenerate semiconductors. The conductivity and Hall coefficients are shown to vary with the orientation of the normal to the film with respect to its crystallographic axes.

537.311.33:621.314.63 3156

**Investigation of the Growth of an *n*-Type Semiconductor Layer at the Contact between Cadmium and Selenium**—V. A. Dorin, B. I. Kuznetsov, and D. N. Nasledov. (*Fiz. Tverdого Tela*, vol. 1, pp. 734-739; May, 1959.) An investigation in the temperature range 240°-300°C showed the square of the thickness of the CdSe layer to be directly proportional to the heating time. Data obtained can be used to calculate the thickness of the *n* type layer in a selenium rectifier.

537.311.33:621.317.3.029.6 3157

**Microwave Measurement of Semiconductor Carrier Lifetimes**—H. A. Atwater. (*J. Appl. Phys.*, vol. 31, pp. 938-939; May, 1960.) A mathematical treatment is given of the propagation of dominant-mode waves in a waveguide containing an imperfect dielectric medium in which the conductivity is a function of time.

537.311.33:[546.28 + 546.24 3158

**Field Emission of Silicon and Tellurium Single Crystals**—C. Kleint and R. Fischer. (*Z. Naturf.*, vol. 14, p. 753; August, 1959.) Current/voltage characteristics obtained at room temperature are given for three Si and three Te crystals; the Te characteristics are linear, whereas the Si characteristics flatten out at low strengths owing to surface conditions.

537.311.33:546.28 3159

**Dislocations in Si Single Crystals**—T. Furuya and Y. Sasaki. (*J. Phys. Soc. Japan*, vol. 15, pp. 205-206; January, 1960.) The disappearance of dislocations in pulled Si crystals is discussed.

537.311.33:546.28 3160

**Measurement of Minority-Carrier Lifetime in Silicon**—T. Asakawa. (*Rep. Elec. Commun. Lab., Japan*, vol. 7, pp. 382-383; October, 1959.) Describes a modified photoconductivity-

decay method for obtaining approximate values.

537.311.33:546.28 3161

**Transmitted Phonon Drag Measurements in Silicon**—K. Hubner and W. Shockley. (*Phys. Rev. Lett.*, vol. 4, pp. 504–505; May 15, 1960.) Experimental observation of the phonon-drag effect, and discussion of further possible methods of investigation.

537.311.33:546.28:535.215 3162

**On the Spectral and Temperature Dependences of the Quantum Yield in Silicon**—V. S. Vavilov and K. I. Britsyn. (*Fiz. Tverdogo Tela*, vol. 1, pp. 1629–1631; October, 1959.) Data obtained by a method which excludes the effect of trapping centers are given. They are based on measuring the short-circuit current between the *p* and *n* regions of an illuminated crystal.

537.311.33:546.28:538.63 3163

**Nernst and Ettingshausen Effects in Silicon between 300°K and 800°K**—H. Mette, W. W. Gärtner, and C. Loscoe. (*Phys. Rev.*, vol. 117, pp. 1491–1493; March 15, 1960.) Measured coefficients are in good agreement with theoretical predictions.

537.311.33:546.28:538.632 3164

**Low-Temperature Hall Coefficient and Conductivity in Heavily Doped Silicon**—G. A. Swartz. (*J. Phys. Chem. Solids*, vol. 12, pp. 245–259; February, 1960.) Measurements have been made of Hall coefficient in the range 15°–300°K and of conductivity at 3°–30°K. Results are similar to those observed with other semiconductors exhibiting impurity conduction. Two types of conduction were found, of nonband and band type, the latter requiring impurity concentrations of  $10^{18}/\text{cm}^3$  or more.

537.311.33:546.28:538.632 3165

**Dependence of the Hall Constant on Magnetic Field Intensity in Silicon**—N. S. Orlova and V. M. Tuchkevich. (*Fiz. Tverdogo Tela*, vol. 1, pp. 1631–1634; October, 1959.) Measurements at 114°, 136° and 300°K are reported. Saturation occurs in both *p* and *n* type Si at field strengths of 10–12 kilo-oersteds.

537.311.33:546.289 3166

**Optical Constants of Germanium in the Region 0–10 eV**—M. D. Rimmer and D. L. Dexter. (*J. Appl. Phys.*, vol. 31, pp. 775–777; May, 1960.)

537.311.33:546.289 3167

**Optical Absorption by Degenerate Germanium**—J. I. Pankove. (*Phys. Rev. Lett.*, vol. 4, pp. 454–455; May 1, 1960.) Measurements made on wafers of Ge doped with known concentrations of As indicate that the shrinkage of the energy gap is greater than the rise of the Fermi level.

537.311.33:546.289 3168

**[111] Direct Transition Exciton and Magneto-reflection in Germanium**—B. Lax. (*Phys. Rev. Lett.*, vol. 4, pp. 511–513; May 15, 1960.) Some theoretical predictions about parameters of the  $I_{31}$  valence band, and suggestions for experimental investigations are given.

537.311.33:546.289 3169

**Mobility in High-Resistivity Germanium at D.C. Electric Fields**—J. Zucker. (*J. Phys. Chem. Solids*, vol. 12, pp. 350–352; February, 1960.) Measurements of mobility have been made on samples similar to those used by Seeger (3371 of 1959). Discrepancies between the dc pulse data and Seeger's microwave data are discussed.

537.311.33:546.289 3170

**Field Effect and Reactions on the Surface of Germanium**—H. Flietner. [*Ann. Phys.*

(*Leipzig*), vol. 3, pp. 414–427; July 2, 1959.] On the basis of Kingston's model of phenomena (2108 of 1956), results are interpreted of field-effect measurements on CP4-etched specimens of *p* and *n* type Ge whose surfaces were exposed to dry and humid  $\text{O}_2$ ,  $\text{N}_2$  and ozone in different sequences.

537.311.33:546.289 3171

**A.C. and D.C. Field Effects on Cleaned Germanium Surfaces**—S. Kawaji. (*J. Phys. Soc. Japan*, vol. 15, pp. 95–99; January, 1960.) The density of fast states was estimated from measurements of the ac field effect; it decreased after exposure of the surface to oxygen. Measurements of a dc field effect showed that the slow states are caused by absorbed gases on the outer surface of the oxide layer.

537.311.33:546.289 3172

**Investigation of "Fast" Surface States of Germanium**—V. G. Litovchenko and V. I. Lyashenko. (*Fiz. Tverdogo Tela*, vol. 1, pp. 1609–1621; October, 1959.) The topography of fast surface states has been investigated using a pulsed field method. The effect of a constant transverse field on the concentration of surface states lying near the middle of the forbidden zone and the effect of dry air absorption on the concentration of one type of level are particularly discussed.

537.311.33:546.289 3173

**Diffusion and Solubility of Cadmium in Germanium**—V. E. Kozenko. (*Fiz. Tverdogo Tela*, vol. 1, pp. 1622–1626; October, 1959.) The diffusion coefficient is  $1.75 \times 10^8 e^{-102000/RT}$  and the solubility at 840°C  $2 \times 10^{18} \text{cm}^{-3}$ .

537.311.33:546.289 3174

**Infrared Properties of Gold in Germanium**—L. Johnson and H. Levinstein. (*Phys. Rev.*, vol. 117, pp. 1191–1203; March 1, 1960.) Investigation of fundamental parameters by absorption, photoconductivity and lifetime measurements between 60 and 300°K.

537.311.33:546.289 3175

**The Possibility of Creating Ohmic Contact with Silicon by Rubbing the Metal on to the Semiconductor using Dry Friction**—I. D. Kirvalidze and V. F. Zhukov. (*Fiz. Tverdogo Tela*, vol. 1, pp. 1583–1586; October, 1959.) Good ohmic contact is obtained on polished *p* and *n* type Si surfaces by rubbing with Al, bronze, brass or tin. Mo and Ta give rectifying contacts. Al and Ni give good ohmic contacts on etched *p* and *n* type Si.

537.311.33:546.289:535.215 3176

**Photoconductivity in Nickel-Doped Germanium**—Y. Furukawa. (*J. Phys. Soc. Japan*, vol. 15, p. 353; February, 1960.) Steady-state intrinsic photoconductivity has been measured at fields up to  $10^3$  volts/cm to examine the effects of contacts. An explanation is given of the observed results.

537.311.33:546.289:537.32 3177

**The Effect of Strain on the Seebeck Coefficient of *n*-Type Germanium**—J. R. Drabble and R. D. Groves. (*J. Phys. Chem. Solids*, vol. 12, pp. 285–294; February, 1960.) A study of the anisotropy of the phonon-drag Peltier tensor for a single valley in *n* type Ge by observing the effect of strain on the Seebeck coefficient with simultaneous measurements of piezo-resistance. Results are given for a number of specimens.

537.311.33:546.289:538.63 3178

**Investigation of the Hall Effect and Transverse Resistance in Germanium in Fields up to 400 Kilo-oersteds**—V. P. Kaesik. (*Dokl. Akad. Nauk SSSR*, vol. 130, pp. 521–522; January

21, 1960.) Results show that the dependence of the Hall EMF on the magnetic field in *n* type and *p* type Ge at 77° and 20.4°K is linear.

537.311.33:546.289:539.12.04 3179

**Influence of Fast Neutrons on the Recombination of Electron-Hole Pairs in Germanium**—N. van Dong and A. Barraud. [*Compt. rend. acad. sci. (Paris)*, vol. 249, pp. 2181–2183; November 23, 1959.] A study of recombination processes in *p* and *n* type Ge. The abnormal behavior observed is similar to that reported by Curtis, *et al.* (868 of 1959), but a different hypothesis is proposed to explain it.

537.311.33:546.289:939.12.04 3180

**Annealing of  $\gamma$ -Ray Damage in Germanium**—T. Asada, H. Saito, K. Omura, T. Oku, and M. Oak. (*J. Phys. Soc. Japan*, vol. 15, pp. 93–94; January, 1960.) The variation of conductivity with time is studied.

537.311.33:546.3–31 3181

**The Conduction Mechanism of Oxide Semiconductors at High Temperatures**—J. Rudolph. (*Z. Naturforsch.*, vol. 14a, pp. 727–737; August, 1959.) Extension of earlier investigations on BaO and (Ba, Sr)O (1685 of May) covering measurements of conductivity as a function of temperature and oxygen pressure on SrO, CaO, ThO<sub>2</sub>, ZrO<sub>2</sub>, La<sub>2</sub>O<sub>3</sub>, CeO<sub>2</sub>, TiO<sub>2</sub>, and ZnO with or without doping, are given.

537.311.33:546.3–31 3182

**Change in the Work Function of Doped Oxide Semiconductors**—E. Kh. Enikeev, L. Ya. Margolis, and S. Z. Roginskii. (*Dokl. Akad. Nauk SSSR*, vol. 130, pp. 807–809; February 1, 1960.) The solution of Li<sub>2</sub>O in the lattice of NiO, CuO or ZnO semiconductors resulted in a lowering of the work function by 0.6 to 0.8 ev. Graphs also illustrate the effect of ThO<sub>2</sub>, ZnSO<sub>4</sub>, Fe<sub>2</sub>O<sub>3</sub> and MgO admixtures on the work function.

537.311.33:546.47–31 3183

**Infrared Absorption of ZnO Crystals**—R. Arneth. (*Z. Phys.*, vol. 155, pp. 595–608; August 5, 1959.) Measurements were made on synthetic single crystals of ZnO with or without doping in the wavelength range 1–13  $\mu$ . See also 878 of 1959 (Bogner and Mollwo).

537.311.33:546.47–31:541.135 3184

**The Charge and Potential Distributions at the Zinc Oxide Electrode**—J. F. Dewald. (*Bell Sys. Tech. J.*, vol. 39, pp. 615–639; May, 1960.) An experimental method of measuring capacitance of single-crystal ZnO electrodes in contact with aqueous electrolytes is described. Tables of results show capacitance variations with bias and frequency. Results agree quantitatively with the capacitance calculated from the Poisson-Boltzmann equation under non-degenerate surface conditions, and with the Poisson-Fermi equation in the degenerate case.

537.311.33:546.623'86 3185

**Electrical Properties of *n*-Type AlSb**—D. N. Nasledov and S. V. Slobodchikov. (*Fiz. Tverdogo Tela*, vol. 1, pp. 748–754; May, 1959.) Investigation in the range 80–1200°K of the temperature dependence of conductivity, Hall effect, and thermoelectric power of AlSb samples doped with Se and Te. Calculated and experimental results are shown graphically.

537.311.33:546.681'19 3186

**High-Temperature Hall Coefficient in GaAs**—L. W. Aukerman and R. K. Willardson. (*J. Appl. Phys.*, vol. 31, pp. 939–940; May, 1960.)

537.311.33:546.681'86 3187

**Thermoelectric Properties of Gallium Antimonide (GaSb)**—A. I. Blum. (*Fiz. Tverdogo*

*Tela*, vol. 1, pp. 766-773; May, 1959.) The temperature dependence of the carrier density, mobility, and effective mass in the impurity conduction region are calculated from results of measurements of conductivity and Hall effect. Formulas are derived, relating the thermal EMF to the width of the forbidden zone and the carrier mobility ratio. This ratio is calculated for the intrinsic conduction region.

537.311.33:546.682'86 3188  
**Electrical and Galvanomagnetic Properties of High-Purity InSb**—N. I. Volokobinskaya, V. V. Galavanov, and D. N. Nasledov. (*Fiz. Tverdogo Tela*, vol. 1, pp. 755-760; May, 1959.) An investigation of the conductivity and Hall effect in the range 77°-500°K in magnetic fields from 60 to 25,000 oersteds. Some anomalies were noticed in the Hall effect and the dependence of conductivity on the transverse magnetic field intensity at low temperatures. The transition to intrinsic conduction takes place at 140°K.

537.311.33:546.714-31 3189  
**Semiconductor Behaviour of Dioxides of Manganese with Added Foreign Ions as a Function of Frequency**—J. P. Chevillot and J. Brenet. [*Compt. rend. acad. sci. (Paris)*, vol. 249, pp. 1869-1871; November 9, 1959.] The influence of  $Li^+$  ions on the resistivity of  $\beta$ - $MnO_2$  specimens is examined as a function of frequency in the range 300-15,000 cps at 25°, 40° and 60°C. See also 3783 of 1959.

537.311.33:546.824-31:537.312.9 3190  
**Piezoresistivity in the Oxide Semiconductor Rutile (TiO<sub>2</sub>)**—L. E. Hollander, Jr., T. J. Diesel, and G. L. Vick. (*Phys. Rev.*, vol. 117, pp. 1469-1472; March 15, 1960.)

537.311.33:546.873'863'241:537.324 3191  
**Solid Solutions of Bi<sub>2</sub>Te<sub>3</sub> and Sb<sub>2</sub>Te<sub>3</sub> as p-Type Materials for Semiconductor Thermoelements**—K. Šmirous and L. Štourač. (*Z. Naturforsch.*, vol. 14a, pp. 848-849; September, 1959.) Good thermoelectric properties and efficiencies  $> 3.5 \times 10^{-3}$  per °C were obtained on specimens of Bi<sub>0.5</sub>Sb<sub>1.5</sub>Te<sub>3</sub>.

537.533:537.311.31 3192  
**Contribution on the Problem of Exo-electron Emission of Metals**—W. Schaaffs. (*Z. angew. Phys.*, vol. 11, pp. 220-223; June, 1959.) The relation between exo-electron emission and contact potential is discussed, with reference to measurements on oxidized metal surfaces (550 of February).

537.533.8 3193  
**Inelastic Scattering and Electrons and Secondary-Electron Emission in Certain Metals: Part I & 2**—I. M. Bronshtein and R. B. Segal'. (*Fiz. Tverdogo Tela*, vol. 1, pp. 1489-1508; October, 1959.) A detailed report of an experimental investigation of Be, Bi and Ag is given.

538.22 3194  
**Magnetic Property of Mn<sub>2</sub>Cr<sub>2</sub>O<sub>7</sub>**—K. Siratori and S. Iida. (*J. Phys. Soc. Japan*, vol. 15, pp. 210-211; January, 1960.) Variation of magnetic properties with composition and temperature is considered.

538.22 3195  
**Evidence for an Antiferromagnetic-Ferromagnetic Transition in Cr-Modified Mn<sub>2</sub>Sb**—T. J. Svoboda, W. H. Cloud, T. A. Bither, M. S. Sadler, and H. S. Jarrett. (*Phys. Rev. Lett.*, vol. 4, pp. 509-511; May 15, 1960.)

538.22:537.311.3:546.72'241 3196  
**Magnetic and Electrical Anomalies of Iron Telluride Single Crystals**—R. Naya, M. Murakami, and E. Hirahara. (*J. Phys. Soc. Japan*,

vol. 15, pp. 360-361; February, 1960.) Experimentally observed anomalies are interpreted.

538.221 3197  
**On the Ferromagnetic Iron-Aluminum Alloys**—M. Sugihara. (*Rep. Elec. Commun. Lab., Japan*, vol. 7, pp. 333-338; September, 1959.) The magnetic properties of specimens containing various percentages of Al are given.

538.221 3198  
**Studies on the Magnetic Anisotropy Induced by Cold Rolling of Ferromagnetic Crystal: Part 2—Iron-Aluminum Alloys**—S. Chikazumi, K. Suzuki, and H. Iwata. (*J. Phys. Soc. Japan*, vol. 15, pp. 250-260; February, 1960.) The investigation reported in Part I (1797 of 1958) is extended to body-centered cubic crystals.

538.221 3199  
**Variational Principles in Determining the Main Characteristics of a Ferromagnetic by the Calculation of its Hysteresis Loop**—V. I. Skobelnik. (*Dokl. Akad. Nauk SSSR*, vol. 130, pp. 1012-1014; February 11, 1960.) Formulas are derived which can be used in a quantitative evaluation of the hysteresis loop.

538.221:538.569.4 3200  
**"Foldover" Effects caused by Spin Wave Interactions in Ferromagnetic Resonance**—H. Suhl. (*J. Appl. Phys.*, vol. 31, pp. 935-936; May, 1960.) Whereas current theory supposes the real part of the susceptibility to be zero, at high powers this assumption is unjustified. An expression is given for the uniform precession amplitude when the phase shift is not tuned out, and this is shown to account for multi-valued results.

538.221:539.23 3201  
**Magnetic Anisotropy in Single-Crystal Thin Films**—E. L. Boyd. (*IBM J. Res. & Dev.*, vol. 4, pp. 116-129; April, 1960.) The preparation of single crystals of Ni, Fe and Ni-Fe and Ni-Co alloys and the measurement of their magnetic crystalline anisotropy by a torque balance method is described.

538.221:539.23 3202  
**External Fields from Domain Walls of Cobalt Film**—B. Kostyshy, J. E. Brophy, I. Oi, and D. D. Roshon, Jr. (*J. Appl. Phys.*, vol. 31, pp. 772-775; May, 1960.) Domain pattern on thin Co films are mapped with a Hall probe by measuring peak fields at domain boundaries.

538.221:539.23 3203  
**Thickness Dependence of Domain Orientation in Thin Nickel Films**—K. Kuwahara and M. Goto. (*J. Phys. Soc. Japan*, vol. 15, p. 359; February, 1960.)

538.221:539.23 3204  
**Thin Nickel Films with Very High Coercive Force and High Energy Product**—W. Ruske. [*Ann. Phys. (Leipzig)*, vol. 3, pp. 323-326; May 12, 1959.] A multilayer system of Ni films with or without intermediate Cu film electrolytically deposited on hollow cylindrical Cu rods was subjected to axial pressure and the effect on coercivity was measured. For measurements on similar systems not subjected to elastic or plastic deformation, see 3804 of 1959.

538.221:539.23 3205  
**Domain Walls in Thin Ni-Fe Films**—S. Methfessel, S. Middlehoek, and H. Thomas. (*IBM J. Res. & Dev.*, vol. 4, pp. 96-106; April, 1960.) A description is given of experimental investigations into the processes taking place in the transition region between Bloch and

Néel walls where the domain walls have their highest energy.

538.221:539.23 3206  
**The Influence of Edge Effects on Domain Structure and Coercive Force of Circular Nickel-Iron Films**—M. Beckerman and K. H. Behrndt. (*IBM J. Res. & Dev.*, vol. 4, pp. 198-201; April, 1960.) The coercive force can be decreased by removal of the shadowed edge.

538.221:539.23:538.23 3207  
**Theoretical Hysteresis Loops of Thin Magnetic Films**—H. J. Oguey. (*Proc. IRE*, vol. 48, pt. 1, pp. 1165-1166; June, 1960.) Gives analytical and graphical methods of determining hysteresis loops; good agreement with experiments is obtained.

538.221:539.23:681.142 3208  
**Chemically Deposited NiCo Layers as High-Speed Storage Elements**—R. J. Heritage and M. T. Walker. (*J. Electronics Control*, vol. 7, pp. 542-552; December, 1959.) A simple, inexpensive method giving switching constants of 0.15  $\mu$ sec oersted.

538.221:539.234 3209  
**Angle-of-Incidence Anisotropy in Evaporated Nickel-Iron Films**—E. W. Pugh, E. L. Boyd, and J. F. Freedman. (*IBM J. Res. & Dev.*, vol. 4, pp. 163-172; April, 1960.) The anisotropy is incompatible with the fiber-axis and stress models. The angle-of-incidence effects appear to originate in anisotropically oriented imperfections, and an attempt is made to deduce their nature.

538.221:539.234:538.63 3210  
**Film-Thickness and Temperature Dependence of the Coercivity of Thin Vapour-Deposited Nickel Films Measured by means of the Magnetic Variation of Resistance**—W. Hellenthal. (*Z. Naturforsch.*, vol. 14a, pp. 722-727; August, 1959.) The results of measurements on Ni films deposited at 20°, 200° and 400°C are discussed. See 1944 of 1959.

538.221:539.234:538.632 3211  
**Measurement of the Temperature Dependence of the Ferromagnetic Hall Effect of Vapour-Deposited Nickel Films for the Determination of the Curie Temperature**—L. Reimer. (*Z. Phys.*, vol. 155, pp. 524-530; August 5, 1959.) Extension of earlier investigations (1280 of 1959). Hall-effect variation with temperature in the range 20°-400°C is measured at a constant field strength of 6000 oersteds. The Curie temperatures are derived from the curves obtained.

538.221:621.318.134 3212  
**Thermal Variations of the Anisotropy Constants and Spontaneous Magnetization of Magnetoplumbite**—R. Pauthenet and G. Rimet. [*Compt. rend. acad. sci. (Paris)*, vol. 249, pp. 1875-1877; November 9, 1959.] See 1717 of May.

538.221:621.318.134:538.569.4 3213  
**High-Power Effects on Ferrimagnetic Resonance**—M. T. Weiss. (*J. Appl. Phys.*, vol. 31, pp. 778-782; May, 1960.) Measurements on single-crystal Mn ferrite spheres are reported. The variation of susceptibility with power level is in agreement with Suhl's theoretical treatment of the saturation process (1309 of April).

538.221:621.318.134:538.569.4 3214  
**L-Band Ferromagnetic Resonance Experiments at High Peak Power Levels**—E. Schlömann, J. H. Saunders, and M. H. Sirvetz. (*IRE TRANS. ON MICROWAVE THEORY AND TECHNIQUES*, vol. MTT-8, pp. 96-100; January, 1960. Abstract, *PROC. IRE*, vol. 48, p. 972; May, 1960.)

538.221:621.318.134:538.569.4 3215  
**High-Power Ferromagnetic Resonance at X Band in Polycrystalline Garnets and Ferrites**—J. J. Green and E. Schlömann. (IRE TRANS. ON MICROWAVE THEORY AND TECHNIQUES, vol. MTT-8, pp. 100-103; January, 1960. Abstract, PROC. IRE, vol. 48, p. 972; May, 1960.)

538.221:621.318.134:538.652 3216  
**On a Consequence of Similarity of Magnetization in Mixed Ferrites**—L. N. Syrkin. (Fiz. Tverdogo Tela, vol. 1, pp. 1538-1539; October, 1959.) An expression is derived which is useful in the treatment of experimental data on magnetostriction of mixed ferrites. A family of magnetostriction curves corresponding to various values of concentration of the non-ferromagnetic ferrite can be constructed.

538.221:621.318.134:621.318.57 3217  
**Studies in Partial Switching of Ferrite Cores**—R. H. Tancrill and R. E. McMahon. (J. Appl. Phys., vol. 31, pp. 762-771; May, 1960.) The characteristics of Mg-Mn ferrite cores in a partially switched state are investigated experimentally. A model is proposed to describe the behavior observed and applications to storage systems are discussed.

#### MATHEMATICS

519.281 3218  
**A Variant Least-Squares Method of Solution of a System of Observation Equations**—J. L. Stearn and H. Richardson. (J. Geophys. Res., vol. 65, pp. 1308-1309; April, 1960.) A mathematical device which allows a suspect equation to be excluded without the need for a new set of normal equations.

#### MEASUREMENTS AND TEST GEAR

621.3.018.41(083.74):[529.786+525.35 3219  
**Frequency Variations of Quartz Oscillators and the Earth's Rotation in Terms of the N.P.L. Caesium Standard**—L. Essen, J. V. L. Parry, and J. M. Steele. (Proc. IEE, vol. 107, pt. B, pp. 229-232; May, 1960. Discussion, pp. 232-234.) Frequency variations of ring type oscillators at the N.P.L. and other laboratories were linear to within  $\pm 5$  parts in  $10^9$  over a 3-year period. A steady retardation in the period of rotation of the earth of 1 part in  $10^9$  from September, 1955, to January, 1958, was superimposed upon the annual seasonal variation of  $\pm 8$  parts in  $10^9$ .

621.317(083.74):53.081.6 3220  
**Electrical Units and Standards**—P. Vigoureux. (Proc. IEE, vol. 107, pt. B, pp. 235-240; May, 1960.) Recent advances in experimental techniques, such as atomic-beam frequency standards, the measurement of the gyromagnetic ratio of the proton, and the development of an accurately calculable capacitor, are reviewed in relation to their application to the determination of electrical standards. 57 references.

621.317.337:621.372.413 3221  
**Q of Resonant Cavities**—M. Y. El-Ibiary. (Electronic Tech., vol. 37, pp. 284-286; July, 1960.) The phase delay which occurs in the modulation envelope of a signal passed through a resonant system is measured by comparison with that caused by a calibrated RC network. The Q of the resonant system is then evaluated from the phase shift.

621.317.351:621.397.6 3222  
**The Oscillographic Recording of the Non-linear Part of the Phase Characteristics**—L. A. Wegner. (Rundfunktech. Mitt., vol. 3, pp. 114-122; June, 1959.) A method is given for recording the difference between the actual and the specified linear phase characteristics of

video networks using the equipment described in 219 of 1958 (Kroebel and Wegner).

621.317.444:538.569.4:551.507.362.2 3223  
**Magnetometer at Work in Outer Space**—D. Mansir. (Radio and Electronics, vol. 31, pp. 38-41; April, 1960.) Description of a proton free-precession magnetometer of the type used in the Vanguard III satellite.

621.317.729.1:621.3.032.269.1 3224  
**Study of Electron Optics by Electrolyte Tank for Space-Charge Conditions by the Method of Current Injection**—J. Bonnerot. [Compt. rend. acad. sci. (Paris), vol. 249, pp. 1878-1880; November 9, 1959.] The design of a universal model is discussed, and an investigation of electron trajectories in a reflex klystron is described. See also 2708 of 1959.

621.317.755:621.382.23.012 3225  
**Test Set for Displaying the Volt/Ampere Characteristics of Tunnel Diodes**—A. M. Goodman. (Rev. Sci. Instr., vol. 31, pp. 286-288; March, 1960.) Principles of design, construction and operation are given. Circuit instabilities which can occur with negative resistance devices have been suppressed. I-V characteristics can be displayed on any suitable CRO.

621.317.757 3226  
**A Spectrum Analyser for Video Frequencies**—A. L. Whitwell and N. Williams. (Electronic Engrg, vol. 32, pp. 268-274; May, 1960.) A description of a general purpose equipment designed to operate in the frequency range 500 cps-95 kc with a threshold sensitivity of about  $0.2 \mu\text{v}$  in a 70-cps band is given. The dynamic range is 50 db.

621.317.77:621.391.812.63.029.45 3227  
**Phase-Measuring Equipment**—G. E. Ashwell and C. S. Fowler. (Electronic Tech., vol. 37, pp. 252-255; July, 1960.) The equipment described has been developed to investigate the influence of ionospheric changes on the phase of a VLF signal received at two sites separated by up to 400 km. A reference signal at both sites is derived from the VLF transmissions of the Gee navigational system, and measurement of phase difference is made via a line-telephone circuit.

621.317.794 3228  
**Sensitivity and Natural Limit of Response of Nickel Bolometers**—G. Barth and W. Maier. [Ann. Phys. (Leipzig), vol. 3, pp. 260-282; May 12, 1959.] Comprehensive measurements were made on specially constructed Ni bolometers to determine the effect on their sensitivity of changes in various parameters which are functions of ambient conditions and bolometer constructional features. The results obtained are discussed with reference to theoretical work. A table is given for the comparison of figures of merit and response limits of Ni bolometers and various other thermal-radiation measuring devices.

#### OTHER APPLICATIONS OF RADIO AND ELECTRONICS

535.376:681.6 3229  
**Data Storage and Display with Polarized Phosphors**—H. P. Kallmann and J. Rennert. (Electronics, vol. 32, pp. 39-41; August 28, 1959.) The persistent internal polarization (PIP) phenomenon is discussed: information may be stored by producing a separation of charges in the phosphor, using dc fields and radiation.

537.311.33:537.312.9:531.78 3230  
**Semiconductor Strain Transducers**—F. T. Geyling and J. J. Forst. (Bell Sys. Tech. J., vol. 39, pp. 705-731; May, 1960.) The piezo-

resistive properties of semiconductors and their application in strain transducers are discussed. Both ac and dc signals can be handled, and signal amplification is not usually necessary. Problems of bond rigidity and temperature compensation are mentioned.

621.372.029.64:531.717 3231  
**Microwave Thickness Detector**—J. B. Beyer, J. Van Bladel, and H. A. Peterson. (Rev. Sci. Instr., vol. 31, pp. 313-316; March, 1960.) A device is described for continuous measurement of the thickness of moving conducting materials. Increments of 1/40 mm are clearly detectable. Two methods, based on (a) the amplitude and (b) the phase variations of reflected microwave energy are compared; the former is preferred.

621.375.9:621.372.44:513.6 3232  
**Parametric Oscillatory and Rotary Motion**—H. E. Stockman. (Proc. IRE, vol. 48, pt. 1, pp. 1157-1158; June, 1960.) A note on the application of variable inductance devices to give oscillatory or rotary movement.

†621.383.5:616-073 3233  
**An Improved Recording Oximeter**—A. W. Melville, D. H. Smith, and J. B. Cornwell. (Electronic Engrg., vol. 32, pp. 296-300; May, 1960.) An analysis of the theory of ear oximetry is given, and an instrument is described which provides a continuous record of absolute arterial oxygen saturation.

621.387.462:621.382.3 3234  
**Detection of Alpha Particles with Commercially Available Transistors**—A. I. Yavin. (Rev. Sci. Instr., vol. 31, pp. 351-352; March, 1960.) Measurements show that an acceptable accuracy can be obtained for certain experiments and for demonstration purposes.

621.397.9:612.84 3235  
**TV Tracker records Eye Focus Points**—E. L. Thomas, R. Howat, and N. H. Mackworth. (Electronics, vol. 33, pp. 57-59; April 22, 1960.) See 930 of 1959 (Mackworth and Mackworth).

621.398:551.507.362.2 3236  
**Telemetry Transmitter for Radiation Satellite**—A. J. Fisher, W. R. Talbert, and W. R. Chittenden. (Electronics, vol. 33, pp. 68-69; May 6, 1960.) The transmitter was designed for an investigation of the Van Allen radiation belt. It operates on 108.03 Mc with an output of 300 mw and incorporated a phase modulator based on a bridged-T network.

621.398:621.387.462 3237  
**Balloon-Borne Circuits Sort High-Altitude Cosmic Rays**—D. Enemark. (Electronics, vol. 35, pp. 52-55; August 28, 1959.) Details of transistor circuits which are stable over wide temperature and pressure ranges are given; the modulator and transmitter have been described earlier (2373 of 1959).

786/789:621.37/.38 3238  
**Electronic Music Synthesis**—H. F. Olson, H. Belar, and J. Timmens. (J. Acoust. Soc. Amer., vol. 32, pp. 311-319; March, 1960.) The synthesizer described has been developed from an earlier model [3068 of 1955 (Olson and Belar)].

#### PROPAGATION OF WAVES

621.391.812.6:537.56 3239  
**Signal Transmission through Ionized Media**—W. A. Greenhow. (Electronics, vol. 33, pp. 81-85; May 20, 1960.) The process of ionization in the atmosphere and their effects on signal transmission are discussed with particular reference to ionization associated with nuclear

vehicles, hypersonic re-entry vehicles, rocket-motor exhausts, and nuclear explosions.

621.391.812.62 3240

**Tropospheric Fields and their Long-Term Variability as Reported by TASSO**—P. L. Rice. (PROC. IRE, vol. 48, pt. 1, pp. 1021-1029; June, 1960.) Curves are given for predicting field strength over a smooth earth for frequencies between 40 and 1000 Mc based on long-term recording over many paths.

621.391.812.62 3241

**Propagation in the Frequency Bands 460-470, 585-605 and 6660-6700 Mc/s over the Gulf of Naples**—A. Bruno. (*Alla Frequenza*, vol. 28, pp. 425-440; June/August, 1959.) Statistical analysis of propagation measurements for various paths across the Gulf of Naples to assess the effect of seasonal factors and of the height above sea level of the transmission path.

621.391.812.621 3242

**Refraction of Radio Waves at Low Angles within Various Air Masses**—B. R. Bean, J. D. Horn, and L. P. Riggs. (*J. Geophys. Res.*, vol. 65, pp. 1183-1187; April, 1960.) The conclusions of Schulkin (2576 of 1952) are extended by identifying abnormal refraction of radio waves with abnormalities in the refractive-index structure in the lower layers of air masses. A method of classifying air masses in terms of their refractive properties is described.

621.391.812.623 3243

**Radio Transmission Beyond the Line of Sight between Kyushu and Amami-Oshima Island**—K. Kakita, F. Iwai, and S. Ieiri. (*Rep. Elec. Commun. Lab., Japan*, vol. 7, pp. 350-361; October, 1959.) Diffraction effects of a mountain at the mid-point of a 340-km path over sea can reduce the propagation loss at VHF and UHF by 20 db.

621.391.812.63:551.510.535 3244

**Radio Wave Propagation Characteristics of a Simple Ionospheric Model based on Rocket Data**—L. Zhekulin. (*Planetary Space Sci.*, vol. 2, pp. 110-120; April, 1960.) The wave treatment of the propagation of a radio wave in an ionospheric layer is given, and the solution expressed in Airy functions. Transient signals are also dealt with. When absorption is low, the solutions are approximately the same as for those depending on geometrical optics. See 3811 of 1958 (Gringauz).

621.391.812.63:551.510.535 3245

**The Reflexion of Radio Waves from a Stratified Ionosphere Modified by Weak Irregularities: Part 2**—M. L. V. Pitteway. [*Proc. Roy. Soc. (London)* A, vol. 254, pp. 86-100; January 19, 1950.] "The results of an earlier paper are applied to an ionosphere containing weak random irregularities, statistically specified only. It is supposed that the shape of the irregularities is described by a Gaussian autocorrelation function, and that their intensity varies in a known way with height. Possibilities of obtaining slow and rapid fading characteristics from forward and back scatter by the irregularities are considered briefly. Certain conclusions of the earlier paper, concerning the importance of scattering by irregularities near the reflexion level, are modified. A mechanism for explaining the occurrence of 'spread F' signals is suggested." Part 1: 225 of 1959.]

621.391.812.63.029.62 3246

**Angles of Arrival of a V.H.F. Signal in Ionospheric Forward Propagation**—K. Miya, T. Sasaki, and M. Ishikawa. (*Rep. Ionos. Space Res. Japan*, vol. 13, pp. 187-200; September, 1959.) Newly developed equipment is described for measuring the voltage ratio of two signals at low signal-to-noise ratios. This equipment is used to study bearing and eleva-

tion of a signal received on 50 Mc over a 1560-km path. The results obtained are described and discussed.

## RECEPTION

621.391.812.3 3247

**Rapid Periodic Fading of Medium-Wave Signals**—H. Misrar. (PROC. IRE, vol. 48, pt. 1, pp. 1167-1168; June, 1960.) Unusually fast fading is reported on medium- and short-wave bands.

621.391.821 3248

**A Study of Atmospheric Radio Noise Received in a Narrow Bandwidth at 11 Mc/s**—C. Clarke. (*Proc. IEE*, vol. 107, pt. B, pp. 311-319; May, 1960.) The amplitude probability distribution of the noise envelope was determined by a pulse counting technique. A graphical presentation of the distribution indicating its limits, combined with a burst-width distribution, is suggested as the most useful way of providing data required by communication engineers.

621.396.625:621.391.812.3 3249

**Measuring the Mean Square Amplitude of Fading Signals using a Selected Quantile Output Device (SQUOD)**—A. E. Adam and J. D. Whitehead. (PROC. IRE, vol. 48, pt. 1, pp. 1172-1173; June, 1960.) The principle of the method and circuit details are given.

621.396.662.6 3250

**Frequency-Tuning Drive for Commercial [Communication] Receivers**—F. Laubach. (*Telefunken Ztg.*, vol. 32, pp. 125-129; June, 1959. English summary, pp. 139-140.) Details are given of a coarse-to-fine tuning mechanism and its applications.

## STATIONS AND COMMUNICATION SYSTEMS

621.391 3251

**Analytical Representation of a Time Function with an Unlimited Spectrum**—I. T. Turbovich. (*Radiotekhnika*, vol. 14, pp. 22-27; March, 1959.) This function is represented in the form of the sum of time functions with limited spectrum. The mean-square value of each consecutive term of the series is shown to be less than the preceding one, so that an approximate method can be applied. The coefficients of the series are calculated from the values of the approximate function at discrete times.

621.391 3252

**The Reliability of a Communication Circuit with Reserved Finite Bandwidth**—H. Wolter. (*Arch. elekt. Übertragung*, vol. 13, pp. 267-270; June, 1959.) A general theorem derived in 2161 of June, giving the reliability of a communication channel is used to obtain an estimate of the quantity of correctly recognized bits per total number of bits for a channel of given interference-free bandwidth disturbed by adjacent transmitters, as well as white noise.

621.391:621.396.6 3253

**The Speed of Transmission of Information and the Carrying Capacity of a Multipath System and Reception by the Linear-Operator Conversion Method**—I. A. Ovseevich and M. S. Pinsker. (*Radiotekhnika*, vol. 14, pp. 9-21; March, 1959.) Mathematical analysis shows that the speed of transmission of information over a multipath system does not vary if some linear function of the channel output signals is taken as the output signal. Filter transmission coefficients are derived defining the form of this function.

621.394.3:621.376.53:681.142 3254

**An Evaluation of A.M. Data System Performance by Computer Simulation**—R. A.

Gibby. (*Bell Sys. Tech. J.*, vol. 39, pp. 675-704; May, 1960.) This simulation technique provides a means of answering complex problems relating to delay distortion, influence on performance of the variation of bit speed, location of carrier frequency, and length and type of transmission medium used.

621.394.5:621.391 3255

**Recent Telegraphy Receiving Installations for Long-Distance Traffic on Short and Long Waves**—W. Hasselbeck. (*Telefunken Ztg.*, vol. 32, pp. 103-118; June, 1959. English summary, pp. 138-139.)

621.396:523.1:535-1 3256

**Search for Artificial Stellar Sources of Infrared Radiation**—F. J. Dyson. (*Science*, vol. 131, pp. 1667-1668; June 3, 1960.) The energy metabolism of technically highly developed extraterrestrial beings may consist of the large-scale conversion of starlight into far-infrared radiation. A search for sources of infrared radiation is suggested to accompany the search for interstellar radio communications [320 of January (Coconi and Morrison)].

621.396.4:621.396.65 3257

**Frequency Patterns for Multiple-Radio-Channel Routes**—B. B. Jacobsen. (*Proc. IEE*, vol. 107, pt. B, pp. 241-249; May, 1960. Discussion, pp. 249-252.) The selectivity requirements are considered in detail, and a specific frequency pattern is worked out for a route with six two-way channels, each capable of carrying 600 telephone channels or a single television channel. This pattern was adopted by the C.C.I.R. in 1956.

621.396.65 3258

**Convention on Radio Links**—(*Alla Frequenza*, vol. 28, pp. 209-524; June/August, 1959.) Third and last issue covering the proceedings of a convention held in Rome, June 5-8, 1957, with cumulative index. Second issue: 2014 of 1959. Abstracts of some of the papers are given individually; titles of others are as follows:

(a) **The Design and Realization of Microwave Filters**—I. Caroli and U. Cucina (pp. 211-232).

(b) **Modulators for Multichannel Radio Links**—E. Dalla Volta (pp. 233-244).

(c) **Electronic Stabilizers for the Power Supply of Klystrons in a Radio Link**—M. Saba (pp. 245-259).

(d) **Directional Couplers in Coaxial Lines**—I. Bucci (pp. 260-276).

(e) **Reference Cavity Resonators for Automatic Frequency Control**—B. Basini (pp. 277-284).

(f) **Application of Compander Circuits to Radio Links**—P. Chiesa (pp. 330-338).

(g) **Radio Links with Travelling-Wave Valves**—L. Barbaglio (pp. 339-355).

(h) **Tropospheric-Scatter Radio Links**—A. Favilli (pp. 356-369).

(i) **Interference between F.M. Radio Links**—M. Federici (pp. 383-393).

(j) **Noise Measurements on F.M. Radio Links**—O. Fabbri (pp. 454-468).

(k) **Panoramic Measurement Systems for Wide-Band Radio Link Equipment**—F. Polastrello (pp. 469-480).

(l) **Results of Acceptance Tests on Multichannel Radio Telephone Links**—A. Cardarelli (pp. 481-497).

621.396.65 3259

**The Radio-Link Installation Berne-Breitenrain**—F. Füllemann. (*Tech. Mitt. PFT*, vol. 37, pp. 188-189; May 1, 1959.) The operation is described and constructional details are given of a radiotelephony relay station operating at frequencies near 4 kMc.

621.396.65:621.391.826.2 3260  
**Multiple Paths in Radio Links with Passive Repeaters**—F. Fabbri. (*Alta Frequenza*, vol. 28, pp. 394–404; June/August, 1959.) The types of echo likely to affect the performance of multi-channel radio links are discussed, and curves of harmonic distortion as a function of echo, amplitude and delay are given. Methods of minimizing interference and results achieved in practical repeater systems are mentioned.

621.396.65:621.391.826.2 3261  
**The Reflected Ray in Radio Links over the Sea or over Smooth Plane Ground**—V. Montevicchi. (*Alta Frequenza*, vol. 28, pp. 410–424; June/August, 1959.) Propagation measurements made on various radio links were analyzed to assess the influence of the reflected ray on reception conditions, and from this a design and alignment procedure for radio links has been developed. The procedure is tested experimentally and appears to be economically advantageous compared with a diversity reception system.

621.396.65:631.391.832 3262  
**Transmission Distortion in Frequency-Modulated Radio Relay System (Especially on the Relation between Harmonic Distortion due to Amplitude Characteristics and Differential Gain Characteristics)**—T. Uchino. (*Rep. Elec. Commun. Lab., Japan*, vol. 7, pp. 362–365; October, 1959.) A theoretical treatment of various forms of distortion is given.

621.396.712:621.396.66 3263  
**Programme Switching, Control, and Monitoring in Sound Broadcasting**—R. D. Petrie and J. C. Taylor. (*BBC Engrg. Div. Monographs*, no. 28, 32 pp.; February, 1960.)

621.396.934:629.19 3264  
**Radio Communication with a Lunar Probe**—W. T. Blackband. [*Proc. Roy. Soc. (London) A*, vol. 253, pp. 511–515; December 29, 1959.] See 2167 of June.

#### SUBSIDIARY APPARATUS

621.314.6:621.382.3 3265  
**Controlled Rectification using Transistors**—K. Homilius. (*Arch. Tech. Messen*, no. 281, pp. 129–132; June, 1959.) The suitability of a transistor as a switching device is discussed in terms of its operating characteristics, and an equivalent circuit is derived. A switched rectifier circuit for use in a chopper-type dc amplifier is described which incorporates a transistor oscillator providing the control frequency.

**TELEVISION AND PHOTOTELEGRAPHY**  
 621.397.12 3266  
**Slow-Scan Image Transmission: a Progress Report**—C. Macdonald (*QST*, vol. 44, pp. 36–40; April, 1960.) Report of transatlantic tests of a system described earlier (276 of 1959).

621.397.12:629.19 3267  
**Pictorial Data Transmission from a Space Vehicle**—J. F. Baumunk and S. H. Roth. (*J. Soc. Mot. Pict. Telev. Engrs.*, vol. 69, pp. 27–31; January, 1960.) Specifications are given of a FM subcarrier system for transmitting pictures from a satellite in the vicinity of the moon.

621.397.13 3268  
**Sound-to-Picture Power Ratio**—K. McIlwain. (*Proc. IRE*, vol. 48, pt. 1, pp. 1097–1102; June, 1960.) The effect of changing this ratio from 50 per cent to 10 per cent is examined.

621.397.13:389.6 3269  
**The Results so far Achieved in the Work of the C.C.I.R./C.C.I.T.T. Mixed Commission on Television Transmission (C.M.T.T.)**—H. A. Laett. (*Tech. Mitt. PTT*, vol. 37, pp. 217–224;

June 1, 1959.) The work of the Monte Carlo conference of October, 1958 is reviewed, and the text is given of the recommendations regarding standards for long-distance transmission of monochrome television signals, which were approved by C.C.I.R. in Los Angeles, April, 1959. See also 3306 of 1957.

621.397.13:621.317.328 3270  
**The Measurement of Television Field-Strengths in the V.H.F. and U.H.F. Bands**—H. T. Head and O. L. Prestholdt. (*Proc. IRE*, vol. 48, pt. 1, pp. 1000–1008; June, 1960.) Details are given of the TASO specification. The program of field strength measurements and a summary of results are presented.

621.397.13:621.391.81 3271  
**Presentation of Coverage Information**—D. C. Livingston. (*Proc. IRE*, vol. 48, pt. 1, pp. 1102–1112; June, 1960.) Two methods are described for finding boundaries within which television reception is of a particular grade.

621.397.13:621.391.812.8 3272  
**Forecasting Television Service Fields**—A. H. Lagrone. (*Proc. IRE*, vol. 48, pt. 1, pp. 1009–1015; June, 1960.) An empirical method is suggested for forecasting service areas taking account of meteorology, terrain and vegetation. Estimates compare well with measured values.

621.397.13:621.391.814.2.029.63 3273  
**The Influence of Trees on Television Field Strengths at Ultra High Frequencies**—H. T. Head. (*Proc. IRE*, vol. 48, pt. 1, pp. 1016–1020; June, 1960.) Measurements show that typical woods are essentially opaque at UHF sites near woods receive a diffraction field plus a small leakage field.

621.397.13:621.391.82 3274  
**Picture Quality—Procedures for Evaluating Subjective Effects of Interference**—G. L. Fredendall and W. J. Behrend. (*Proc. IRE*, vol. 48, pt. 1, pp. 1030–1034; June, 1960.) Details of test design and laboratory facilities are given.

621.397.13:621.391.82 3275  
**Measurements of the Subjective Effects of Interference in Television Reception**—C. E. Dean. (*Proc. IRE*, vol. 48, pt. 1, pp. 1035–1049; June, 1960.) Results are given of the tests described in 3274 above.

621.397.13:621.391.83 3276  
**Studies of Correlation between Picture Quality and Field Strength in the United States**—C. M. Braum and W. L. Hughes. (*Proc. IRE*, vol. 48, pt. 1, pp. 1050–1058; June, 1960.) An analysis of data gathered from a house-to-house survey in conjunction with field strength measurements is given.

621.397.132 3277  
**First Results of Colour-Television Propagation Tests in Switzerland**—K. Bernath. (*Nachrichtentech. Z.*, vol. 12, pp. 281–285; June, 1959.) See 336 of January.

621.397.132 3278  
**Sequential Receivers for French Colour T.V. System**—R. Chaste, P. Cassagne, and M. Colas. (*Electronics*, vol. 33, pp. 57–60; May 6, 1960.) Description of the Henri de France system for compatible color television using sequential transmission of chrominance information and delay line storage of one-line duration. Details are given of an experimental 625-line receiver for band III.

621.397.2:621.372.553 3279  
**A Quadrature Network for Generating Vestigial-Sideband Signals**—G. G. Gouriet and G. F. Newell. (*Proc. IEE*, vol. 107, pt. B pp.,

253–260; May, 1960. Discussion, pp. 281–284.) A four-terminal linear quadrature network, comprising a tapped delay line, is used to produce a distortion free vestigial-sideband version of a 405-line television signal with a video bandwidth of 3 Mc.

621.397.331.222 3280  
**Some Aspects of Vidicon Performance**—H. G. Lubszynski, S. Taylor, and J. Wardley. (*J. Brit. IRE*, vol. 20, pp. 323–334; May, 1960.) The effect of operating voltages and illumination on sensitivity and transfer characteristics, response time, resolution, geometry and spectral response are discussed with particular reference to the EMI vidicon.

621.397.331.24 3281  
**Television Field Scan Linearization**—H. D. Kitchin. (*J. Brit. IRE*, vol. 20, pp. 357–379; May, 1960.) Conventional linearizing networks of the feedback type produce an S shaped deflection current under certain conditions. This current gives the desired shape of field scan for wide-angle CR tubes in domestic receivers.

621.397.334 3282  
**Flying-Spot Scanning for Opaque Colour Pictures**—N. Mayer. (*Rundfunktech. Mitt.*, vol. 3, pp. 123–131; June, 1959.) The advantages of a flying-spot system, such as Vitascan [279 of 1959 (Haines and Tingley)], are outlined, and the operation of the system is considered quantitatively. A photograph of a color television picture obtained with experimental scanning equipment is reproduced.

621.397.6:621.372.55 3283  
**Techniques of Delay Equalization**—A. N. Thiele. (*Proc. IRE, Australia*, vol. 21, pp. 225–241; April, 1960.)

621.397.6:621.396.677 3284  
**Determining the Operational Patterns of Directional TV Antennas**—Kear and Kershner. (See 3003.)

621.397.61 3285  
**Findings of TASO Panel I on Television Transmitting Equipment**—H. G. Towson and J. E. Young. (*Proc. IRE*, vol. 48, pt. 1, pp. 1081–1087; June, 1960.) Indicates the technical and economic factors involved in operation in the VHF and UHF bands.

621.397.61:681.42.089 3286  
**The Objective Lens in Television and its Transmission Properties as given by Amplitude and Phase Characteristics**—H. Grabke and F. Below. (*Rundfunktech. Mitt.*, vol. 3, pp. 145–152; June, 1959.) The concept of contrast transmission factor in optical systems is related to modulation depth in electrical communication theory. Methods of measuring and evaluating the transmission characteristics of optical systems are reviewed. 15 references.

621.397.612 3287  
**Remote TV Control by Blanking-Interval Pulses**—K. Kazama and T. Ishino. (*Electronics*, vol. 33, pp. 79–81; May 13, 1960.) Circuits are described for transmitting and receiving colour control pulses during unused line scans in the vertical blanking interval. Possible applications to local program control at subsidiary stations are suggested.

621.397.62 3288  
**VHF and UHF Television Receiving Equipment**—W. O. Swinyard. (*Proc. IRE*, vol. 48, pt. 1, pp. 1066–1080; June, 1960.) Data are given for antennas, transmission lines and receivers with particular reference to RF amplifiers and mixers. Community antennas and distribution systems and the effects of transmitter

sound power reduction on receiver performance are also discussed.

621.397.62 3289

**Relative Performance of Receiving Equipment as Reported by Television Servicemen**—H. W. Taylor. (Proc. IRE, vol. 48, pt. 1, pp. 1059-1065; June, 1960.) Statistical results of a six-page questionnaire are presented, covering VHF and UHF, color and monochrome.

621.397.62.001.4(083.74) 3290

**IRE Standards on Television: Methods of Testing Monochrome Television Broadcast Receivers, 1960**—(Proc. IRE, vol. 48, pt. 1, pp. 1124-1154; June, 1960.) Standard 60 IRE, 17.S1.

621.397.621 3291

**The Fine Contrast of Television Picture Tubes**—F. Arp. (*Rundfunktech. Mitt.*, vol. 3, pp. 105-113; June, 1959.) The results are given of photometric measurements of the brightness of differently sized test patterns in relation to the constant brightness of the background. The transfer characteristics for the contrast of a picture tube are derived; these cannot be described by an equivalent linear quadripole so that improvement of contrast by electrical compensation is not feasible. The influence of tube screen absorption and safety front plates on picture contrast are discussed; optimum results should be obtainable by using transparent CRT screens without safety plates.

621.397.621:621.373.444.1 3292

**Multi-triode Flywheel Synchronizing Circuit for 525- and 625-Line Receivers**—M. C. Gander and P. L. Mothersole. (*Mullard Tech. Commun.*, vol. 4, pp. 284-287; August, 1959.) See 3500 of 1959.

621.397.712(47) 3293

**Video-Frequency Equipment for Television Centres of the Soviet Union**—B. A. Berlin. (*J. Brit. IRE*, vol. 20, pp. 381-386; May, 1960.) Present and future requirements are outlined. Equipment designed for mass production and the performance of television cameras are described.

621.397.743:621.372.553 3294

**Phase Equalization in the Repeater Stations of the Television Radio Link Milan-Palermo**—A. Luna. (*Alta Frequenza*, vol. 28, pp. 441-453; June/August, 1959.) The procedure of group-delay equalization for the repeaters of the Milan-Palermo radio link [see also 2254 of 1958 (Carassa)] and group delay measurement equipment are described.

621.397.743.001.4 3295

**Alignment and Maintenance Tests on the Television Link Milan-Rome-Palermo**—E. Castelli. (*Alta Frequenza*, vol. 28, pp. 498-512; June/August, 1959.) The procedure and equipment for routine measurements of linearity, pass band frequency response and matching for the terminal and relay stations are described.

621.397.9:621.397.331.2 3296

**Television Transmission of Objects of Low Brightness by using Long Storage Times**—F. Pilz and W. Habermann. (*Rundfunktech. Mitt.*, vol. 3, pp. 132-144; June, 1959.) The performance is investigated of commercial-type camera tubes under conditions of extended storage time; only the image iconoscope is capable of storage times extending to several minutes. A storage tube of the image-iconoscope type is described in which harmful ionization effects are eliminated by the use of an external scanning beam ("photoscan"). The application of display storage tubes [see, e.g., 976 of 1958 (Smith)] for viewing objects of low brightness is proposed.

## TUBES AND THERMIONICS

621.382 3297

**A Proposed Space-Charge-Limited Dielectric Triode**—G. T. Wright. (*J. Brit. IRE*, vol. 20, pp. 337-350; May, 1960. Discussion, pp. 351-355.) Recent experiments on dielectric diodes using insulating crystals of CdS have shown that large controllable space-charge-limited current can be obtained. Possible forms of a triode are suggested, and its static and frequency characteristics are forecast. These indicate that the device should have a high-gain bandwidth product, a high mutual conductance and a high input resistance, and be insensitive to temperature changes.

621.382-71 3298

**Problems of Cooling Diode and Transistor Semiconductor Elements. Simple Calculation of the Thermal Resistance of Radiators and the Determination of Maximum Dissipative Power**—J. P. M. Setrot. (*Onde élect.*, vol. 40, pp. 164-182; February, 1960.)

621.382.2 3299

**Breakdown and Light Emission in Gallium Phosphide Diodes**—J. W. Allen and P. E. Gibbons. (*J. Electronics Control*, vol. 7, pp. 518-522; December, 1959.) Avalanche breakdown is discussed in alloyed or point-contact junctions on *n* type GaP.

621.382.2 3300

**Improvement in the Square-Law Operation of IN23B Crystals from 2 to 11 kMc/s**—A. Stanforth and J. H. Craven. (IRE TRANS. ON MICROWAVE THEORY AND TECHNIQUES, vol. MTT-8, pp. 111-115; January, 1960. Abstract, Proc. IRE, vol. 48, p. 972; May, 1960.)

621.382.23 3301

**The Electrical Characteristics of the Silicon Alloyed Junctions at Very Low Temperature**—H. Izumi. (*Rep. Elec. Commun. Lab., Japan*, vol. 7, pp. 339-344; September, 1959.) Large negative resistance effects have been observed in *p-n* junctions at liquid-helium temperatures. See also 691 of February.

621.382.23 3302

**Microwave Diode Cartridge Impedance**—R. V. Garver and J. A. Rosado. (IRE TRANS. ON MICROWAVE THEORY AND TECHNIQUES, vol. MTT-8, pp. 104-107; January, 1960. Abstract, Proc. IRE, vol. 48, p. 972; May, 1960.)

621.382.23:621.318.57 3303

**Theory of the Germanium Diode Microwave Switch**—R. V. Garver, J. A. Rosado, and E. F. Turner. (IRE TRANS. ON MICROWAVE THEORY AND TECHNIQUES, vol. MTT-8, pp. 108-111; January, 1960. Abstract, Proc. IRE, vol. 48, p. 972; May, 1960.)

621.382.23:621.372.44 3304

**Anomalous Reverse Current in Varactor Diodes**—K. Siegel. (Proc. IRE, vol. 48, pt. 1, pp. 1159-1160; June, 1960.) In Varactor diodes with a high-frequency pump source applied, reverse current flowed for dc bias voltages nearer to forward conduction than reverse breakdown. Possible explanations are given.

621.382.23:621.373.029.64 3305

**High-Frequency Negative-Resistance Circuit Principles for Esaki Diode Applications**—M. E. Hines. (*Bell Sys. Tech. J.*, vol. 39, pp. 477-513; May, 1960.) A comprehensive theoretical treatment of the negative resistance characteristic of the Esaki diode for use in microwave oscillator and amplifier circuits is given. Appreciable amounts of power should be obtained in circuits using diodes in pairs, in narrow strip form, and in traveling-wave distributed circuits with ferrite nonreciprocal

attenuation. Stabilization problems and amplifier noise figure are also discussed.

621.382.23.012:621.317.755 3306

**Test Set for Displaying the Volt/Ampere Characteristics of Tunnel Diodes**—Goodman. (See 3225.)

621.382.233 3307

**A Curious Characteristic of *p-n-p-n* Junctions**—T. Kurata and K. Komatsubara. (*J. Phys. Soc. Japan*, vol. 15, pp. 362-363; February, 1960.) Variations in the *V/I* characteristics with temperature are discussed.

621.382.3 3308

**The Possibilities of the Tecnetron**—S. Handel. (*Brit. Commun. Electronics*, vol. 7, pp. 282-285; April, 1960.) A summary of the theory of operation of the device and a brief account of some recent developments in its application are given. See also 303 of 1959.

621.382.3:621.317.3 3309

**On the Determination of the Minority-Carrier Lifetime in the Base Region of Transistors**—M. E. Das and A. R. Boothroyd. (*J. Electronics Control*, vol. 7, pp. 534-539; December, 1959.) The technique described involves measurements of the base width modulation parameters and the base transport time, and provides a simple method of determining also the extrinsic base resistance and collector capacitance.

621.382.3:621.317.7.029.55/63 3310

**Measurement of Transistor Characteristic Frequencies in the 20-1000-Mc/s Range**—J. Bickley. (*Proc. IEE*, vol. 107, pt. B, no. 33, pp. 301-304; May, 1960.) A description of apparatus for rapid determination of the cutoff frequencies.

621.382.3:621.318.57 3311

**Applications of the Storage-Type Switching Transistor**—W. V. Münch and H. Salow. (*Nachrichtentech. Z.*, vol. 12, pp. 301-310; June, 1959.) A number of multivibrator circuits are described which incorporate transistors with thyatron-like input characteristics [see 696 of February (V. Münch)].

621.382.333.33 3312

**Combined Transistor Simplifies Circuitry**—(*Electronics*, vol. 33, pp. 82-83; April 22, 1960.) A short note describing a multijunction drift-field transistor in which the two emitters function independently. The device is suitable for use as a combined mixer-oscillator to which AGC may be applied.

621.382.333.34:621.318.57 3313

**Turn-On Transient of *p-n-p-n* Triode**—T. Misawa. (*J. Electronics Control*, vol. 7, pp. 523-533; December, 1959.) Experiments are described on Si *p-n-p-n* power triodes to determine current waveform during the transient. Expressions are derived for the relation between base current and delay time.

621.382.333.34:621.318.57 3314

**The Silicon Transistor Thyatron, New Semiconductor Element of Silicon for Rapid Switching of Large Powers**—A. Petitclerc. (*Onde élect.*, vol. 40, pp. 155-160; February, 1960.) Characteristics of a *p-n-p-n* junction transistor with a forward current of 15 amperes and a reverse voltage of 300 volts are given. Different applications are described.

†621.383.292 3315

**Resistance-Strip Magnetic Photomultiplier for the Extreme Ultraviolet**—L. Heroux and H. E. Hinteregger. (*Rev. Sci. Instr.*, vol. 31, pp. 280-286; March, 1960.) The multiplier comprises a high-resistance coated class dynode strip with a cathode area at one end, and a

parallel strip with a metal grid at the cathode end. A stainless steel anode is mounted close to the ends of the dynode and field strips. Crossed electric and magnetic field between the strips focus the electrons emitted from the cathode area. Current gain is  $10^8$  for wavelengths below 1400 Å. As a photoelectron counter the normal background is  $<0.1$  count/sec.

†621.383.53 3316\*  
**Calculation of Relaxation Processes of a Phototriode for Low-Intensity Illumination**—N. D. Potekhina. (*Fiz. Tverdogo Tela*, vol. 1, pp. 1509–1515; October, 1959.) Formulas are derived from Shockley's theory for the relaxation of the potential difference between emitter and base and also for the change of collector current of a  $p$ - $n$ - $p$  junction when illumination is applied or turned off. Relaxation curves are shown, and the dependence of the attenuation constant on the intensity of light absorbed is considered.

621.385.029.6:061.3 3317  
**Microwave Valves**—(*Wireless World*, vol. 66, pp. 391–394; August, 1960.) Review of some of the papers presented at the International Congress held in Munich, June 7–11, 1960, which are to be published as vol. 22 of *Nachrichtentechnische Fachberichte*.

621.385.032.21:537.29 3318  
**Electrical Stability and Life of the Heated Field-Emission Cathode**—W. P. Dyke, F. M. Charbonnier, R. W. Strayer, R. L. Floyd, J. P. Barbour, and J. K. Trolan. (*J. Appl. Phys.*, vol. 31, pp. 790–805; May, 1960.) The theory of transport phenomena in heated metals is applied to a quantitative study of cathode stability in dc and pulsed fields. Results of tests on 85 cathodes are reported.

621.385.032.212:537.29 3319  
**Stable, High-Density Field-Emission Cold Cathode**—E. E. Martin, J. K. Trolan, and W. P. Dyke. (*J. Appl. Phys.*, vol. 31, pp. 782–789; May, 1960.) Instability of emission is shown to be due to contamination and sputtering, causing surface changes. Experimental techniques are described whereby a single needle tungsten cathode can be operated at  $10^7$  amperes/cm<sup>2</sup> dc emission over a 1000-hour period. Reconditioning extends its life indefinitely.

621.385.032.213:621.391.822.33 3320  
**Thermal Positive-Ion Emission and the Anomalous Flicker Effect**—S. Datz, R. E. Mintura, and E. H. Taylor. (*J. Appl. Phys.*, vol. 31, pp. 880–883; May, 1960.) Recent measurements on tungsten filaments are used to correlate the intensity and duration of the electron pulses associated with the anomalous flicker effect and of the positive ion pulses causing it. A quantitative explanation is given of the periodic structure of the electron pulse

621.385.032.213.13 3321  
**Evolution of Gases and Ions from Different Anodes under Electron Bombardment**—J. R. Young. (*J. Appl. Phys.*, vol. 31, pp. 921–923; May, 1960.) Evolution of Cl from anodes of Ag, Cu, Ni, Mo, Ta, Ti and W has been detected. It is believed to be responsible for the early fall in emission commonly observed at low anode voltages. Evolution of O<sup>+</sup> ions from oxidized anodes reduces oxide-cathode dc emission capabilities considerably.

621.385.032.213.13:548.74 3322  
**Electron-Microscope Study of the Decomposition Process of Oxide-Coated Cathodes**—S. Hirota and T. Imai. (*J. Phys. Soc. Japan*, vol. 15, pp. 137–144; January, 1960.) The technique of electron microscopy on oxide cathodes is described. Oxide crystal growth becomes significant at 1100°C for (BaSrCa)CO<sub>3</sub> but at a lower temperature for BaCO<sub>3</sub>.

621.385.032.266 3323  
**Exact Electrodes for the Formation of a Curved Space-Charge Beam: Part 2**—R. J. Lomax. (*J. Electronics Control*, vol. 7, pp. 482–490; December, 1959.) An extension of an analytical method previously described (see 651 of 1958) for determining the design of Pierce electrodes for curved space-charge beams.

621.385.032.269.1 3324  
**Triode Pierce Guns**—B. Melzer. (*J. Electronics Control*, vol. 7, pp. 491–496; December, 1959.) "The range of application of high-perveance Pierce guns may be increased by converting them to triode and multitriode systems. A method is given, and its implications for tube design in general are pointed out."

621.385.032.269.1 3325  
**The Calculation of Electrostatic Electron-Gun Performance**—M. R. Barber and K. F. Sander. (*J. Electronics Control*, vol. 7, pp. 465–481; December, 1959.) The cathode current density and trajectories in the space-charge-limited gun are derived by an iterative procedure.

621.385.3:621.396.61:621.315.612 3326  
**The Application of Ceramics in the Development of Techniques for the Construction of Transmitting Valves**—G. Gallet. (*Onde élect.*, vol. 40, pp. 201–206; February, 1960.)

621.385.6 3327  
**Determination of the Sign of Power Flow in Electron-Beam Waves**—W. R. Beam. (*PROC. IRE*, vol. 48, pt. 1, p. 1170; June, 1960.) A method for determining this sign is given.

621.385.624 3328  
**Theoretical Study of Klystron Power Amplifiers for the U.H.F. Band**—C. Zlotykamin. (*Onde élect.*, vol. 40, pp. 133–138; February, 1960.) Geometric and electrical parameters are discussed in relation to conditions for maximum gain and bandwidth. A klystron is proposed,

having a narrow high-density beam and its advantages are noted.

621.385.624 3329  
**Technical and Practical Aspects of the Construction of Klystron Power Amplifiers**—R. Champeix. (*Onde élect.*, vol. 40, pp. 139–142; February, 1960.) Two types of medium-power klystron are described, based on theoretical consideration discussed in a companion paper (3328 above).

621.385.63 3330  
**Beam Focusing by R.F. Electric Fields**—E. Suguta, M. Terada, K. Ura, and Y. Ikebuchi. (*PROC. IRE*, vol. 48, pt. 1, pp. 1169–1170; June, 1960.) It is shown that waves traveling faster than the electron beam (in the same direction) have a defocusing action.

621.385.63:621.372.56 3331  
**Some Measurements of Travelling-Wave-Tube Attenuators in 2000 Mc/s**—C. H. Dix. (*IRE TRANS. ON MICROWAVE THEORY AND TECHNIQUES*, vol. MTT-8, pp. 121–122; January, 1960.) Results are given of measurements of surface resistivity, phase velocity, and attenuation made along steatite rods sprayed with Aquadag mixture.

621.385.63:621.375.9:621.372.44 3332  
**A Transverse-Field Traveling-Wave Tube**—E. I. Gordon. (*PROC. IRE*, vol. 48, pt. 1, p. 1158; June, 1960.) The electron beam moves in a spatially varying electric quadrupole field; the fast cyclotron wave is amplified and after extraction of energy in the output coupler, the electrons can be collected at a potential close to that of the cathode.

621.385.632 3333  
**Improvements in a C.W. Power Travelling-Wave Tube**—M. O. Bryant, J. F. Gittins, and F. Wray. (*J. Electronics Control*, vol. 7, pp. 505–517; December, 1959.) Improvements are described in a "clover-leaf" amplifier for the 3-cm band. An output of 1 kw or more can be obtained with a high-level gain  $\pm 10$  db.

621.387:621.316.722 3334  
**The Corona Discharge and its Application to Voltage Stabilization**—E. Cohen and R. O. Jenkins. (*Proc. IEE*, vol. 107, pt. B, pp. 285–294; May, 1960.) The properties of corona discharges are outlined, and the various factors determining the design of stabilizing tubes for the range 350–7000 volts are discussed.

#### MISCELLANEOUS

621.396:061.3 3335  
**New Radio Regulations**—C. F. Booth. (*J. IEE*, vol. 6, pp. 431–433; July, 1960.) The main conclusions of the Administrative Radio Conference, Geneva, August–December, 1959, are summarized, including the frequency allocations for space research and the nomenclature of the frequency and wavelength bands for radio communication.

# Translations of Russian Technical Literature

Listed below is information on Russian technical literature in electronics and allied fields which is available in the U. S. in the English language. Further inquiries should be directed to the sources listed. In addition, general information on translation programs in the U. S. may be obtained from the Office of Science Information Service, National Science Foundation, Washington 25, D. C., and from the Office of Technical Services, U. S. Department of Commerce, Washington 25, D. C.

PUBLICATION	FREQUENCY	DESCRIPTION	SPONSOR	ORDER FROM:
Acoustics Journal (Akusticheskii Zhurnal)	Quarterly	Complete journal	National Science Foundation—AIP	American Institute of Physics 335 E. 45 St., New York 17, N. Y.
	Monthly	Complete journal	National Science Foundation—MIT	Instrument Society of America 313 Sixth Ave., Pittsburgh 22, Pa.
Automation and Remote Control (Avtomatika i Telemekhanika)	Monthly	Abstracts only		Office of Technical Services U. S. Dept. of Commerce Washington 25, D. C.
	Monthly	Abstracts of Russian and non-Russian literature		Office of Technical Services U. S. Dept. of Commerce Washington 25, D. C.
Journal of Experimental and Theoretical Physics (Zhurnal Eksperimentalnoi i Teoreticheskoi Fiziki)	Monthly	Complete journal	National Science Foundation—AIP	American Institute of Physics 335 E. 45 St., New York 17, N. Y.
Journal of Technical Physics (Zhurnal Tekhnicheskoi Fiziki)	Monthly	Complete journal	National Science Foundation—AIP	American Institute of Physics 335 E. 45 St., New York 17, N. Y.
Proceedings of the USSR Academy of Sciences: Applied Physics Section (Doklady Akademii Nauk SSSR: Otdel Prikladnoi Fiziki)	Bimonthly	Complete journal		Consultants Bureau, Inc. 227 W. 17 St., New York 22, N. Y.
Radio Engineering (Radiotekhnika)	Monthly	Complete journal	National Science Foundation—MIT	Pergamon Institute 122 E. 55 St., New York 22, N. Y.
	Monthly	Abstracts only		Office of Technical Services U. S. Dept. of Commerce Washington 25, D. C.
Radio Engineering and Electronics (Radiotekhnika i Elektronika)	Monthly	Complete journal	National Science Foundation—MIT	Pergamon Institute 122 E. 55 St., New York 22, N. Y.
	Monthly	Abstracts only		Office of Technical Services U. S. Dept. of Commerce Washington 25, D. C.
Solid State Physics (Fizika Tverdogo Tela)	Monthly	Complete journal	National Science Foundation—AIP	American Institute of Physics 335 E. 45 St., New York 17, N. Y.
Telecommunications (Elekprosviaz')	Monthly	Complete journal	National Science Foundation—MIT	Pergamon Institute 122 E. 55 St., New York 22, N. Y.
	Monthly	Abstracts only		Office of Technical Services U. S. Dept. of Commerce Washington 25, D. C.
Automation Express	10/year	A digest: abstracts, summaries, annotations of various journals		International Physical Index, Inc. 1909 Park Ave., New York 35, N. Y.
Electronics Express	10/year	A digest: abstracts, summaries, annotations of various journals		International Physical Index, Inc. 1909 Park Ave., New York 35, N. Y.
Physics Express	10/year	A digest: abstracts, summaries, annotations of various journals		International Physical Index, Inc. 1909 Park Ave., New York 35, N. Y.
Express Contents of Soviet Journals Currently being Translated into English	Monthly	Advance tables of contents of translated journals		Consultants Bureau, Inc. 227 W. 17 St., New York 22, N. Y.
Technical Translations	Twice a month	Central directory in the U. S. of translations available from all major sources in the U. S.	OTS and Special Libraries Assoc.	Superintendent of Documents U. S. Gov't Printing Office Washington 25, D. C.